The development of secondary porosity and permeability in fractured rock

Anthony Robin Westerman

TITLE

The development of secondary porosity and permeability in fractured rock.

OUTLINE

Theory from several fields related to engineering geology is compared with experimental results and with observations in caves and limestone quarries; then used towards the prediction of the sizes and distribution of the voids caused by solution in rock.

A thesis submitted to the University of Durham, England for the degree of Doctor of Philosophy in the Faculty of Science

by Anthony Robin Westerman B.Sc., November 1981.

DECLARATION.

The content of this thesis is the original work of the author (any joint research, where included, is acknowledged by reference). It has not been previously submitted for a degree at this or any other University.

A. R. Westerman

A.R.Westerman.

Durham, November, 1981.

ABSTRACT

Systems of faults and joints are observed to span many scales of length and displacement. Spacing and orientation are rarely constant within any area of interest to groundwater engineers.

It is suggested that the methods used by engineering surface topographists should be applicable to geological fracture surfaces. Each fissure is regarded as resulting from the displacement of two, initially matched, rough surfaces.

It is argued that a fractured aquifer is best modelled as a pipe network. This would be a similar system to the pore network in a small unfractured subvolume of that aquifer. However, the manipulation of models having an infinite number of elements and many scales of length is not in an advanced state. Accordingly, the fissure sytem is treated as a pipe network, and the joint blocks are regarded as being subject to one dimensional diffusion.

The concept of Pore Span Distribution can be developed from the extensive literature on petroleum reservoir engineering. Experimentally determined values of porosity and permeability should be functions of lithology, and also of specimen size and shape. It is a measurable lithological property which describes the degree of interconnection displayed by a pore network.

A falling head gas method is developed and used to determine the low permeabilities found in weathered limestone joint block margins.

Unusually high seismic anisotropy is observed in the Corallian Limestone due to layering of weathered and unweathered rock, parallel to a dominant joint set.

A new interpretation of the deformational phase affecting the Scourie dykes near Loch Torridon, Ross-shire is included. It is related to the problem of describing fault and joint sets adequately.

The secret of healthy tubes
is to keep a good steady flow.

Anon, Sheffield.

ACKNOWLEDGEMENTS

The author would like to express his gratitude to the following for their advice and assistance during the execution of the projects described in this thesis:-

Mr. and Mrs. A.Westerman and Miss K.J.Wilkinson.

Professors P.B.Attewell and M.P.H.Bott and their staff.

Dr. M. J. Reeves, the project supervisor, for his continued availability and support.

Dr. J. G. Holland for opportunities to map the Lewisian, North of Loch Torridon, and for discussions on it's structural analysis.

Mr. B. Lander and the staff of the Computer Unit, Durham University.

Dr. T. Thomas of Teeside Polytechnic, Middlesborough.

Mr. J. M. Lucas for designing electronic circuitry, writing microprocessor programs, and collaboration in the development of a computer program to process X-ray fluorescence counts to major element analyses.

Messrs. J.K.Mierzejewski, H.Jonasson, K.L.Riemer, G.R.Dowlen, and R.I.Kendrick, whose M.Sc. theses are relevant to the subject matter of this thesis.

Messrs. G. Randall and B. McEleavey for numerous useful suggestions in the laboratory.

Mr. G. Richardson of the Institute of Geological Sciences, Leeds for discussions on the geology of the Vale of Pickering, North Yorkshire.

Dr. D. Chadha and Mr. I. Barker of The Yorkshire Water Authority, York for discussions on the hydrogeology of North and East Yorkshire, and for the provision of river gauging station records and borehole logs and cores.

Hargreaves Quarries Limited for access and for discussion on the attenuation of blasting induced vibrations.

Mr. Keith Bell of Hovingham Quarry, North Yorkshire for providing a sawn slab of Corallian Limestone, and for access.

Members of Durham University Speleological Association and of Trent Polytechnic Caving Club for their patience underground.

Mr. P.R. Ryder and Dr.G.Stevens of Moldywarps Speleological Group, and Mr. A. C. Waltham for information on known occurences of bedding plane anastomoses in Britain.

Also to many others whose goodwill and helpfulness was much appreciated.

The Natural Environment Research Council is thanked for financial support.

Note on formulae:

* means raised to the power, e.g. 'd*2' means 'd' squared, and 'd*0.5' means the square root of 'd'.
. means multiplied by, e.g. 'a . b' means 'a' multiplied by 'b'.
/ means divided by, e.g. 'dp / dl' means 'dp' divided by 'dl', or grad 'p'.

Note on symbols:

s, second,
N, Newton,
Pa, Pascal, or (N / m*2)

Dimensions, expressed in terms of: Length, L; Time, T; and Force, F, are enclosed in square brackets.

The SI code is followed except where oil industry units are more commonly used.

CONTENTS.

CONTENTS. PAGE.

1.1 Aims and scope of study.

1.1.1 Synopsis

Most previous studies of groundwater flow have assumed that aquifer properties are constant with time. Darcy's law and the Laplace equation allow analysis where the geometry and hydraulic conductivity of the aquifer, and the fluid's viscosity and hydraulic head are known. Where fissure flow has been taken into account, the hydraulic conductivities of the individual fissures have been integrated with that of the unfractured aquifer. In order to model the development of secondary porosity and permeability two other considerations must be made. The chemical aggressivness of the fluid towards aquifer lithologies must be known, as must it's rate of decrease with reaction time. A realistic description of the fracture pattern is also required. One large fissure is no longer directly equivalent to several smaller ones in a purely additive manner, Chapter 5. Discrete flows must be calculated for each fissure in the network. Darcy's law is therefore no longer applicable.

A numerical model that accurately described the fracture pattern and change in aggressiveness could also take account of the phenomenon of mischungkorrosion, Bogli (1971). Although pipe networks can be analysed for discrete flows, a satisfactory numerical model of dynamically increasing fracture permeability cannot yet be constructed. The outstanding problems relate to the description of fracture networks and are dealt with in Chapter 4. Theoretical work which will allow realistic models of fracture patterns to be generated is becoming available. Much field and laboratory work is required before the hydraulic conductivities of individual fractures can

be calculated, Chapter 3.

1.1.2 Sources and related work.

Since so many phenomena need to be taken into account, a variety of studies have contributed to this thesis. Their inter-relationship within the text is shown in Fig 1. They have been grouped into three main areas of study, i.e.: fieldwork, laboratory work, and numerical modelling. Observations relating to the two outstanding areas of: fracture pattern description; and engineering surface metrology, or roughness studies have been made both in the field and in the laboratory. Studies which now seem to be of peripheral importance are referred to in the appendices.

Within the County of Yorkshire it is possible to compare cavern development within three limestones of very different lithology and age. Yorkshire is also a classic area for speleological studies. Flow tracing in the Jurassic Corallian aquifer of North Yorkshire has been undertaken by Mierzejewski (1978) and Kendrick (1979) in related M.Sc. studies. The search for examples of the very early stages of the solutional development of secondary porosity took the author to the Carboniferous Limestones of South Wales and the Mendip area as well as West and North Yorkshire.

Since the rate of development of a flow network depends upon its initial topology as well as the hydraulic conductivities of it's individual elements, descriptions of fracture patterns are of importance. Fracture patterns have been observed and the heterogeneity of their effects on seismic properties studied by Dowlen (1979), in an M.Sc. linked to this thesis. Although the anisotropies observed are far in excess of those reported in

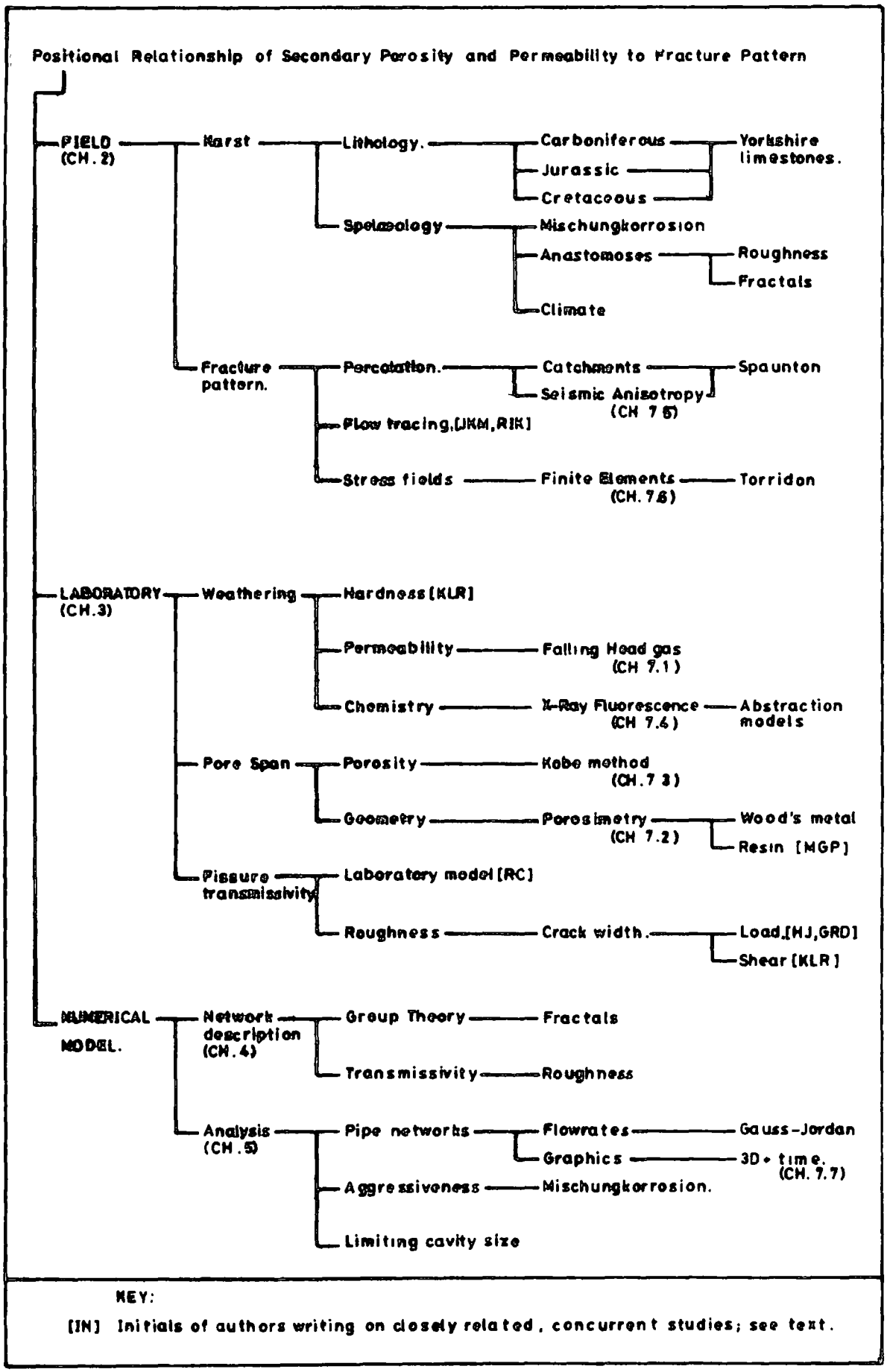

KEY:

[IN] Initials of authors writing on closely related, concurrent studies; see text.

Fig 1

the literature, this work is of purely illustrative value. Seismic properties are summed over a large body of rock and depend upon the number, the width, and the weathering of the fissures reponsible. An attempt to solve for the variables of fissure frequency and fissure porosity using existing empirical relations and observed attenuation and velocity anisotropies, led to large error bounds, Appendix 7.5. Resistivity is an analogue of permeability, but in most engineering applications varying saturation in the vadose zone makes it an unreliable data source. Consequently, the direct detection of bulk properties cannot supply the detailed information required for a predictive dynamic model.

The mathematical description of fracture patterns, which are observed to occur on many scales of length, does not yet allow a good predictive model to be generated. The controlling mechanisms which generate the observed fracture patterns are becoming well understood. The Scourie dykes of the Loch Torridon area were studied during this research, and their mechanism of emplacement can be related to the fracture pattern observed at Spaunton Moor. In the Lewisian the fracture pattern has been infilled by basic dykes so there is no question of any development of secondary porosity; and the permeability remains effectively zero, except along late brittle fractures. The importance of relating the two study areas lies in the fact that the mappable distribution and size of the basic dykes illustrates the dependence of primary hydraulic conductivities upon the stress field which generated the fracture pattern. A Finite-Element model was used to illustrate the mechanism, Appendix 7.6.

Laboratory studies involved the use of standard oil industry

apparatus for the measurement of porosity and permeability in small samples of rock. Weathering studies were undertaken by Riemer (1978) in a related M.Sc. and pore geometry has been studied using the scanning electron microscope. Patsoules (pers comm) has used similar methods on a concurrent study of the chalk. The relevance of studies on weathered margins lies in comparing the rate of development of secondary permeability in different limestone types. Apparently limestones of low porosity do not develop weathered margins. All solution is concentrated on fissure widening, and large cavern systems develop. Reeve's (1979) piston mechanism for the recharge of the chalk aquifer represents the converse case.

An important laboratory study upon which much more work needs to be done for the purposes of engineering geology was undertaken by Jonasson (1980). Fracture roughness has been described before by engineering geologists and it's importance recognised for slope stability studies. However theory relating measurable, and eventually predictable properties of a fissure to it's hydraulic conductivity under varying loads has been developed by engineering surface metrologists. This theory will eventually allow individual fissure hydraulic conductivities to be predicted for various depths. At present, evidence from boreholes and seismic experiments are the only sources of such information, Snow (1968). It should eventually be possible to model the distribution of initial fissure hydraulic conductivities from the stress field deduced from the partially observable fracture pattern, and a knowledge of the roughness parameters associated with the shear strain history and normal load on each fissure.

Observations made in the field enable one to justify the

modelling of a fissure system by a pipe network. The relationship between intersecting rough fissures and the pipe observed at their intersection during later stages of solutional development must be considered, Chapter 5 and Fig 28. Pipe networks are solvable for flow rate, and so in theory a viable model can be made. This numerical model compares with previous electric analogues and physical models involving frameworks of small tubes. A numerical model will allow: calculation of the mischungkorrosion effect; statistical analyses; and computer graphic descriptions of the development of the model through time. Natural systems are far too large and complex for any model to be useful in a predictive manner at present.

1.1.3 Summary and applications.

It must be concluded that for engineering geological purposes, the description of roughness parameters and of fracture patterns observed will not only allow indices of speleological potential and mineralisation potential to be mapped, but will eventually allow the construction of realistic predictive models. Prediction of the position, shape and size of fracture controlled mineral deposits and of cave systems are related problems. Attempts are made at direct detection backed by exploration models.

Many factors have been recognised as influencing the size and distribution of the voids caused by solution in rock. They can be split into those related to the fissure porosity, and those related to the intrinsic porosity. The different ways in which pore space has been described are related to groundwater modelling requirements. In this study local flowrates through

the fissure network are required so that the rate of growth of each element can be predicted. Existing theories and experimental results on solution rates can only be applied where the provenance, flow rate, and consequently the aggressiveness of the pore fluid is known. System sources (infiltration and stream sinks) and system sinks (resurgences) should be represented. Observations of karst suggest that the early stages of subterranean development do correspond to a system of anastomosing solution tubes. Later, more cavernous stages involve several other mechanisms, in addition to solution, which are not treated here.

Natural systems occur on a vast scale, and the basic data describing them are not usually sufficiently well known to allow predictive numerical modelling. A numerical model is of interest for testing theories of speleogenesis. Predictions of solution tube development would be of use in site investigation work for dams, barrages and wells in fissured aquifers. It is possible that similar mechanisms operate during the inceptive stages of fault controlled hydrothermal deposits.

Mineral veins may not follow the same developmental path as cave systems. Fissure controlled orebodies result from a depositional process which often involves ion exchange with the wallrock. If the depositional phase is preceeded by an erosional phase, then pipe-like cavernous systems may be expected. If, as in most gold-quartz veins, emplacement was purely depositional, then roughness studies and stress analysis will be of importance in understanding the distribution of ore.

1.2 Basic concepts and definitions.

1.2.1 Porosity.

The porosity, N (dimensionless) of a rock or soil is defined as:-

$$N = Vv / V \quad \ldots\ldots(1)$$

where:

Vv (cc) is the volume of voids, and

V the volume of the specimen.

The specimen volume may be determined to a high accuracy, by displacement. The volume of voids is also determined by displacement; but indirectly since:-

$$V = Vv + Vg \quad \ldots\ldots(2)$$

Various assumptions are made in determining the grain volume, 'Vg'; depending on the method used. If a non-destructive method is adopted, there is an implicit assumption that the whole of the void space is accessible from the surface of the specimen. Since the sampling fluid cannot be injected into them, closed voids within the specimen will behave as part of the grain volume, Appendix 7.3.1. Thus the effective porosity, 'Ne' may be defined as that part of the total porosity which is accessible to the sampling fluid:-

$$N = Ne + Nresidual \quad \ldots\ldots(3)$$

In the case of soils and poorly-cemented, coarse-grained rocks the pore space is probably infinitely connected, so that 'Ne = N'. In the case of 'tight' rocks such as granites and well-cemented limestones this assumption is harder to justify. Norton and Knapp (1977) subdivide porosity as follows:-

$$N = Nflow + Ndiffusion + Nresidual \quad \ldots\ldots(4)$$

and show that "the major portion of total porosity in pluton

environments is due to residual pores not interconnected to either flow or diffusion porosity".

For present purposes, it is better to redefine the flow porosity, the diffusion porosity, and the residual porosity using equation (1). The volume of voids, 'Vv' then subdivides into 'Vf', 'Vd', and 'Vr'. 'Vf' comprises the volumes of those pores, {Pf} which provide continuous flow channels. 'Vd' comprises the volumes of those pores, {Pd} which "either have apertures that are too small to permit significant fluid flow or are discontinuous". 'Vr' comprises the volumes of those pores, {Pr} which are not interconnected to either flow or diffusion pores.

Figure 2 shows that the set of pores {P} does not subdivide uniquely into {Pf;Pd;Pr}. The faces of two schematic specimens are shown by dashed lines. In general, the volume of an individual pore may become attributed to any one of: 'Vf', 'Vd', or 'Vr'; during specimen preparation.

In a sufficiently thin specimen:

Vv = Vf, and:

Vd = Vr = 0.

In Section 3.2, it will be suggested that the effective porosity of a small subvolume, 'Nes' may vary with distance from the main specimen face. When the subvolume is at the main specimen face, 'Ves = Vvs', and 'Vrs = 0'. As the subvolume is moved into the specimen and away from the main specimen face, 'Ves' reduces until 'Vrs = Vvs'.

It is also possible to subdivide the porosity by:-

N = Nfissure + Nintrinsic.....(5)

where the intrinsic porosity is taken as the porosity characteristic of the unfractured lithology. Again, there are

THE PUTATIVE EFFECT OF SPECIMEN SIZE ON THE CLASSIFICATION OF POROSITY

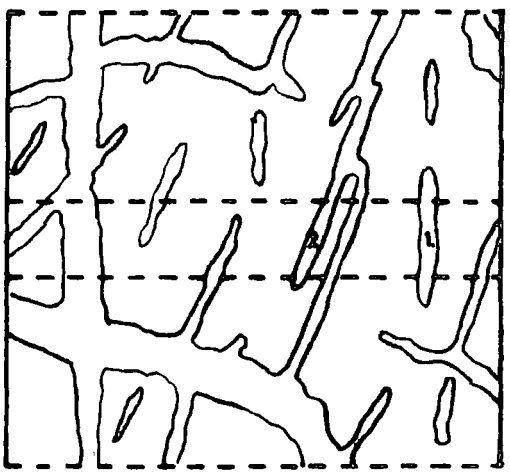

Pore (1) is a residual pore in the large specimen and a flow pore in the small

" (2) " diffusion " " " " " " " "

Fig 2

problems of scale. Norton and Knapp (1977) show that in igneous rocks, most of the small pores are microcracks. In Chapters 2 and 4, it will be argued that, even on a large scale, the fissure porosity is not necessarily equal to the flow porosity. Faults and joints are observed to have distributions of characteristic lengths. The relationship between the land surface and such a fracture pattern is analogous to the relationship between the faces of a laboratory specimen and the intrinsic porosity.

Finally, the effective porosity has been divided into:-

$$Ne = Nmicro + Nmacro \quad \ldots\ldots\ldots\ldots\ldots\ldots\ldots\ldots (6)$$

where:

Nmicro is the microporosity, and

Nmacro is the macroporosity.

Scott Russell (in Schaffer, 1972) assumed a value of 5 microns for the limiting size of a micropore. He used a microscope to measure the macroporosity, due to pores above that size. The effective porosity was measured by water absorption in vacuo. In Schaffer (op cit) it is shown that rocks having a high microporosity degrade quickly under natural weathering conditions and crystallisation tests. The mechanisms proposed involve the growth of product crystals in the pore space. The rock suffers disruptive interference during expansion and contraction, wetting and drying.

Jones and Hurt (1978) used the rock suction characteristic curve to rank the susceptibilities of natural limestone aggregates to frost heaving. This osmotic method produces a full effective pore size distribution curve, similar to that obtained from a mercury capillary pressure curve. Such curves can be integrated to estimate the internal surface area of a

lithology.

1.2.2 Permeability

Darcy's law may be written as:

$$Q = [\ c / u\ ].[\ d^2 . A\ ].(\ dp / dl) \quad \ldots\ldots\ldots (7)$$

where:

Q is the flowrate [L^3 / T],

c is a dimensionless constant dependent upon grain size, shape, sorting and porosity etc.,

d is the grain size [L],

u is the absolute viscosity (10 poises = 1 Pa.s)

A is the cross-sectional area across which flow is measured, and

(dp / dl) is the pressure loss per unit length of flow line.

Darcy (1865), first defined his law as:

$$Q = K . A . (\ dh / dl\ ) \quad \ldots\ldots\ldots\ldots\ldots\ldots (8)$$

where:

K is the hydraulic conductivity [L / T]

(dh / dl) is the headloss such that:

$$dp = w . dh \quad \ldots\ldots\ldots\ldots\ldots\ldots (9)$$

where:

w is the specific weight (N / m^3).

Raudkivi and Callander (1976, p15) show that:

$$k = c . d^2 \quad \ldots\ldots\ldots\ldots\ldots\ldots\ldots\ldots (10)$$

where:

k is the coefficient of permeability, or the permeability [L^2].

They also show that:

$$K = k . w / u = c . d^2 . w / u \quad \ldots\ldots\ldots\ldots (11)$$

The permeability is therefore independent of the fluid type, and was defined by Bear (1972) as follows: "a porous medium is said to have a permeability of one darcy if a single-phase fluid of one centipoise viscosity that completely fills the pore space of the medium will flow through it at a rate of 1 cm*3 / s per cm*2 of cross-sectional area under a pressure gradient of 1 atm. per cm". So 1 darcy = 0.987 x 10*-8 cm*2.

The remarks associated with Fig 2 may be pertinent for low porosity specimens. Pores that behave as flow pores in a thin specimen could become accessible only by diffusion, in a thick specimen. Permeability is not a scalar quantity. It has been represented as a tensor by Scheidegger (1954, 1956, 1957), so that variations with direction must be taken account of. Geological materials are usually inhomogeneous, and anisotropic. Raudkivi and Callander (op cit, p115-126) following Scheidegger (1956), show that for hydraulic conductivity measured parallel to the streamlines:

KS1 = Kx . Kz / (Kz . cos*2(Beta) + Kx . sin*2(Beta))

.....(12)

where:

KS1 is the hydraulic conductivity measured,

Kx , Kz are orthogonal minimum and maximum hydraulic conductivities for the anisotropic (planar) medium, and

Beta is the angle between the 'Kx' axis and the direction of 'KS1'.

For hydraulic conductivities measured parallel to the head gradient, or perpendicular to the equipotentials:

KS2 = Kx . cos*2(Alpha) + Kz . sin*2(Alpha).....(13)

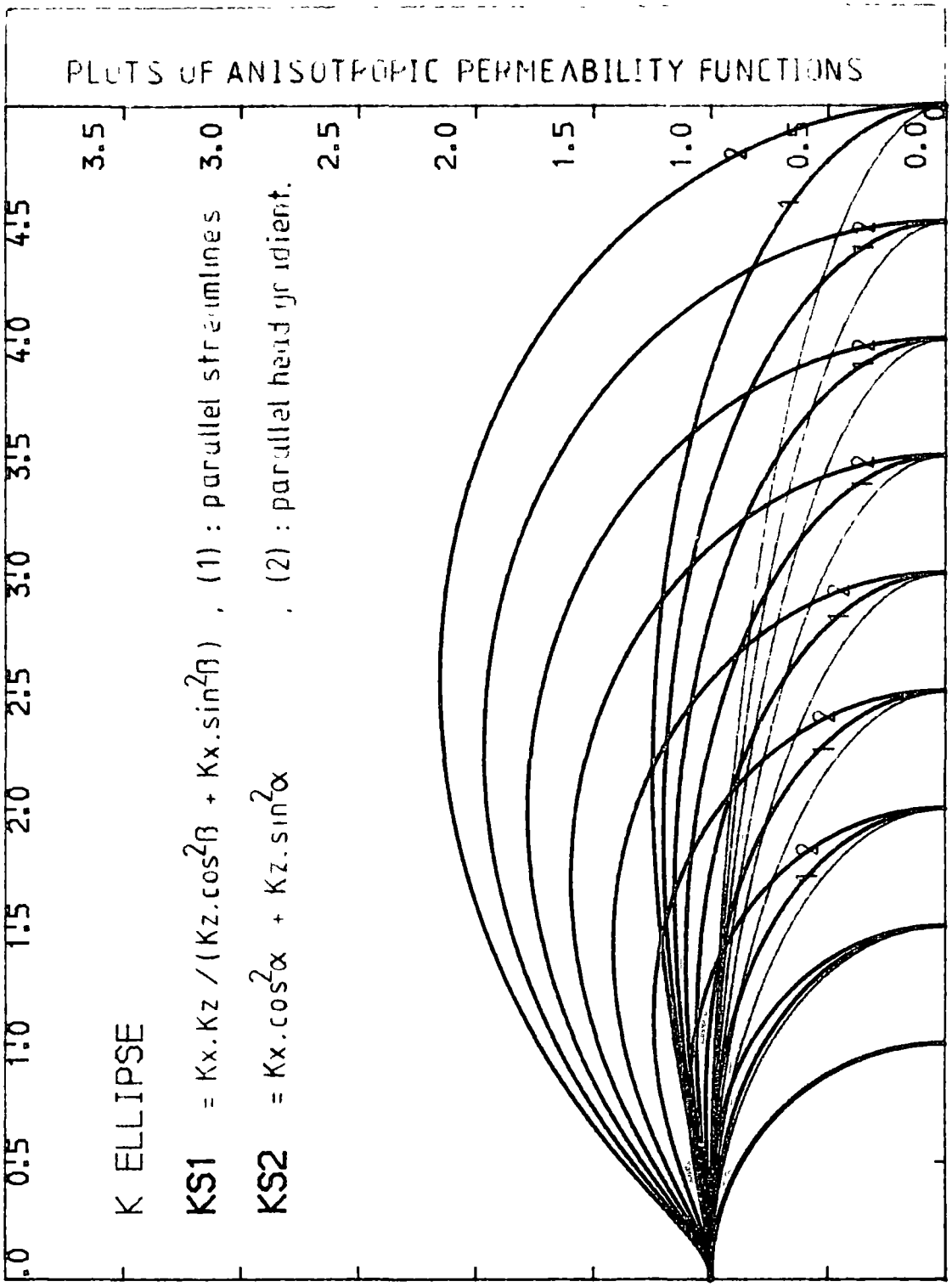
PLOTS OF ANISOTROPIC PERMEABILITY FUNCTIONS
K ELLIPSE
KS1 = Kx.Kz / (Kz.cos²β + Kx.sin²β) , (1) : parallel streamlines
KS2 = Kx.cos²α + Kz.sin²α , (2) : parallel head gradient.
0.0
0.5
1.0
1.5
2.0
2.5
3.0
3.5
4.0
4.5

Fig 3

where:

KS2 is the hydraulic conductivity measured, and

Alpha is the angle between the 'Kx' axis and the direction of 'KS2'.

The equations for 'KS1' and 'KS2' are different forms of inverse ellipse and have been plotted for comparison in Fig 3.

The permeability,'k' has been separated into:-

k = kfissure + kintrinsic.....(14)

compare equation (5).

Norton and Knapp (op cit) define permeability as a function of the abundance and geometry of continuous flow channels. The functional relationship between the permeability and the flow porosity is usually derived by using simple models, Scheidegger (1957). These rely on known relationships between pore or pipe geometry, viscosity and the flowrate.

The hydraulic conductivity of a system of fissures is usually described as if the system were an equivalent continuum. Romm (1966) has shown that the hydraulic conductivity of anisotropically fissured media varies in a similar manner to 'KS2', above.

Louis and Maini (1967) have shown empirically that for flow parallel to a joint set:

K = { w / 12 . u }.[e*3 / sp].....(15)

where:

e is the joint opening, and

sp is the joint spacing.

Howard and Fast (1970) give the permeability of an open fracture in laminar flow as:

k = 10*8 . hf*2 / 12.....(16)

where:

k is the permeability (darcies), and

hf is the fracture width (inches).

For the permeability of a packed fracture they give:

$$k = n^3 / Ck \cdot S^2 \cdot (1 - n)^2 \quad \text{.....(17)}$$

where:

n is the porosity,

Ck is the Kozeny-Carmen constant, approximately equal to 5.0, and

S is the area of particle surface per unit volume of packed space (per inch).

The last relationship is noted since fault planes are usually packed with gouge, and values for 'S' and 'n' will depend upon the shear history of the fracture and variables such as the normal load and the shear strength of the apophyses.

Patir and Cheng (1978) have used flow simulation by a Finite-difference method to derive an expression for the flow though a rough fissure:

$$Q = [Pff / 12 \cdot u].[h^3 \cdot 1].(dp / dl) \quad \text{.....(18)}$$

where:

h is the average gap of the fissure between mean surface heights,

i is the fissure width (L), and

Pff is the pressure flow factor (dimensionless) given by:

$$Pff = 1 - 0.9 \cdot \exp(-0.56 \cdot h / sigma) \quad \text{....(19)}$$

where:

sigma is the standard deviation of the combined roughnesses of the two surfaces such that:

$$sigma = (sigma(a)^2 + sigma(b)^2)^{0.5} \quad \text{.....(20)}$$

where:

sigma(a) , sigma(b) are the standard deviation surface roughnesses of the heights from surface profiles for sides 'a' and 'b' of the fissure.

Patir and Cheng (op cit) also give expressions for the effect of anisotropic surface roughness.

The Reynold's number for pipes is given by:

$$Re = V \cdot D.w/ u.g \quad \ldots\ldots(21)$$

where:

Re is the Reynold's number (dimensionless),

V is the average velocity through the pipe [L/T]

D is the diameter of the pipe [L].

Jeppson (1976) describes the Darcy-Weisbach equation as "the most fundamentally sound method of computing head losses". The Darcy-Weisbach equation can be written for flowrate as:

$$Q = \{ Pi / 128 \cdot u \}.\{ D*4 \}.(dp / dl) \quad \ldots\ldots(22)$$

where:

Pi is the ratio of a circle's circumference to it's diameter.

Nikuradse (1933) described the variation in the friction factor [dimensionless], which is equivalent to Patir and Cheng's Pressure flow factor, over laminar and turbulent flow regimes for pipes of different relative roughnesses. His extensive experiments showed that flow was laminar below 'Re=2100', independently of roughness, and that in this region the friction factor was given by:

$$f = 64 / Re \quad \ldots\ldots(23)$$

where:

f is the friction factor.

In the equations given above, for flowrates in:

Darcy flow, (equation 7);

fissure flow, (equation 18); and

pipe flow, (equation 22),

the square-bracketed terms have been arranged to be of dimension [L*4]. The curly-bracketed terms are of dimension [L*2 / F.T] since they contain the inverse of the absolute viscosity. In Darcy flow, the hydraulic conductivity is the product of terms in all three brackets, (compare equations 9 and 11). For a given fluid, the hydraulic conductivity will vary as the square of the grain size (d*2) as solution of the rock proceeds; though in fact the constant 'c' varies as porosity increases, and the grain size diminishes. In porous media the grain size is usually small, so that the specific surface is large. Large volumes of material must be removed in solution to significantly change the porosity.

For fissure flow, the flowrate varies as the cube of the fissure width (h*3) multiplied by the pressure flow factor which is itself an exponential function of the fissure width. For pipe flow, the flowrate increases as the fourth power of the diameter (D*4). Accordingly pipes will grow at a faster rate than fissures, and both will grow at a much greater rate than the intrinsic permeability in a given rock. However, rocks with a large number of small fractures and a high intrinsic porosity such as Chalk may contribute material to solution by diffusion, so that fissure size only increases slowly. Rocks of low intrinsic porosity and fracture frequency will conversely show a high rate of increase in fracture permeability. Variations in the separation and width of fissures lead to rapid variations in permeability, for the same fissure

porosity.

A static model of a flow system solves Laplace's equations, which are governed by conservation of mass. A dynamic model is required for investigating the development of secondary porosity and permeability. Following an initial static solution for discrete local flowrates, flowchannels will be modified according to the flowrate and composition of the water in each channel. In the dynamic model, local flowrates are important because flows will concentrate exponentially. Local flowrates are not merely a function of the geometry of the local flow channel. As in a road network, the position and size of each flow channel in the system must be known before local flows can be predicted, Chapter 5.

The dynamic analysis of a discrete flow system depends upon it's being described as a network of nodes and arcs , or junctions and pipes, Section 1.2.4. Because a rough crack is bridged by asperities, it is suggested that it can be replaced by an equivalent pipe network. Flows can then be calculated for each pipe in the system.

1.2.3 Homogeneity and scale.

Geological phenomena are usually described by verbal and graphical means. Some can be modelled in the laboratory,using scale model theory. Scheidegger (1958) finds that most or all mathematical models of geological processes suffer from serious defects. Difficulties arise from the range of time and length scales involved; and because data must be collected at various scales and with irregular density. Usually, an homogeneous material is assumed. If anisotropy is allowed, Neumann's

principle that the solid behaves as a large centrosymmetric crystal is applied (Nye, 1957)

The hydrogeology of an area should describe the several rock types and their distribution. For the purposes of a dynamic model the solubility, porosity and intrinsic permeability of each should be known. Typically the whole would be cut by a system of fractures. Descriptions of the fracture pattern dominate the calculation of permeability. In Sections 2.2 and 7.7, two naturally occuring fracture patterns are described which are not regular. A model is required to describe discrete flows in an irregular network. Fractures from several ranges of scale can be important, so that the model is limited to describing only a small part of a natural system.

1.2.4 Nets and trees.

The integral descriptions of fissure flow summarised in Section 1.1.2 have proved very satisfactory for most groundwater flow problems. However, it was argued that integral descriptions do not form an adequate basis for the modelling of a dynamic flow system. In Chapter 2, field evidence is assembled which suggests that a pipe network constitutes a realistic model of the flow paths in a system of fractures. Two other attributes are required of a numerical model apart from a topological similarity to the natural system. It must be able to utilise computational algorithms that already exist, or that can be invented for the purpose. It must be capable of describing a sufficiently large part of the natural system, so that significant problems can be analysed.

The initial pipe network is formed by the lines of

intersection between the various fracture sets, and the lines of intersection between the fracture sets and the bedding planes. The position of the initial net with respect to the topography will determine where the inputs and outputs will be. Deo's (1974) theorem no.3-11 states that every connected graph has at least one spanning tree. A fissure flow network, contrasts with a surface stream drainage system in being 3-dimensional so that 6-fold nodes are more frequent than 3-fold nodes. Any net comprises nodes and arcs. The arcs may represent pipes, or roads, or resistors, etc..

Three main analytical techniques are available for flow net analysis. The method chosen depends upon the relationship between the potential across a single element of the network, and the flow induced in it:

In road networks and traffic flow problems, it is usually assumed that each arc has a limiting capacity associated with it. Ford and Fulkerson (1957) provide the Maximum Flow - Minimum Cut algorithm for the analysis of such problems.

In electrical resistance networks, the flow within each arc is governed by Ohm's Law. In this case, a gradient is associated with each arc which describes a linear relationship between electrical potential and current. Jennings (1977) describes alternative methods of solution using either the Node Conductance Matrix, or the Loop Resistance Matrix.

In hydraulic pipe networks, the flow within each arc bears a non-linear relationship to the drop in hydraulic head across it. The Darcy-Weisbach equation empirically describes the experimental results of Nikuradse (1933) most exactly, but cannot be solved explicitly. Jeppson (1976) describes the Newton-Raphson method of obtaining a solution iteratively. He

also gives several other methods based on approximate descriptions of Nikuradse's curves. For laminar flow at low Reynold's numbers the relationship between headloss and the flowrate in a pipe is linear. Accordingly, the Node Conductance Matrix can be used to solve for flowrates, provided that Reynold's numbers above 2100 are not involved. In this region permeability is an analogue of diffusivity. Reeves's (pers comm, 1981) method of Monte Carlo simulation of the diffusion process can then be applied to flow problems.

It will be shown in Chapter 5, that the the position of a pipe in a flownet is more important than it's initial size, in determining the flowrate through it. The positional relationship of fissures which conduct waters of different qualities, is also important in the mischungkorrosion effect, Fig 28. Consequently, a dynamic model requires a more detailed description of the fracture network than a static model. In the dynamic model, local solubilities and flowrates are important, because flowrates will concentrate exponentially into certain pipes. The rate at which a pipe increases in size will be a function of the flowrate and aggressiveness of the fluid, and the solubility of the rock. The aggressiveness of the fluid depends upon it's history. The initial concentration of carbon dioxide in water can be modified, both by gaseous diffusion, and by mixing of waters. Whilst in contact with a reactive lithology, the aggressiveness declines exponentially with time, Harrison (1973), Mercado (1972).

Much of the field and laboratory work in this thesis is background towards the design of a dynamic model of groundwater flow.

CONTENTS. PAGE.

Fig 4:

Geological environment of the study area:

a) large scale, after Kent (1974).

b) small scale, after Geological Survey 6 inch sheet.

Fig 5:

a) General view of Spaunton Moor Quarry top bench from the southeast. The length of the bench is approximately 500m east-west.

b) View down the eastern graben and over the Vale of Pickering to the south. Scale: Miss K.J.Wilkinson.

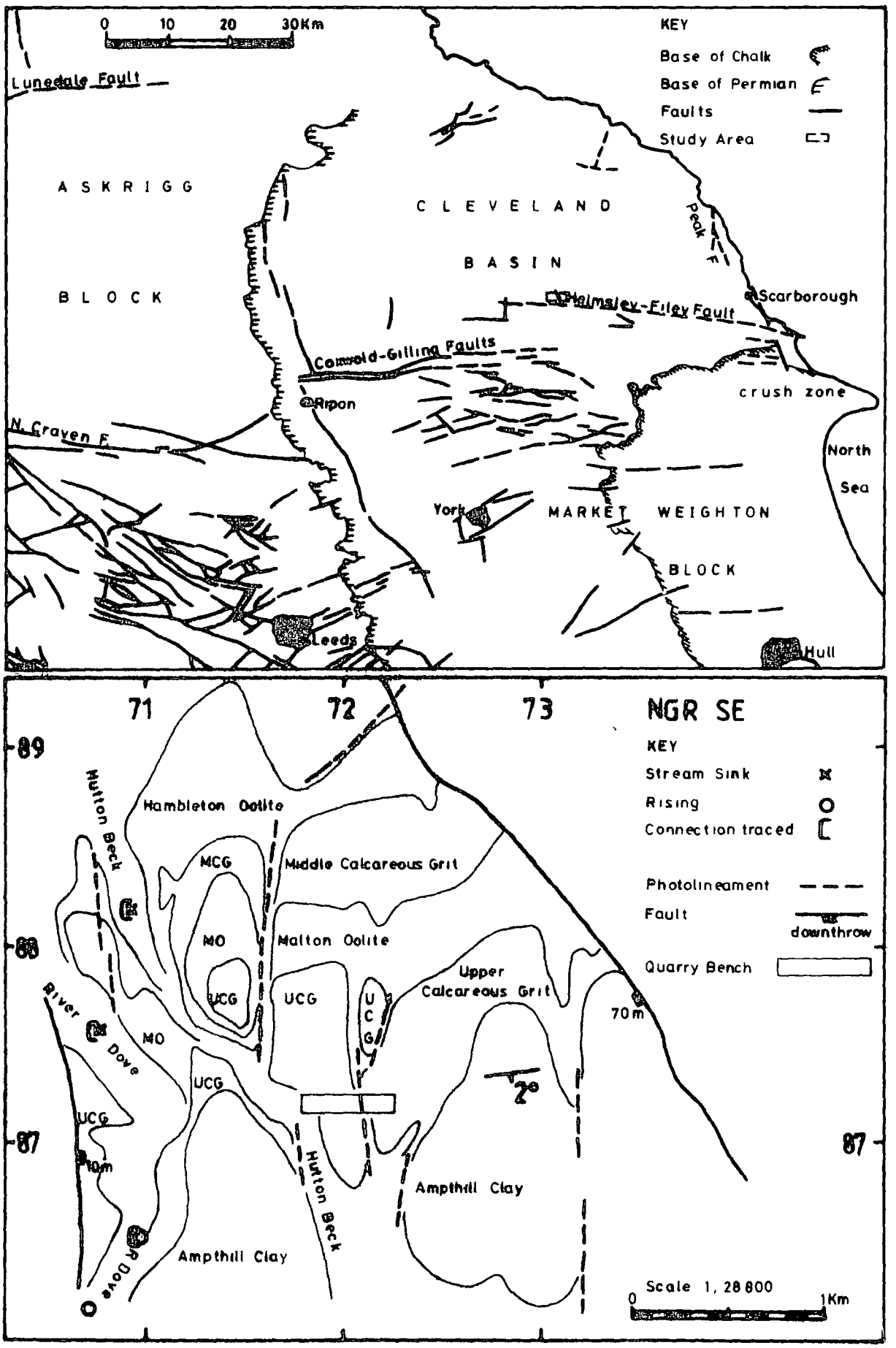
0 10 20 30Km
KEY
Base of Chalk
Base of Permian
Faults
Study Area
Lunedale Fault
ASKRIGG
BLOCK
CLEVELAND
BASIN
Peak F.
Scarborough
Helmsley-Filey Fault
Cowold-Gilling Faults
crush zone
Ripon
N. Craven F.
North
Sea
York
MARKET WEIGHTON
BLOCK
Leeds
Hull
71
72
73
NGR SE
89
88
87
KEY
Stream Sink
Rising
Connection traced
Photolineament
Fault
downthrow
Quarry Bench
Hambleton Oolite
Hutton Beck
MCG
Middle Calcareous Grit
MO
Malton Oolite
UCG
Upper
Calcareous Grit
River Dove
70m
Ampthill Clay
Scale 1, 28800
0
1Km

Fig 4

Fig 5

2.1 Fracture patterns

2.1.1 Spaunton Moor case study.

General geology.

Spaunton Moor Quarry (NGR SE 720 872) lies just north of the east-west fault system which bounds the Askrigg Block and Cleveland Basin on their southern margins, Fig 4a. The area has been studied in M.Sc. dissertations by Mierzejewski (1978), Kendrick (1979) and Dowlen (1979). Rocks from Spaunton Moor Quarry have been studied in M.Sc. theses by Jonasson (1980) and Riemer (1979). The quarry lies within the Corallian Aquifer which has been intensively studied by The Yorkshire River Authority (Reeves, 1974a and 1974b), Harrison (1973), and Reeves et al. (1978).

Wilson (1948) tabulates the Corallian Series as comprising from top to bottom:-

Upper Calcareous Grit

Osmington Oolite

Middle Calcareous Grit

Hambleton Oolite

Lower Calcareous Grit.

The Series is about 67m thick and is underlain by the Oxford Clay, and overlain by the Ampthill, and then Kimmeridge Clays. Around Kirbymoorside and Spaunton Moor Quarry, the Osmington Oolite has the local name of the Malton Oolite Coral Rag, or Malton Oolite. In the vicinity of the quarry the beds dip gently at about 2 degrees south, Fig 4b.

Photolineaments striking north-south are evident on the air photographs, but the mapped intensity of faulting is much lower within the Cleveland Basin than it is in the Vale of Pickering

to the south. The Vale of Pickering is underlain by Kimmeridge Clay and occupied by faults of overall east-west strike. Springs from the Corallian Aquifer are often close to the boundary with the Kimmeridge Clay, (Mierzejewski, 1978). Groundwater tracing by Kendrick (1979) suggests that the minor north-south trending faults within the Corallian Aquifer control the flow within it, Fig 4b.

Site description

Spaunton Moor Quarry is operated by Hargreaves Quarries Limited. It was chosen for detailed study because fault controlled solutional development is well displayed, and the exposure is excellent. Viewed from the southeast, Fig 5a, the top bed of the Malton Oolite can be seen cleared of the weathered Upper Calcareous Grit which forms the overburden of the quarry, Fig 4b. A thin but distinctively blue-weathering laminar bed of the Upper Calcareous Grit marks the base of the overburden. The Upper Calcareous Grit has been classified as overburden because it has become deeply weathered and easily bull-dozed, in complete contrast to the Malton Oolite which is drilled, blasted and broken with a drop-weight before being crushed and screened to roadstone mesh sizes. The sequence of beds at the top of the Malton Oolite is also quite distinctive with a blocky micrite being particularly regular in development, Fig 6. (The uppermost shelly limestone varies in thickness, and the topmost bed appears to thin out away from the centre of the quarry as an original depositional feature). This means that a survey of the quarry's top bench is a structural map of the top of the Malton Oolite. Figure 7 presents in summary the fault pattern from the detailed survey

Fig 6:

Stereo pair looking north, to show the stratigraphy in Spaunton Moor Quarry. Part of the western worked face with 30m tape for scale.

Fig 7:

a) Summary map of faults on Spaunton Moor Quarry top bench.

b) Section showing faults in relation to the western syncline and the eastern anticline.

Fig 8:

Tachymetric survey of the top bench, Spaunton Moor Quarry, near Pickering, Yorkshire.


Shelly Limestone
Micrite
Oolitic and shelly Limestones.
30m tape

Fig 6

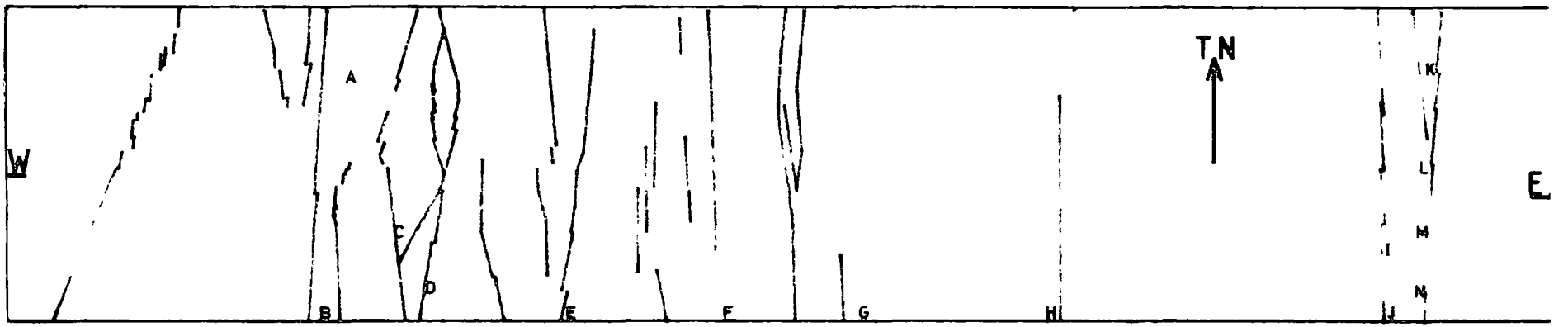

Faults of Spaunton Moor Quarry, top bench, in plan (ABOVE) and section (BELOW)

An arbitrary datum is used, and the survey is not tied in to the National Grid

Solutional features are labelled A to N

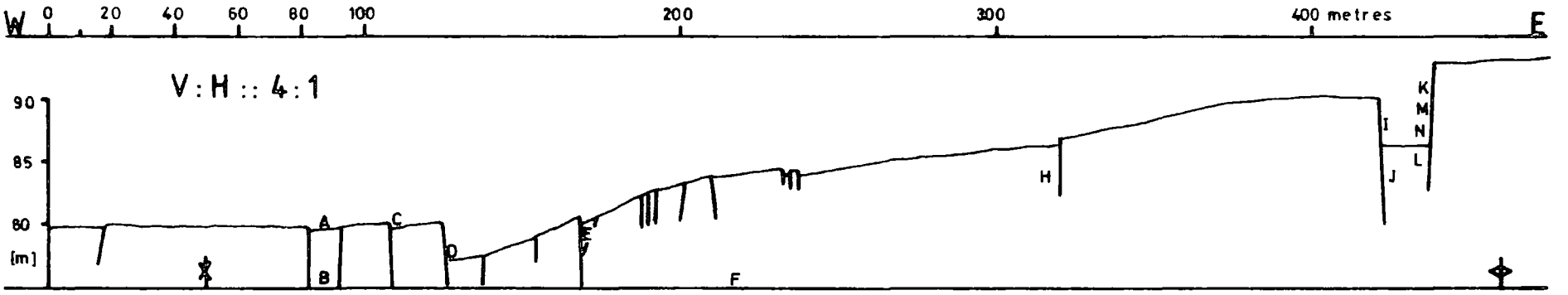

Tachymetric Survey by R I Kendrick & A R Westerman, 30,6 - 1,7,1979.

of Fig 8. Ideally, such maps should be contoured to define the structural lows and highs. Contouring routines to handle break points (or fault lines) are not yet generally available and have limitations of applicability, Grassie (pers comm). Cubic splines may be fitted with break points on a rectangular grid; but at Spaunton Moor break points die out laterally and have varied orientations.

The general view of Fig 5a shows that superimposed on the general southerly dip are cross folds with axes trending north-south. The fault pattern associated with the western synclinal area differs markedly from that in the eastern anticlinal part of the quarry. Figure 5b shows the keystone graben of subparallel faults in the anticline. These are the largest faults in the quarry and have been a nuisance throughout it's life. The many small caves developed within the downthrown keystone, are infilled with overburden. The faults associated with the western syncline are far more numerous, and not only vary in throw over a short distance but ramify in plan. Figure 9 shows a view to the west across the faults of the syncline and Fig 10 shows the central members of this fault set viewed from the north.

In Fig 10, the relationship between solutional activity and the fault pattern is clearly seen. The cavern entrance labelled 'C' in Fig 7 is seen at the foot of a fault scarp, and the mud cracked site of a small pond can be seen in a structural low formed by the scissors faults. The unfaulted Malton Oolite appears as an aquiclude to the percolating waters descending through the Upper Calcareous Grit. Fault blocks form underground catchments so that percolation from a relatively large area is directed towards the lowest point in the fault

Fig 9:

Stereo pair looking west, to show scissors faults at the western end of the top bench, Spaunton Moor Quarry. Scale: 5m ranging pole, and Ford Transit van.

Fig 10:

Stereo pair and sketch looking south across the area in Fig 9, to show scissors faults and the position of solutional features. Scale: vehicle tracks.

Fig 11:

a) Stereo pair looking south-southeasterly at the western flanking face, Spaunton Moor Quarry, to show long wavelength waviness of major joint surfaces.

b) Stereo pair looking north-northeastly at the eastern fault face of the eastern anticlinal graben in Spaunton Moor Quarry. Note en echelons joints in fault zone. Scale: Mr. H.Jonasson with plumb bob.

Fig

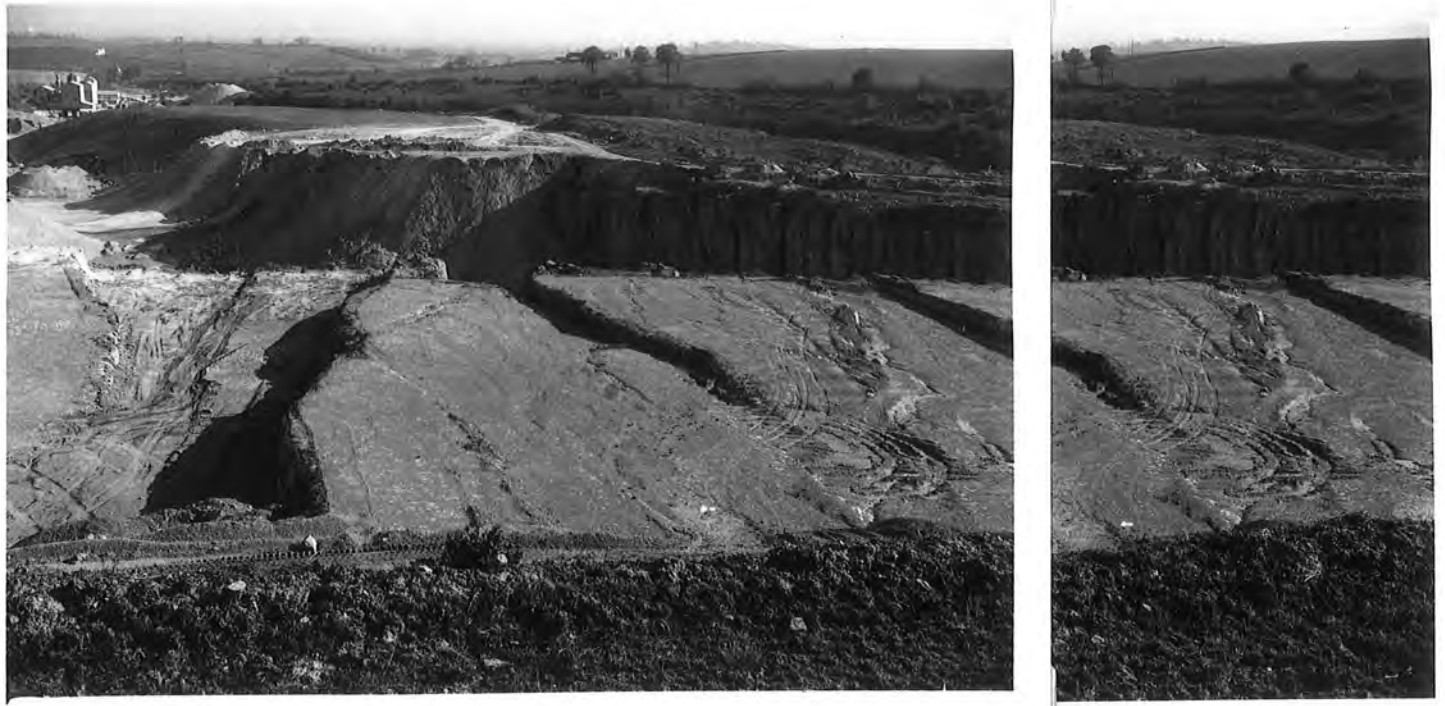

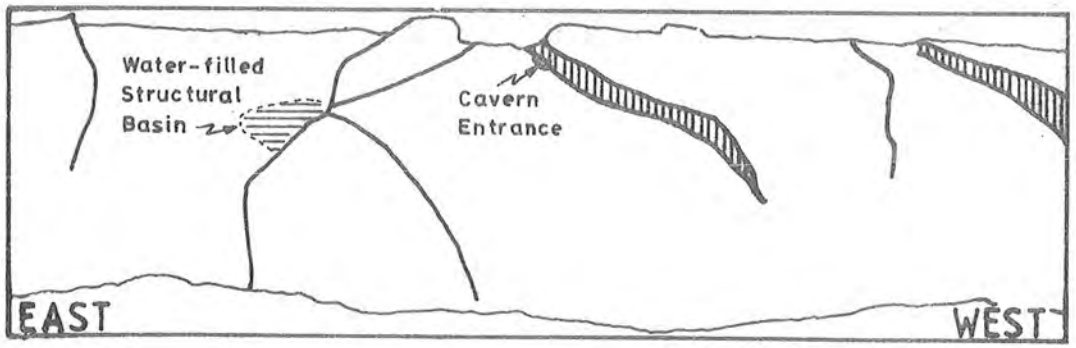
Water-filled
Structural
Basin
Cavern
Entrance
EAST
WEST

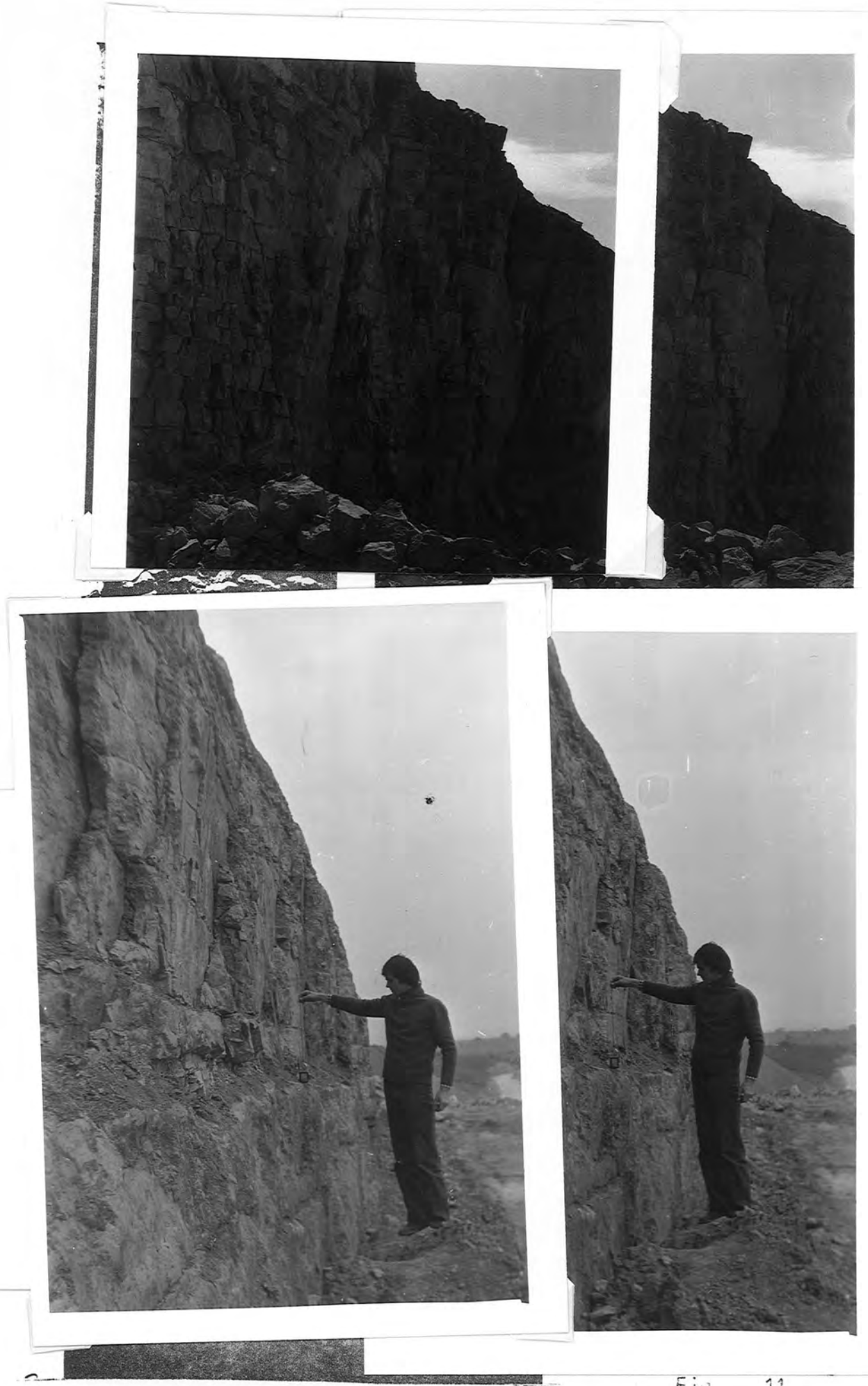

Fig 11

system. The lowermost point here corresponds to a fault having one of the larger throws in the system. It will be argued that there is a proportional relationship between the throw on a fault and it's hydraulic conductivity.

Figures 11 and 6 illustrate the generally vertical dip of the faults and joints in the quarry. The large surface area seen in Fig 11a shows the joint surfaces to be wavey rather than planar. Clearly the shearing of such surfaces will create a room problem and a relationship between throw and transmissivity may be expected. The surface may be said to have large scale and long wavelength surface roughness. Shear of a rough surface creates a fissure, Hoek and Bray (1975, p85).

Stress analysis.

Comparing Figures 11b and 7a illustrates the relationship between faults and joints at Spaunton Moor. Joints are used by the faults en echelons. In the eastern, anticlinal part of the quarry, the obtuse angle subtended by the two joint sets used by conjugate pairs of faults is greater than that subtended by the faults. In the central and synclinal part of the quarry the two obtuse angles are about the same. In the west of the quarry, corresponding perhaps to the axis of the syncline, (Fig 7b), the angle subtended by the joint sets is less than that subtended by the later faults.

Near localities 'C' and 'D' in Fig 5a sections of fault faces can be seen with horizontal slickensides. Coupled with the vertical dips and the angles subtended between conjugate sets, this suggests that all the fractures at Spaunton Moor were first formed in shear. Since the dihedral angle of the joints is more uniform than that of the faults, it seems that

the joints formed before the folds, and that the faults formed later as the folds grew and locally modified the stress field.

A theory describing the energy balance criteria during the propagation of an elliptical crack, was first given by Griffith (1920). Griffith's crack theory has been extended to predict a parabolic Mohr envelope for tensile stresses, and a linear envelope for compressive stresses, Brace (1960), compare Fig 88. The parabolic envelope takes the form:-

$$T^{*2} + 4Sn^{*2} - 4Sn.St = 0 \quad \ldots\ldots\ldots\ldots\ldots\ldots (24)$$

where:

T is the maximum shear stress along the plane at failure,

St is the tensile strength of the rock, i.e. the intercept of the Mohr envelope on the normal stress axis, and

Sn is the stress normal to the shear plane at failure.

The linear envelope has the familiar form of the Mohr-Coulomb failure criterion:-

$$T = 2.St + Sn.\tan(Phi) \quad \ldots\ldots\ldots\ldots\ldots\ldots (25)$$

where:

Phi is the angle of internal friction, and

2.St=C, is the cohesion of the rock, or the intercept of the Mohr envelope on the shear stress axis.

Muelhberger (1960) has shown that the parabolic shape of the tensile portion of the Mohr envelope can be used to relate tension gashes and conjugate shear sets subtending an obtuse angle near to 180 degrees. A plastic yeild criterion is proposed in Section 7.6.4, Westerman and Holland (submitted). This closes the Mohr envelope at the high pressure end, and is

based on thermodynamic considerations comparable to those which form the basis of Griffith's crack theory. Systems of brittle failure planes can then be related to plastic failures in rock, and a coherent body of theory applied to the study of fracture patterns, Fig 88.

Hydraulic conductivity.

From these observations it can be seen that the normal stresses to the failure surfaces in jointing and faulting can be worked out from the Mohr envelope. The throw on the fracture surfaces is known and can be related to fault length. In Chapter 3 the surface roughness of geological fractures will be discussed. It will be shown that an improved knowledge of the surface roughness characteristics of rocks would allow the primary hydraulic conductivities of individual geological fractures to be calculated. In Appendix 7.6 a comparison is made with the Inverian fracture pattern affecting Lewisian rocks near Loch Torridon. There the primary fracture pattern is infilled with basic dykes, emplaced at hydrostatic stress. Groundwater will also exert an hydrostatic stress in a tectonically active sedimentary basin, though it's head is less due to a lower density. The main relevance of the Torridon study is that conjugate shear bounded blocks can be seen to have rotated slightly, and that the rotational couple was an important mechanism in controlling the distribution of primary fracture permeability. Finite-Element models are useful in calculating the stress trajectories in such a system.

Figure 12 shows that the ratio of throw to length in the map areas of Figs 4b and 7a appears to have a maximum of 1:30. Anderson (1954) found a similar ratio of 1:50 for faults in the

Fig 12:

Log. log. plot of throw vs. length for faults in the vicinity of Spaunton Moor Quarry, North Yorkshire.

Fig 13:

Plot of projected elevations of the top of the Malton Oolite across the eastern anticlinal graben, Spaunton Moor Quarry.

Fig 14:

Diagram to illustrate the dependence of primary fracture hydraulic conductivity upon surface roughness and shear displacement across a normal fault.

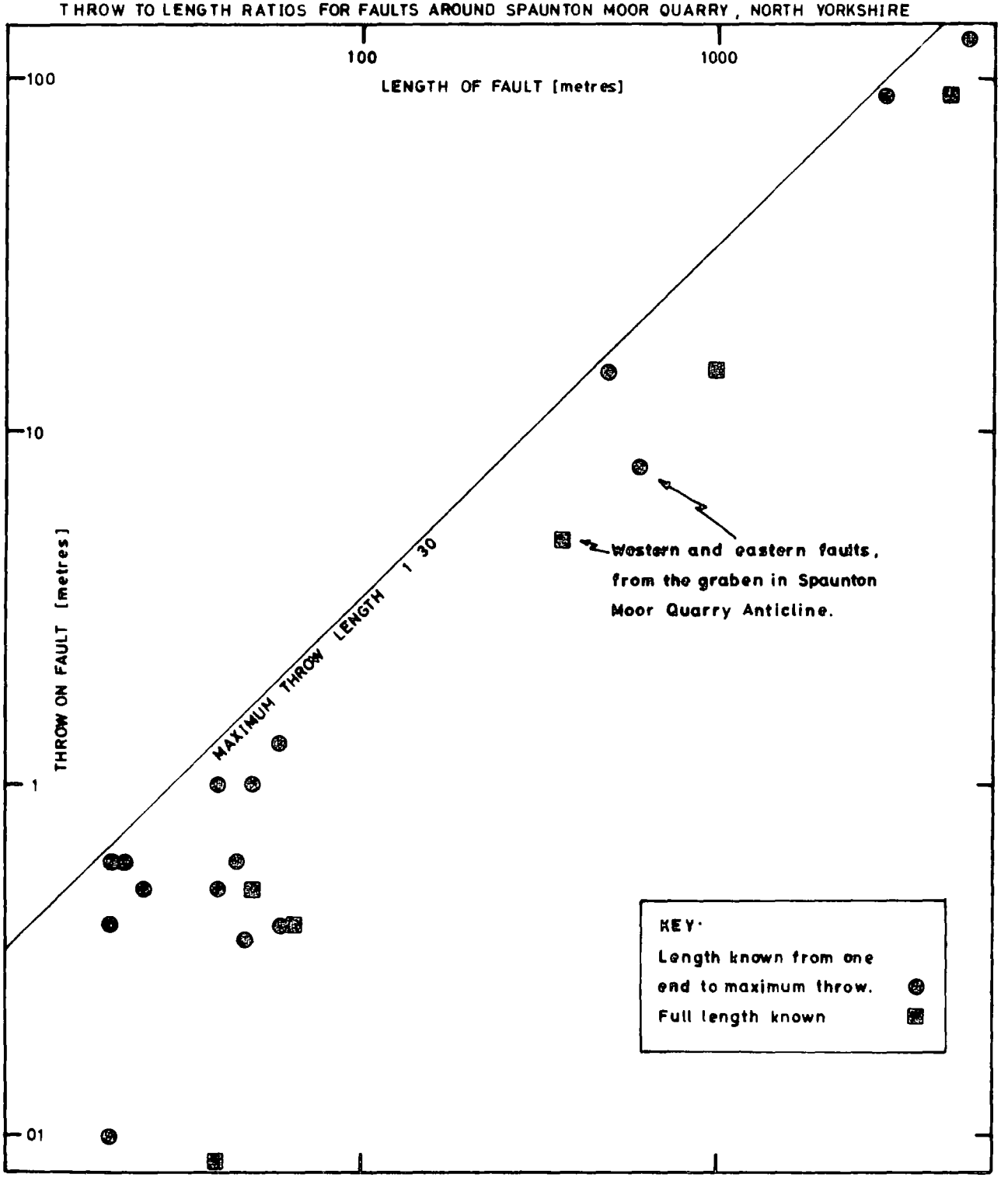
THROW TO LENGTH RATIOS FOR FAULTS AROUND SPAUNTON MOOR QUARRY, NORTH YORKSHIRE
100
1000
LENGTH OF FAULT [metres]
100
10
1
01
THROW ON FAULT [metres]
MAXIMUM THROW LENGTH 1 30
Western and eastern faults, from the graben in Spaunton Moor Quarry Anticline.
KEY:
Length known from one end to maximum throw.
Full length known

Fig 12

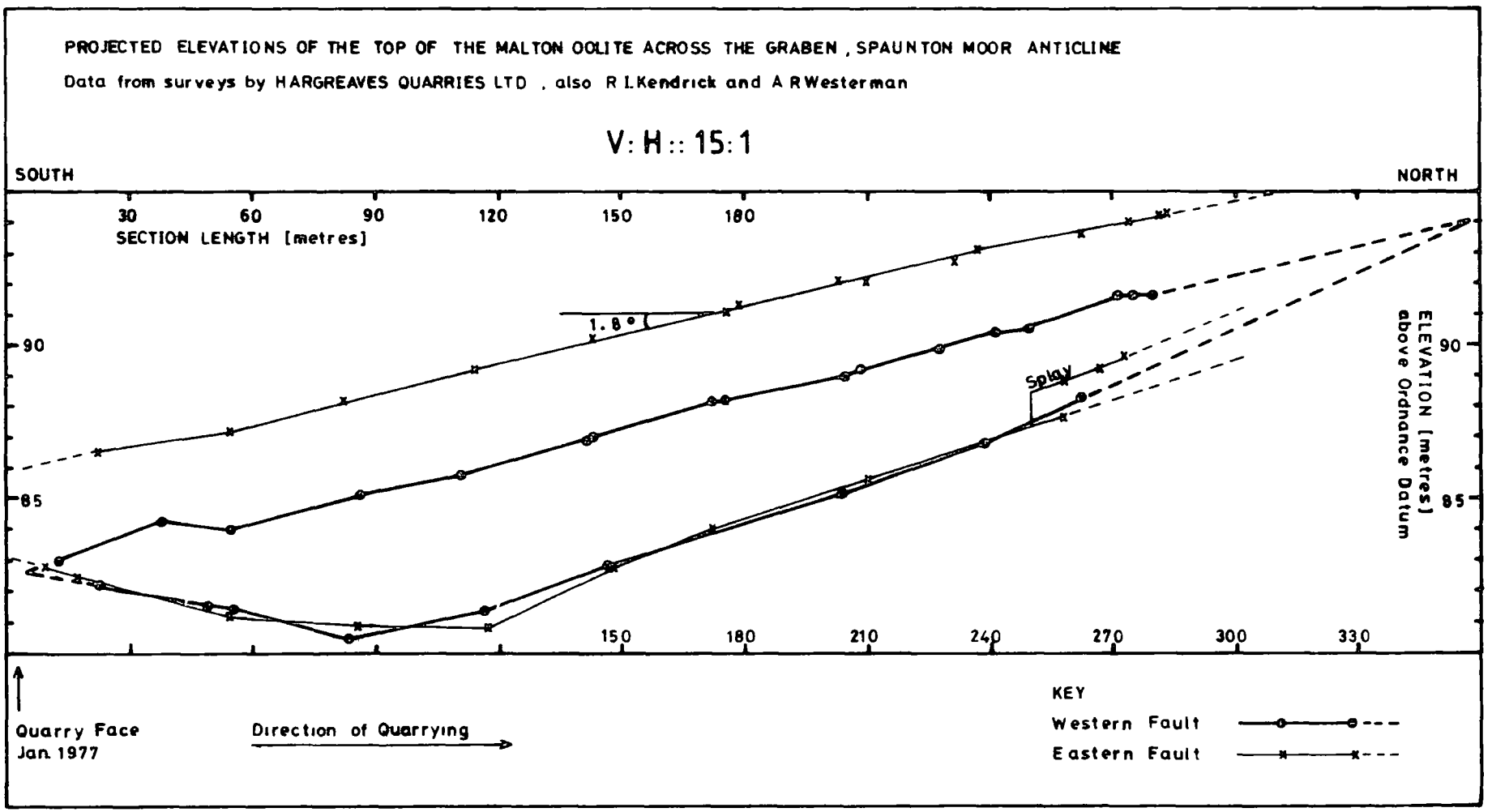
PROJECTED ELEVATIONS OF THE TOP OF THE MALTON OOLITE ACROSS THE GRABEN, SPAUNTON MOOR ANTICLINE
Data from surveys by HARGREAVES QUARRIES LTD. also R I Kendrick and A R Westerman
V: H :: 15: 1
SOUTH
NORTH
30
60
90
120
150
180
SECTION LENGTH [metres]
1.8°
90
85
Splay
ELEVATION [metres] above Ordnance Datum
150
180
210
240
270
300
330
Quarry Face Jan. 1977
Direction of Quarrying
KEY
Western Fault
Eastern Fault

Fig. 13

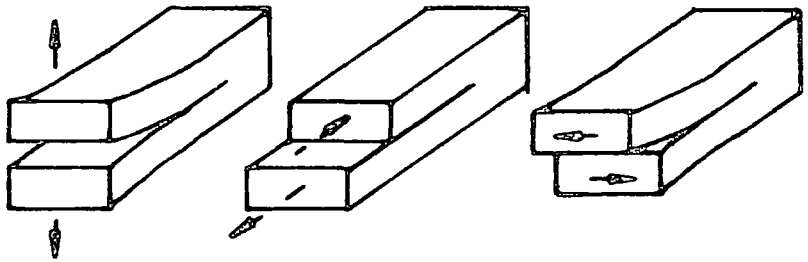

Three modes of fracture , after Lawn and Wilshaw ,(1975)

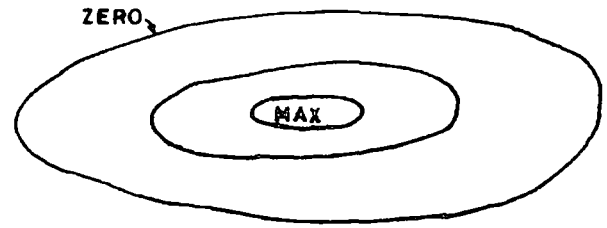

Distribution of throw within a 'penny-shaped' Griffith's crack like fault

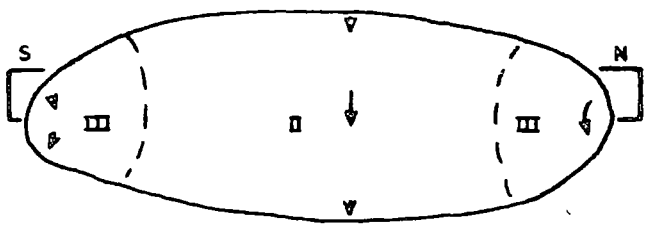

Equivalent of section fig 12.

Distribution of main fracture mode within a 'normal' fault

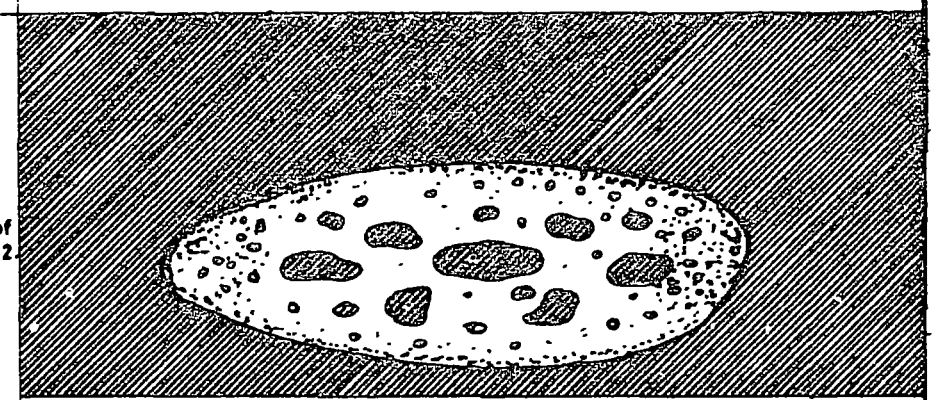

Distribution of apophysis contact across a sheared , rough Griffith's crack - like fault

Diagrams to illustrate the dependence of primary fracture transmissivity upon surface roughness and shear across a normal fault

Fig 14

Scottish coalfields. Because the graben faults at Spaunton Moor have been a problem to the quarrying operation, heights of the top of the Malton Oolite, near to the graben, have been recorded in some detail on the quarry surveys. These are superimposed in Fig 13 which shows a profile of both faults. Most of the faults in Spaunton Moor Quarry have well developed subvertical slickensides. If they die out vertically as well as laterally, they would appear as large penny-shaped Griffith's cracks, Fig 14.

Lawn and Wilshaw (1975) classify failure modes as:-

I - opening mode.

II - sliding mode.

III - tearing mode.

As the faults die out horizontally the two surfaces have rotated relative to each other by approximately arctan(1/30) or 2 degrees, and the failure has been in mode III. The central area of the faults have failed in the sliding mode II. It is possible that slickensides on several overlapping joints within the fault zone have varying angles of dip because they were formed at different stages during the growth of the fault; and so with different components of tearing and shearing failure. Lawn and Wilshaw (op cit, pp 60-61) show that the stress intensity factor for a plane crack with an elliptical border " will always be greatest where the elliptical crack front intersects the minor axis. The implication here is that a crack free from interference from outer boundaries will tend to extend on a circular front ". It is not known whether the faults at Spaunton Moor have elliptical fronts as depicted in Fig 14, due to interference from bedding planes; or whether they are circular: but this is of importance if a full

Fig 15:

a) View looking east at the eastern fault face of the eastern anticlinal graben in Spaunton Moor Quarry. Note that solutional features alternate with fault gouge. Scale: Miss K.J.Wilkinson.

b) Detail from the far right of Fig 15a. Note slickensides.

Fig 16:

Stereo pair of detail from Fig 15b. Note: slickensides; marked solution of fault/joint and fault/bedding plane intersections; and early stage, peripheral anastomosing solution tubes with dominant development parallel to the slickensides. Scale: ruler in 6 inch (15.24 cm) sections.

Fig 17:

Stereo pair and sketch looking north at the western worked face near the quarry floor at Spaunton Moor Quarry. Note the development of solution tubes within a block between conjugate normal faults.

Fig 15

Fig 16

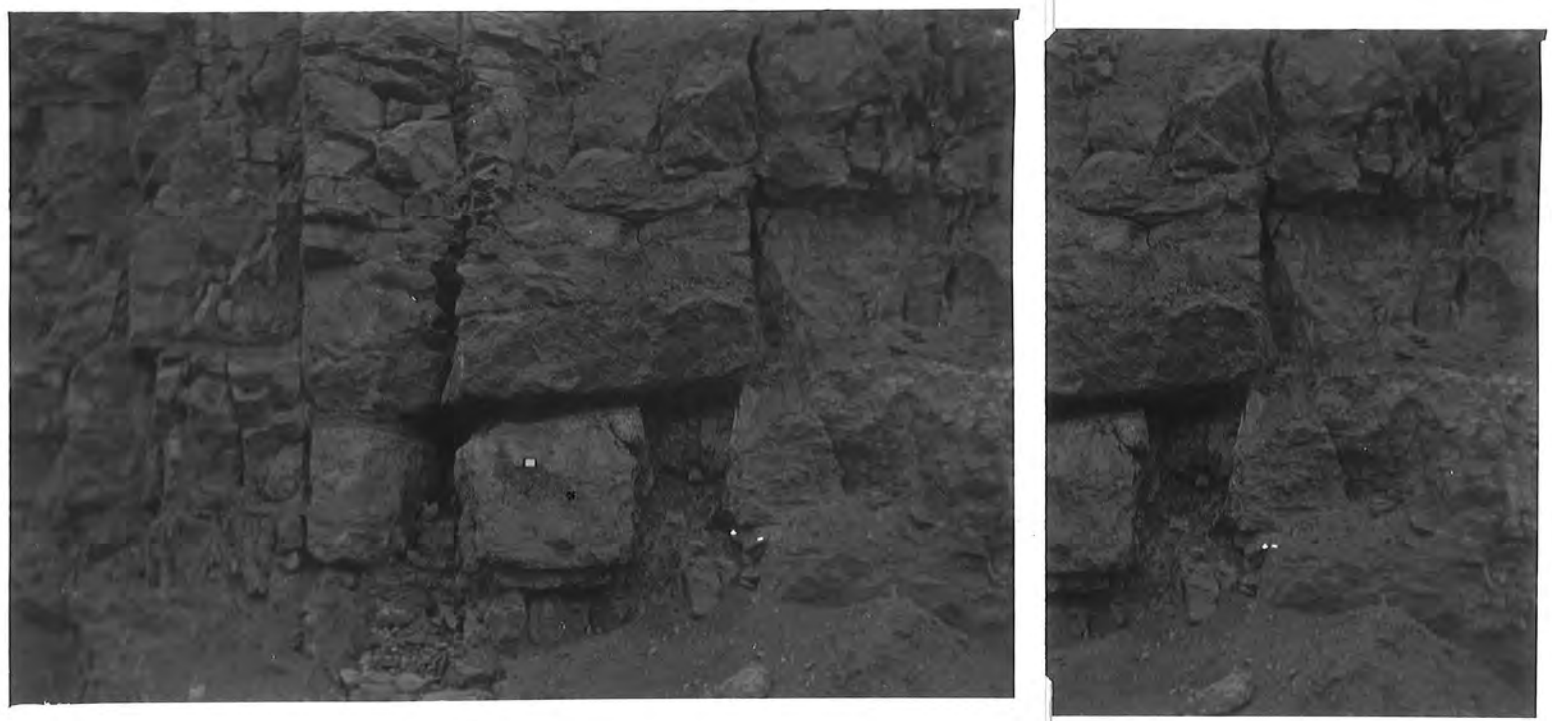

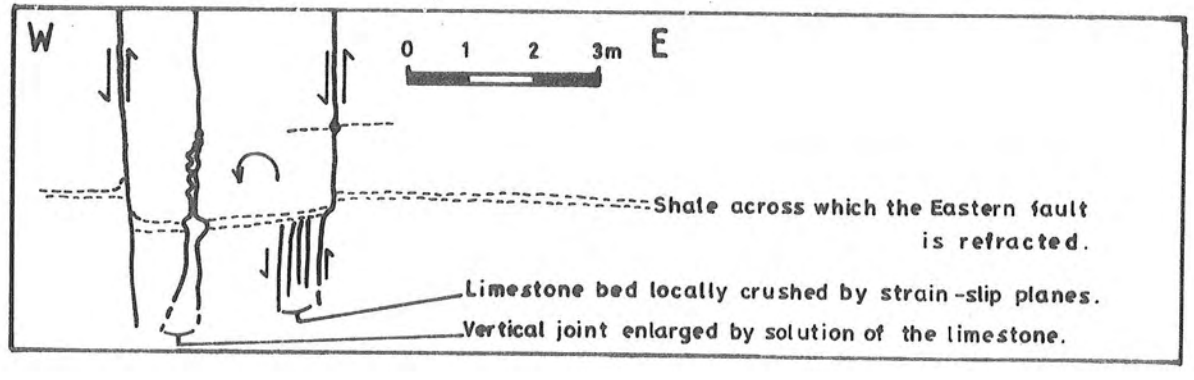
W
0 1 2 3m
E
Shale across which the Eastern fault is refracted.
Limestone bed locally crushed by strain-slip planes.
Vertical joint enlarged by solution of the limestone.

Fig 17

description of primary fracture permeability is to be known. This work could best be extended with access to coal mining records, where throws have been recorded in several sections through the surface of a single fault.

Figures 11b, 15 and 16 illustrate the nature of the fault scarp on the eastern of the two graben faults at Spaunton Moor Quarry. Because the faults postdate the joints, as discussed above, individual joint slices have been rotated by movement on the fault. At a distance from the fault plane, the earlier joints show no detectable shear displacement. As they approach the fault plane at a small angle tearing mode III failure has ocurred during faulting even where the overall movement on the fault plane is in the sliding mode II. The joint surfaces are also seen to be refracted across shale beds, creating lithologically controlled roughness of the failure surface.

Structural features noted along the fault plane fall into two groups, Fig 15:

Zones of strong slickensiding and fault gouge produced by the tearing of joint slices are strongly developed.

Zones of dog tooth spar and of later solutional activity occur between them.

It is thought that the dog tooth spar is an early feature which developed soon after faulting by pressure-solution and redeposition. Solutional development of cross joints and the development of flowstone - seen on the western graben fault - is a feature of the vadose zone. The alternation between these two groups of structures along the fault plane, is not regular. It does suggest that the shear of a surface with large scale waviness, as seen in Fig 11a, leads to patches of asperity contact surrounded by net-like zones of open fissure.

Consequently, calculations based upon statistical descriptions of fracture surfaces are expected to lead to a good description of primary hydraulic conductivities.

It was found that roughness profiles could be collected from fracture surfaces in the field by Rawl-bolting on about 2m length of angle iron as a reference straight-edge and offering up a profile gauge (Vitrex, regd. design A921942) to the surface of the rock, so that a linked sequence of small profiles could be traced. A more elegant method of gathering roughness data in the field would be to use a surveyor's camera to take stereo photographs. Photogrammetric methods have been developed for contouring and digitising surfaces directly from such stereo photographs. The small scale roughness would be studied by conventional profiling machines operating on hand specimens of the surface, Section 3.2.2.

Figure 17 shows a further mechanism for the formation of primary fissure permeability. Here the failure is in the opening mode I, and is caused by the rotation of conjugate fault bounded block due to the refraction of one of the fault planes across a lensoidal shale bed.

Solutional features.

The location of observed solutional features is shown in Fig 7. Locality 'A' is exceptional in that there is solutional widening of a joint having no vertical displacement. However it is along strike from locality 'B' which is decribed above and in Fig 17, and so may also result from opening mode I failure between conjugate normal faults. Localities 'C', 'D', and 'E' are enterable cavities developed on fault planes. Locality 'H' has also developed in joints opened in mode I where flexure has

occurred on the downthrown side of a normal fault. Sites 'I' to 'L' are described above and lie within the graben, the keystone or downthrown block of which is occupied by man-sized potholes on a spacing of about 20m. Figures 15 and 16 show that solution has progressed most rapidly where cross joints intersect the fault plane so that a network of small pipes develops within the zone affected by solution. Solutional activity tapers rapidly downwards. Locality 'F' is the only observed solutional development in an east-west striking minor joint. As with 'B', the solutional pipe is horizontal in development and lies only 1.5m above the present water-table, at the quarry floor.

Dowlen (1979) studied the seismic velocity anisotropy of the Spaunton Moor Quarry top bench. Anisotropy was predicted from the strongly directional fault and joint pattern shown in Fig 18. Weathering of the joint block faces has lead to an increase in porosity and a reduction in Young's modulus. Figure 19 summarises Dowlen's (op cit), and other field results which are discussed in more detail in Appendix 7.5. The heterogeneity of the fault and joint pattern and of subsequent weathering and solutional development can be seen. The array 'Farrthree' shows 160% seismic anisotropy, compared with a previously recorded maximum of about 20% found in the Carboniferous limestone of the North of England, Bamford and Nunn (1979). In the array 'DBARRAY' attenuation results were gained using a dropweight and the gain levels of the 'Bison' recorder. However it was not possible to calculate useable values of hydraulic conductivity from these results, although in theory there are relationships between fracture porosity, intrinsic porosity, and seismic velocity and attenuation, Tourenq et al, (1971).

The promise of the seismic refraction results is that

Fig 18:

Joint rose diagram for the western worked face of Spaunton Moor Quarry, North Yorkshire, after G.R.Dowlen (1979).

Fig 19:

Map and diagram summarising the results of radial seismic velocity arrays on Spaunton Moor Quarry top bench. Most results are from Dowlen (1979).

JOINT ROSE DIAGRAM FOR THE FACE OF SPAUNTON MOOR QUARRY, NORTH YORKSHIRE
After G R Dowlen, 1979

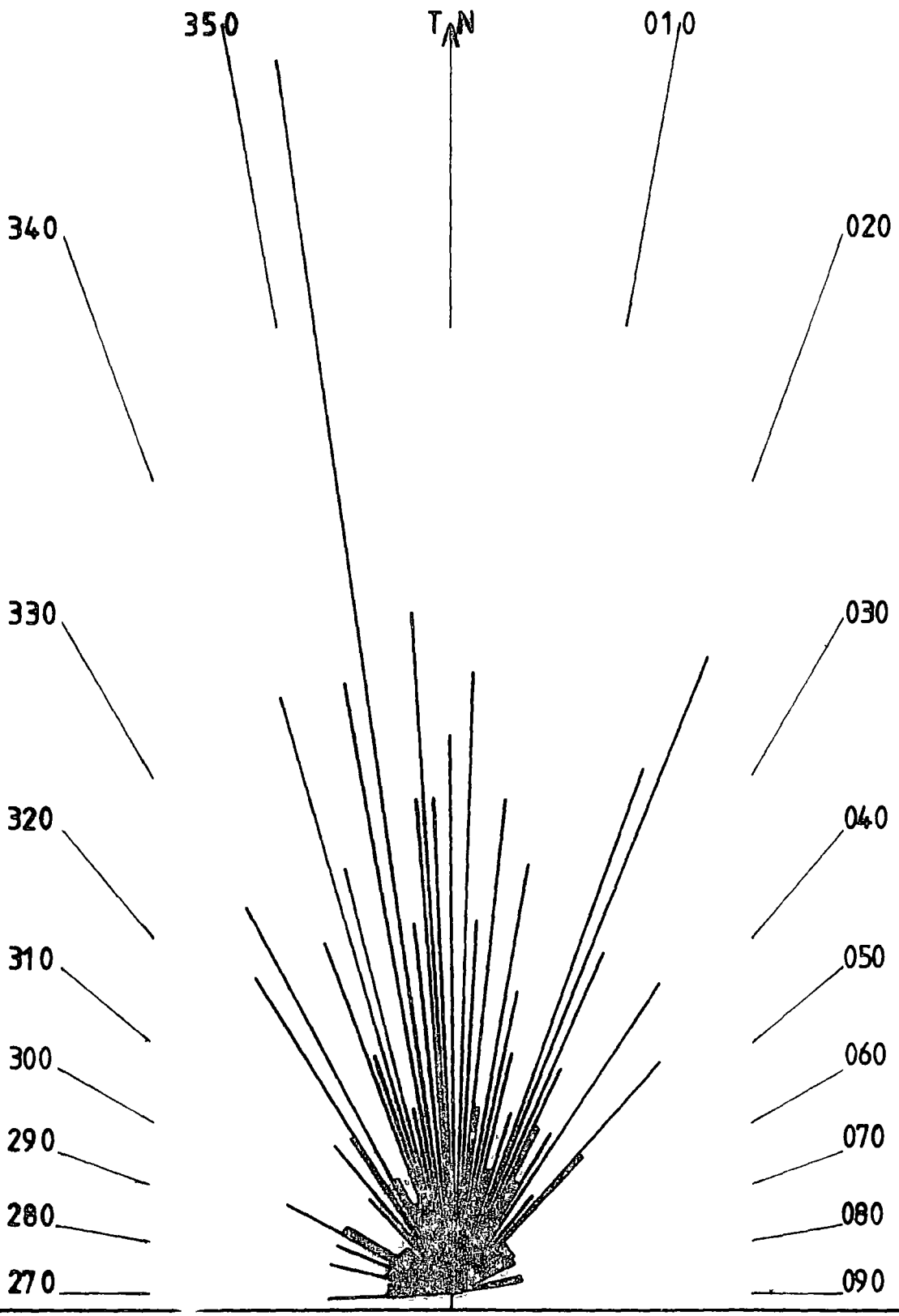

Fig 18

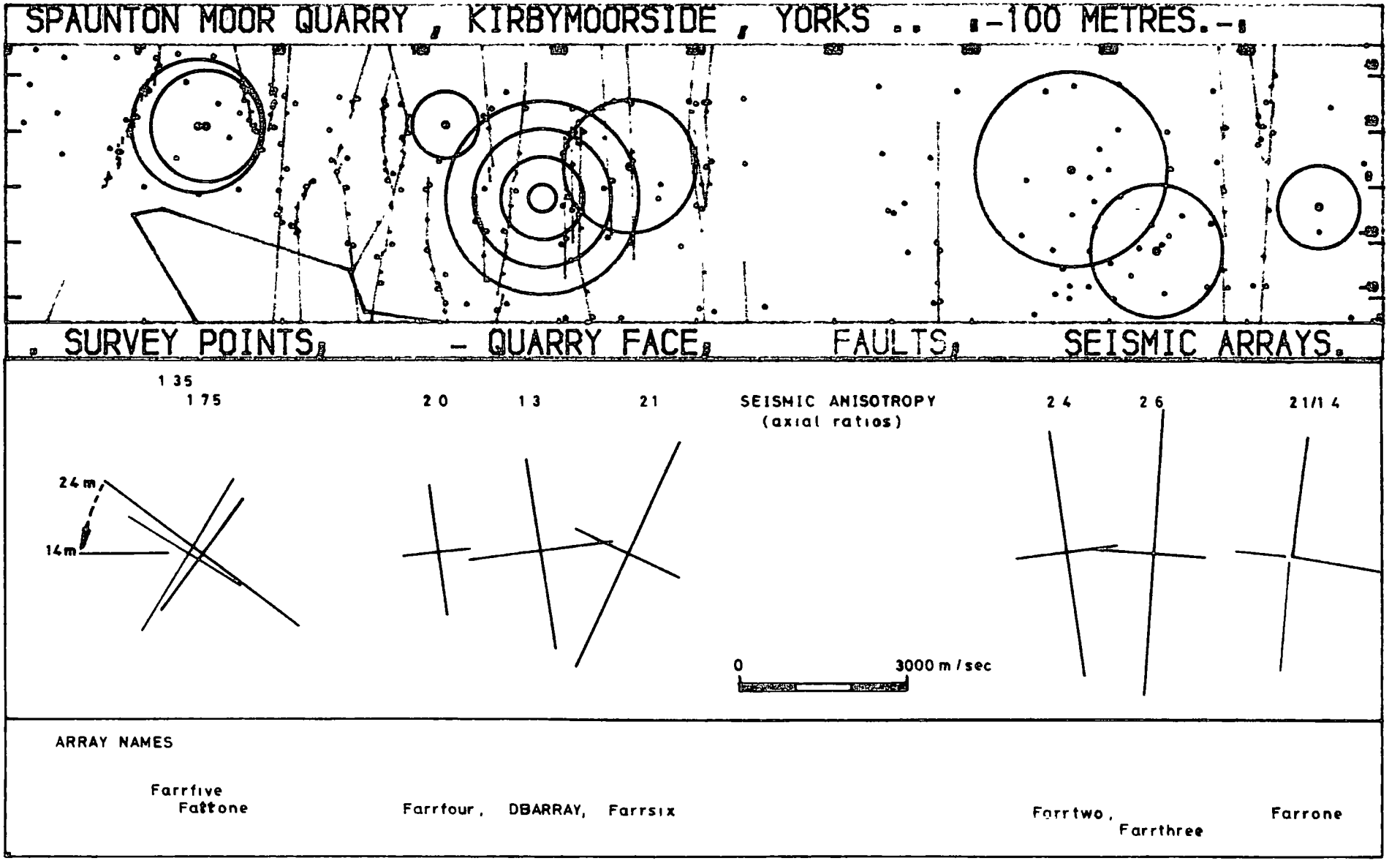
SPAUNTON MOOR QUARRY , KIRBYMOORSIDE , YORKS .. .-100 METRES.-.
. SURVEY POINTS, - QUARRY FACE, FAULTS, SEISMIC ARRAYS.
1 35
1 75
2 0
1 3
21
SEISMIC ANISOTROPY
(axial ratios)
2 4
2 6
21/1 4
24 m
14m
0
3000 m / sec
ARRAY NAMES
Farrfive
Farrone
Farrfour, DBARRAY, Farrsix
Farrtwo, Farrthree
Farrone

Fig 19

heterogeneity of development, and principal orientations of fissures can be well illustrated. Backus (1965) have shown that the method is applicable at great depths. Thus, when the development of secondary porosity and permeability associated with Mississippi Valley type orebodies, hydrothermal areas, and fracture controlled oil reservoirs is of interest, the method could be considered as a useful tool. In particular, when casing is being perforated using explosives in one of the many wells from an oil production platform, downhole geophones placed in the other wells could gather data on the anisotropy of fissure permeability within the most critical zone of the reservoir. The amount of cable required to log several holes at once will prevent this from being done on offshore installations; but the method should be considered for site investigation purposes in nuclear waste disposal. Large volumes of rock can be tested for heterogeneity, at depths where the probability of intersecting a vertical fissure in a borehole is low.

2.2 Speleology.

A great deal is known about the mechanisms controlling cave formation and Ford and Cullinford (eds. 1976) provide a thorough summary. Waltham (1971, 1974) has discussed morphology, and has pointed out the over-riding influence of climate and lithology on the rate of cavern development in different parts of the world. The solutional features described at Spaunton Moor Quarry are very well displayed in relation to the fracture pattern and should be placed in perspective. Similarly, the observations made by speleologists can be compared with the solutional mechanisms generating fracture controlled orebodies of the Mississippi Valley type.

Solutional development at Spaunton Moor is predominantly vertical. Horizontal pipes are observed near the quarry floor just above the present water table. The extent to which fissures are dissolved away tapers markedly downwards. Pitty (1968) shows from calcium carbonate concentrations, that most most of the limestone dissolved is removed from the surface since "more limestone is removed" from the southern Pennines "in a single year than the volume of known cave systems". Mercado (1972) has shown that the rate of increase of calcium carbonate concentration in groundwater decreases exponentially with time; Harrison (1973) has demonstrated the same time dependancy in the laboratory. The resurgence near Bogg Hall at NGR (SE 710 865), Figs 4b and 20b, represents the flow system developed in a horizontal plane at or below the water table. An impression is gained of percolating waters rapidly losing their chemical aggression on first contact with limestone. The large size of cave systems such as that represented by the Bogg Hall

Fig 20:

a) View looking west at the cliff section below Kirkdale Ford (NGR SE 6795 8525). Anastomosing solution tubes seen in section. Scale: 1 foot, (30.5 cm).

b) View looking east at Bogg Hall resurgence. (NGR SE 710 865).

Fig 21:

Survey of Kirkdale cave after G.Stevens and P.F.Ryder (1973) and photograph looking east at Kirkdale Quarry cliff section (NGR SE 677 856).

Fig 22:

Stereo pair of bedding plane anastomoses seen in plan looking upwards at the cliff section below Kirkdale Ford, near the view of Fig 20a.

Fig 20

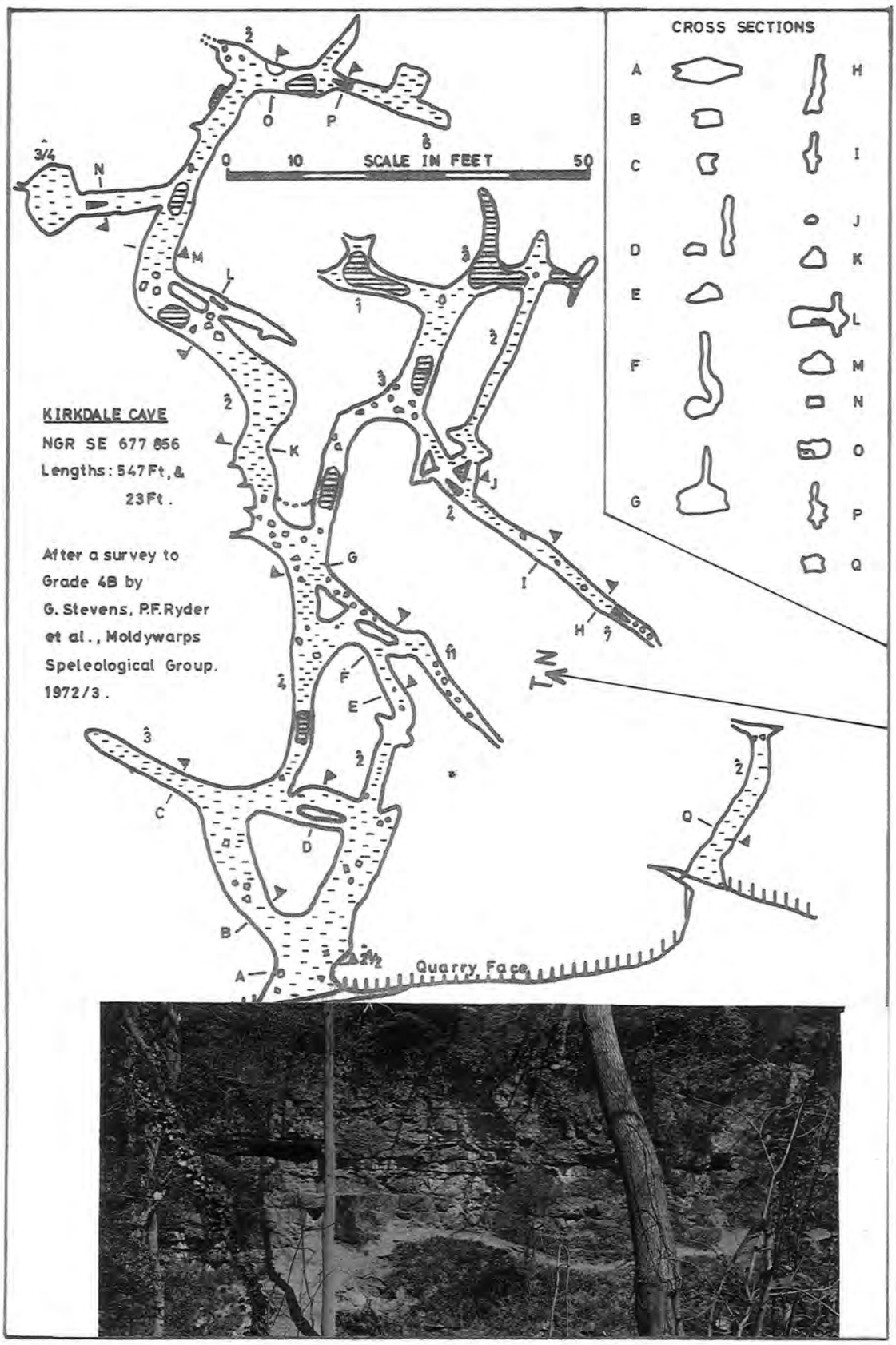
CROSS SECTIONS
A
B
C
D
E
F
G
H
I
J
K
L
M
N
O
P
Q
0 10 SCALE IN FEET 50
KIRKDALE CAVE
NGR SE 677 856
Lengths: 547Ft, &
23Ft.
After a survey to
Grade 4B by
G. Stevens, P.F. Ryder
et al., Moldywarps
Speleological Group.
1972/3.
Quarry Face
N

Fig 21

Fig 22

resurgence may be explained by either the great volume of coalescing flows, or by the mechanism of mischungkorrosion, first pointed out by Bogli (1971). Probably both factors contribute.

Four kilometers west of the Spaunton Moor area, and also in the Corallian, lies the Kirkdale Cave, Fig 21, and the cliff section of Hodge Beck, Figs 20a and 22. Kirkdale Cave is very similar in appearance to Bogg Hall although it is now dry. A survey by the Moldywarps Speleological Group shows the strong joint control and maze-like pattern of the cave system, Ryder and Stevens (1973). It has developed along one particular bed and has not cut down significantly into the bed below.

Cross-correlation of storm pulses recorded at gauging stations above and below Bogg Hall Resurgence by Kendrick (1979) resulted in smooth correlograms with a long correlation length (days). The single-shot fluorescein tracer between the sinks in Hutton Beck and Bogg Hall also emerged as a diffuse peak. Ashton (1965, 1966) gives a method of digitising flood pulses and dye peaks that have been convolved by passing through cave systems having several loops. He presents a way of deconvolving the record and solving for the topology of a flooded system. It seems that, in the Corallian aquifer, a multiplicity of overlapping peaks prevents analysis at the resolution available from tracing techniques. The caves appear to be confined to single beds, providing a baseflow through the phreatic zone, near to the water table.

Of the Upper Limestone or Malton Oolite seen in Spaunton Moor Quarry and at Kirkdale Cave, Fox-Strangeways (1881) wrote '' In a quarry near the roadside at Kirkdale are the remains of the famous Kirkdale Cave in which were found the bones of no

less than 27 species of Mammalia and Birds. The cave, which has now been mostly quarried away, is situated about half way up the face of the quarry along an irregular line formed at the junction of the Chemnitzia limestones with the more earthy limestones above; the upper surface of the Chemnitzia limestones throughout this region is very hummocky, and is known to the quarrymen of Pickering and Hutton as "hilly and holey;" on this irregular surface repose the more earthy limestones above with soft marly partings which are easily worked away and form the cave line throughout the district. It is probable that at this horizon in the limestone are formed the numerous "swallows" or underground channels, in which most of the streams in the neighbourhood lose a part or all of their water, and if the denudation of these valleys was carried 100 feet lower, it is probable that a fine series of caves would be exposed in this region.''

Atkinson and Smith (in Ford and Cullingford, eds 1976) consider that lithological differences between limestones are of minor importance compared to other chemical factors; but Ford (1971) describes the avoidance of reef limestones in Derbyshire by stream valleys. In the Hodge Beck section below Kirkdale Ford the concentration of solutional features within a few beds is clearly seen, Mierzejewski (1978). Furthermore, the smaller solution tubes are invariably developed upwards from the bedding plane, and not downwards, Fig 20a.

By comparison with solution tubes, or anastomoses, described from other areas it seems that the earliest stages of cave formation occur in the base of beds selected by jointing and solubility. Doughty (1968) has shown that limestone beds are often better sorted and exhibit a higher joint frequency at the

base. Porosity increases with sorting. Also, by comparison with the cave systems of the Great Scar Carboniferous Limestone it would seem that thin bedding and alternating lithologies have prevented the second stage of cave development in the Malton Oolite. Large cave systems in the Carboniferous limestone appear to have formed as solution has cut down into underlying beds, leaving the first formed solution tubes in the roof. Little is known of solution tubes in the Chalk, though they are known to exist. Large (2m diameter) caverns with high hydraulic conductivities have been intersected by water-supply boreholes in East Yorkshire (Chadha, 1979 pers comm) and the South of England. There is an example of sea cliffs intersecting a chalk cave in France. The high frequency of small joints in the chalk probably lead to the collapse of pipes in the vadose zone, so that they are active in the phreatic zone but rarely observed.

Efforts were made to find examples of early solution tubes; called "anastomoses" by Ewers (1966). Commonly they appear to have been destroyed by roof falls in cave systems that are now large enough to enter. Where the cave system is phreatic they (should they have existed) will have been removed by radial growth of the solution tube, Lange (1959 and 1968).

Figure 22 shows that some joint control has been exercised. Figure 23, from Yapley Quarry, adjacent to the Bogg Hall resurgence shows anastomoses intermediate in size between an enterable cave and those of Fig 22. Figure 24 shows a similar, rare example from the Great Scar limestone of West Yorkshire. Joint control is clearly evinced here by parallelism between the solution tubes and lines of later stalagtites.

Figures 25, 26, and 27 all come from the entrance chamber of Ogof Ffynon Ddu II cave in the Carboniferous limestone of South

Fig 23:

Stereo pair of a section through bedding plane anastomoses at Yapley Quarry (NGR SE 710 868), near Bogg Hall resurgence. Scale: 6 inches (15.24cm).

Fig 24:

Stereo pair of bedding plane anastomoses with minor joints marked by lines of stalactites. The roof of Straw Chamber, County Pot, Easegill System (NGR SD 673 818). Scale: Mr. D.Chester.

Fig 25:

Oblique and close up photographs, with sketch, to show bedding plane anastomoses in plan looking upwards. Entrance to Ogof Ffynon Ddu II cave, South Wales, (NGR SN 8637 1590). Scale: 6 inch (15.24 cm).

Fig 26:

Stereo pair of bedding plane anastomoses seen in plan looking upwards. Adjacent to location of Fig 25. Note the rough bedding plane surface.

Fig 27:

Stereo pair of bedding plane anastomoses and rough bedding plane surface seen in plan looking upwards. Adjacent to the location of Figs 25 and 26. Note the vertical joint surface left by the fallen block which revealed this texture.

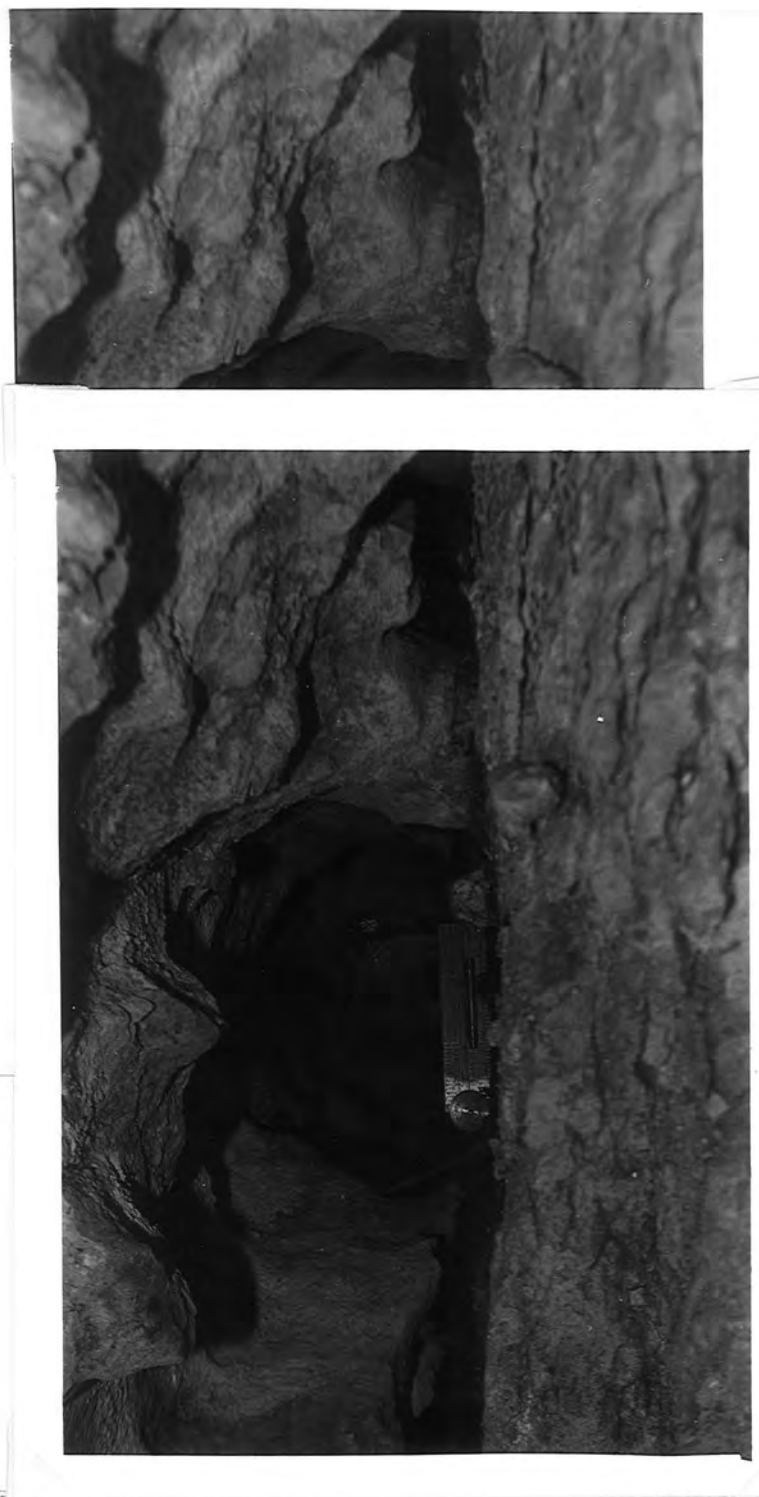

Fig 23

Fig 24

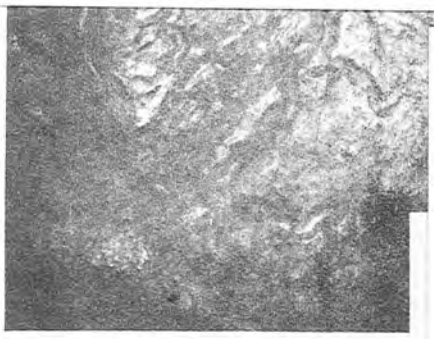

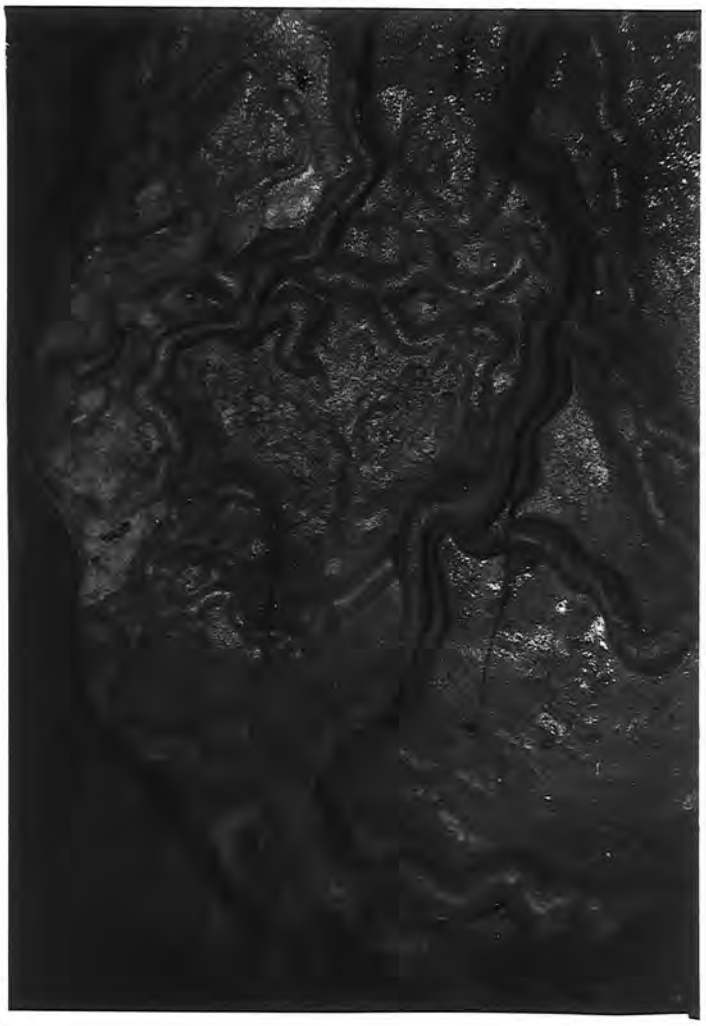

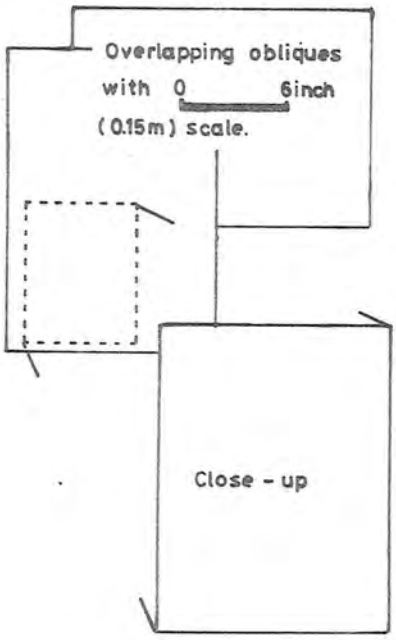

Fig 25

Fig 26

Fig 27

Wales, whence the author was directed by Mr. A.C. Waltham. The survey of Ogof Ffynon Ddu (South Wales Caving Club, undated) - a very large system - shows strong joint control on a large (Km) scale; some areas have a similar plan to pillar and stall mine workings. In Fig 25 some joint control still appears in evidence. Figures 16, 26 and 27 show smaller and presumably earlier developments of anastomoses. They appear to be entirely random and to die out laterally into the rough surface of an undissolved bedding plane. Figure 16 is rare in that anastomosing solution tubes do not appear to have been described from fault surfaces before. They are particularly well developed parallel to the slickensides, so that the anisotropy of the surface roughness appears to have been a controlling factor. Consequently, it would seem that joint control of solution tube development is a later feature of solutional development. The earliest, rarely preserved stages appear to be random. It is proposed that slight movement across bedding and joint planes creates fissures by shearing the rough surfaces. Stress concentration at joint block corners leads to comminution of the joint/joint and joint/bedding intersections. This would be comparable to the distribution of primary fractures described in Appendix 7.6, though on a much smaller and less obvious scale.

A calculation of primary fracture hydraulic conductivity based upon descriptions of surface roughness, distance sheared, and normal load should therefore give an accurate value for primary fracture permeability. Once the comminuted corners of joint/joint intersections have been dissolved away, the pipe like tubes so formed will have the fastest flow fronts. Fluid at the centre of intersecting fissures of equal size is at

least square-root(2) as far from the nearest rock as the fluid at the centre of either individual fissure.

Cave systems are being described on increasingly large scales; particularly as interconnections are found between known systems, and exploration proceeds by diving and water tracing. On a scale of 3-10 kilometers cave systems appear particularly pipe-like with cross sections of 5-10 meters, see surveys presented by Waltham et al (1980) and Brooks et al (1974, 1976). The vadose zone open to most explorationists often presents a slot-like section due to subaerial downcutting and roof collapse, but phreatic systems are notable for their tubular cross-section and lack of gravitational control.

The mischungkorrosion effect proposed by Bogli (1971) may also favour the development of pipe-like solutional forms at fissure intersections. Figure 28a illustrates the mechanism whereby two saturated solutions become undersaturated on mixing due to the nonlinearity of limestone solubility with respect to carbon dioxide concentration. Provided that the cave system is large enough to receive waters from sources with different carbon dioxide concentrations, cavern development can occur where waters mix after travelling through undeveloped primary fissures. Mixing will occur at fissure intersections, and the high hydraulic conductivity pipes so formed, will have a different orientation, in general, to those of the confluent flowlines. This may also apply to the meeting of meteoric and connate waters and in hydrothermal systems. The mischungkorrosion effect depends simply on a nonlinear solubility curve, and it has since been extended to include many common-ion effects, e.g. Picknett and Stenner (1978). Thus not only must the carbon dioxide concentration of surface waters be known over the last

DIAGRAM AFTER PICKNETT ET AL (1976) TO ILLUSTRATE THE MISCHUNGKORROSION EFFECT.

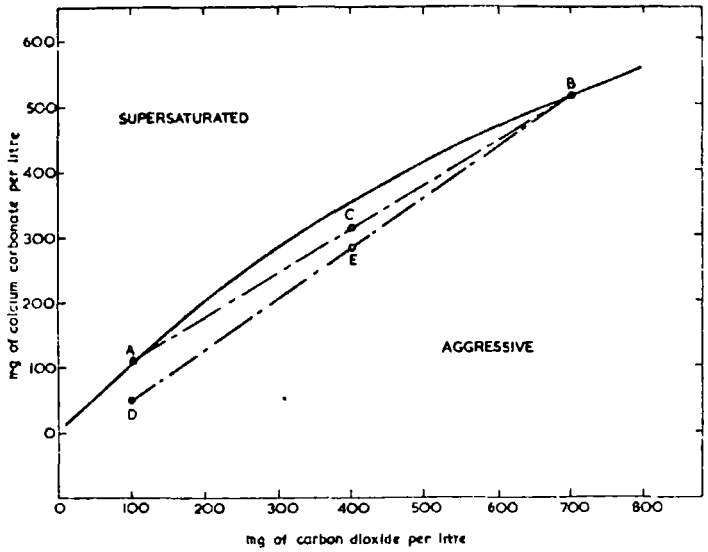

Mischungskorrosion effect. The solid curve shows the solubility of calcium carbonate (calcite) at 10°C with respect to the total carbon dioxide in solution. The mixing of two saturated solutions A and B results in increased aggressiveness as at C

DIAGRAM TO ILLUSTRATE THE LOCALISATION OF MISCHUNKORROSION-BASED AGGRESSIVENESS NEAR FISSURE INTERSECTIONS

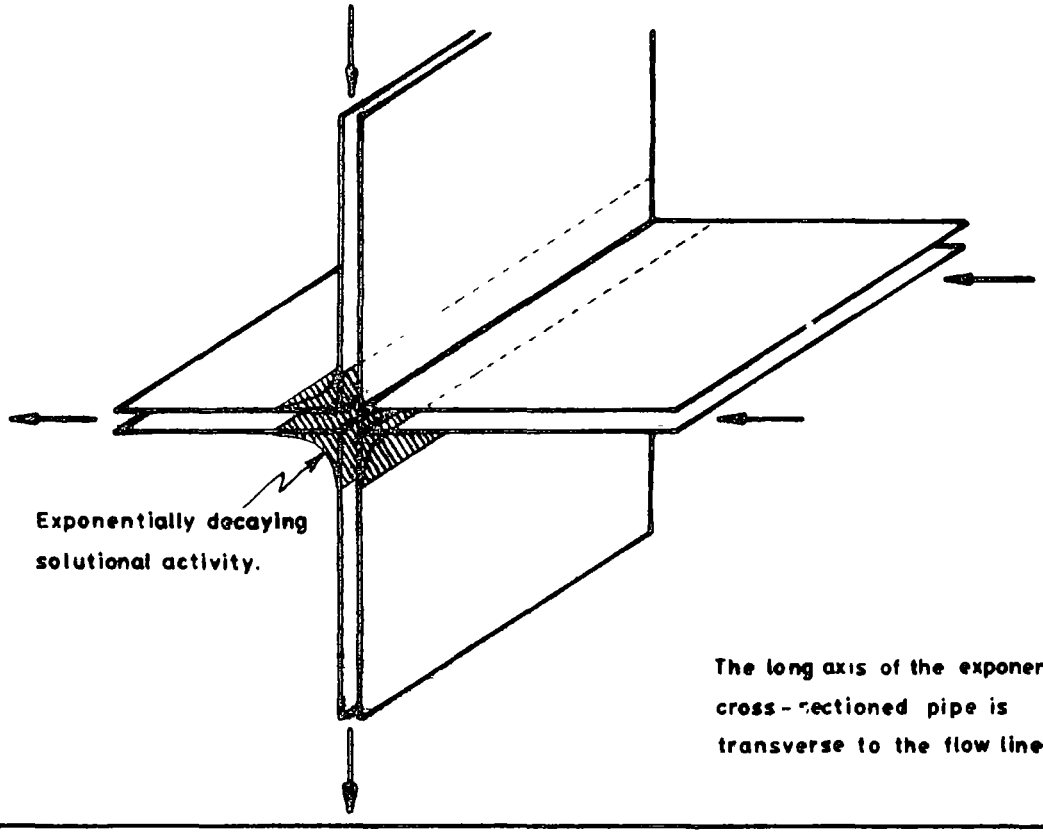

Fig 28

10,000 years, but the chemical effect on the groundwater of all the lithologies present must be traced throughout the flownet before an accurate description of chemical aggressiveness could be made for the system.

It is also clear that at an early stage of development, the flownet comprises a very large number of small tubes. The number can be reduced for the purposes of analysis by using the principal of "equivalent pipes", Jeppson (1976), so that only pipes joining six-fold nodes are considered. The pipes formed at the intersection of minor joints with another surface join three or four-fold nodes only. However solution tube numbers cannot be further reduced, since position within a spanning tree could be as important as initial size in deciding future growth-rate. Even with these provisos, too little is known about the detailed fracture pattern of any area to allow the development of a realistic predictive flow model.

Lange (op cit) and Mowat (1962) have described progressive changes of shape in theory, in the field, and in the laboratory. In purely solutional erosion, centres of curvature for the cavern walls are constant for concave surfaces, and migrate outwards along the bisectrix for sharp convexities. Solutional histories are not back-calculatable in the general case since surrounded blocks drop out to create space that could have been formed by several sequences. One must therefore know the primary hydraulic conductivities of all the fissures from structural geological, and other independent considerations. The effect of Lange's description of erosional processes is the same as that of the Minkowski Sausage used to smooth out a class of non-differentiable curves studied by Wiener, and described in Mandelbrot (1977).

2.3 Summary.

Anastomosing solution tubes are described from a fault surface as well as from bedding planes. It seems that they are controlled by the character of the fissure formed between two, initially matched, sheared, rough surfaces. As the size of individual solution tubes increases, the number of tubes through which the majority of the flow is transmitted decreases. Three stages of development can be recognised, each dominated by solution tubes of a different type:

1) The earliest stage. A large number of solution tubes, most of which are randomly disposed anastomoses, is controlled by the roughness characteristics of the fault, joint, and bedding plane fissures.

2) The intermediate stage. A smaller number of solution tubes, most of which are linear anastomoses, is controlled by the intersection lines between minor joints and major joints, faults, and bedding planes.

3) The final stage. Relatively few, large solution tubes are controlled by the intersection lines between major joints and faults and bedding planes.

Underground catchments can be controlled by the fault pattern, each fault block forming a drainage area. Large faults are fed by such catchments on their downthrown side. Faults may be considered as large Griffith's cracks with a distribution of surface roughness and shear which results in a maximum fissure hydraulic conductivity at the lowest point of the underground catchment.

CONTENTS. PAGE.

3.1 Intrinsic Porosity.

3.1.1 Relevance.

In general, changes in permeability will be mainly controlled by the solution of wallrock, and the enlargement of existing fissures; but changes in bulk porosity may also be controlled by the leaching of matrix from the rock mass. The leaching of matrix from joint blocks is observed to occur in the Oolitic limestones of the North York Moors, and the changing character of the wallrock may be expected to affect the rate of growth of the fissure.

Karstic landforms are described from rocks such as: granites; the Roraima Formation conglomerates, grits and sandstones; as well as from limestones and evaporites. Under appropriate conditions, internal and external erosion of rock masses of most lithological types is possible by solution. Yet, in the limited lithological and geographical ranges of the limestones of the North of England, the rate of chemical erosion, the landform produced, the response of water-supply boreholes drilled in them to pumping, and their (theoretical) classification as oil reservoir rocks is diverse.

Lithological controls of solubility such as geochemistry and mineralogy are well researched, but only in recent years has a rapid method of determining the porosity at varying suction pressure (pF), or effective pore diameter been applied to rocks, Jones and Hurt (1978). The Building Research Establishment have shown that microporosity - i.e. the porosity determined when only pores less than 5 microns in diameter are saturated - is the main variable in determining the resistance of building stone to chemical attack, as well as to disruption

of the fabric by the crystallisation of ice or weathering products.

Solution tubes are demonstrably more common in particular beds of the Corallian rocks of the North York Moors. The width of the tubes often varies with position in an apparently uniform bed, Fig 20a. Microporosity could be a relatively unexplored key to the understanding of the large variation in the susceptibility of limestones to chemical attack.

Doughty (1968) has shown that coarse grained limestones and shelly limestones have higher joint densities than carbonate mudstones. He states that "bed thickness does not control densities" of jointing, whereas Ladeira and Price (1981) find a relationship between bed thickness and joint frequency. Reeves (1977) and Gaida et al (1973) have shown the general decrease in porosity with geologic age. The Yorkshire limestone types compare as:

Carboniferous; low joint density, low porosity (0-2%), thickly bedded, large cave systems with several cycles of interglacial development;

Jurassic; higher joint density, moderate porosity (5%), thinly bedded, small cave systems with one cycle of development;

Cretaceous; very high joint density, high porosity (30%), thickly bedded, cave systems stable in the phreatic zone only and less well developed than in Jurassic limestones.

Rocks with a high porosity seem to develop a higher joint density, being mechanically weaker.

Both a high joint density and a high intrinsic porosity result in percolating waters becoming rapidly saturated and in

flow being diffuse, almost Darcyan. With low joint density and low intrinsic porosity, flow is distinctly non-Darcyan and all solution within the aquifer leads to fissure widening. Doughty (op cit) has shown that the base of limestone beds tend to be better sorted than the tops. The base of a bed will consequently tend to have a higher porosity and a higher joint frequency, with joints dying out upwards in the bed, compare Section 2.2 and Fig 29b.

3.1.2 Work done.

In the Malton Oolite, oolites, micrites, and shelly limestones occur. Primary intrinsic porosities are of the order of 5%. Secondary intrinsic porosity increases hyperbolically in the weathered margins towards a thin powdery surface layer. The fresh rock is blue-grey but the weathered margins are yellowish, Fig 29. In Fig 29b minor joints can be seen terminating within the bed. This is frequently observed in the micrites at Spaunton Moor but has not been observed in the shelly limestones or oolites. This may be due to varying strength characteristics within an apparently uniform bed or it may be a beam bending phenomenon: the micrites occur at the top of the Malton Oolite, Fig 6, and the Quarry represents a section from syncline to anticline through the limb of a fold of 1 kilometer wavelength, Figs 5a and 7b.

Riemer (1979) has shown the usefulness of the NCB cone indenter for detailing the rock strength characteristics of thin weathered margins. His results on porosity variations through the weathered margin correlate well with the point hardness profile and have a hyperbolic distribution, showing that weathering is by the diffusion of soluble rock materials

Fig 29:

Photographs of lithologies from Spaunton Moor Quarry, North Yorkshire, to show the yellow weathering margins of the joint blocks. Scale: transparent ruler marked in inches and cm.

a) Shelly limestone,

b) Micritic limestone with terminating cracks.

Fig 29

towards the fissure. In rocks that comprise a soluble matrix around an insoluble skeleton of grains this process would limit the development of fissure porosity. Mechanical erosion is required to detatch the insoluble residue from the fissure wall and remove it from the system.

A falling-head gas method based on the Ruska Gas Permeameter was developed for testing the permeability of these low porosity limestones, it is described in Appendix 7.1. Shelly limestones show considerable anisotropy when the axes of accurately cut cubes are tested separately, but they also show great heterogeneity.

Swanson (1979) has described the injection of porous rocks with Wood's metal. His technique was modified using a high pressure cell and the pore space down to 8 microns diameter was stereoscopically photographed under the scanning electron microscope, (SEM), Appendix 7.2. Patsoules (pers com) further modified the method by using resin and found Chalk pore sizes down to 0.1 microns diameter. He describes pore coordination numbers of about 16 for the Chalk of Flamborough Head, East Yorkshire. Similar values were found for the Corallian shelly limestone from Hovingham Quarry at NGR (SE 678 748), Fig 59b. The coordination number is characteristic of packing, not grain size. Surface roughness is well displayed in SEM photographs of pore space. Morrow (1975) has discussed the influence of pore surface roughness on petroleum recovery. Within the diffusively weathering margin of a joint block, both pore surface roughness and microporosity increase the internal surface area, and so reduce the growth rate of fissure porosity.

3.1.3 Pore Span Distribution.

In Fig 2, and Section 1.2.1, Norton and Knapp's (1977) division of porosity into: flow porosity, diffusion porosity and residual porosity was illustrated. Clearly specimen size is of importance since residual porosity and diffusion porosity are defined in terms of connectedness with respect to the test specimen or joint block surface. The Kobe method was used for porosity determinations in the Ruska Porometer and is described in Appendix 7.3. A number of one inch cubes and slices from a 9 inch concrete block made with 6 mm diameter aggregate show a trend of porosity values with increasing specimen thickness. The mean is equivalent to a mean pore span of 6 mm. The pores in concrete are considered to form preferentially at the interface between the aggregate and the matrix. The idea of a pore span distribution can be applied at all scales in both intrinsic and fissure pore systems with low levels of connectedness. Since fissure systems with low joint density host the largest cave systems and by analogy the highest grade, least diffuse orebodies, this concept is of interest. The intrinsic pore span distribution is also an experimentally determinable characteristic of a rock.

The pore span distribution is equivalent to the site percolation problem of classical probability theory (Broadbent and Hammersley, 1957), redefined in terms of the openness of pore throats. If any given pore throat has a probability (p) of being unblocked what is the probability P(p) that a given pore throat belongs to an infinite cluster? And what is the distribution of cluster span? The heirarchy of pore lengths and diameters can be compared with the Sierpinski Sponge and the

Appollonian Gasket fractals of Mandelbrot (1977).

Budworth (1970) describes the increase in closed porosity and decrease in open porosity during the sintering of ceramics. Open porosity and permeability fall to zero and closed or residual porosity reaches a maximum of 4 to 5% at a relative density of 96.4%. In general the mean pore span will increase with porosity and also with connectedness and coordination number. For intrinsic porosity, it is a measure of the depth to which diffusive processes can operate within a joint block.

Coats and Smith (1964) have considered dead end pore volume and dispersion in porous media. Chatzis and Dallien (1977) have made statistical numerical models of 2 and 3-dimensional pore networks. Purcell (1949) and Pickell et al (1966) have described the use of capillary pressure curves with the injection of mercury and the calculation of the effective pore size distribution. In all such experimental work the assumption made is that all the porosity can be reached from the specimen surface. The pore size distribution curve may be expected to change with specimen size. Large specimens will have a lower proportion of small pores since they are more likely to become ascribed to residual porosity. This makes little difference to permeability and storage calculations within the range of porosities of interest in petroleum engineering; but microporosity is the major influence on the specific surface of a rock. The effective specific surface presented by a joint is important to diffusive processes such as weathering and mineralisation. Probably the most satisfactory description of a rock for diffusive processes would be to measure the internal surface area by nitrogen condensation, as a function of specimen thickness.

Chemical analysis by X-Ray diffraction, carbon dioxide train and thermal balance is described in Appendix 7.4. A relative increase in silica and alumina is evident with increasing weathering of joint block margins in impure limestones, Fig 65. An abstraction model was constructed for comparison with porosity variations but limestones have too restricted a chemical range for this to be useful.

3.2 Fissure porosity

3.2.1 Engineering Surface Metrology.

The statistical description of surfaces for engineering purposes is generally traced back to Longuet-Higgins (1957). Thomas and King (1977) provide a bibliography and the 'Short Course Notes' available from Teesside Polytechnic, Middlesborough provide a useful working state-of-the-art reference to the subject. Williamson et al (1969) point out that most naturally occurring surfaces will have a Gaussian height distribution as a consequence of the Central Limit Theorem, by which a large number of events is shown to produce a Gaussian distribution whatever the distribution associated with an individual event. They show (op cit) that non-Gaussian distributions occur in transitional topographies, as a Gaussian surface produced by one process is partially worn into the eventually Gaussian surface produced by a different process. Nayak (1971) has shown that the statistical geometry of an isotropically rough surface can be defined by the moments of the power spectum of any profile through it. Thus, five radially disposed profiles are required to specify an anisotropic Gaussian surface. Of course, the discussion of geological surface roughness in Section 2.1 implies that natural surfaces will be heterogeneously, as well as anisotropically rough.

Patir (1977) has shown that satisfactory numerical models of rough surfaces can be generated from two parameters: the standard deviation roughness - a measure of the surface-normal roughness, and the correlation length - a measure of the surface-parallel waviness. However, Thomas and Sayles (1978) show that since natural surfaces taken across eight orders of

magnitude are non-stationary, the autocorrelation length is dependent upon the sampling interval, which is effectively a low-pass filter. (Perhaps engineering surface metrology should be reworked in terms of geostatistics, which has been designed specifically to deal with non-stationary, 2-dimensional populations.) Care is therefore required in using statistical surface descriptions: the sampling interval and profile length should be quoted. This caution particularly applies to the shear of two initially matched rough surfaces, see Section 3.2.3.

Thomas and Sayles (op cit) point out that the development of stochastic theories of surface geometry has permitted the quantification of surface roughness in a form suitable for input to tribological theories. Insofar as the present study is concerned, Patir and Cheng's (1978) solution by numerical modelling of the flowrates through a rough fissure, illustrate the promise of this approach to surface roughness, equations (18) and (19), Section 1.2.2. Models of asperity deformation are not yet advanced enough to take account of the extreme plastic deformation of asperities seen in the production of fault gouge under high normal loads. However, numerical modelling coupled with further laboratory work of the type described below should illuminate the problem.

Geological surfaces are much rougher than most engineering surfaces so that the sliding stylus instruments with resolutions of 2 microns cannot be operated. The experiment described below was therefore conducted with a sawn block of rock which was acid etched to produce a tolerably rough surface. Weissbach (1978) has developed a profile measuring machine employing a stepping stylus, so that extremely rough

geological surfaces can now be automatically digitised. A profile gauge was used in the field at Spaunton Moor Quarry to trace fault roughness profiles successfully, Section 2.1.1.

3.2.2 Experimental work.

New and West (1980) describe an experiment whereby a PUNDIT (Portable Ultrasonic Non-destructive Digital Indicating Meter) was used to monitor the acoustic closure of an artificial crack subjected to normal load. This experiment was extended by:

a) monitoring the intact rock as a control, before sawing it in half and etching the crack so produced for the main experiment,

b) monitoring the surface roughness both before and after loading,

c) comparing the effects of increasing surface roughness,

d) using a Demec gauge to take strain measurements across the site of the crack, both before and after sawing, and

e) the monitoring of seismic attenuation using the Pundit and an oscilloscope, as well as the P-wave velocity monitored by New and West (op cit).

The experiment was performed by Jonasson (1980) and Dowlen (1979) and is summarised in Figs 30 and 31.

By comparison with Fig 30b the sample S3, etched for 90 seconds had a more Gaussian height distribution and a more 'normal' exponential autocorrelogram. Sample S1, etched for 60 seconds, has a transitional topography between a sawcut and an etched profile. Whitehouse and Archard (1970) proposed an asperity contact model from which they derive a plasticity

Fig 30:

Profile taken with a continuous profiling machine, with computed correlogram and histograms, after Jonasson (1980). Micritic Corallian limestone, sawn and etched.

Fig 31:

Variations in strain, sonic velocity and attenuation, for rough cracks under normal load. After Jonasson (1980) and Dowlen (1979).

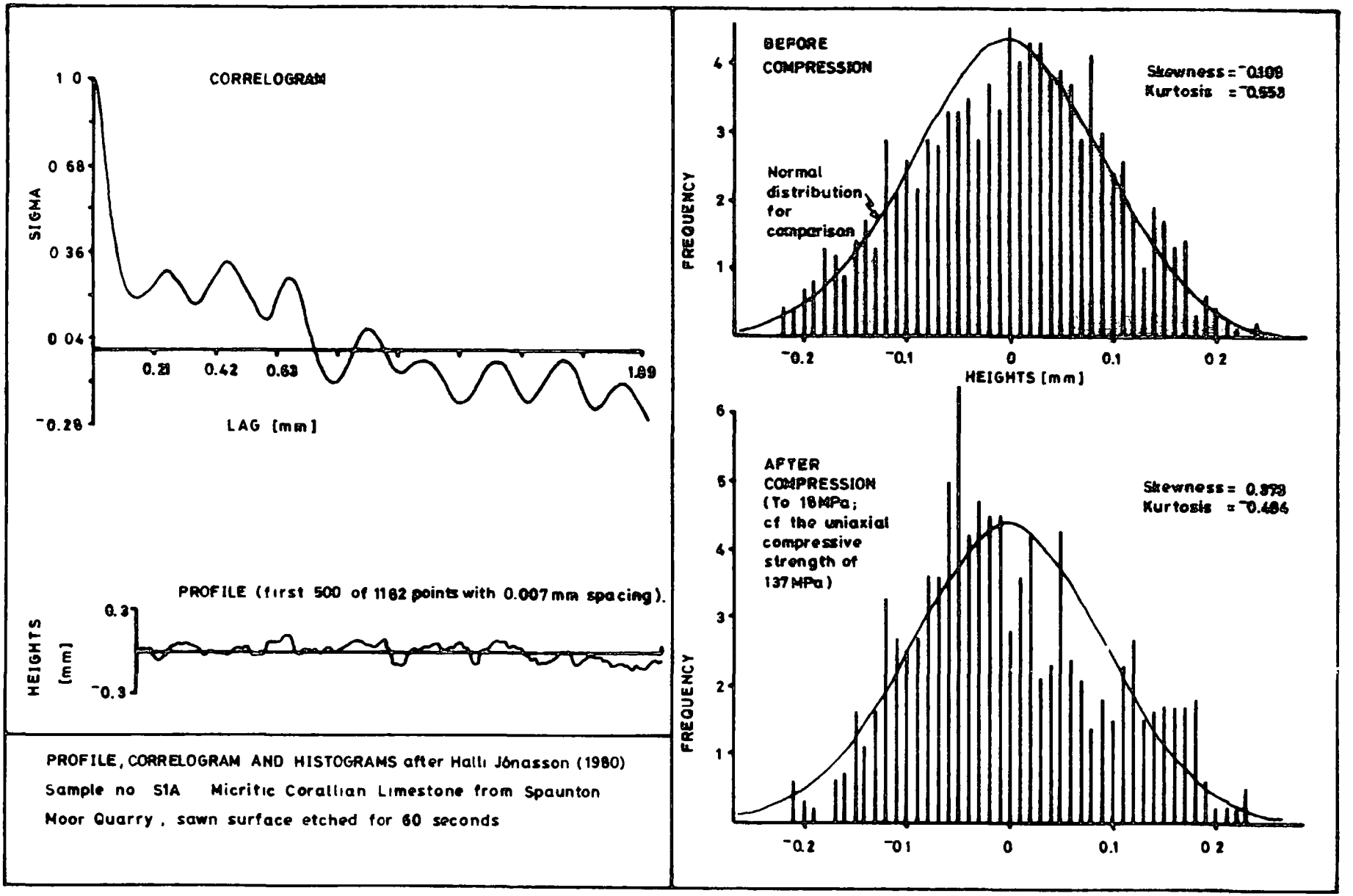

PROFILE, CORRELOGRAM AND HISTOGRAMS after Halli Jónasson (1980)
Sample no S1A Micritic Corallian Limestone from Spaunton Moor Quarry, sawn surface etched for 60 seconds

Fig 30

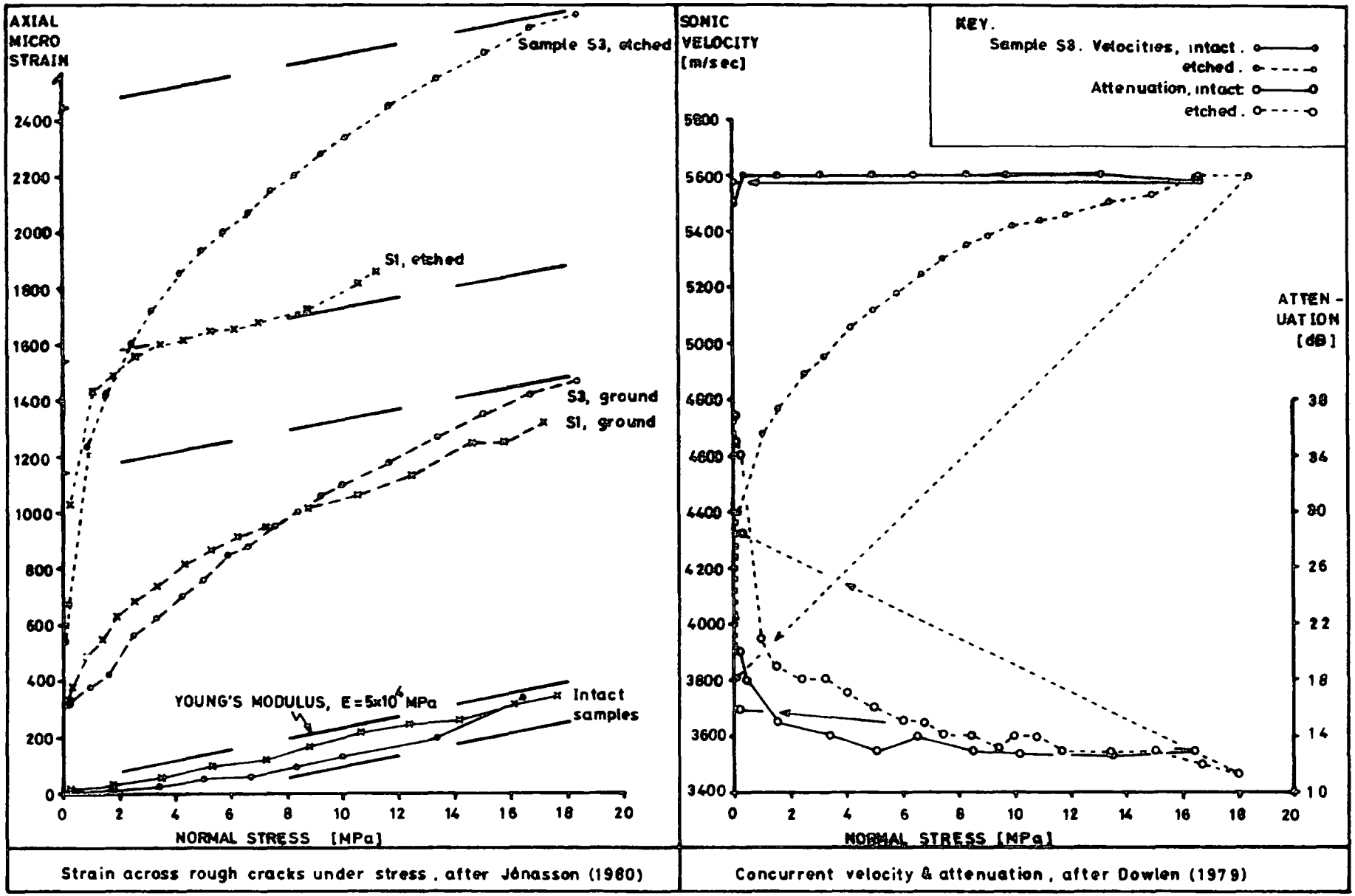

Strain across rough cracks under stress, after Jönasson (1980)

Concurrent velocity & attenuation, after Dowlen (1979)

Fig 31

index, expressed in terms of surface roughness and material strength parameters. Jonasson (op cit) used their expression to calculate that most asperity deformation will be plastic, i.e. by crushing. This was found to be the case, Fig 30b.

Figure 31a shows that the maximum strain across the cracks at any given load increases with surface roughness. Bearing in mind the extreme surface roughness of natural geological surfaces in comparison to these test specimens, one must question New and West's (op cit) conclusion that natural cracks close at relatively low stresses of 1.0 MPa. Their conclusion is valid only for lapped surfaces, as used in their experiment, and for joints across which no shear displacement has occurred so that the two surfaces are still perfectly matched. Walsh and Brace (1966) state that pressures of 100MPa are required to close cracks, but that pores do not close. Attenuation results are not convincing, but both strain and sonic velocity (P wave) show that the the roughest sample, S3 was not accoustically closed until a normal load of 17MPa; equivalent to a depth of 600 metres, or 1 kilometer in the presence of groundwater, and three times these depths if the crack is oriented vertically.

Surface roughness characteristics for the two samples: S1 etched for 60 seconds, and S3 etched for 90 seconds, are given by Jonasson as:

	S1	S3
TOTAL SURFACE.		
Number of samples:	1162	1042,
Sample interval:	7 microns	10 microns,
Vertical resolution:	2 microns	2 microns,
Roughness range:	0.24 mm	0.8 mm,
Standard deviation roughness:	0.05 mm	0.15 mm,
Skewdness:	-0.11	-0.2,
Kurtosis:	-0.55	-0.004.
PEAKS.		
Number of peaks:	96	73,
Number per mm:	9.9	7.0,
Range:	0.18 mm	0.7 mm,
Standard deviation:	0.04 mm	0.12 mm,
Skewdness:	-0.3	-0.05,
Kurtosis:	-0.4	0.3.

The bearing area equation describes the surface contact as a Gaussian surface is planed away and so corresponds to the cumulative Gaussian height distribution function:

A(h) = (erfc(h / s . (2*0.5))) / 2.....(26)

where:

A(h) is the bearing area at separation 'h', and

s is the standard deviation roughness, for a single surface.

The combined roughness of the two surfaces 'sc' is given by:

sc = (s*2 + s*2)*0.5 = s . (2*0.5).....(27)

The strain across the crack at 17 MPa in specimen S3 was 0.0024, less 0.002 strain across the intact sample, or control. This corresponds to 0.11 mm for a 5 cm Demec gauge, and converts to a bearing area of 46% using the total surface standard deviation, and 37% using the peak standard deviation. Acoustic closure at only 46% bearing area can be explained by the fact that the surface is not being planed away, but crushed outwards into the remaining fissure. Also some peaks intermesh, since as Jonasson has pointed out, some high asperities are preserved, Fig 30b.

Asperity contact models which are valid to bearing areas of 100% and under both plastic and elastic asperity deformation are required. In further experiments, moments of the power spectrum (Nayak, op cit) should be calculated and fissure closure related to Francis's (1977) mixed elastic-plastic asperity deformation model. Experiments should be conducted for surfaces modified under varying conditions of load and shear, Celestino and Goodman (1979).

3.2.3 Numerical modelling.

As an initially matched rough surface is sheared it can be expected that a transition topography will be produced between: the surface typical of a propagating crack in the lithology with the fracture mode pertaining; and the surface typical of a surface worn in shear. Surface waviness of at least the length of the shear should be included in the profile or profiles. Fortunately, on a fault plane, several samples taken in parallel will sample roughness of the two distinct characters: that due to heavily modified asperities in contact areas; and that which is partially original in non-contact areas. Provided

the mechanics of mixed mode roughness production on fault planes is understood, the two topographies could be separated for stress analysis, and for hydraulic conductivity calculations. It would be interesting to know whether the surface waviness of fault surfaces is partially a function of normal load, and whether fault surfaces are more nearly planar at great depths. If they are wavey, considerable hydraulic conductivity must be present albeit in sporadic and convoluted 'pipes'. Gash (1971) has described fracture surface markings and related them to stress trajectories and interface conditions at the time of formation.

There is an essential difference between the surfaces described by engineering surface metrologists, and those which create geological fissures. Engineering surfaces can be regarded as being independently and randomly rough so that their standard deviation surface roughnesses may be combined by equation (27), regardless of relative position in surface contact problems. Geological surfaces form from cracks within the material. Initially the two sides of the crack are matched and they remain a perfect fit whilst undisplaced. The concept of an autocorrelation length must be applied at all scales; from that of the individual grain, to the diameter of the penny-shaped crack. The displacement varies over the crack, Fig 14, as do the lithologies intersected, so that two independent heterogeneities are involved, as well as an anisotropy controlled by the direction of the displacement vector.

A simple model can be designed to compare the size of the autocorrelation length with the size of the displacement vector. One would expect that surface roughness features with a wavelength less than the displacement vector, will interact in

an unrelated or random fashion. Surface roughness features with a wavelength greater than the displacement vector will control the dilation of the fissure as it forms. It will be important to know how the autocorrelation length and standard deviation surface roughness of geological surfaces vary as a function of lithology, and of the surface-normal stress at the time of formation.

Patir's (1978) algorithm was used to create a numerical model of a surface with an isotropic, linear autocorrelation function having a length of ten sample intervals. The surface generated was one hundred samples square, so that only a small section is displayed in Figs 32 and 33. The generating function 'RELATE' is given in Fig 34. The surface, 'S' has a mean of zero and a standard deviation surface roughness of one, Fig 32. To model the shear of a rough crack with no dilation, the surface, 'S', is shifted with respect to a copy of itself and the two surfaces are then subtracted. The surface, 'T', Fig 32, is then a model of the fissure width created, such that negative values are areas of asperity contact, expressed in terms of the unit standard deviation surface roughness of one original surface, 'S'. They represent material that has been plastically deformed, or comminuted to gouge. These negative areas are elongate, aligned normally to the displacement vector, and have widths that are approximately equal to the length of the displacement vector, i.e. three for Fig 32, and seven for Fig 33. As the length of the displacement vector approaches the autocorrelation length of the original surface, the areas of contact become less elongate, Fig 33.

A function 'SHEAR' was written to apply this modelling principle to the situation in which dilation is allowed. For a

Fig 32:

Numerical model of heights on a rough surface, S, generated to have a linear autocorrelation function, using an algorithm due to Patir (1978). Shear with no dilation produces the fissure, T, illustrated. Negative areas are asperity overlaps and positive areas are inter-surface gaps. Numerical values are units of the standard deviation surface roughness of the original surface, S.

Fig 33:

Numerical model of the fissure, T, between a sheared, originally matched surface, S. Here asperity contact areas are isotropic since the shear displacement is close to the autocorrelation length of the original surface, S. In Fig 32, the shear displacement is less than the autocorrelation length of the surface, S, and anisotropic areas of asperity contact are aligned normal to the direction of shear.

Fig 34:

APL functions used in Figs 32 and 33.

```
      MOMENTS ,S

  M1=M1   , SD=M2 , M3     , M4     , M5     , M6   .
     .00     1.00      .53     1.33     1.14     1.60
M[4]-M[2] =      1.33
M[5]-M[3] =      2.13
```

```
      2 0↑36 36↑T←S-3Φ[1]S
```

```
 0 0 0 1 0 1 1 1 1 1 1 2 1 1 1 1 1 0 0 0 0 0 0 0 0 1 0 0 0 0 1 0 1
 0 1 0 0 0 0 0 0 0 0 0 0 1 1 1 1 1 0 0 0 0 0 0 0 0 1 1 1 1 1 0 0 0 0 1 1
 0 0 0 0 0 0 0 0 0 0 0 0 1 0 0 0 0 0 0 1 1 1 1 1 1 1 2 1 0 0 0 0 0 0 0
 0 1 0 0 0 0 0 0 0 0 0 0 0 0 1 1 1 1 1 1 1 1 1 1 2 2 1 1 1 0 1 0 0 0 0
 1 0 0 0 0 0 0 0 0 1 1 2 1 1 2 1 1 2 2 1 1 1 1 1 1 1 2 2 1 1 1 1 0 0
 1 0 0 0 0 0 0 0 0 1 1 1 1 1 1 1 1 1 1 1 1 1 1 1 1 1 1 1 1 1 0 1 0 0 1 1
 1 0 0 0 0 0 0 0 0 1 1 1 1 1 0 0 0 0 0 0 0 0 0 1 0 1 1 1 1 0 0 0 0 1 1
 1 1 1 1 0 0 1 1 0 0 0 0 0 0 0 0 0 0 0 0 0 0 1 0 0 0 1 1 1 1 1 1 1 1 1
 0 0 0 0 1 1 1 0 1 1 1 1 1 1 1 1 1 1 1 0 0 0 0 0 0 1 1 1 1 1 1 0 1
 0 1 0 0 0 0 1 0 1 2 2 2 2 2 2 2 2 2 1 1 0 0 0 0 0 1 1 1 1 1 1 0 1
 1 1 1 1 1 2 2 1 2 2 2 2 2 2 2 2 2 2 1 1 1 1 1 1 0 1 1 0 0 0 1
 1 1 1 0 0 1 1 0 1 1 1 2 2 2 1 2 2 2 2 2 2 1 1 1 1 1 1 1 1 1 0 1
 1 1 0 0 0 0 0 0 0 0 0 1 0 0 0 0 0 0 0 0 0 0 0 0 1 1 1 1 1 1 1 0 0
 1 1 1 0 0 0 0 0 0 0 0 1 0 0 0 1 1 0 1 1 1 1 1 0 0 1 1 1 1 1 1 1 1
 0 0 0 1 0 0 0 0 0 0 1 1 1 1 1 1 1 1 1 1 1 1 1 0 1 0 0 0 1 1 0 1
 0 0 0 1 1 1 1 1 1 0 0 0 0 0 1 0 0 0 0 0 0 0 0 0 0 0 0 1 1 1 1 1 1
 0 0 0 1 0 0 0 1 1 0 1 1 1 1 1 1 1 0 0 0 0 0 0 0 1 1 0 0 0 1 1 1 0 0
 0 0 0 0 0 1 1 1 1 1 1 1 1 1 1 1 1 0 1 1 1 1 1 1 0 0 0 1 2 1 1 1 1
 0 0 0 1 1 0 0 0 0 0 0 0 0 0 0 0 0 0 1 0 0 0 0 0 0 1 1 1 2 1 1 1 2
 0 0 0 0 1 1 0 0 1 1 1 1 1 1 1 1 1 1 0 0 0 0 0 0 0 1 1 1 1 1 1 1 2
 1 1 1 1 1 1 1 0 1 1 1 1 1 1 1 0 1 1 1 1 0 0 0 0 0 1 1 1 1 1 1 1 2
 0 1 0 0 0 0 0 0 0 0 0 1 1 1 0 0 1 1 1 1 1 1 0 0 0 0 0 0 0 0 1 1
 0 1 1 1 0 0 1 0 0 0 0 0 0 0 1 1 0 0 0 0 0 0 0 0 0 0 0 0 0 0 0 1
 0 1 1 1 0 1 1 0 1 1 0 0 0 0 0 1 0 0 0 1 1 1 1 1 1 0 0 0 1 1 1 0
 0 0 0 0 0 0 0 0 0 0 0 0 0 0 0 0 0 0 0 1 1 2 1 1 1 1 1 0 0 1 1 1 1
 1 1 1 1 1 1 1 1 0 1 1 1 1 1 1 1 1 0 0 0 1 0 0 1 1 0 0 0 1 1 1 1
 1 1 2 2 2 2 1 1 1 2 2 2 2 1 1 1 1 0 0 0 1 0 1 1 0 0 0 0 0 1 0 0
 1 1 1 1 1 1 1 1 1 1 1 1 1 1 1 0 0 0 0 0 0 0 1 1 0 0 0 0 1 0 0 0 1
 0 0 0 0 1 0 0 0 0 1 0 1 0 1 0 1 0 0 0 0 0 0 0 0 0 0 1 0 1 1 1 1 1 2
 0 0 0 0 0 0 0 0 0 0 0 0 0 1 1 1 0 0 1 1 1 0 1 0 0 0 1 1 1 1 1 2
 1 1 1 1 1 1 1 0 0 0 0 0 0 0 1 1 1 1 1 1 1 1 1 1 1 1 1 2 2 1 1 2
 1 1 1 2 1 1 1 1 1 0 0 0 0 0 0 1 1 1 1 1 1 1 1 1 1 1 1 1 0 0 0 0
 0 1 1 1 1 1 1 0 0 0 0 1 0 0 0 0 1 1 1 0 1 1 1 1 1 1 1 1 1 1 1 1
 0 0 1 1 0 0 1 0 0 0 0 0 0 0 0 0 0 0 0 0 0 0 0 0 0 1 0 0 0 0 1 0 0
 1 1 0 0 1 1 1 1 1 1 0 1 1 1 1 1 1 1 1 1 2 1 1 1 1 0 0 0 0 0 1 1 1 1
 2 2 2 1 1 1 1 1 0 1 0 0 0 1 1 1 1 1 1 1 1 1 1 0 0 0 0 0 0 0 0 0
```

```
      MOMENTS ,T
  M1=M1   , SD=M2 , M3     , M4     , M5     , M6   .
     .00      .80      .42     1.09      .98     1.38
M[4]-M[2] =      1.37
M[5]-M[3] =      2.35
```

Fig 32

```
      2 0+36 36↑T←S-7Φ[2]S
```

```
 0 0 1 1 1 1 0 1 1 0 0 0 0 1 1 1 1 1 1 0 1 1 2 3 3 2 1 2 1 0 1 1
 1 1 2 1 1 1 0 1 0 1 0 0 0 1 1 1 1 1 1 1 1 1 1 3 3 3 3 2 2 2 1 1 0
 1 2 2 2 2 2 0 1 0 1 0 1 1 0 1 1 1 0 0 0 2 2 3 3 4 3 2 2 1 0 0 0
 1 2 2 2 2 2 0 1 0 1 0 1 1 0 0 0 0 0 0 0 1 2 3 3 3 3 2 2 1 0 0 1
 1 2 2 2 2 2 1 2 0 1 0 1 1 0 1 0 0 0 1 0 1 1 2 2 3 3 2 2 1 1 0 1
 1 2 2 2 2 2 0 1 0 1 1 2 2 0 1 1 0 1 0 0 1 1 2 2 2 2 1 1 0 0 1 2
 1 3 2 1 2 1 0 0 1 2 2 2 2 0 1 0 1 0 1 1 0 0 1 2 2 2 2 1 1 1 0 0
 1 2 1 0 1 1 1 0 1 1 1 1 1 1 0 0 1 0 0 0 1 1 1 2 1 1 1 1 0 0 0 0
 1 2 1 0 1 0 1 0 1 1 1 2 1 0 1 1 0 1 0 0 1 1 0 1 0 1 1 1 1 1 1 1
 1 2 1 0 1 1 0 0 0 1 1 2 1 0 1 1 0 0 0 1 0 0 0 1 0 1 1 1 1 1 1 1
 1 1 0 1 1 0 1 1 1 1 1 2 1 0 1 0 0 1 1 1 1 0 0 0 0 1 1 2 1 2 1 1
 1 1 0 1 0 0 1 1 1 1 1 1 0 1 0 1 1 1 1 1 1 0 0 1 1 1 1 1 1 1 0 0
 0 0 1 2 0 1 2 1 2 1 1 1 0 2 1 1 2 2 2 2 1 1 1 0 0 0 1 1 1 1 0 1
 0 0 1 1 0 1 1 1 2 1 1 1 0 1 0 1 1 2 2 2 2 1 2 0 1 1 0 1 0 1 0 1
 0 1 1 2 1 2 2 2 2 2 2 1 0 1 0 1 2 2 3 2 2 1 1 0 1 1 0 0 0 0 0 1
 0 1 1 2 1 1 2 1 1 1 1 0 0 1 0 1 1 2 2 1 1 0 0 0 1 1 0 0 0 0 0 1
 1 1 2 2 1 1 1 1 1 0 1 0 0 1 1 1 1 2 1 0 0 1 0 0 0 0 0 0 1 1 1 1
 0 0 1 1 0 0 1 1 1 1 1 0 0 1 0 1 1 2 2 0 0 1 1 0 0 1 0 1 0 0 1 0
 1 1 1 1 1 1 1 1 1 1 1 0 0 1 1 1 1 1 2 1 0 0 1 1 1 0 0 0 0 0 1 1 1
 2 2 2 2 2 1 2 1 1 1 0 1 2 3 2 2 2 1 1 0 1 2 2 1 0 0 0 1 1 2 2 2
 1 1 1 2 1 1 2 1 1 0 1 1 2 3 2 2 2 1 1 1 1 2 3 2 2 1 1 0 1 1 2 2 2
 2 2 2 2 2 1 2 0 1 1 0 1 1 2 1 1 1 0 0 1 2 3 2 2 1 1 0 1 1 2 2 2
 2 1 1 1 1 1 2 1 1 1 0 0 1 1 1 1 1 0 0 2 2 3 3 2 2 1 0 1 1 2 3 3
 2 1 1 1 2 1 1 1 0 0 1 1 1 2 2 1 1 1 1 2 3 4 3 3 2 2 1 1 1 2 3 4
 2 1 1 1 1 1 1 1 1 0 1 1 1 2 2 1 1 1 1 2 3 3 3 3 3 2 1 0 1 2 3 4
 2 1 1 1 1 1 1 1 1 1 0 1 0 0 1 1 1 1 1 1 2 2 2 3 2 2 1 0 1 2 2 3
 2 2 1 1 1 0 1 0 0 0 1 0 0 1 1 1 0 1 1 1 2 1 1 2 1 1 1 1 1 2 2 3
 2 1 1 1 1 0 1 0 0 0 1 0 0 0 0 0 0 2 1 1 2 1 1 1 1 1 0 2 2 2 3 3
 2 2 1 1 1 1 1 1 1 1 0 0 1 1 1 0 0 0 2 1 1 2 1 1 1 1 1 0 2 2 2 3 3
 2 1 1 1 1 0 1 1 1 1 1 1 2 1 1 0 1 2 1 1 1 1 0 1 1 1 0 2 2 2 3 3
 2 2 1 1 1 1 1 1 1 1 1 1 1 1 1 2 1 1 1 1 1 1 0 1 0 0 1 0 0 0 2 2 2 3 2
 2 1 0 1 0 0 0 1 1 1 0 1 1 1 0 0 1 1 1 0 0 0 0 0 0 0 0 0 2 2 2 2 2
 2 2 1 1 1 0 1 1 1 1 0 1 1 1 1 0 1 2 1 0 0 0 0 0 1 0 0 2 2 1 1 1
 2 2 1 2 1 1 1 1 1 1 0 1 1 0 0 0 1 1 1 0 0 0 0 0 0 0 0 1 2 1 1 0
 2 2 1 2 1 1 2 1 1 0 1 0 0 0 0 0 1 1 1 0 0 1 1 1 1 0 0 0 1 0 1 0
 2 2 2 2 2 1 2 1 1 1 1 0 0 0 1 0 1 1 1 0 0 0 0 0 0 0 0 0 1 0 0 1
```

```
      MOMENTS ,T
  M1=M1   , SD=M2 , M3    , M4    , M5    , M6  ,
     .00    1.16     .44    1.54    1.02    1.87
M[4]-M[2] =     1.33
M[5]-M[3] =     2.31
```

Fig 33

```
      ∇MOMENTS[□]∇
    ∇ MOMENTS X;XMN;XSD
[1]   XMN←(+/X)÷⍴X
[2]   →L1 IF(⍴X)≠1
[3]   XSD←99
[4]   →L2
[5]  L1:XSD←((+/[1](X-XMN)∘.* 2 3 4 5 6)÷(⍴X)-1)*1÷ 2 3 4 5 6
[6]  L2:M←XMN,XSD
[7]   ' MN=M1(0), SD=M2 , M3(MN), M4(MN), M5(MN), M6  ,'
[8]   □← 8 2 ⍕M
[9]   →0 IF 1=⍴X
[10]  'SKEWNESS = M[3]-M[2]*3 = ', 8 2 ⍕M[3]-M[2]*3
[11]  'KURTOSIS = M[4]-M[2]*4 = ', 8 2 ⍕M[4]-M[2]*4
    ∇

      ∇RELATE[□]∇
    ∇ RELATE X;R;C;F;LC;LR;LRC
[1]   R←C←1
[2]   Z←⍳0
[3]   'SET CORRELATION LENGTHS (LRC)'
[4]   'INPUT AS A VECTOR ; ( ROW,COL ) '
[5]  A
[6]  A LY=LR=N
[7]  A LX=LC=M
[8]  A
[9]   LRC←,□
[10]  LR←1↑LRC
[11]  LC←¯1↑LRC
[12]  →L1 IF(LR≠0)∧LC≠0
[13] A
[14]  'Z←(SD-(LC×LR)*0.5)×SUM,SUM ETA'
[15]  'INDETERMINATE FOR (LC=0)∨LR=0 ! '
[16]  →0
[17] A
[18] A FROM NADIR FATIR (1978)
[19] A       WEAR , 47 PP. 263-277
[20] A
[21] L1:Z←Z,+/+/X[(R+⍳LR);C+⍳LC]
[22]  R←R+1
[23]  →L1 IF R≤(1↑⍴X)-LR
[24]  R←1
[25]  C←C+1
[26]  →L1 IF C≤(¯1↑⍴X)-LC
[27] A
[28]  MNSDI←MNSD,X
[29]  Z←Z×F←MNSDI[2]÷(LC×LR)*0.5
[30]  MNSDO←MNSD,Z
[31]  'MN,SD OF INPUT (MNSDI): ', 10 2 ⍕MNSDI
[32]  'MN,SD OF OUTPUT (MNSDO):', 10 2 ⍕MNSDO
[33]  'SD (LC×LR)*0.5 = ', 10 2 ⍕F
[34] A
[35]  Z←⍉(⍴(⍴X)-LRC)⍴Z
[36]  'O/P IS IN Z ; ⍴Z = ',⍕⍴Z
    ∇
```

Fig 34

constant asperity contact area, expressed as a percentage of the total area, the dilation is a linear function of displacement; as may be expected with a linear autocorrelation function. At low percentages of asperity contact, the contact areas were isotropic, but increasing the amount of surface contact increases the anisotropy, as illustrated in Fig 32.

3.3 Summary.

In similar lithologies, an increase in porosity leads to a lower rate of growth in hydraulic conductivity. The higher joint frequency associated with a high porosity, leads to a more dispersed flow; and the presence of a significant intrinsic mean pore span allows diffusion from a much greater specific surface.

The techniques of engineering surface metrology will be applied to engineering geological problems in the future, and will allow the hydraulic conductivity of individual fissures to be predicted at depths where little direct evidence is available, but where stress conditions and shear histories can still be deduced. An extensive program of research will be required to fully explore the surface topographies produced in naturally occurring surfaces under varying load and shear conditions. With statistical descriptions of surface roughness, continual comparison can be made between: laboratory produced surfaces; surfaces observed in the field; and surfaces produced by numerical models having different mechanisms for the comminution of asperities.

CONTENTS. PAGE.

4. Fractures and networks.

4.1 Observed patterns.

In Fig 35 the maps of apparently different fracture patterns all include the area of Spaunton Moor Quarry. The map of Fig 35a is after Kent (1974), see Fig 4a. The map of Fig 35b is after Richardson, reported in Mierzejewski (1978). The map of Fig 35c is from Fig 4b and is based on air photographs (V1 543/RAF/4278 26 APR 68 DOE numbers 0119, 0120, and 0121). The maps of Figs 35d and 35e are from Figs 7 and 8.

The large jump in scale between Figs 35c and 35d illustrates a common gap in geological mapping scales. Fracture patterns on the scale of Figs 35d and 35e are not usually mapped, as they can only be observed within restricted localities. They are the scales of interest during mining, quarrying and engineering geological investigations. The other three scales illustrate the range considered in mineral exploration and regional geology.

In Fig 35a the predominant trend of the fault pattern is east-west, but at an even greater scale the faults associated with continental drift and the North Sea graben would appear, Whiteman et al (1975). According to Kent (1967) these are northwest-southeast in the west of the southern North Sea Basin, and north-south in the eastern part of it. The very large scale northwesterly and north-10-degrees-easterly trending faults of the southern North Sea Basin are considered to be early transform faults; surfaces parallel to them have low fissure hydraulic conductivity as they are packed with fault gouge. The Dowsing Fault of the southern North Sea Basin belongs to this set and may extend to the Scarborough and Peak

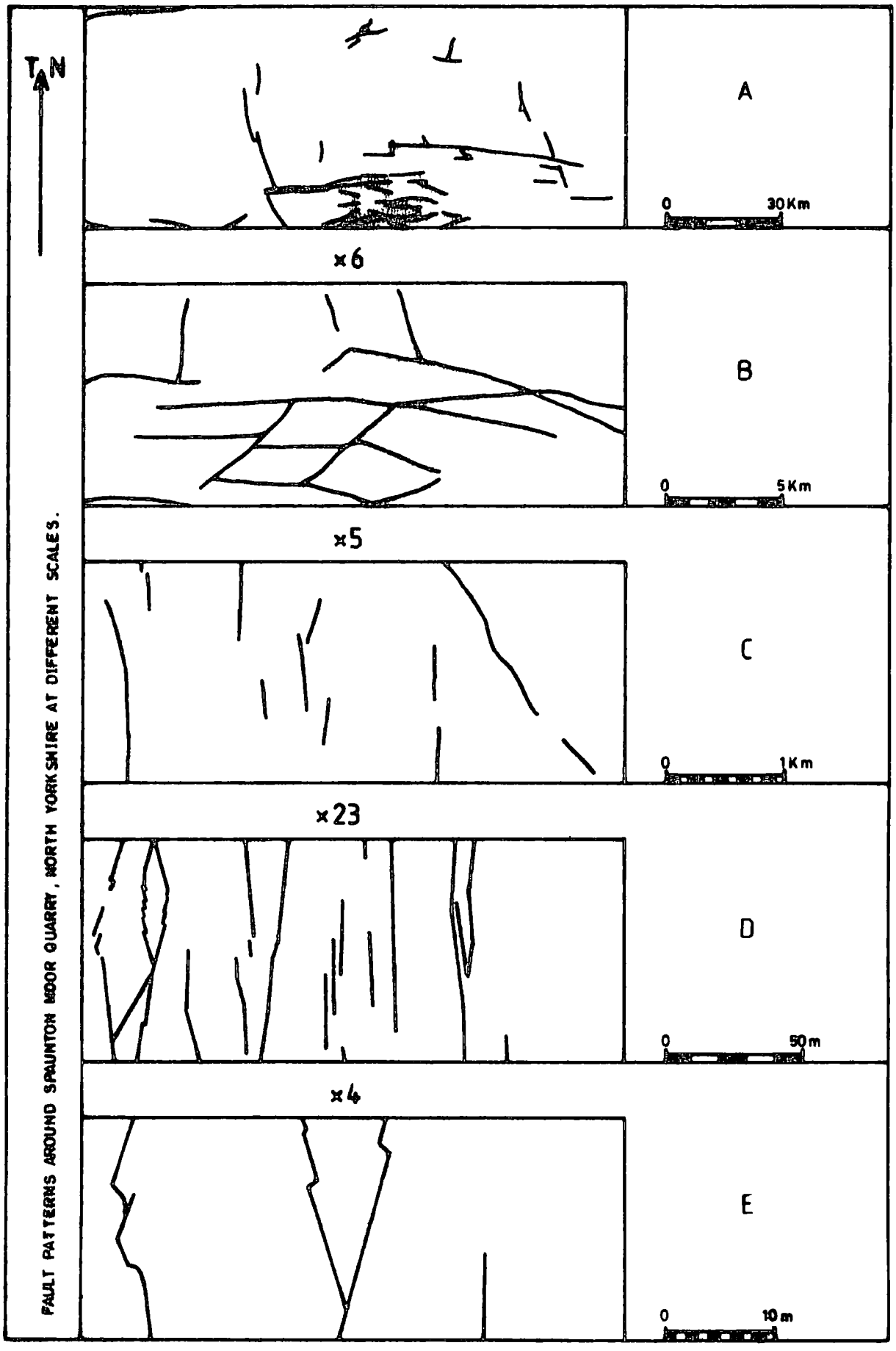
N
A
0
30Km
×6
B
0
5Km
×5
C
0
1Km
×23
D
0
50m
×4
E
0
10m
FAULT PATTERNS AROUND SAUNTON MOOR QUARRY, NORTH YORKSHIRE AT DIFFERENT SCALES.

Figure 35

Faults of Fig 4a. Later faults in the southern North Sea Basin trend northeasterly, supposedly following Charnian trends, and surfaces parallel to them have high fissure hydraulic conductivity, being extensional. Moseley (1973) relates small scale structures to the regional features of: the Borrowdale Volcanics centre; the Weardale Granite; and the Wensleydale granite which underlies the Askrigg Block of Fig 4a. Moseley's (op cit) Fig 1 shows an hexagonal disposition of these large scale igneous structural units. In Appendix 7.6, the formation of a rhombohedral regional fracture pattern is described in the basement of the North West Highlands of Scotland. (The Inverian fracture pattern described in Appendix 7.6 could have controlled the Caledonian and Charnian orogenies in the southern North Sea area, being modified in the North of England by hexagonally centred later igneous intrusions.) Moseley (op cit) gives several examples of fracture patterns formed in the first brittle deformation of the crust being copied into overlying sediments. Indeed, the mobility of a particular zone in the earth's crust may have been predetermined at a very early stage after it's formation.

Ramberg et al (1977) and Johnson and Frost (1977) describe large scale fracture patterns taken from Landsat images. For present purposes it is held to be important that regional fracture patterns be understood, because not only are they the most permeable zones but they also define the structural blocks which control the distribution of minor faults. Huskey and Crawford (1967) have shown experimentally that the total length of a nearby fracture is closely correlated with the producing capacity of a well. Chinnery (1966a, b) has discussed the formation of second order faults due to stress concentrations

near the ends of the first order fault. In Appendix 7.6 it is shown that early formed conjugate-shear bounded blocks can rotate between later shear zones formed in the dominant member of the conjugate shear set. This mechanism produces stress concentrations within shear zones. Not only are large scale fractures the most important hydrologically and for mineral exploration purposes, but they also control the formation of small structures in an heirarchical manner. Mathematical descriptions of the fracture patterns will probably be based on a similar heirarchy.

The small scale cross joints have not been shown on Fig 35e since they do not form mappable features on the quarry bench. However they do form hydrologically important cross-links between the otherwise isolated north-south trending faults at Spaunton Moor. They also influence seismic anisotropy in small scale arrays, Appendix 7.5 and Figs 72 to 77. Individually, they terminate at the north-south trending faults, just as the latter terminate at the east-west trending larger scale faults of the Vale of Pickering, Fig 35b. On a very large scale there may be a similar relationship between the east-west trending Helmsley-Scarborough Fault System of the Vale of Pickering, and the north-south trending North Sea graben faults. Four hydrologically important fracture sets would then be involved in a truncation relationship which is repeated three times. Fractures are discrete, and when observed across four orders of magnitude the pattern exhibits self-similarity. Moseley and Ahmed (1967) show that this pattern may no longer be tenable at the scale of a 1 metre thick bed, since they observe that one bed may develop a minor joint system entirely different from that in the bed above or below, particularly in flaggy

sandstones. It has been shown in Section 2.2 that minor joints control the distinctive linear solution channels in cave roofs, but that the earliest and critical stage of solutional development is controlled by the primary hydraulic conductivity of the bedding planes and master joints, which together form an interconnecting system of flow fissure porosity. Minor joints contribute to the diffusive fissure porosity, and flow within them is parallel to the major surfaces they intersect. Consequently, for hydrological purposes, although fracture patterns are observed across at least eight orders of magnitude, (as are scales of roughness, Section 3.2) fractures less than a metre long may be disregarded.

In Section 2.1 geological fractures were described and compared with 'penny-shaped' rough Griffith's cracks. A relationship between length and throw was observed and a relationship between local stress fields and orientation shown by considering structural position. To generate a fracture pattern purely in plan, the following variables would have to be produced for each fracture:

$$F(i) = \{ L , x , y , A \} \quad \ldots\ldots\ldots\ldots\ldots\ldots (28)$$

where:

L is the length of fracture (i),

x,y are the coordinates of it's centre, and

A is it's angle of orientation with respect to True North.

This would be a very simple description and would not allow intrinsically for truncation by other fractures unless the generating algorithm produced the members of the fracture set {F} in a dynamic and heirarchical sequence. They are also considered as straight - or the centre-line average roughness

plane is described.

Rats and Chernyashov (1966) state that permeability is an additive function of jointing and confirm a lognormal distribution of permeability for oil and water wells. De Wijs (1951, 1953) finds a lognormal distribution of ore assay values. An apparent lognormal distribution can be produced from an hyperbolic distribution by non observation of the low grade or of the impermeable. A plot of pitch, or underground waterfall heights for British caves shows a maximum corresponding to a 10 foot ladder length. This is predetermined by the size of the creatures observing the physical obstacle. Rowlands and Sampey (1977) have proposed that Zipf's law - an hyperbolic distribution - may be used to relate the size and rank of orebodies since it has been applicable to such populations as: word counts, the sizes of companies and cities, and of colonies of bacteria and political parties. They summ up Zipf's law as "the biggest is twice as big as number two, three times as big as number three, and so on"; so that size may be plotted against rank on a log. log. scale. The possibility that the size and grade of orebodies may be controlled by fracture size and frequency should not be overlooked.

4.2 Modelling possibilities.

Hoyle (1953) distinguishes two types of turbulence in the general sense. Ordinary turbulence in fluid flow, and the formation of eddies in a pressure field are both evanescent, as the rise of pressure due to compression tends to disrupt the denser elements of the material. In gravitational turbulence denser materials tend to become permanent concentrations. Novikov and Stewart (1964) have constructed a theory for

ordinary dissipative turbulence based upon the moments of the velocity field. Mandelbrot (1977) provides numerical models illustrating energy condensing and energy dissipating turbulence, and finds that they have different ranges of fractal, or Haussdorff-Bessicovitch dimension.

Richardson (1961) found self-similarity in turbulence and also found an hyperbolic relationship between the apparent lengths of natural boundaries and the basic unit of length used to measure them. Mandelbrot (op cit) shows that Richardson's latter unpublished result is an illustration of the Haussdorf-Bessicovitch, or fractal dimension.

In the models created by Mandelbrot, the algorithms generate heirarchies of scalar values. Two dimensional representation follows fixed and arbitrary rules. He shows that the Sierpinski Sponge, the Appollonian Gasket and percolation models, which are all relevant to studies of intrinsic porosity have fractal dimensions greater than one. The Cantor Set and the models of Hoyle's energy condensing turbulence have fractal dimensions of less than one, and one respectively. The Cantor set has been found applicable to the modelling of error bursts in telegraphy and bears a strong resemblance to the clustered nature of fault patterns. Although faulting and jointing are processes in which strain energy is dissipated, later movements tend to concentrate near preexisting zones of weakness, or to splay from them. Thus energy is dissipated in a spatially concentrated manner. Unfortunately, fractal descriptions of vector sets, such as those needed to describe fault patterns, have not yet been provided.

All the leading contenders for a numerical basis to the generation of fracture patterns are subsets of Group Theory.

The exception is a body of theory known as geostatistics (David, 1977) which gives the best available prediction of scalar values in 2 or 3-dimensions, on the basis of current scalar data. The area of interest is sampled on a grid, and the functional equivalent of a non-stationary correlogram evaluated in several directions.

Group Theory is being used to describe many relations within the physical sciences, including random graphs (or nets), Bollobas (1979). The Renormalisation Group allows complex computational models to be based on energy states, and the interactions between the nodes on a grid. Harris et al (1975) have applied the Renormalisation Group to the percolation problem, but it is notoriously difficult to apply to new problems, Wilson (1975, 1979). Fractals are a group whereby non-differentiable curves are generated across a wide range of scales by repeatedly applying the transformation at the previous, less detailed scale. Nooshin (1979) created the Formex Formulation method of automatically generating double layered grids. Formex is a set of exotically named transformations designed to create groups of vectors. As with fractals, the method of spatial representation is arbitrary, but follows strict rules for each implementation.

The basic ingredients for the numerical generation of fracture patterns thus seems to be contained in a combination of Formex and Fractals. Formex illustrates the manipulation of a few basic vectors into a description of the full set required. Fractals allow inter-relationships to exist between (vector sets at) several different scales. They can both describe sparse, discrete patterns rather than the regular grid of inter-related averages treated by geostatistics.

The first aim would be to match a model with the joint and fault sets observed. Observational detail is not uniform at the scales of interest; though fortunately it is at the larger scale of the controlling block faults. Patterns could be generated in a predictive manner, then tested and modified by subsequently aquired data. That is, it would be used in a similar manner to geostatistics, and where mineralisation is fracture controlled, the two methods would be directly comparable.

4.3 Analysis

The graph that is required to be constructed by the methods discussed above bears a resemblance to the model of conduction on a tree with random links, Ziman (1979, p381). Ziman (op cit) shows that the average conductance of such a net can be calculated, so that maps of fracture permeability could be drawn from a fractal model of the fracture pattern. Consequently the requirements of engineering geology and mineral exploration would be fulfilled by such a model. For dynamic purposes however, the flowrate must be known along each arc of the net and this involves the inversion of an impossibly large conductance matrix. An heirarchical method of flow analysis would have to be developed. Reeves (pers comm, 1981) has proposed a Monte Carlo method of net tracing to avoid the inversion of the conductance matrix. This will be valid where the Reynold's number is less than 2100, so that the relationship between flowrate and headloss is linear, and diffusion is an analogue of permeation.

4.4 Summary

The numerical description of fracture patterns is a fundamental pre-requisite for predicting the dynamics of the development of secondary porosity and permeability in fractured rock; but it is one of the areas in geology where most progress remains to be made. Although it is not possible to solve for discrete flowrates within flownets of natural proportions at present, an algorithm to simulate fracture patterns would be useful in mineral exploration and hydrogeology. Geological data is gathered at a variety of scales, but becomes particularly fragmentary on a small scale; the scale of interest in mining and engineering geology. The modelling of fracture lengths over four orders of magnitude is required. The generation of new fractures is believed to be controlled by the fracture pattern on a larger scale. An heirarchically based numerical model is most likely to be successful. Basic large scale patterns include hexagonal or pentagonal sets controlled by igneous bodies, and rhombohedral sets controlled by early fracture sets, compare Legeza, 1975.

CONTENTS. PAGE.

5.1 Related models.

Models of fissure flow networks may be classified in several ways, including:

two, or three dimensional;

physical or numerical;

electrical or hydraulic; and

pipes or planes.

Numerical models have been made using: the Finite-element method; the Finite-difference method; and by the inversion of conductance matrices describing electrical or hydraulic networks.

Wittke (1970) and Wittke et al (1972) constructed both physical and numerical models of flow through joint planes in a rock slope. The joint planes considered were coaxial, so that the problem was essentially two-dimensional: the edges of the planes were joined by pipes. Wittke (op cit) used the Finite-element method to obtain a numerical solution. Duguid and Abel (1974) developed a two-dimensional Finite-element model to analyse the flow in fractured porous media.

Bedinger (1966) used a two-dimensional physical array of electrical resistors to model the flow through a fissured limestone bench. He iteratively decreased the resistances of those resistors which had the highest current flow. His appears to be the only dynamic model in the literature.

Ollos (1961) constructed a three-dimensional, physical model using pipes, and used it to describe the drawdown near a production well in a fissured aquifer.

Herbert and Rushton (1966) discussed the modelling of Darcy flow by resistance networks. They found that the water table was best modelled by Redshaw's (1948) algorithm. For fissure

flow however, a less complicated algorithm may be used in which the partially empty pipes have a hydraulic conductivity described by their wetted perimeter. This is the Hazen-Williams equation described in Jeppson (1977, p40).

The transition from fissure flow to pipe flow localised along the lines of fissure intersections, would be best modelled using the Finite-element method of Wittke (op cit). His method of 'stitching' the edges of elements from intersecting fissures together, by simply giving them the same node numbers would have to be modified. The cross-section of a fissure intersection differs from that of a single fissure because the fissure intersection has zero flow wallrock conditions at only the four corner points. The fissure intersection would need to be represented by separate elements since their boundary conditions will lead to higher initial hydraulic conductivities parallel to the axis of the intersection. Fluids of different chemical composition will meet at fissure intersections so that the greatest rate of wallrock solution will occur adjacent to these elements, Fig 28.

Finite-element models to explore the transition from fissure flow to a predominance of flow along fissure intersections would be of theoretical interest. That this transition does occur at an early stage has been established in Chapter 2. For practical purposes however, a model which describes as large a system as possible is of more interest.

5.2 Model presented.

A numerical model to illustrate the dynamics of a pipe network subjected to internal erosion does not seem to have

been constructed before. The many complicating factors observed in natural systems, may be added to the model as data sets describing them are acquired. The model is constructed as a simple loop which is iterated to represent time steps. Within one cycle: the size distribution and connectedness of the pipes is determined; conductivities and thence flowrates and headlosses are calculated for each pipe in the system; and finally the internal erosion of each pipe is worked out as a function of flowrate, water aggressiveness, and lithological factors, etc..

The present model is also simple in that pipes are generated to represent major fault/bedding intersections at only one scale. Fault and bedding plane separations can be on any spacing but are oriented rectilinearly. This input is through the function 'STARTSQNET', Fig 44. Several stream sinks and resurgences may be chosen in the function 'FIN', Figs 45 and 46. Flowrates are calculated on the basis of a constant head however; runoff and an internal water table are not computed in the function 'DEV', Figs 47 to 49. Furthermore, the computation is by the inversion of a sparse node conductance matrix, Jennings (1977, pp 38-47). The APL matrix inversion operator is used for the inversion, Smith (1972). The volume of material removed from pipe walls at each iteration is taken as a linear function of flowrate, so that the mischungkorrosion effect is not yet incorporated. The graphical representation is in Fortran, using a program Ignet9, Section 7.7.2, which allows interactive selection of perspective and scale, and a choice of output as an anaglyph, stereopair or three orthoscopic views. Orthoscopic views are commonly used for cave surveys but stereoscopic views are more easily appreciated when complex

systems are involved.

Two runs of this system of programs are presented. Firstly a regular cubic network of equal sized pipes, Fig 36. Figures 37 and 38 show the flowrates in such a system when one input and two symmetrical outputs are available. Note that the three-dimensional position of the pipes in the network is important. Flows concentrate near stream sinks and resurgences, but are diffuse between. Figure 39 shows a lateral orthoscopic view of the flownet in Figs 37 and 38. A cantor set, (Mandelbrot, 1977) was chosen to illustrate the relative magnitudes of the flowrates in the system because an orthoscopic view then presents the maximum flowrate in that plane.

Figures 40 and 41 show tha distribution of pipe sizes used in the second run of the program suite. Equal spacing is used again, though this is not a program restriction. In this run, two inputs and two outputs are used. Figures 42 and 43 illustrate the extreme degree to which the larger flowrates are concentrated near sinks and resurgences in systems of many pipes, regardless of pipe size. Because the version of the program 'DEV' given in Figs 47 to 49 does not examine for a water table or set a maximum flowrate for the system, the pipes increase in size at constant relative rates in subsequent iterations. The model is equivalent to a phreatic system.

The addition of mischungkorrosion criteria and of exponential decay of solvent aggressiveness would alter this picture, as would the presence of a water table. The water table would be lowered in a constant flow system as pipes at deeper levels enlarge. It would be computationally more efficient to perform the matrix inversion using routines designed for sparse matrices. Jeppson (op cit) and Sharir and

Fig 36:

Print of an anaglyphic drawing: red and green, right and left images of a stereopair superimposed. A simple network of pipes formed at the intersections of nine equally spaced, equally sized fissures in three orthogonal directions.

Fig 37:

Left stereo image of pipe network in Fig 36. Flowrates, 'VFL1', calculated in the function 'DEV' for the input and outputs shown in Fig 28, with constant head. Key:

Percentage of maximum flow.	Percentage of gaps in line.	Number of pipes.
80-100%	Full line.	2.
60-80%	20.	6.
40-60%	10, 20, 10.	0.
20-40%	5,10,5,20,5,10,5.	32.
0-20%	Blank.	14.
	Total = 3 . 18 =	54.

Fig 38:

Right stereo image of flowrates in the pipe network of Fig 37. Input and output points are arrowed.

Fig 39:

Orthoscopic view of the flownet in Figs 37 and 38.

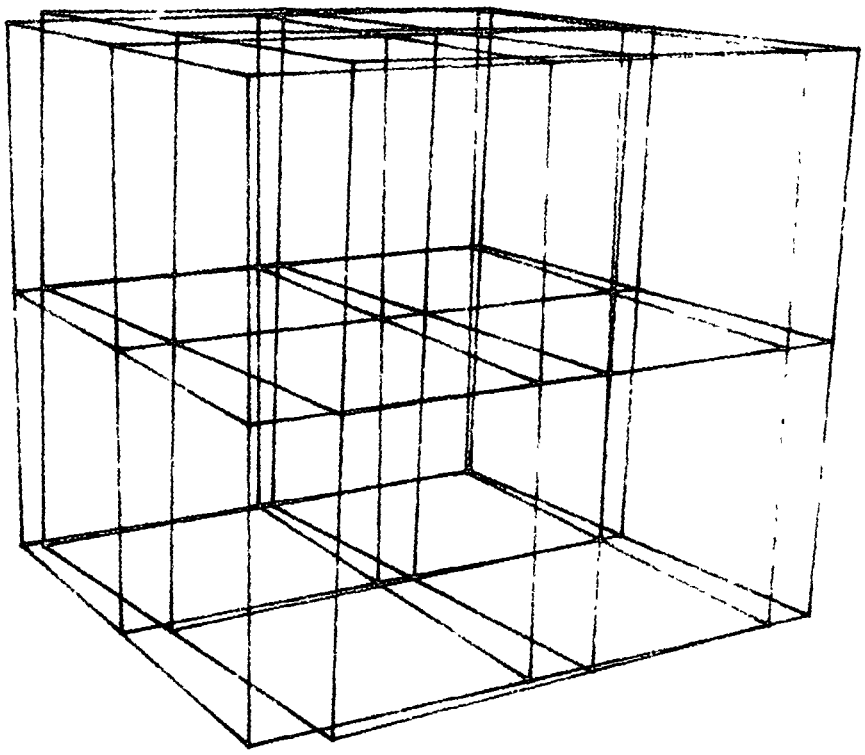

ANAGLYPH OF PIPE NETWORK :-

ITERATION NUMBER 0.

Fig 36

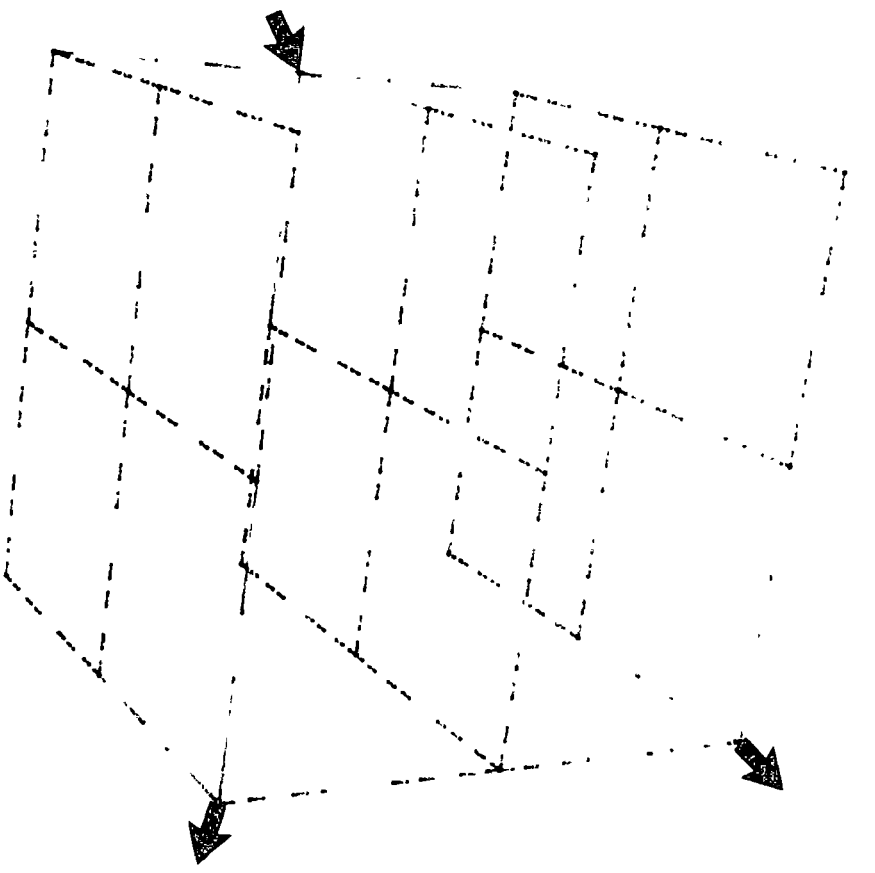

STEREO PAIR OF PIPE NETWORK :

RIGHT IMAGE

ITERATION NUMBER 2.

Fig 38

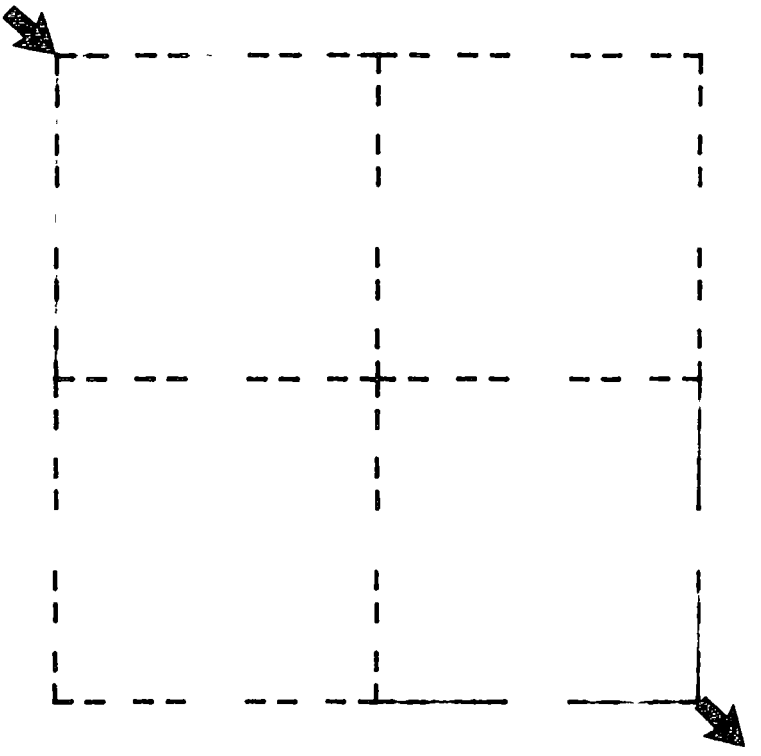

ORTHOSCOPIC PROJECTION .

VIEW DOWN X (SIDE) AXIS .

Fig 3

Fig 40:

Left stereo image of a pipe network, grouped as in the key to Fig 37, but for percent maximum size. Three orthogonal sets of 5 by 5 by 3 fissures with pipe sizes taken as the maximum of each pair of intersecting fissures. There is a linear decrease in fissure size with: the vertical, or depth axis; from right to left; and from back to front.

Fig 41:

Right stereo image of the pipe network in Fig 40.

Fig 42:

Left stereo image to show flowrates, 'VFL1', from the function 'DEV', applied to the pipe network of Figs 40 and 41. Constant head, with the inputs and outputs shown in Fig 43. Flowrates are grouped as in the key to Fig 37.

Fig 43:

Right stereo image of Fig 42, with inputs and outputs arrowed.

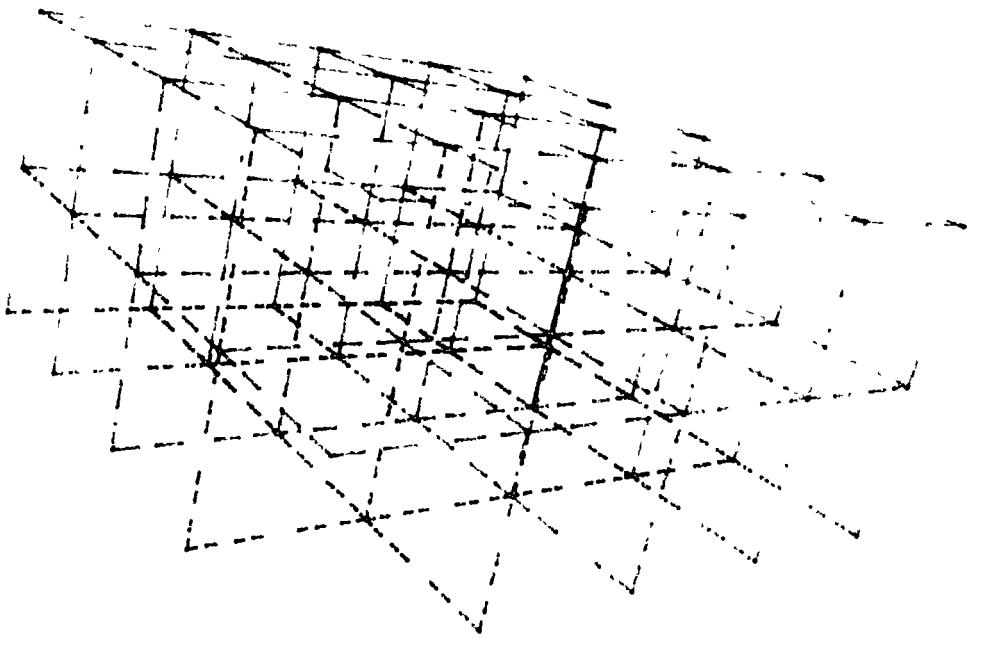

STEREO PAIR OF PIPE NETWORK :

RIGHT IMAGE

ITERATION NUMBER 0.

Fig 41

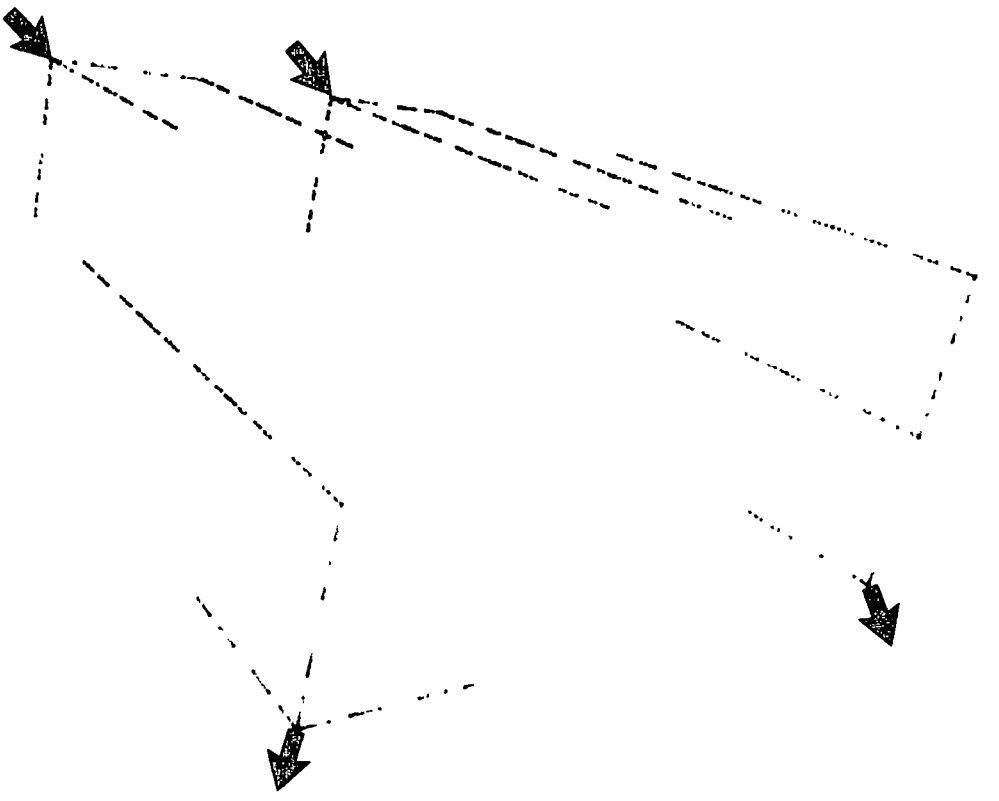

STEREO PAIR OF PIPE NETWORK :

RIGHT IMAGE

ITERATION NUMBER 2.

Fig 43

Fig 44:

APL function 'STARTSQNET' used in Figs 36 to 43.

Fig 45:

APL function 'FIN' used in Figs 36 to 43.

Fig 46:

APL function 'FIN' continued.

Fig 47:

APL function 'DEV' used in Figs 37, 38, 39, and 42, 43.

Fig 48:

APL function 'DEV' continued.

Fig 49:

APL function 'DEV' continued, and the function 'PERSPECTIVE' used in 'STARTSQNET'.

Fig 50:

APL functions 'PIPESF', 'SORT', and 'DEGREE'.

```
      ∇STARTSQNET[□]∇
    ∇ STARTSQNET;N;FERS;FIF
[1]   ⍝ ASSEMBLE MATRICES , FORMAT O/P FOR NETPLOT
[2]   ⍝    IN *PTNX+*GHOST .
[3]   ⍝
[4]     ''
[5]     ' THE Y AXIS IS VERTICAL IN *IG ;'
[6]     '      Z IS POSITIVE AWAY FROM YOU ;'
[7]     ' AND X IS POSITIVE TO YOUR RIGHT .'
[8]     ''
[9]   L1:'INPUT VECTOR OF PLANAR PIPE NET INTERSECTIONS ON X
      AXIS'
[10]    X←⍞□
[11]  L2:'INPUT VECTOR OF PLANAR PIPE NET INTERSECTIONS ON Y
      AXIS'
[12]    Y←⍞□
[13]  L3:'INPUT VECTOR OF PLANAR PIPE NET INTERSECTIONS ON Z
      AXIS'
[14]    Z←⍞□
[15]  ⍝
[16]  L4:FERS←FERSPECTIVE(⌊/X),(⌈/X),(⌊/Y),(⌈/Y),(⌊/Z),(⌈/Z)
[17]    X←X[⍋X]-FERS[2]
[18]    Y←Y[⍋Y]-FERS[3]
[19]    Z←Z[⍋Z]-FERS[4]
[20]    FERS←  1  30  ⍴  30  4  ⍴1↑FERS
[21]  ⍝
[22]  ⍝ ASSEMBLE MATRICES OF COORDINATES ,
[23]  ⍝ PIPES PARALLEL TO X AXIS IN XZ,
[24]  ⍝
[25]    FIF←((X,Z,Y) PIPESF(⍴X),(⍴Z),⍴Y)[⍋ 1 3 2 4 6
      5]
[26]  ⍝
[27]  ⍝ PIPES PARALLEL TO Z AXIS IN ZX,
[28]  ⍝
[29]    FIF←FIF,[1]((Z,X,Y) PIPESF(⍴Z),(⍴X),⍴Y)[⍋ 2 3
      1 5 6 4]
[30]  ⍝
[31]  ⍝ PIPES PARALLEL TO Y AXIS IN YZ,
[32]  ⍝
[33]    FIF←FIF,[1]((Y,Z,X) PIPESF(⍴Y),(⍴Z),⍴X)[⍋ 3 1
      2 6 4 5]
[34]    N←1↑⍴FIF
[35]  ⍝
[36]  ⍝ OUTPUT
[37]  ⍝
[38]    OF←FERS,[1](1 30 ⍴ 30 0 ⍴N),[1](10 *3 ⍴ 0 *3 ↓FIF)
[39]    OF←OF,[1] 10 *3 ⍴ 0 3 ↓FIF
[40]    ''
[41]    'OUTPUT TS IN OF  .'
[42]    ')SINK F4;OF;)SINK *MSINK*;FINISQNET.'
[43]  ⍝
[44]    FILL←1+/(0 *3 ↓FIF)- 0 3 ↓FIF
      ∇
```

Fig 44

```
      ∇FIN[□]∇
     ∇ FIN;DX;DY;DZ;N;MJ
[1]   A ASSEMBLE MATRICES , FORMAT O/F FOR NETPLOT
[2]   A    IN ⍟PIPEX+⍟GHOST ,
[3]   A    THEN USE 'DEVELOP' FOR THE FIRST TIME .
[4]   A
[5]    ''
[6]   L1:'VECTOR OF PIPE INTERSECTIONS ON X AXIS IS :-'
[7]    □← 6 ¯1 ⍕X
[8]    'NOTE : -'
[9]    '          PIPE DIAMETERS ARE TO BE GROUPED INTO'
[10]   '          20 PERCENT BINS ; BIN 5 = 0 TO 20 PCT'
[11]   '          NOT DRAWN .'
[12]   'INPUT VECTOR OF PIPE DIAMETERS INTERSECTING X AXIS'
[13]   DX←,□
[14]   →L-2 IF(⍴DX)-⍴X
[15]   ⎕ERROR
[16]   →L 1
[17]  L2:'VECTOR OF PIPE INTERSECTIONS ON Y AXIS IS :-'
[18]   □← 6 ¯1 ⍕Y
[19]   'INPUT VECTOR OF PIPE DIAMETERS INTERSECTING Y AXIS'
[20]   DY←,□
[21]   →L-3 IF(⍴DY)=⍴Y
[22]   ⎕ERROR
[23]   →L-2
[24]  L3:'VECTOR OF PIPE INTERSECTIONS ON Z AXIS IS :-'
[25]   □← 6 ¯1 ⍕Z
[26]   'INPUT VECTOR OF PIPE DIAMETERS INTERSECTING Z AXIS'
[27]   DZ←,□
[28]   →L-4 IF(⍴DZ)=⍴Z
[29]   ⎕ERROR
[30]   →L 3
[31]  A
[32]  A SELECT LARGEST PIPE DIAMETER FROM EACH TWO PLANES,
[33]  A PIPES PARALLEL TO X AXIS IN XZ,
[34]  A
[35]  L4:DIF←,(,DZ∘.,⌈DY)∘.,X(¯1+⍴DX)⍴1
[36]  A
[37]  A PIPES PARALLEL TO Z AXIS IN ZX,
[38]  A
[39]   DIF←DIF,,(DX∘.,⌈DY)∘.,X(¯1+⍴DZ)⍴1
[40]  A
[41]  A PIPES PARALLEL TO Y AXIS IN YZ,
[42]  A
[43]   DIF←DIF,,(DZ∘.,⌈DX)∘.,X(¯1+⍴DY)⍴1
[44]  A
[45]  A OUTPUT
[46]  A
[47]   OF← 10 0 ⍕ 1 2 ⍴ITN←0
[48]  A THAT WAS THE INITIAL ITERATION NUMBER ,
[49]  A FOR TONEY7 ,
[50]   OF←OF,[1] 10 0 ⍕⍪(2,⍴DIF)⍴(5-⌊5×DIF-
       0.0001+⌈/DIF),(⍴DIF)⍴2
[51]   ''
[52]   'OUTPUT IS IN OF ,'
[53]   ''
```

Fig 45

```
[54]   'OUT FIRST SET OF TOPOLOGY OF JUNCTIONS'
[55]   'AND PIPE NUMBERS , READY FOR DEVELOP.'
[56]   'I/P, O/P, POINTS AND I/P FLOWRATES'
[57]   'WILL BE INPUT NOW UNLESS YOU ANSWER N'
[58]   →L5 IF 'N'=1↑⍞,' '
[59]   ''
[60]   'MATRIX OF JUNCTION NUMBERS (MJ) , FROM BOTTOM TO TOP
       :-'
[61]   ⍞←MJ←⍉ZX⍴,X/⍉ZX←(⍴⍉),(⍴Z),⍴X
[62]   ''
[63]   ⍞←'THERE ARE ',(⍕NP←+/X/(3 3 ⍴⍉ZX)+¯1×(⍳3)∘.=⍳
       3),' PIPES'
[64]   ⍞←'       AND ',(⍕NJ←X/⍉ZX),' JUNCTIONS .'
[65]   ''
[66] A VJS,F , ORDERED VECTORS OF JUNCTION NUMBERS .
[67] A
[68]   VJS←SORT MJ
[69]   VJF←, 0 1 ↓VJS
[70]   VJS←, 0 ¯1 ↓VJS
[71] A
[72] L6:'INPUT VECTOR OF INPUT JUNCTIONS , (VIPJ)'
[73]   'OR ¯1 FOR REPEAT OF MJ :-'
[74]   →L8 IF   ⌊≠1↑VIPJ←⍞,0
[75]   ⍞←MJ
[76]   →L6
[77] A/:'INPUT VECTOR OF INPUT FLOWS (VIPF) :-'
[78] A→L8 IF(⍴VIPJ)=⍴VIPF←⍞,0
[79] AIPERROR
[80] A→L6
[81] L8:VIPF←(⍴VIPJ)⍴1
[82]   'INPUT VECTOR OF OUTPUT JUNCTIONS (VOPJ)'
[83]   'OR ¯1 FOR REPEAT OF MJ :-'
[84]   →L10 IF ¯1≠1↑VOPJ←⍞,0
[85]   ⍞←MJ
[86]   →L8
[87] AL9:'SPECIFY WHETHER RUNOFF ALLOWED FROM IP JUNCTIONS ,
       Y/N : '
[88] A→L10 IF 'N'=1↑⍞,0
[89] AGOV←VIPF-(,(((⍴X)×⍴Z),⍴⍉)⍴⍉)[VIPJ]+1-⌊/⍉
[90] A
[91] A WHAT ELSE COULD G OVERFLOW BE ?
[92] A
[93] A→L5
[94] L10:GOV←(⍴VIPJ)⍴0
[95] L5:'OUTPUT IS IN OP'
[96]   ')SINK F5;OP;)SINK *MSINK*;)ERASE OP;)SAVE NET;)OFF.'
[97]   'EDIT OUT LINES 1 OF F4 AND F5 .      '
[98]   'AND CHANGE ALL NOTS TO -'
[99]   'IN *API;)LOAD NET2;DEVELOP N;ETC..'
[100]  '                              N TIMES .'
     ∇
```

Fig 46

```
      ∇DEV[[]]∇
    ∇ DLV N;I;J;G;GIF;E;VH;VFL0;VFL1;NCM;NV;LH;GOF;TOTG;LS;K
      ;RE;M;H;MFH
[1]   A THIS FUNCTION WILL TAKE THE VARIABLES :-
[2]   A G(NET) , GIF , GOF , GOV(OVERFLOW)
[3]   A AND [1] FORM THE NODE CONDUCTANCE MATRIX (NCM),
[4]   A       [2] SOLVE FOR NODE VOLTAGES USING TOTAL FLOW (TOT
      F),
[5]   A       [3] CHECK FOR WATER TABLE POSITION (REDSHAW) ,
[6]   A       [4] UPDATE FLOW , DIF , VFL ETC ,
[7]   A       [5] LOOPING N TIMES , WITH )SINK 15
[8]   A
[9]    □← 10 0 ⍕ITN,ITN+N
[10]   NV←(¯1↓1↑⍉ZX)××X/1↓⍉ZX
[11]   TOTG←(+/VIFF)-2÷(⌈/Y)-L/Y
[12]   GOF←(+/VIFF)-⍴VOFJ
[13]   T←1⋄K←0
[14]  A
[15]  A       [1] SET ORDERED VECTOR OF PIPE CONDUCTANCES,
[16]  A
[17]   G←-32×1.31E¯6×PI×L-9.808×DIF*2
[18]  L1:J←1
[19]   NCM←(NJ,NJ)⍴0
[20]  A
[21]  A INFILL OFF-DIAGONAL ELEMENTS OF NCM,
[22]  A
[23]  L2:NCM[VJS[J];VJF[J]]←G[J]
[24]   J←J+1
[25]   →L2 IF J≤NF
[26]   NCM←¯1×NCM+⍉NCM
[27]   J←1
[28]  A
[29]  A INFILL DIAGONAL ELEMENTS OF NCM,
[30]  A
[31]  L3:NCM[VJS[J];VJS[J]]←NCM[VJS[J];VJS[J]]+G[J]
[32]   NCM[VJF[J];VJF[J]]←NCM[VJF[J];VJF[J]]+G[J]
[33]   J←J+1
[34]   →L3 IF J≤NF
[35]  A
[36]  A NOW ADD O/F , I/F CONDUCTANCES (GOF) , (GIF),
[37]  A
[38]   J←1
[39]  L6:NCM[VOFJ[J];VOFJ[J]]←NCM[VOFJ[J];VOFJ[J]]+GOF
[40]   J←J+1
[41]   →L6 IF J≤⍴VOFJ
[42]   J←1
[43]  L7:NCM[VIFJ[J];VIFJ[J]]←NCM[VIFJ[J];VIFJ[J]]+GOV[J]×
      VIFF[J]
[44]   J←J+1
[45]   →L7 IF J≤⍴VIFJ
[46]  A
[47]  A FROM G×H_F , H=1 ; GIF=VIFF
[48]  A
[49]   GIF←(+/((⍳NJ)∘.=VIFJ)\VIFF
[50]   '''EAD W] GO ',⍕K←K+1
[51]   ''
```

Fig 47

```
[52] A□←'NCM : '
[53]  NCM←(NCM,(NJ,1)⍴GIF),[1] GIF,TOTG++/VIFF
[54]  ''
[55] A□←'⍴NCM    ',⍕⍴NCM
[56] A''
[57] A□←'NCM≠0     :-'
[58] A□←NCM≠0
[59] A''
[60] A
[61] A      CONDENSE NCM TO REMOVE ROWS AND COLUMNS OF ZEROS,
[62] A      [2] AND SOLVE FOR JUNCTION POTENTIALS .
[63] A
[64]  NCM←LS/[1](LS←∨/NCM≠0)/NCM
[65]  ''
[66]  □←'⍴NCM ',⍕⍴NCM
[67]  ''
[68]  □←'NCM≠0    :-'
[69]  □←NCM≠0
[70]  ''
[71]  □←'LS   :   ', 6 0 ⍕LS
[72]  ''
[73]  □←'VH :- ', 6 ¯1 ⍕VH←¯1↓LS\,((((+/¯1↓LS),1)⍴0),[1]+/
      VIFF)⌹NCM
[74]  ''
[75] A
[76] A      [3] REDSHAW/BUSHTON ITERATIVE ALGORITHM TO RESET
      G VALUES
[77] A          MT/HR , ELEVN./FLOW HEADS , START/FIN. ORDERE
      D PIPES.
[78] A
[79] AMTH←SORT ↑ΣX⍴Q((X/1↓↑ΣX),⍴T)⍴T+1-⍳/T
[80] A□←'MTH          MFH          '
[81] A□← 6 ¯1 ⍕MTH,MFH←SORT ↑ΣX⍴VH
[82] A''
[83] ARF←((NF-NV)⍴1),NV⍴0
[84] A□←'G   :- ', 6 ¯1 ⍕G←(GX∼RE)+GXRE∧∧/LS←MTH⍷MFH
[85] A''
[86] A□←'G   :- ', 6 ¯1 ⍕G←(GX∼RE)+(RE∧≠/LS)X(0⍲(⌈-/MFH)-(⌈/MF
      H-MTH)
[87] A''
[88] A□←'IF¯6)+/MFH      ,      ∧/LS      ,      ∧      : '
[89] A→L1 IF 0<+/□←|(□←∧/LS)-□←1E¯6)+/MFH
[90] A
[91] A      [4] NOW SOLVE FOR FLOWS (VFL1) FROM POTENTIALS (V
      H).
[92] A
[93]  VFL1←GXVH[VJS]-VH[VJF]
[94]  DIF←VFL1xDIF 1.31E¯6
[95] A
[96] A UPDATE DIF AS FN.(VFL1 , DIF)
[97] A NOTE : NEEDS AGGRESSIVENESS BUILT IN.
[98] A NOTE : DISTANCE FROM SOURCE TO BE BUILT IN
[99] A          FOR BOTH MERCADO/HARRISON AND
[100]A          BOGLI EFFECTS .
[101] DIF←((DIF*2)+(4x|VFL1)-01)*0.5
[102]A
```

Fig 4c

```
[103]A RESET VFL0 VFLΔ , FROM VFL1 ; FORMAT OUTPUT TO MTS F5
      .
[104]A
[105] →L8 IF ITN≠0
[106] VFL0←VFL1
[107]L8:VFLΔ←VFL1-VFL0
[108] VFL0←VFL1
[109] OF← 10 0 ⍕ 1 2 ⍴ITN
[110]A OF←OF,[1] 10 0 ⍕⍉(2,⍴VFLΔ)⍴(10.5+5×VFL1 (+/VIFF)-+/GO
      VxVH[VIFJ]),1+VFLΔ≤0
[111] OF←OF,[1] 10 0 ⍕⍉(2,⍴VFL1)⍴(5 15×|VFL1-
      0.0001+⌈/VFL1),(⍴VFL1)⍴2
[112] I←I+1
[113]A
[114]A      [5] ITERATE TO TIME STEP ,
[115]A          IF MAX. REYNOLD'S NO. < 2100.
[116]A
[117] →L9 IF 2100<⌈/RE
[118] →L1 IF I≤N
[119] →L10
[120]L9:'TURBULENT FLOW IN ≥1 PIPE INVALIDATES CALCULATION .'
      .
[121] 'REPLACE ITS,ITF IN OF BY :', 10 0 ⍕ITN,ITN+I
[122] 'PRESENT LINE READS      :', 10 0 ⍕ITN,TTN+N
[123]L10:'REYNOLD''S NUMBERS ARE:-', 10 3 ⍕RE
[124] ITN←ITN+I
    ∇
```

```
      VCROSSECTIVE[⎕]∇
    ∇ RES←CROSSECTIVE IF;R;C
[1]   A R      RADIUS OF SPHERE OF INTEREST .
[2]   A XYZ C  CENTRE OF S,O,I,
[3]   A
[4]    R←0.5×⌈/IF[1 3 5]-IF[2 4 6]
[5]    C←IF[2 4 6]+R
[6]    R←(+/R*2)*0.5
[7]    RES←R,C
    ∇
```

FIG 49

```
      ∇F[⎕]∇
    ∇ RES←ABC PIPESF S;PS;FF;A;B;C;M;I;FC
[1]   ⍝ ASSEMBLES MATRIX OF START , FINISH , XYZ COORDS
[2]   ⍝ FOR PIPES IN PARALLEL PLANES GIVEN BY ABC ;
[3]   ⍝ SPLIT BY S ; AND THROUGH 3D ARRAY M .
[4]   ⍝
[5]    A←S[1]↑ABC
[6]    B←S[2]↑S[1]↓ABC
[7]    C←(¯1⌽S[3])↑ABC
[8]   ⍝
[9]    RES←⍬
[10]   FC←3,×/ ¯1 0 +2↑S
[11]   I←1
[12]  L1:M←(⍳2↑S)⍴A
[13]   M←M,[0.5]⍉(2↑S)⍴B
[14]   M←M,[1](⍳2↑S)⍴C[I]
[15]   PS←⍉FC⍴, 0 0 ¯1 ↓M
[16]   FF←⍉FC⍴, 0 0 1 ↓M
[17]   RES←RES,[⍳] PS,FF
[18]   I←I+1
[19]   →L1 IF I≤S[3]
[20]   RES← 1 0 ↓RES
    ∇

      ∇SORT[⎕]∇
    ∇ SF←SORT M;S;F
[1]   ⍝ OUTPUTS ORDERED VECTORS S,F
[2]   ⍝ AS TWO COLUMN MATRIX OF PIPE
[3]   ⍝ START/FIN. JUNCTION NUMBERS .
[4]   ⍝
[5]   ⍝ M , MATRIX OF JUNCTION VALUES .
[6]   ⍝ S/F , VECTORS OF ORDERED JUNCTION VALUES.
[7]   ⍝
[8]    S← , 0 0 ¯1 ↓M
[9]    F← , 0 0 1 ↓M
[10]   S←S,, 1 3 2 ⍉ 0 ¯1 0 ↓M
[11]   F←F,, 1 3 2 ⍉ 0 1 0 ↓M
[12]   S←S,,⍉ ¯1 0 0 ↓M
[13]   F←F,,⍉ 1 0 0 ↓M
[14]  ⍝
[15]   SF←⍉(2,⍴S)⍴S,F
    ∇

      ∇DEGREE[⎕]∇
    ∇ D←DEGREE XYZ;C
[1]   ⍝ OUTPUTS VECTOR OF NODAL DEGREES ;
[2]   ⍝ GIVE PT. ABC. (⍴X),(⍴Y),⍴Z .
[3]   ⍝
[4]    D←(((XYZ⍴1),[1] 0),[2] 0),[3] 0
[5]    C←(D=¯1⌽[1] D)+(D=1⌽[1] D)
[6]    C←C+(D= 1⌽[2] D)+D=1⌽[2] D
[7]    D←C+(D=¯1⌽[3] D)+D=1⌽[3] D
[8]    D←,XYZ↑D
    ∇
```

Fig 5C

Howard (1968) describe the analysis of flowrates in pipe systems taking account of non linearity at Reynolds numbers greater than 2100.

5.3 Summary.

A model is presented which solves for flowrates in a system with constant head and with erosion dependent only on flowrate. To model conditions near and above the water table, and to take account of the mischungkorrosion effect and the decrease of aggressiveness with reaction time additional algorithms would be required. The graphical presentation is adequate for the model presented since relative flowrates remain constant, but a more complex model will have a more complex evolutionary history and it would be advantageous to place output on microfilm. Anaglyphs will allow the presentation of the erosional history of a fissure system as a three-dimensional motion picture. It is not yet possible to produce computer graphics on microfilm at Durham.

6. Conclusions.

Several lines of investigation have been followed. The inter-relationship of data on: seismic anisotropy, rock chemistry, hardness, pore network characteristics, and solution kinetics, could best be studied through a numerical model. Two characteristics of faults and joints must be better understood before an adequate numerical model can be constructed. Firstly, rock surface metrology, or roughness parameters must be known for different types of fracture. Existing statistical theory will then allow the calculation of mean fissure widths and hydraulic conductivities at given stresses. Secondly, realistic numerical models of geological fracture patterns are required. Several fracture sets, covering a length range of 10 kilometers to 1 meter are typically involved in hydrological problems. A combination of two subsets of Group Theory is seen as the most promising approach.

A larger system of 3-dimensional fissures may be solved for fluid flowrates if it is modelled as a pipe network. Evidence has been presented to show that a pipe network model is in fact realistic. However, in the early stages of naturally occurring fissure flow systems, extremely large numbers of flow lines or 'pipes' are involved. The computation to solve for discrete flows is too large for existing algorithms. Effects such as mischungkorrosion could be illustrated on a model of analysable size, for theoretical purposes.

Compared with the design requirements of a computer based numerical model, speleogenesis is a complex process requiring an impracticably large and poorly known database. Empirical

analyses and direct exploration methods based on descriptive works such as those by Waltham,(1971) and Ford and Cullingford (eds, 1976) will probably continue to be the most practicable lines of investigation.

The work described in Chapter 3 indicates that studies of rock surface roughness which follow the methods of engineering surface metrology will prove very powerful in the analysis of engineering geological problems. For mineral exploration purposes, emphasis must be placed on the development of a mathematical description of fracture patterns observed across four orders of magnitude.

CONTENTS. PAGE.

7.1 Falling-head gas permeability.

7.1.1 Falling-head gas method in Ruska permeameter.

The Department of Geological Sciences in Durham acquired a Ruska Gas Permeameter in 1977.This instrument comprises:

a) three flowmeter tubes.

b) a selection switch,

c) a sensitive bourdon gauge (0-1 atm. in steps of 0.01 atm. above atmospheric pressure),

d) a sample holder with thermometer, and

e) an inlet pressure controlling valve.

It is designed for the Constant Head method which is based on Darcy's Law for gas:

$$Qav = (Kapp . A . Pm)/(u . L) \quad \ldots\ldots\ldots\ldots (29)$$

compare equations (7) and (8), where:

A (cm*2) is the cross-sectional area of the specimen,

L (cm) is it's length,

Pm (atm) the pressure drop across the specimen, measured on the bourdon gauge,

u (centipoise) is the viscosity,

Qav (cc/sec) is the volumetric flowrate, which is taken at the centre of the specimen, because the local volumetric flowrate depends upon the local pressure in the specimen.

Kapp (darcys) is the apparent permeability at the average pressure Pav (atm), where

$$Pav = (Pm + (2 \times Pa)) / 2 \quad \ldots\ldots\ldots\ldots (30)$$

where:

Pa is the atmospheric pressure.

The flowmeter tubes are calibrated against upstream pressure

at 1.0, 0.75 and 0.25 atm. (see Anon.). Three determinations of 'Kapp' are made and plotted against reciprocal 'Pav'. The intercept (Kinf [darcys]) of the best fitting line on the 'Pav=infinity' axis is taken as being equivalent to the permeability for an inert liquid. The extrapolation proceedure is based on the Klinkenberg equation:-

$$Kapp = Kinf \times (1 + (b / Pav)) \quad \ldots\ldots\ldots\ldots\ldots (31)$$

Klinkenberg (1941), Rose (1948). A program was written to solve (Pressure, time) values for 'Kinf' and the constant 'b' directly, but the matrix is ill conditioned, so the method to be described below was retained.

The flowmeter tubes cover the range 0.185 to 60.0 [cc/sec] and since gauge pressures (Pm) of 1.0 and 0.25 atm. should be used, a specimen which is say a one inch cube will allow a range from 1.27 to 1650 [millidarcys] to be covered. Figure 51a, after Raudkivi and Callander (1976) shows that this corresponds to the range of permeabilities for petroleum reservoir lithologies, or 'oil rocks'; and is well above the range of permeabilities associated with 'good limestone'.

Typical values of hydraulic conductivity and intrinsic permeability

$\log_{10} K(m/s)$	0	-1	-2	-3	-4	-5	-6	-7	-8	-9	-10	-11	-12	-13
Permeability	Pervious					Semipervious				Impervious				
Aquifer	Good						Poor			None				
Soils	Clean gravel		Clean sand or sand and gravel				Very fine sand, silt loess, loam, solonetz							
						Peat			Stratified clay			Unweathered clay		
Rocks						Oil rocks				Sandstone		Good limestone dolerite	Breccia granite	

$\log k(m^2)$	-7	-8	-9	-10	-11	-12	-13	-14	-15	-16	-17	-18	-19	-20
$\log_{10} k(md)$	8	7	6	5	4	3	2	1	0	-1	-2	-3	-4	-5

DIAGRAM OF PERMEABILITIES (millidarcies) AFTER RAUDKIVI & CALLANDER (1976)

DIAGRAM OF VOLUMES AND PRESSURES IN RUSKA GAS PERMEAMETER

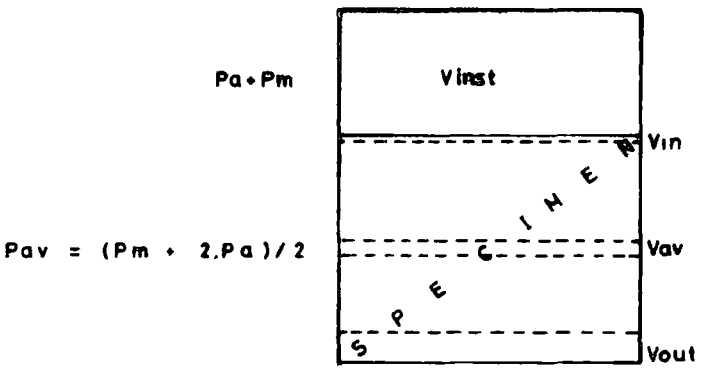

KEY

Pm , measured pressure

Vin , Vav , Vout , infinitessimal expanding volume of gas flowing through specimen

Vinst , volume of gas in permeameter between specimen and pressure-control or shut-off valve.

Fig 51

Low permeabilities in soils and concrete are usually determined by a Falling-head water method, with the attendant difficulties discussed in Section 7.2.1.. In fact three main methods have been used to determine either the permeability of a porous medium, or the viscosity of a gas, employing a falling head of the gas (Calhoun and Yuster, 1947a). They are:

> "1, maintaining a constant upstream pressure, usually atmospheric, and measuring the rise in pressure in an evacuated downstream vessel;
>
> 2, maintaining a constant downstream pressure, usually atmospheric, and measuring the fall of pressure in a closed upstream vessel; and,
>
> 3, measuring the rise in pressure in a downstream vessel and simultaneously measuring the fall in pressure in an upstream vessel".

The pressure controlling valve on the Ruska permeameter is a very efficient seal when turned off. The enclosed gas pressure can be maintained for as long as a week, with a steel blank in the sample holder. Temperature changes accounted for all the observed variations. It is therefore suitable for the second of the above methods.

The governing formula was derived as follows:-

By Boyle's Law:

$$Vout = Vinst \times (Pm1 - Pm2) / Pa \quad \ldots\ldots\ldots\ldots (32)$$

where:

Pm1 is the first, and Pm2 the second of two measured pressures,

Vout is the volume of gas that has flowed through the specimen for the pressure drop of 'Pm1-Pm2', and

Vinst is the instrument volume, see Fig 51b.

So:

(dVout / dt) = (Vout . Vinst . dPm)/(Pa . dt)...(33)

From Fig 51b:

Vav = Vout x (2 x Pa) / (Pm + (2 x Pa))..... (34)

From Darcy's law (27), and equations(31) and (32):

Kapp={2.u.L.Vinst/A.Pm(Pm+2.Pa)}.{dPm/dt}.(1-((Pm1-Pm2)/(Pm+2Pa))..... (35)

As (Pm1-Pm2) tends to zero, the slope of the graph {dPm/dt} can be used to work out the apparent permeability 'Kapp' at a number of different points. These are then regressed against reciprocal average pressure, as described above. If discrete values of the measured pressure are read from the graph, instead of the slope, these should be close together. A 3 to 5% error is introduced for '(Pm1-Pm2)=0.1atmosphere'.

The instrument constant, 'Vinst' was determined by collecting displaced nitrogen over water, and also by testing a sandstone sample by both the falling-head and constant-head gas methods.

The bourdon gauge may be read directly and (Pm , time) values recorded together with 'Pa', 'A' and 'L'. All bourdon gauges are prone to stick, and it is tedious to wait for the full range of pressure drop required to reduce the standard error to reasonable limits. Accordingly, a Y/T chart recorder was attached to a sensitive pressure transducer inserted in the instrument's thermometer mount. The transducer used was kindly lent by Kulite (UK) Ltd. and had a range of 0-50 psi. Circuits for power supply, and partial protection from mains voltage spikes, zero adjustment and scaling were designed by Mr. J.M. Lucas. A typical curve from the chart recorder output shown in Fig 52.

Fig 52:

Falling-head gas (pressure, time) curve.

Fig 53:

APL function 'FALL2' for calculating permeability values from falling-head gas readings.

Fig 54:

APL function 'FALL2' continued.

Fig 55:

APL function 'FALL2' continued.

Fig 56:

Comparison table of falling-head gas and falling-head water permeability values for specimens of Yorkshire Chalk. Data from Patsoules (pers comm).

Falling-head gas Pressure-time curve

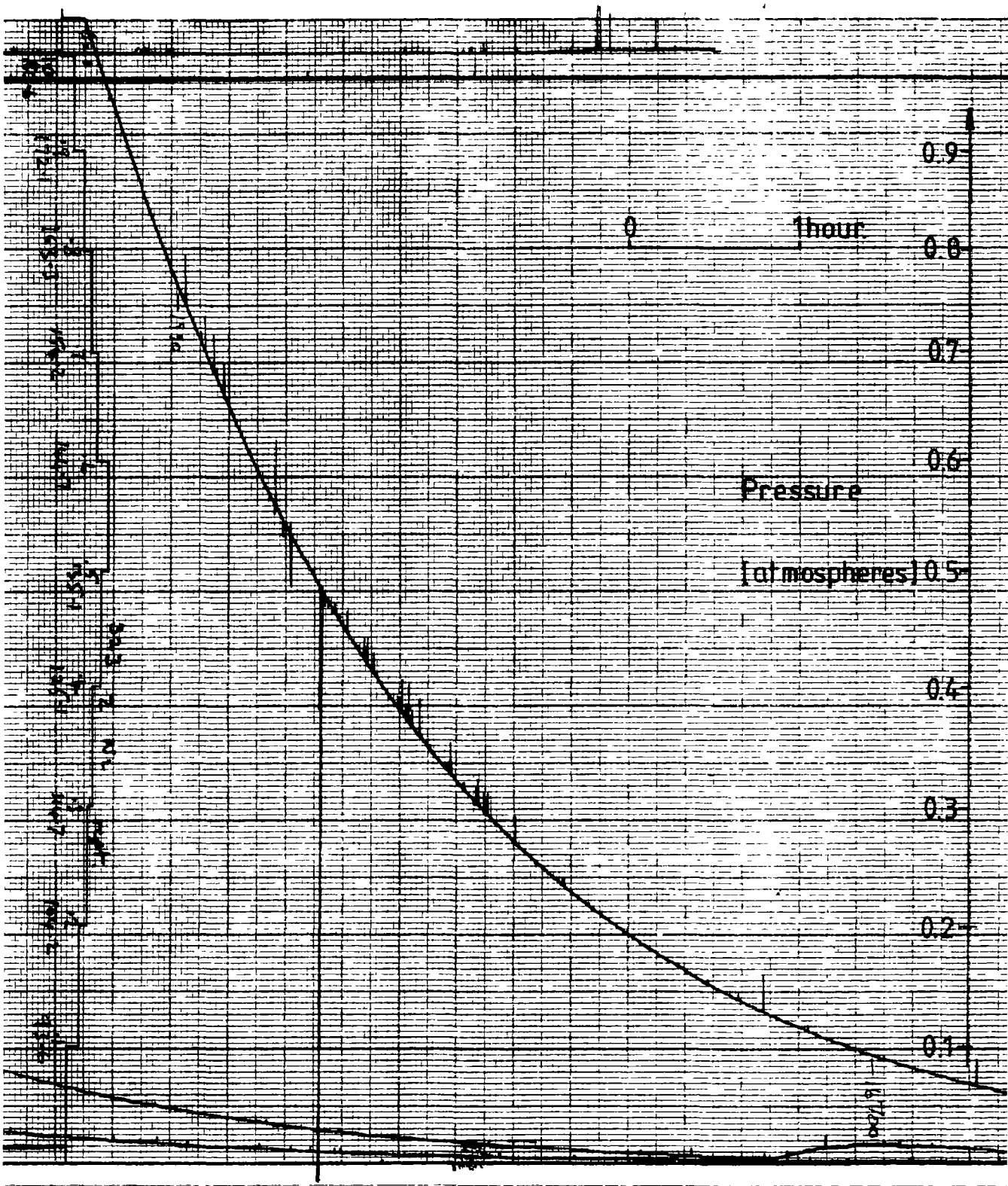

Fig 52

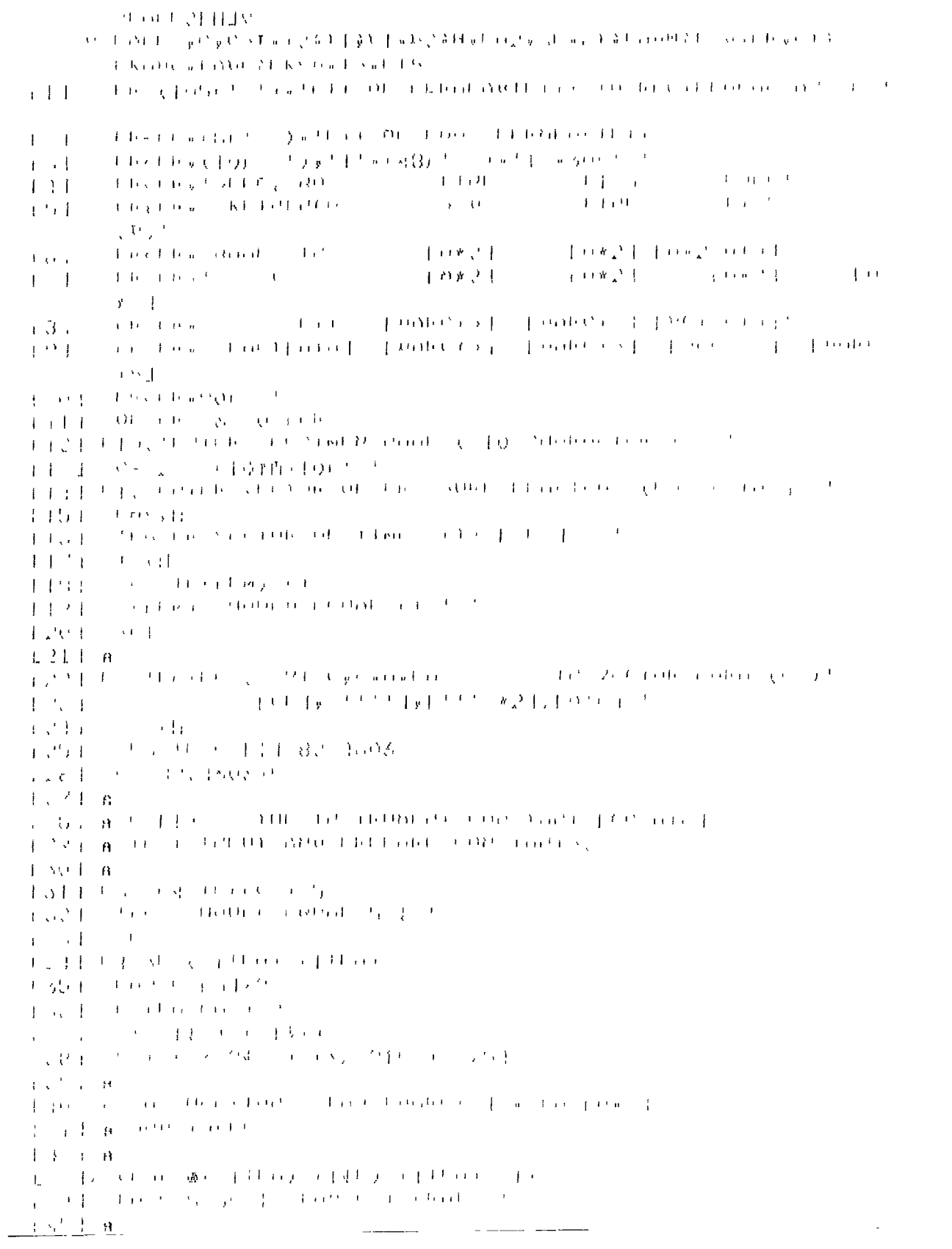

Fig 53

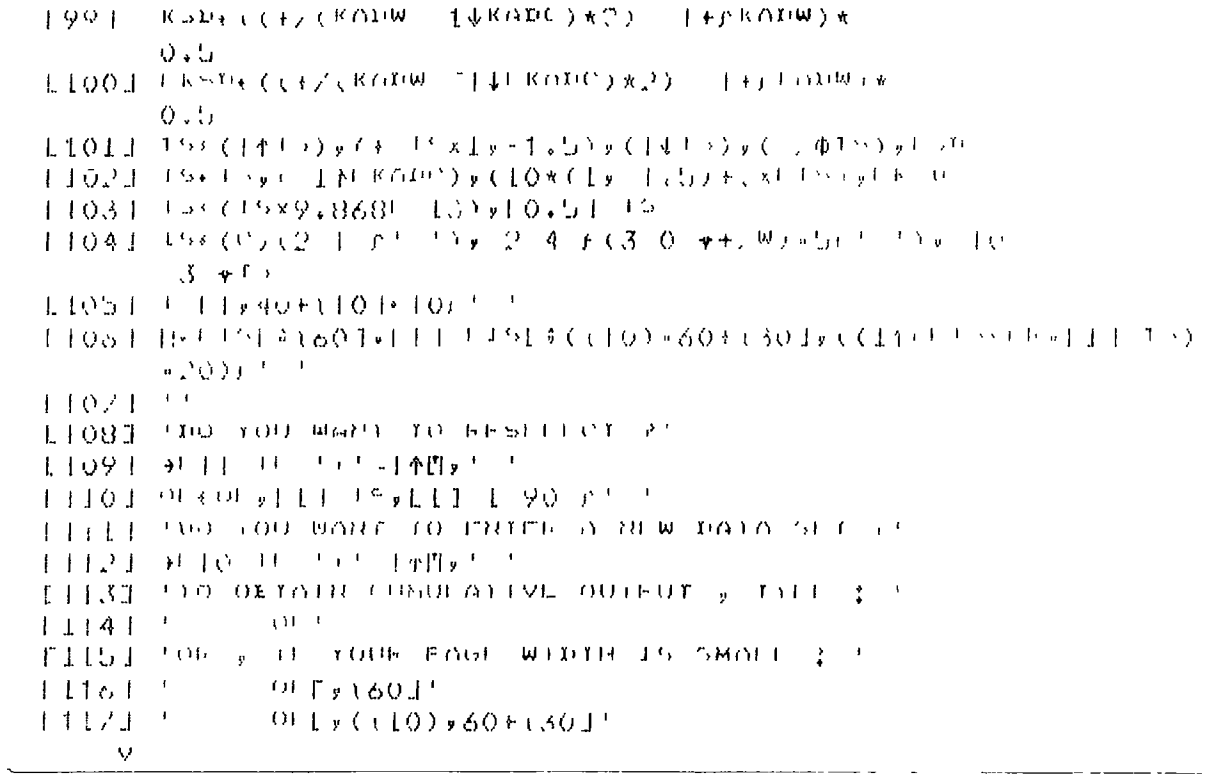

Fig 55

FALLING-HEAD GAS PERMEABILITY VALUES VS WATER PERMEABILITY
After Patsoules (pending)

	Sample	DD1/S	DD1/L	DD2/L	BH1/S	BH1/L	CRH1/L	LTH1/S	LTH1/L	B5A/L18S	B5A/50S
	Kwater	0.029	0 037	0 066	0 036	0 031	1. 08	0.021	0 018	0 045	0.056
○	Kgas (1 5atm)	0 087	0 062	0 017	0.16	0 18	0.086	0.06	0.077	0 2	0.069
◉	Kgas (infinite)	0 0008	0 012	0.002	0.03	0.054	0.001	0.004	0 013	0.087	0.029
+	$\frac{K1\ 5 + Kinf}{2}$	0 044	0.037	0 088	0.1	0 117	0 045	0 032	0 045	0 147	0.049

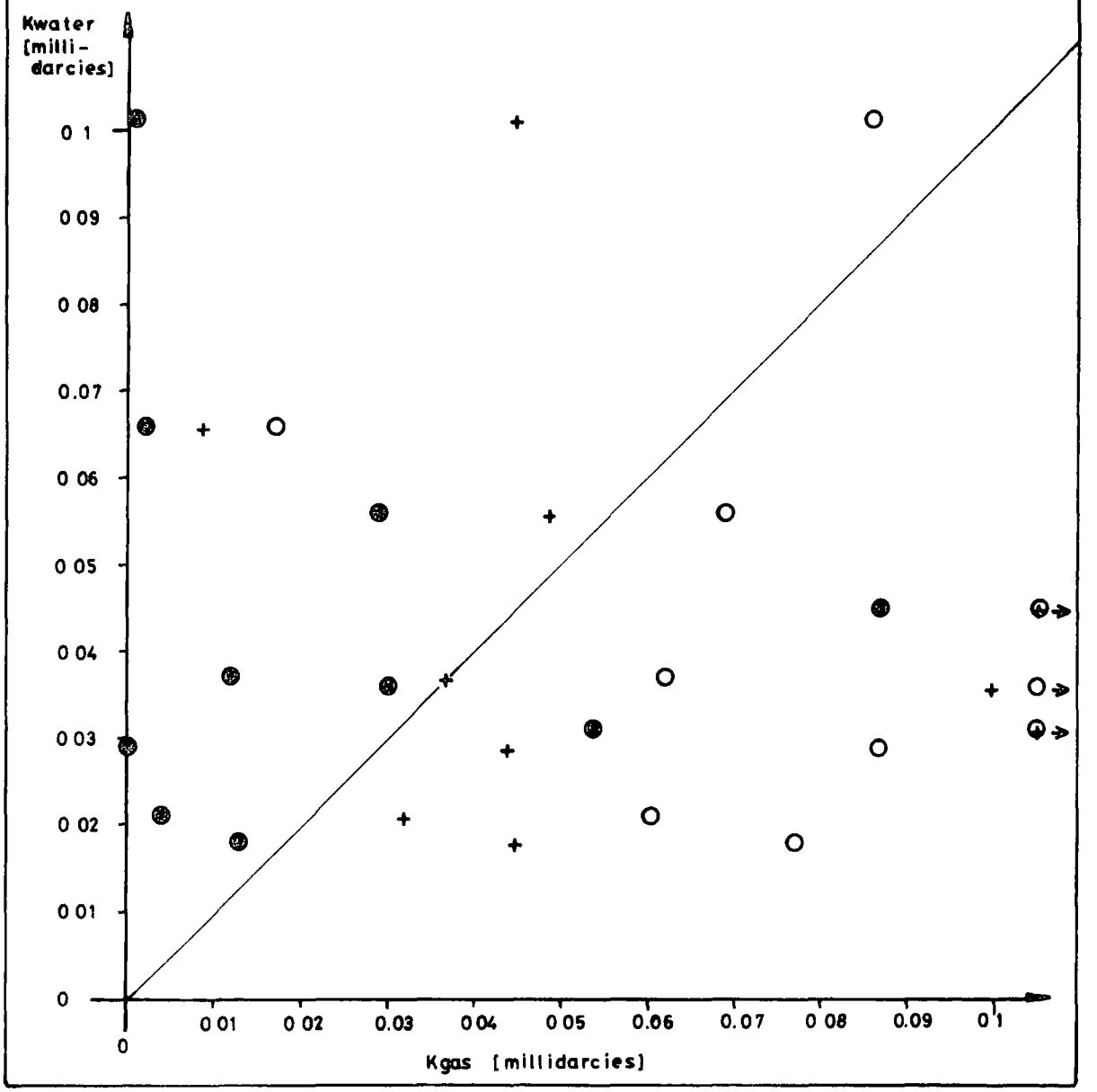

Fig 56

The function 'FALL2' is written to display the input data and the least sqares fitted lines, Figs 53 to 55. The program uses an integrated form of equation (35):

$$Kapp=\{u.L.Vinst/A.Pa.(T1-T2)\}.\ln\{(Pm1-Plav)/(Pm2-P2av)\} \quad .....(36)$$

where:

(T1-T2) is the time difference [seconds] between readings 'Pm1' and 'Pm2',

Plav, P2av are the average pressures corresponding to 'Pm1' and 'Pm2', and

ln is the natural logarithm.

This is only valid when 'Pm1-Pm2' is small, as discussed above, since second order terms in 'Pm1' and 'Pm2' have been dropped. Provision is made for selecting out unlikely looking data points: however this is no substitute for a full data set. (Time, Pm) values should be taken every 0.1 atm. or thereabouts, and seven or eight points are a minimum. It would be much better if apparatus were made to allow measurements to be made at much higher pressures since an extrapolation is made to infinite pressure. For the purposes of comparison without full extrapolation, the gas permeability is also quoted at 'Pav=1.5 atm'; equivalent to 'Pm=1.0 atm', equation (30).

Samples of Yorkshire Chalk tested by the falling-head water method in a triaxial cell at Sheffield University, by Mr. M. Patsoules were also tested by falling-head gas, Fig 56. With very low permeability samples, the standard error may be greater than the intercept value which has occasionally been negative. A fit of the logarithm of the permeability against reciprocal 'Pav' is incorporated in the program to avoid this,but such an extrapolation is without theoretical

justification. It was found that the method was adequate for measuring the low permeabilities found in weathered limestone joint block margins.

7.1.2 Anisotropy and mapping of permeability.

A sawn slab of shelly Corallian limestone was given to the author by Mr. Keith Bell, the manager of Hovingham Quarry, North Yorkshire. It represents a section through a weathered bed, most of the fresh blue colouration being replaced by cream. It was cut into one inch thick cubes to an accuracy of four thousandths of an inch. Permeability determinations were made in the two directions parallel to bedding, and in one direction normal to it.

The purpose of this was to test the variation in permeability within a specimen, and to test the suitability of the falling-head method for limestone of about 5 percent porosity. It is not relevant to the study of weathered margins; but predated it. Technical difficulties made it impossible to process large specimens that had not been acquired as sawn slabs, at that time.

Evers et al. (1967) describe the mapping of cement permeabilities for petroleum reservoir modelling purposes. Their measurements were taken in just one direction. The results for Hovingham limestone showed anisotropy due to bedding and heterogeneity due to variations in shellyness.

7.2 Wood's metal porosimetry and SEM stereopairs.

Amongst others, Swanson (1979), and Pittman and Duschatho (1970) have described the use of pore casts as a conceptual tool for visualising the nature of the pore space in rock. In this study, a very high saturation of the pore space was required so that fine detail could be seen.

It is considered to be impossible to achieve full saturation of a porous medium that is not completely dry beforehand (Turner, 1977). Air pockets are almost certain to be trapped in the network of pores with the water present forming seals across the pore throats. Soils are often tested under back pressured conditions in order to overcome this problem by dissolving the air into the water. It should be possible to thoroughly dry most rocks, without destroying their internal structure. For limestones, this is done after the samples have been cut to size by keeping them in a drying oven at 60 degrees C. for one or two days. Temperatures of 105-110 degrees C. which are used to dry soil samples, would boil off the water explosively.

To saturate with water, a vacuum dessicator with three inlets is used. One inlet is to the vacuum pump, another is to atmosphere via a tap, and the last is to a water reservoir. The water reservoir is also deaired via a line to the vacuum pump. The line connecting it to the vacuum dessicator reaches to the bottom of the latter. The sample is placed on a wire mesh several inches above the base of the dessicator. When both sample and water have been deaired for 24 hours, water is slowly run into the vacuum dessicator whilst still under vacuum. This is done slowly, so that the wetting front in the

sample is allowed to stay above the water level outside. Once the sample has been covered, the vacuum pump is switched off and the vent to atmosphere slowly opened. All voids within the pore space of the specimen should be empty. Atmospheric pressure should force water into them if the rock is water wettable, Turner (op cit).

Both Wood's metal and mercury are non-wetting liquids. Even when the pore space is evacuated, high pressure is required to achieve any degree of saturation. The Pressure of Displacement Equation (Purcell 1949, equation 3):

$$Pc = (2 \cdot It \cdot \cos(Ca)) / R \quad \text{.....(37)}$$

governs the saturation of a pore space comprising cylindrical tubes, where:

Pc is the minimum pressure required to displace a wetting liquid, or to inject a non-wetting liquid,

R is the radius of the tube,

It is the interfacial or surface tension, and

Ca is the contact angle.

The effective surface tension, 'Ite' is used where the contact angle is unknown:

$$Ite = It \times \cos(Ca) \quad \text{.....(38)}$$

'It' is calculated by comparing Wood's metal with mercury capillary pressure curves. Swanson (1979) calculates the effective surface tension for mercury to be 0.368 [J/m*2], and deduces it to be 0.210 [J/m*2] for Wood's metal.

Wood's metal is an alloy of bismuth containing lead, tin and calcium. It's melting point is 70 degrees C; and it's intrusion into rocks is done in nearly the same manner as in mercury intrusion porosimetry, except that it is done at a temperature above the melting point. A high pressure cell with two inlets

was used: both inlets had taps attatched. A cylinder of nitrogen gas and a vacuum pump were connected to the cell which was placed in the oven. The rock samples were held down inside the cell by a spring to prevent their floating in the Wood's metal. Chunks of Wood's metal were packed into the remaining space over an aluminium foil liner.

The cell was sealed by an 'O' ring and vacuum grease then evacuated for about two hours. Next, the oven was switched on and the cell brought to about 100 degrees C and held there for about three hours. The vacuum pump was then switched off and it's tap was closed. Next, the nitrogen gas cylinder's tap was opened and 900 psi (3.3 MPa) applied to the surface of the liquid Wood's metal. The oven was switched off, and the cell allowed to cool to room temperature for about twelve hours whilst under pressure.

The rock samples were sawn out of the Wood's metal and broken across before being treated with dilute hydrochloric acid. The exposed pore casts were mounted on Scanning Electron Microscope studs. Carbon coating of the specimens was not necessary as they were sufficiently conductive.

At the highest resolution reached a distinctly botryoidal or mammiliform surface is seen on the Wood's metal cast, Figs 58 and 59a. This could be a curious feature of the lithology, or it could represent the limiting pore size enterable by the nitrogen saturated Wood's metal. Using equations (37) and (38) with 'Ite=0.21' [J/m*2] gives 'R=0.06' [microns]. The radii of the Wood's metal globules in Fig. 59a are about 4 microns. It could be that the texture is caused by the Wood's metal withdrawing from the smaller pores as it cools, and it's surface tension rises. Backcalculating from a radius of 4

Fig 57:

a) Stereo pair of Wood's metal injected pore space at a relatively large scale. Shelly and oolitic Corallian limestone from Hovingham Quarry, North Yorkshire.

b) Smaller scale view of detail in Fig 57a.

Fig 58:

a) Stereo pair of detail from Fig 57b.

b) Stereo pair of detail from Fig 58a.

Fig 59:

a) Stereo pair of detail from Fig 58b.

b) Stereo pair showing grain coordination in the same lithology as Figs 57a to 59b.

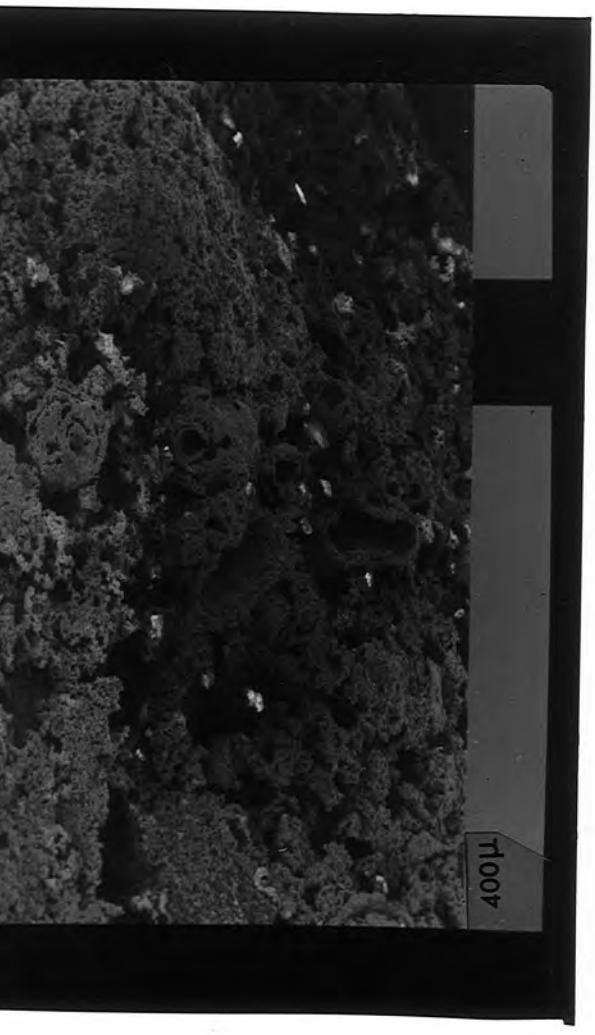

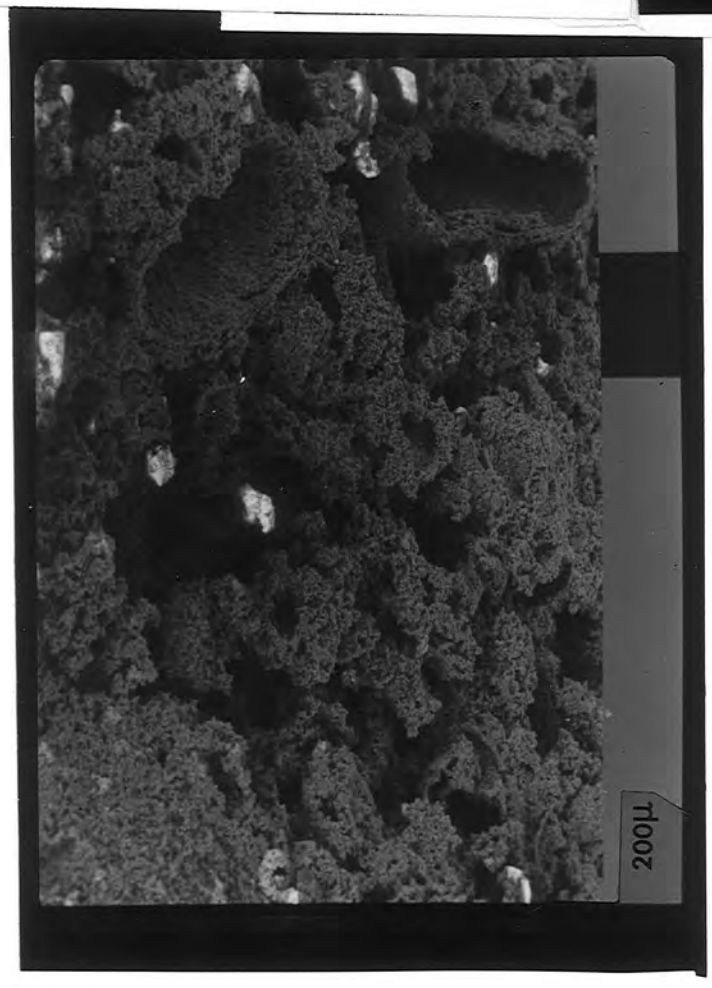

Fig 57

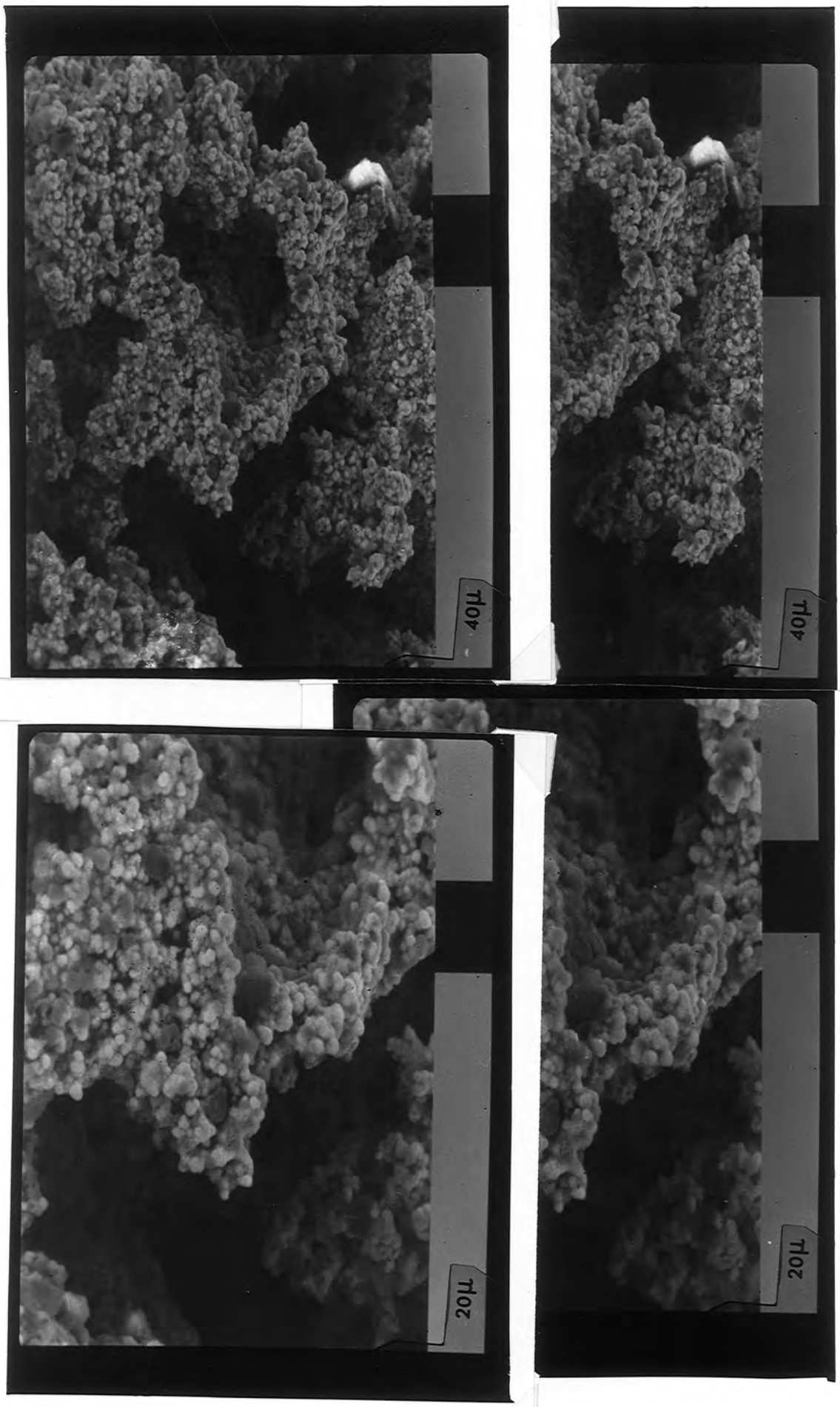

Fig 58

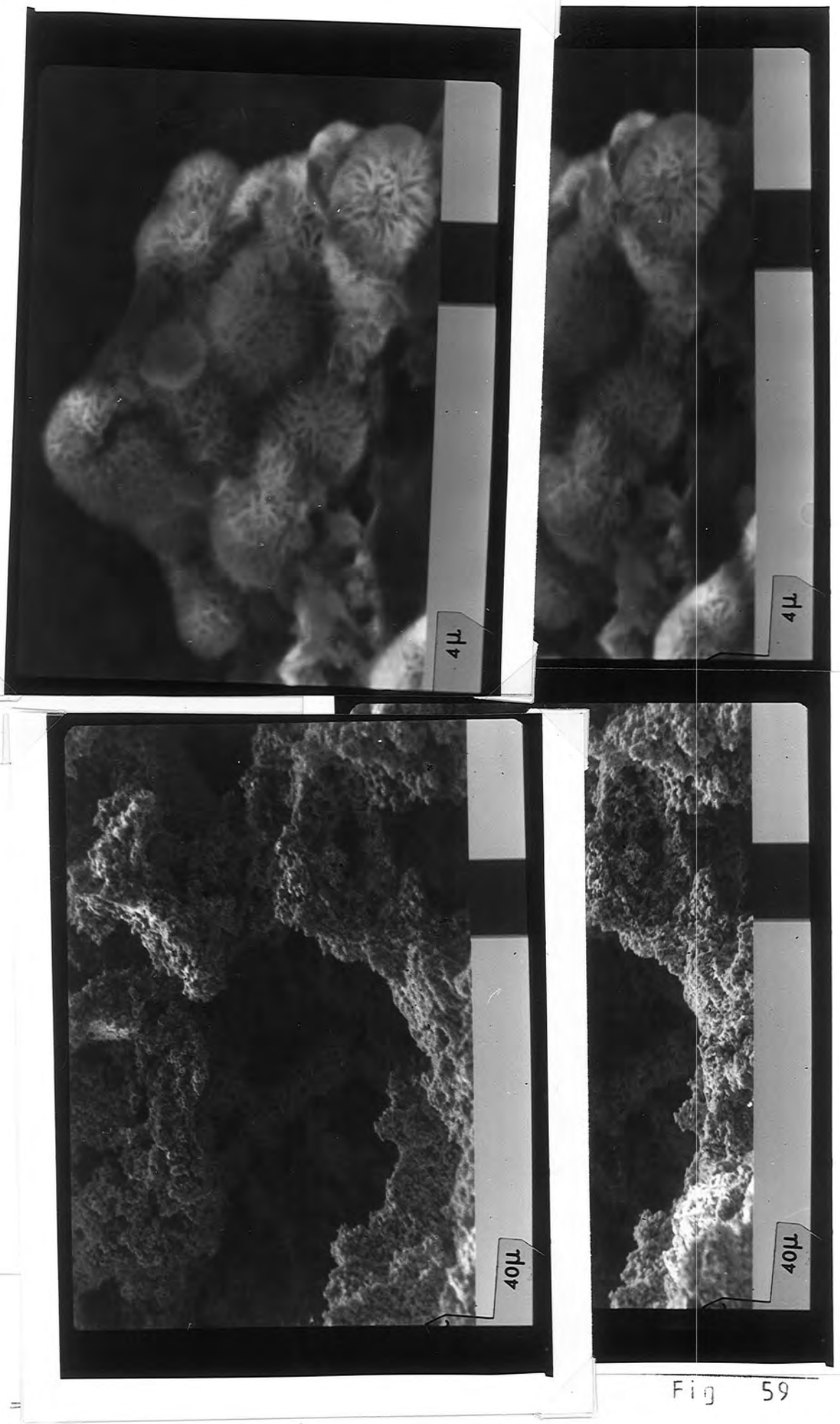

Fig 59

microns gives an effective surface tension of 13.1 (J/m*2).

It seems that the method is only capable of resolving textures down to 10 microns. Patsoules (pers com) accordingly used resin in order to obtain pore casts of the Yorkshire Chalk. There, the pore diameters are in a range of 1-10 microns.

SEM photographs were taken as stereo pairs, separated by 6 degrees of arc. The sequence presented in Figs 57 to 59a is in specimens from a Corallian shelly limestone from Hovingham Quarry. All the photographs centre on the same detail as the magnification is increased. In Fig 59b the coordination number of a single grain can be estimated from the network of grain contacts visible around the bowl that it has left in dissolving away.

7.3 Kobe method and Mean Pore Span.

7.3.1 Kobe method in Ruska porometer.

Total porosity can be determined by:-

a) Determining the specimen volume, 'Vt', by displacement.

b) Crushing the specimen.

c) Determining the grain volume, 'Vg', by displacement.

Equations (1) and (2) combined then give the porosity, N as:-

$$N = (Vt - Vg) / Vt \quad \text{.....(39)}$$

Norton and Knapp (1977) have shown that the porosity value so obtained may increase as the particle size in (b) is decreased. Lithologies such as granites, and some limestones, which have a high residual porosity show this effect markedly. It can also be difficult to ensure that all air bubbles are removed when measuring the volume of fine powders by displacement.

The Kobe, or Boyle's Law Method also estimates the grain volume by displacement. Since air is the fluid used, the whole of the effective pore space is accessible provided the specimen is dry. It was found that low permeability specimens required several minutes equilibration time when the pyncnometer pressure had been increased. Effectively, a falling-head gas permeability test is being performed between the pyncnometer and the centre of the specimen. The estimation of the total porosity is described in Section 7.3.2.

The operation of the Ruska porometer follows the directions given in the manufacturer's manual, (Anon). Each reading was taken at several pressures, from 10 to 50 psi, so that about

seven values were available for every variable. Some estimate of the error was then possible. The program, Figs 60 and 61, allows selection of the calculated values. Weighing the specimen allows the bulk density and the grain density to be calculated. The latter is a good check on the accuracy of the determination if the mineralogy of the specimen is known.

Errors are usually very small. Large errors were noticed when specimens had not been dried properly as described in Section 7.2.1.. This is probably because the pore throats in rocks such as chalk, which have a high microporosity, should be bridged by residual water. Differences in pressure might be maintained across such bridges and prevent the porometer from sampling the pore space beyond. When the pyncnometer pressure reaches a threshold value dependant upon the size of the pore throat, the bridge will break and a larger pore volume may be sampled.

Applying equation (38), and using an effective surface tension of 0.073 (J/m*2) for water and a differential pressure of say 10 psi gives a pore diameter of 4 microns. The improperly dried specimens referred to were of Yorkshire Chalk (Patsoules, pers com), with a pore diameter of 1-10 microns. Typically, the apparent grain volume should decrease with increasing pycnometer pressure.

7.3.2 Mean Pore Span determination.

A nine inch concrete test cube was cast for an undergraduate project supervised by Mr. R.H.Scott of the Department of Engineering Sience, Durham University. Six mm diameter aggregate was used, and the test cube was cut into one inch cubes and residual slices which were just over one inch square.

Fig 60:

APL function 'POROMETER' used in calculating porosity values by the Kobe, or Boyle's Law method.

Fig 61:

APL function 'POROMETER' continued.

Fig 62:

Normal probability plot of volume or thickness vs. percent inferred total porosity, for slices of a concrete cube with a 6mm aggregate.

```
      ∇ VOLUME[[]]∇
    ∇ VOLUME;TITLE;ΔV;I1;ΔVG;GV;MGV;TB
[1]     ⍝ ⍝
[2]     'ENTER SELECTMER NAME  (A20)'
[3]     TITLE←20↑□←20↑' '
[4]     'FOR OUTPUT SELECTMER: ',TITLE,40↑' '
[5]     'FOR OUTPUT CORRECTION:',[0.5] ' POSITION   FOR OUTPUT    OVER
        OVER=,   GREATER VOLS     VOLUME          MASS      '
[6]     FOR←OUTPUT←'FOR OUTPUT:',[1.5] '   (   Y     ',60↑' NO       >0   '
[7]     'ENTER VALUES OF CORRECTION VALUES X   ( OF SELECTMER)',[1.5] 'POSITI
        ON',(10↑'X')
[8]     I←0⍴0
[9]     'INPUT VECTOR OF PRESSURES FROM 0 ',(⍕I)
[10]    I←□
[11]    'INPUT VECTOR OF REFERENCE VOLUMES ',[1.5] (⍕I)
[12]    V1←0⍴0
[13]    'INPUT VECTOR OF REFERENCE VOLUMES 2 ',(⍕I),'.'
[14]    V2←0⍴0
[15] ⍝
[16] ⍝ CALCULATE PRESSURE FACTORS
[17] ⍝
[18]    I←(⍳⍴V1)-1↓ΔV←V2-V1
[19]    'INPUT VECTOR OF DEL. VOL. [ CONTAINING GREATER VOL. ',(
        ⍕I)'
[20]    V0←□
[21] ⍝
[22] ⍝ CALCULATE GREATER VOLUMES
[23] ⍝
[24]    GV←(⍳⍴I)+.=I←I,[0.5] I↓ΔV0←V0-V1
[25] ⍝
[26] ⍝ READING FOR DELETIMERS 0/1
[27] ⍝
[28]    ''
[29]    ''
[30]    'FOR SELECTMER NAME ',TITLE,' ',(40↑'DESIGNATION (0,OR1)'),[1.5
        ]0 0⍴''
[31]    'DEL PRESSURE FACTOR ΔV[I] ΔV[I] ΔV      ',(40↑'GREATER V
        OLUME [CC]')
[32]    ''
[33]    'READING',(⍳⍴I),'    V1[CC]    V2[CC] ΔV ',(⍳⍴V1),'    I
          V0[CC]'
[34]    'I READING',(⍳⍴ΔV0),'    ΔV[CC]'
[35]    'FOR (1/0) ',(⍳⍴V0),' ',V1,V2
[36]    ''
[37] ⍝
[38] ⍝ DELETIMER 0/1 TABLE
[39] ⍝
[40]    DT←(⍳⍴I)∘.≥(⍳⍴I)
[41]    DT←DT,[2] 0 ⍝ +⌿((⍳⍴V1),1)↑V1
[42]    DT←DT,[2] 0 ⍝ +⌿((⍳⍴V2),1)↑V2
[43]    DT←DT,[2] 0 ⍝ +⌿((⍳⍴ΔV),1)↑ΔV
[44]    DT←DT,[2]((⍳⍴I),9)⍴(9↑' '),9 ⍝ +DT
[45]    DT←DT,[2] 9 ⍝ +⌿((⍳⍴V0),1)↑V0
[46]    DT←DT,[2] 9 ⍝ +⌿((⍳⍴ΔV0),1)↑ΔV0
[47]    DT←DT,[2]((⍳⍴I),9)⍴(9↑' '),9 ⍝ +DV
[48]    □←DT
[49]    ''
```

Fig 60

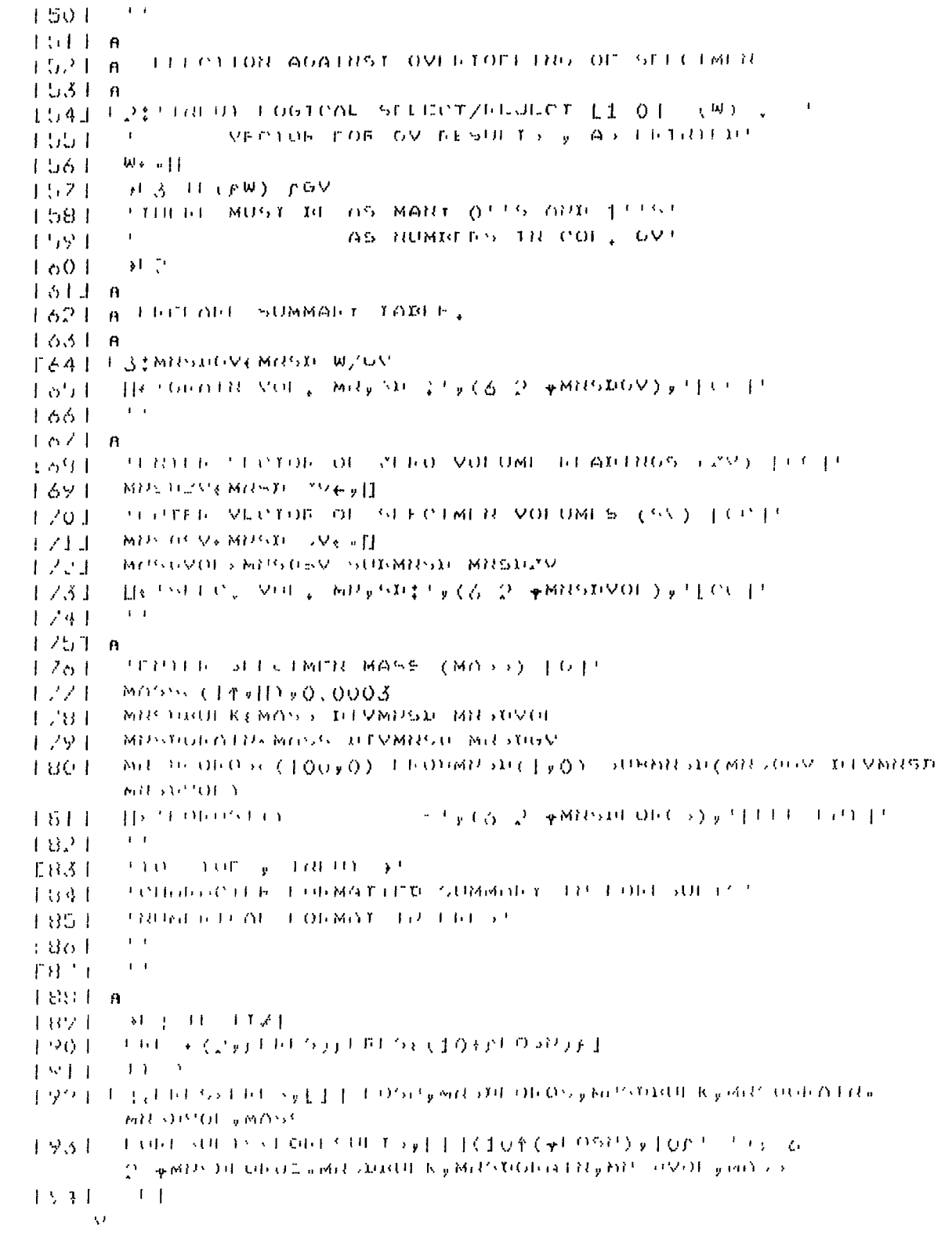

Fig 61

NORMAL / PROBABILITY PLOT OF VOLUME VS. OBSERVED POROSITY AS A PERCENTAGE OF OF INFERED TOTAL POROSITY FOR SLICES OF A CONCRETE CUBE MADE WITH 0.6 cm DIAMETER AGGREGATE.

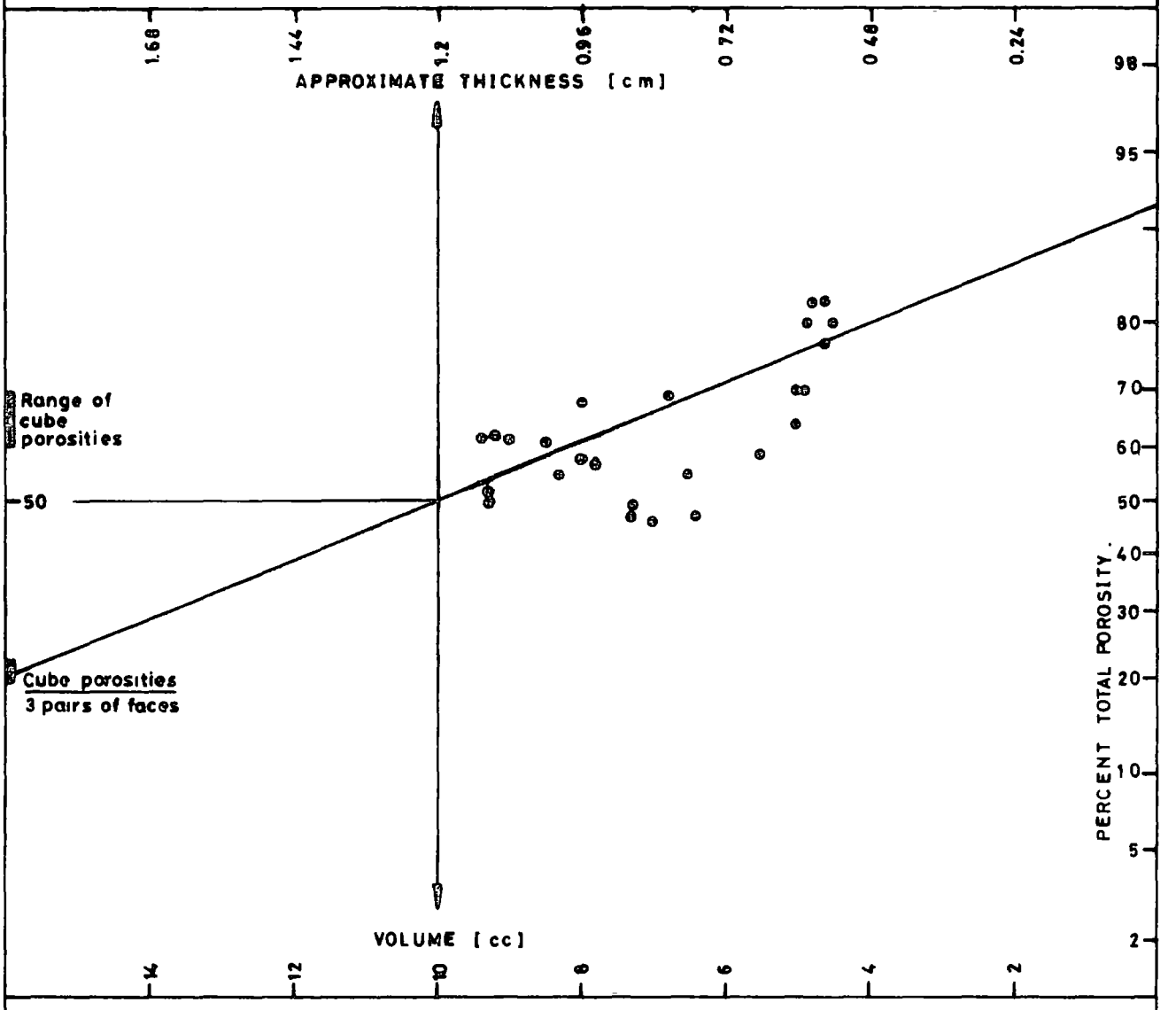

Note

Linear regression of the observed porosities of thin, approx. 2.9 cm square slices of concrete gives a maximum porosity of 20 65 at zero volume , slope -1 05 [per cc]

Porosity values have been re-expressed as "percent total porosity" and plotted ● , ▬

The pore space is provisionally regarded as mainly accessible through the square faces

Fig 62

They were tested in the Ruska porometer, and the data was processed by Mr. C.Postgate. It was found that the observed porosity varied with specimen volume, both parameters being determined to 1% accuracy. Figure 62 shows a plot of these porosities expressed as a percentage of the inferred total porosity. The assumption made is that the intrinsic porosity has a gaussian size distribution and can be characterised by a mean pore span. The mean pore span appears to be of the same order as the diameter of the aggregate in the concrete.

The pore space is envisaged as a three-dimensional maze in which the probability of entering a cul-de-sac increases with distance gone. A diffusing particle begins at the centre of a network of flowpores distributed as a Gaussian sphere about it. Many paths are available for diffusion over short distances, but the number of possible paths dwindles as the distance to be travelled increases.

7.4 Chemical Analyses and calculations.

7.4.1 Chemical analysis of limestones.

The Department of Geological Sciences, Durham University acquired a new Philips X-ray Spectrometer System PW1400 during 1979. The system installed had no inbuilt data processing facility; the counts read out being transferred to the Northern Universities Multiple Access Computer, (NUMAC). The X-ray fluorescence of a group of four samples is controlled by a microprocessor which is part of the Philips system. This was programmed by Mr. Ron Hardy so that the output table was as in Fig 63. The first counting round (line MN....) is a dummy to allow sufficient time for the system to reach the requisite vacuum level. MG+, NA+ etc. are background counts taken with the angle '2theta' set just off the peak for the element. Background counts are subtracted from the peak counts before the main data processing routines begin.

There were already several data processing packages which converted counts into chemical analyses. Usually a minimal number of fourteen or sixteen standards were used to calculate influence factors from the known chemical analyses and corresponding counts. With lesser numbers of standards, influence factors have sometimes been individually adjusted so that reasonable results are obtained. Graphs of counts versus weight percent for one element taken across a full range of standards are rarely linear. The relationship is a multivariate one due to matrix effects (Westbrook, Holland and Hardy, 1974). Since a data processing system was to be attached using software written 'in house', the programs used here were developed in APL with Mr. J.M.Lucas as a precursor to his

Fig 63:

Output table from Philips X-ray spectrometer system PW-1400.

Fig 64:

Table of standard samples used for analysing limestones.

Output table from Philips X-ray Spectrometer System PW-1400.

```
C=SMX1
SAM.POS :=1 2 3 4 I
<1> :=S29
<2> :=SIO2
<3> :=USGSW1
<4> :=SSCSY1

MP  1  4 SAMPLES 17 CHANNELS  MOPS  0
     1 : S29          2 : SIO2         3 : USGSW1       4 : SSCSY1
MN        964  20.000       52  20.000     2284  20.000     5135  20.000
SI     479577   4.000  1388150   4.000   454339   4.000   584429   4.000
AL     488662   8.000     3022   8.000   312800   8.000   195909   8.000
FE     855377   4.000     4258   4.000   998694   4.000   738553   4.000
MG      35701  50.000      598  50.000    84576  50.000    58678  50.000
MG+       540  50.000      281  50.000      492  50.000      503  50.000
CA      12266   4.000      896   4.000   471831   4.000   400359   4.000
NA      13032 100.000     2589 100.000    58876 100.000    88415 100.000
NA+      1510 100.000     1190 100.000     2732 100.000     2764 100.000
K      546272   4.000     1280   4.000    94439   4.000   373352   4.000
TI     667935   4.000     9640   4.000   629177   4.000   248755   4.000
MN       3889  80.000      206  80.000     9206  80.000    20728  80.000
MN+       281  80.000      156  80.000      309  80.000      334  80.000
S      851154  40.000    11218  40.000    28632  40.000    18867  40.000
S+       5628  40.000      893  40.000     1703  40.000     1779  40.000
P        9897  40.000     1190  40.000    18448  40.000    27589  40.000
P+        922  40.000      745  40.000      788  40.000      957  40.000
C=
```

Fig 63

SAMPLE NO.			LITHOLOGY					ANALYST	PELLET CONDITION				
SIO2	AL203	FE203	MGO	CAO	NA20	K20	TI02	MNO	S	P205	C02	H20	
SIO2			ANALAR						NEW				*
100.00	0	0	0	0	0	0	0	0	0	0	0	0	
CACO3			SPEC. PURE						NEW				*
0	0	0	0	56.08	0	0	0	0	0	0	43.92	0	
SU1			MIXED CANADIAN SULPHIDE ORE					INTERNAT. GOOD					*
34.52	9.46	32.70	3.93	3.96	1.03	0.63	0.81	0.11	12.04	0.10	0	0.71	
SU3			1:9::SU1:CACO3						NEW				*
3.45	0.95	3.27	0.39	50.88	0.1	0.06	0.08	0.01	1.20	0.01	39.53	0.07	
SU4			1:3:6::SU1:SIO2:CACO3						NEW				*
33.45	0.95	3.27	0.39	34.05	0.1	0.06	0.08	0.01	1.20	0.01	26.36	0.07	
NBSS8A			DOLOMITIC LST.					31.1.67 USDC		REMADE			*
1.20	0.19	0.28	21.30	30.10	0.01	0.12	0.02	0.03	0	0.01	46.60	0.14	
SU1A			2:1::SU1:NBS88A						GOOD				*
23.42	6.37	21.90	9.71	12.68	0.69	0.46	0.54	0.47	8.03	0.07	15.53	0.13	
SU2A			7:1::SU1:NBS88A						REMADE				*
30.36	8.30	28.65	6.10	7.24	0.90	0.57	0.71	0.09	10.54	0.09	5.83	0.62	
NBS1A			ARGILLACEOUS LST.					8.1.31 USDC		REMADE			
14.11	4.16	1.63	2.19	41.32	0.39	0.71	0.16	0.03	0.25	0.15	34.90	0	
T1			MSUSULE TONALITE					INTERNAT.(10-14)MNSD			NEW		*
62.69	16.55	6.03	1.85	5.19	4.35	1.24	0.59	0.11	0.01	0.13	0	1.26	
SSC-SY1			SYENITE						OLD BUT OK.				*
59.50	9.60	8.20	4.20	10.20	3.30	2.67	0.49	0.40	0	0.22	0.37	0.85	
USGS-W1			DIABASE						OLD BUT OK.				*
52.64	15.00	11.09	6.62	10.96	2.15	0.64	1.07	0.17	0	0.14	0.06	0.15	
NBS99A			FELDSPAR					26.3.65 USDC		REMADE			*
65.20	20.50	0.06	0.02	2.14	6.20	5.20	0.01	0	0	0.02	0	0.56	
NBS98			PLASTIC CLAY					31.8.31 USDC		REMADE			
59.11	25.54	2.05	0.72	0.21	0.28	3.17	1.43	0.01	0.06	0.08	0.06	7.28	
NBS97			FLINTY CLAY					31.8.31 USDC		REMADE			
42.87	38.77	0.98	0.26	0.10	0.33	0.54	2.38	0.01	0.04	0.08	0.29	13.35	
NBS93			BOROSILICATE GLASS					10.7.33 USDC		REMADE			*
80.60	1.94	0.08	0.03	0	4.16	0.16	0.03	0	0.01	0	12.99	0	
NBS91			OPAL GLASS					15.6.31 USDC		REMADE			
67.53	6.81	0.08	0.01	10.48	8.48	3.25	0.02	0.01	0	0.02	0	3.31	
NBS76			BURNT REFRACTORY					15.3.27 USDC		REMADE			
54.68	37.67	2.38	0.58	0.27	0.38	1.37	2.21	0.02	0	0.07	0.15	0.22	
S3			MANSFIELD MARINE BAND SHALE					D.A.SPEARS GEOCHEM.			REMADE		+
56.68	21.42	5.72	1.92	0.38	0.84	3.95	1.03	0.06	0.31	0.15	0.15	7.39	
S23			M.M.B.SH.					D.A.S.		COSMOCHEM.		R.THIN	+
47.15	21.91	8.88	1.75	0.53	0.74	4.46	0.71	0.13	5.42	0.07	0.03	8.22	
S27			M.M.B.SH.					D.A.S.		ACTA		REMADE	+
53.42	23.31	5.72	1.64	0.30	0.63	3.88	0.88	0.06	2.42	0.12	0.07	7.55	
S29			M.M.B.SH.					D.A.S.		1964 V.28		REMADE	+
51.81	23.36	6.00	1.66	0.39	0.64	3.85	0.93	0.05	3.07	0.14	0.60	7.50	
S30			M.M.B.ANKERITIC SHALE					D.A.S.		PP.1679-96		REMADE	*
9.60	5.56	7.56	8.33	26.56	0.36	0.82	0.30	0.71	0.53	0.74	35.40	3.53	
E1/10			SHALE						OLD , THIN				*
57.62	24.50	2.56	1.68	0.18	0.83	4.54	0.89	0	0.01	0.04	0	7.15	
E1/14			SH.						OLD , THIN				+
56.60	23.28	3.64	1.88	0.22	0.77	4.05	0.89	0	0.01	0.04	0	8.62	
E18/14			SH.						OLD CHIPPED				+
67.03	18.79	1.97	1.58	0.01	0.76	3.43	1.15	0	0.06	0.03	0	5.19	
RB57			ROOKHOPE BOREHOLE SHALE					RON LAMBERT		OLD SHINEY			*
51.50	19.80	2.84	1.35	6.93	0.40	4.30	0.81	0.04	0.87	0.13	2.40	8.63	
RB172			ROOKHOPE BH CALCSILICATE					R.L. DURHAM		OLD CHIPPED			
70.79	2.21	2.62	0.17	14.09	0.09	0.52	0.19	0	1.55	0.16	7.61	0	
RB173			ROOKHOPE BH CALCSILICATE					R.L.		OLD CHIPPED			
83.20	0.36	0.40	0.12	10.40	0.10	0.23	0	0.13	0	0.14	4.92	0	

Fig 64

writing an equivalent suite in Z80 machine code and Basic, now operational.

Twenty-nine standards were assembled to cover the sedimentary range of compositions with as many high calcium content standards as possible - see Fig 64 and Flanagan (1968). Mr. Ron Hardy increased the number originally available by blending some standard powders with others and with pure chemicals.

Limestone samples comprising a section across a bed of shelly limestone, and a section across a weathered margin in micritic limestone, were dried as described in Section 7.2.1., and comminuted using a jaw crusher and a disc mill. A teaspoonful of powder was mixed with five drops of Mowiol and pressed into 1 1/4 inch diameter discs with a force of 6 tons. Both borax backed and unbacked discs were prepared: differences in the final analyses were small and randomly distributed, so were used to estimate the standard error for each of the major elements determined. Samples were oven dried at 60 degrees C. for about two hours before being irradiated. This was found to decrease the time taken to reach high vacuum.

Specimen powders were run through the CO2 Train described in Groves (1951), under the supervision of Mr. Ron Lambert. Some were run in the Stanton Thermal Balance. The thermal balance curves showed no break in slope. No separation into H2O+, H2O-, and CO2 was possible using the thermal balance output other than by using arbitrary dividing temperatures. Since carbon and oxygen are close together in the periodic table, and below XRF detection limit, these major oxides are combined as 'CO2'.

7.4.2 XRF data processing.

A suite of APL functions was written which contains three main functions. FIDDCAL calculates the matrix of influence factors, [IF] from the linear matrix relationship:-

$$[\text{STANDARD COUNTS}]_{[n;m]} +.\times [\text{IF}]_{[m;m]} = [\text{STANDARD ANALYSES}]_{[n;m]} \quad \ldots\ldots\ldots\ldots(40)$$

where:

n is the number of standards analysed, and

m is the number of major oxides analysed.

Major oxides such as CO2, H2O+ and H2O- are not quoted and the total is not normalised. COMPCAL calculates unknown analyses from the unknown's counts using the same relationship. RCYCLE and CYCLE are alternative monitoring functions which call on FIDDCAL and COMPCAL as subroutines.

In FIDDCAL, the covariance matrix, described by Jennings (1977, equation 7.50) is output to describe the chemical correlation of the standards used. Selection of standards is facilitated in FIDDCAL and the standard analyses are backcalculated. The absolute normalised differences were defined as the (standard analysis - backcalculated value) divided by the (standard analysis). They are used to check on the stability of the influence factor matrix. A further check is that the analyses computed from the unknown samples counts should total an expected value of 100%; or about 60% for limestones.

Checks for machine drift are made by rerunning a subset of the standards on a regular basis. All the standards are rerun, and a new influence factor matrix is calculated if drift is

detected. During trial calculations it was found that a minimum of about thirty standards, chosen to cover the limited range of unknown whole rock chemistries, gave the most satisfactory results. It is more important to have a large number of standards than to arrive at an influence factor matrix which backcalculates almost exactly. Normalised differences indicate which standards fit least well, or most non-linearly into the range of chemistries covered. Individual normalised differences indicate in which major oxides the fit is poor.

Since a sufficient number of standards was available for the samples tested few problems arose. In the case of other data sets aquired over the same period, much tedious selection of standards was required before an influence factor matrix was calculated which seemed to match the range of unknown chemistries. Further work by J.M.Lucas substantiates these conclusions, and is reported in Lucas and Holland (1980).

7.4.3 Least squares abstraction model.

Abstractive processes affecting the major element composition of rocks include crystal settling and weathering . The Mass Balance Equation (41) governs such processes; and it can be solved by trial and error or by a least squares fit. Wright and Doherty (1970) and Wood (1978) have used the least squares method. Here the calculation is done, and errors are considered using the APL computer language. Crystal fractionation is considered first; and a data set from a weathered limestone margin is considered last.

In modelling crystal fractionation, a number of crystalline phases (or minerals) are removed from an initial liquid to produce a final liquid. The proportions in which the phases are

removed are to be calculated. The initial liquid corresponds to a starting whole rock composition (WRS) which may be taken as the analysis of a chilled margin or of an early apophysis to a major intrusion. The final liquid corresponds to a finishing whole rock composition (WRF) which may be taken as the analysis of late phase extrusives, etc.. The mineral compositions corresponding to the abstracted phases (PLG, etc.) may be taken from electron microprobe analyses of cumulate mineral grains.

The Mass Balance Equation may be expressed for one mineral phase (e.g. plagioclase) as:-

$$(WRS.100) - (PLG.PLGR) = (100-PLGR).WRF \quad .....(41)$$

where:

all vectors WRS, WRF, PLG are of (say) length 9 (or 10) and comprise analytical percentages of major oxides in the order (say) { SIO2, AL2O3, (TOTAL IRON) FE2O3, MGO, CAO, NA2O, K2O, TIO2, MNO, (P2O5) },

PLGR is the unknown amount of plagioclase removed expressed as a percentage of the mass of initial liquid.

Equation (41) can be rewritten as:-

$$(PLG-WRF).PLGR = 100.(WRS-WRF) \quad .....(42)$$

and generalised, for more than one mineral abstracted into a matrix form:-

$$\begin{array}{l} ([PLG,OPX,...,..]\ [WRF,WRF,WRF,..]) \quad (PLGR) \quad [WRS-WRF] \\ ([\ .\ \ .\ \ .\ \ ]\ [\ .\ \ .\ \ .\ \ ]) \quad (OPXR) \quad [\ .\ \ .\ ] \\ ([\ .\ \ .\ \ .\ \ ]-[\ .\ \ .\ \ .\ \ ])+.\times(\ .\ \ ) = 100\times[\ .\ \ .\ ] \\ ([\ .\ \ .\ \ .\ \ ]\ [\ .\ \ .\ \ .\ \ ]) \quad (\ .\ \ ) \quad [\ .\ \ .\ ] \\ ([\ .\ \ .\ \ .\ \ ]\ [\ .\ \ .\ \ .\ \ ]) \quad (\ .\ \ ) \quad [\ .\ \ .\ ] \\ \quad [9;n] \quad - \quad [9;n] \qquad\qquad [9;1] \\ \qquad\quad [9;n] \qquad\qquad +.\times [n;1] = \quad [9;1] \end{array}$$

such that n<=9 (or 10).....(43)

where the matrices are formed from the original vectors expressed in column vector form.

Equation (43) has the form :-

A +.x X = B.....(44)

so that 'X = B (matrix divide by) A'. Matrix division is accomplished by using the APL Inverse (or 'domino') Operator, which will provide a least squares solution if the number of phases abstracted is less than the number of major oxides analysed for, (Smith 1972). The system of equations is insoluble if there are more abstracted phases than major oxides in the analyses.

If a diagonal matrix of weighting factors [W] is to be incorporated, then equation (44) is shown by Jennings (1977 , equations 2.16 to 2.25) to be replaceable by:-

(At . W . A) . X = At . W . B.....(45)

where 'At' is the ordinary transpose of 'A'.

Wood's (1978) table 7 for an igneous abstraction problem were recalculated and it was found that differences from his published table were small and probably due to the different matrix inversion algorithm used. Both Wright and Doherty (1970) and Wood (op cit) fitted assumed mineral compositions accumulating in unobservable magma chambers in Hawaii and Iceland respectively, to the analyses of observed whole rocks. Accordingly Wright and Doherty's program incorporated a method of selecting the most likely phases to abstract, using the simplex algorithm.

Mr. Robert Hunter (1980) used the program on suites of analyses from Carrock Fell where the magma chamber is exposed. In that situation all the phases and whole rock analyses

involved can be analysed directly and the amounts of material separated are of greatest interest. Problems remain in that there is zonation of phases, and alteration has affected the rocks; so that observed compositions do not necessarily represent those abstracted during fractionation.

The calculation for specimens from the weathered margin of a micritic joint block is subject to similar problems. Weathering processes do not necessarily remove entire minerals, and local variations in clay mineral composition may well occur. The method can be applied only as an alternative to the more usual assumption that one or more reference elements remains unaffected by the weathering process. The abstracted percentage of 16.76 weight percent, compares with an increase in porosity of 2% in adjacent specimens, Fig 65 and Riemer (1979).

In addition to the functions listed in Figs 66 to 68, the functions PLOT and VS from the public library PLOTFORMAT may be used in the main functions FIT and MODE.

Fig 65:

Least squares abstraction model applied to weathering:

a) data, and

b) fit.

Specimens are from a micritic Corallian limestone from Spaunton Moor Quarry.

M105F, fresh rock, 105mm from the joint block margin.

M45W, weathered rock, 45mm from the joint block margin.

Fig 66:

APL function 'MODE' for calculating the least squares fitted modal composition of a rock analysis in terms of mineral analyses.

Fig 67:

APL function 'MODE' continued and function 'FIT' to calculate the least squares fitted percentages of mineral phases removed in moving from one whole rock composition to another.

Fig 68:

APL function 'FIT' continued.

LIST

	SIO2	FE2O3	MGO	CAO	CO2	SUM :-
CCT	.00	.00	.00	48.27	51.72	99.99
FE2O3	.00	100.00	.00	.00	.00	100.00
MGCO3	.00	.00	47.92	.00	52.07	99.99
M105F	3.67	1.69	.30	52.75	40.40	98.81
M12W	5.40	1.58	.52	52.94	39.12	99.56
M45W	4.57	1.65	.43	52.93	37.71	97.29
M75F	3.74	1.76	.29	52.80	40.12	98.71
QTZ	100.00	.00	.00	.00	.00	100.00

LEAST SQUARES ABSTRACTION MODEL; FROM M105F TO M45W:-

	CCT	MGCO3	M105F	M45W	BACK CALC	RESIDUALS	REL. ERRS	WTS.
SIO2	.00	.00	3.67	4.57	4.46	.11	.02	1.00
FE2O3	.00	.00	1.69	1.65	1.97	-.32	-.20	1.00
MGO	.00	47.92	.30	.43	.41	.02	.05	1.00
CAO	48.27	.00	52.75	52.93	53.74	-.81	-.02	1.00
CO2	51.72	52.07	40.40	37.71	38.23	-.52	-.01	1.00
	16.83	-.08	TOTAL	16.76				

REMOVED AS WEIGHT FCT, M105F.

MEAN ERROR AND RMS ERROR :- -.30 .46

PLOT OF (LOG10 WRF) VS (LOG10 WRFCALC)

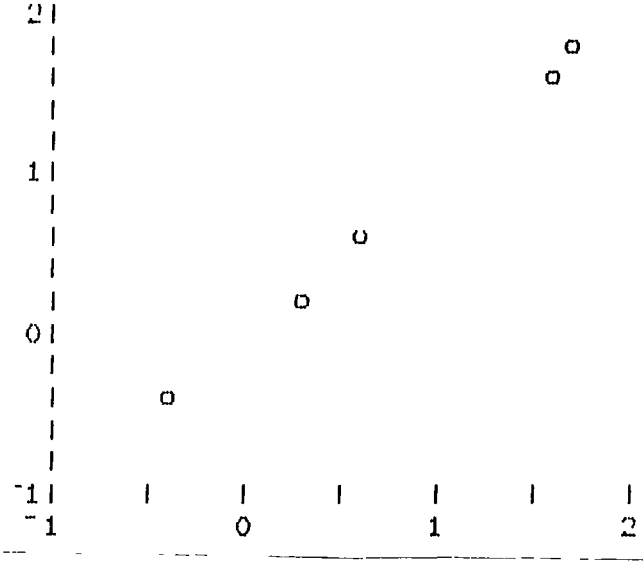

Fig 65

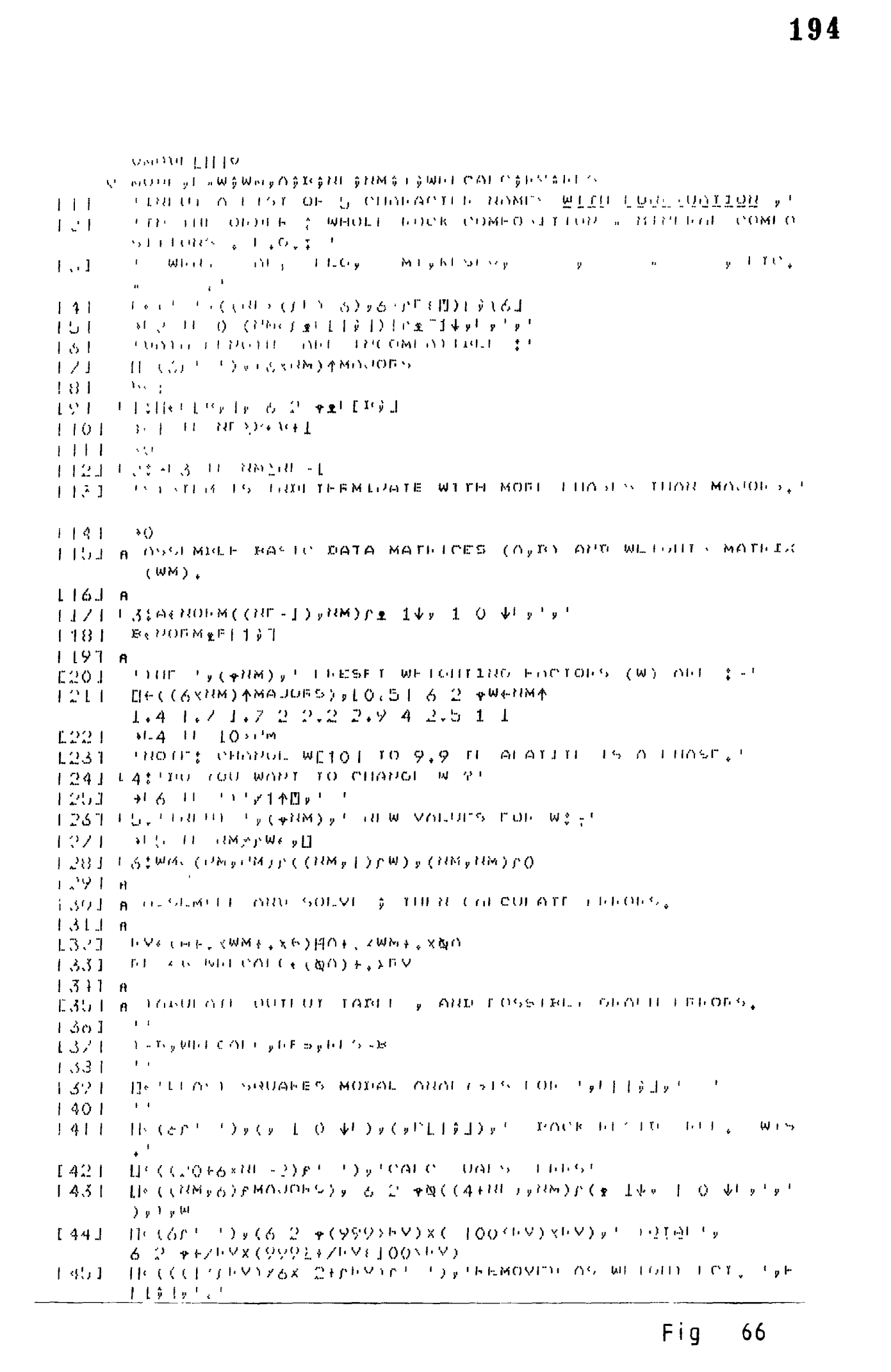

Fig 66

```
[46]  ⍞←'OR;     ',(5 2 ⍕(999)⊥V)×(  100<⌈/V←|⍎⍞)/'  TOTAL',
      6 2 ⍕+/⊥V←NORM T⊥V
[47]  ⍞←'MEAN ERROR OVER RMS ERROR :     ',6 2 ⍕NORMS ÷ 5
[48]  ''
[49]  →18 ⍴⍳ 1 ⍝ 1  100(T)^999>T←T,+/T
[50]  ⍞←'OPTIMAL VALUES WERE :  ',8 2 ⍕T
[51]  '8,3⍴⍝ ⍞  (4,+/'LOT'≠'F' ⍷NL 3)^2≠+/'VS'≠'''' ⍷NL
      3
[52]  ''
[53]  'FIT OF  (LOG10 WHOLELOOK) VS (LOG10 BACKCALC)'
[54]  ''
[55]  20 40 ⍞ OT(⌊10⊗⍷CT+IC) VS 10⊗⌊WRFCALC+⍷CT
[56]  ''
[57]  ''
[58]  ⍞←'DO YOU WANT TO CHANGE WEIGHTS ?'
[59]  →(5 ⍞ '''-⌶⍷,' '
      ∇
```

```
      ∇FIT[⍷]∇
    ∇ FIT;F;W;WM;A;B;NP;NM;T;WRFCALC;RV;RES
[1]   'INPUT A LIST OF 5 CHARACTER NAMES WITH PUNCTUATION ,'
[2]   'IN THE ORDER : PARENT , DERIVED , ABSTRACTED PHASES .
       E.G.;-'
[3]   '  WRS,  WRF,  FLG,   MT,KFSP9,     ,     ,     , ETC.
      ,     .'
[4]   F←(' ',((NP←(⍴P)-6),6)⍴F←⍷)[;⍳6]
[5]   →L2 IF 0=(NM←⍴⍎F[1;])|⍴⍎¯1↓,F,','
[6]   'DATA LENGTHS ARE INCOMPATIBLE :'
[7]   ⍷←(6↑' '),(6×NM)↑MAJORS
[8]   B←1
[9]  L1:⍷←F[B;], 6 2 ⍕⍎F[B;]
[10]  →L1 IF NF≥B←B+1
[11]  →0
[12] L2:→L3 IF NM≥NF-2
[13]  'SYSTEM IS INDETERMINATE WITH MORE PHASES THAN MAJORS.'
```

Fig 67

```
[14]   →0
[15]  ⍝ ASSEMBLE BASIC DATA MATRICES (A,B) AND WEIGHTS MATRIX
        (WM).
[16]  ⍝
[17]  L3:A←(NORM((NP-2),NM)⍴⍉⍪1↓, 2 0 ↓F,',')-((NP-2),NM)⍴
       NORM⍉P[2;]
[18]   B←100×(NORM⍉P[1;])-NORM⍉P[2;]
[19]  ⍝
[20]   'THE ',(⍕NM),' PRESET WEIGHTING FACTORS (W) ARE :-'
[21]   ⎕←((6×NM)↑MAJORS),[0.5] 6 2 ⍕W←NM↑
       1.4 1.7 1.7 2 2.2 2.9 4 2.5 1 1
[22]   →L4 IF 10>NM
[23]   'NOTE: CHANGE W[10] TO 9.9 IF APATITE IS A PHASE.'
[24]  L4:'DO YOU WANT TO CHANGE W ?'
[25]   →L6 IF 'Y'≠1↑⍞,' '
[26]  L5:'INPUT ',(⍕NM),' NEW VALUES FOR W:-'
[27]   →L5 IF NM≠⍴W←,⍞
[28]  L6:WM←(NM,NM)⍴((NM,1)⍴W),(NM,NM)⍴0
[29]  ⍝
[30]  ⍝ ASSEMBLE AND SOLVE ; THEN CALCULATE ERRORS.
[31]  ⍝
[32]   RV←(A+.×WM+.×B)⌹A+.×WM+.×⍉A
[33]   RES←(⍉P[2;])-WRFCALC←(⍉P[1;])-((⍉A)+.×RV)-100
[34]  ⍝
[35]  ⍝ TABULATE OUTPUT TABLE , AND POSSIBLY GRAPH ERRORS.
[36]   ''
[37]   T←(⍉P[1;]),(⍉P[2;]),WRFCALC,RES,RES-⍉P[2;]
[38]   ''
[39]   ⎕←'LEAST SQUARES ABSTRACTION MODEL; FROM ',F[1;],' TO '
       ,F[2;],':-'
[40]   ''
[41]   ⎕←(6⍴' '),(, 2 0 ↓P),(,P[⍳2;]),'  BACK RESID  REL.  WT
       S.'
[42]   ⎕←((20+6×NF-2)⍴' '),'CALC  UALS  ERRS'
[43]   ⎕←((NM,6)⍴MAJORS), 6 2 ⍕⍉((4+NP),NM)⍴(⍉⍪1↓, 2
       0 ↓F,',',')⍪T,W
[44]   ⎕←(6⍴' '),(6 2 ⍕RV),' TOTAL', 6 2 ⍕+/RV
[45]   ⎕←((6×⍳1+⍴RV)⍴' '),'REMOVED AS WEIGHT PCT. ',F[1;],'.'
[46]   ⎕←'MEAN ERROR AND RMS ERROR :-    ', 6 2 ⍕M⍪RMS RES
[47]   ''
[48]   →L7 IF∼(4⍷+/'PLOT'⍷'P' ⎕NL 3)∧2⍷+/'VS'⍷'V' ⎕NL
       3
[49]   ''
[50]   'PLOT OF (LOG10 WRF) VS (LOG10 WRFCALC)'
[51]   ''
[52]   20 40 PLOT(10⍟⍉P[2;]) VS 10⍟⍪WRFCALC
[53]   ''
[54]   ''
[55]  L7:'DO YOU WANT TO CHANGE WEIGHTS ?'
[56]   →L5 IF 'Y'=1↑⍞,' '
    ∇
```

Fig 68

7.5 Seismic anisotropy.

Harrison's (1973) description of the joint sets in the Corallian Series of the North York Moors; and the observation of the structures described in Section 2.1, made it clear that in Spaunton Moor Quarry, north-south joint sets are dominant to an unusual degree, Fig 18. Since this joint set and parallel minor faults seem to control erosion and groundwater flow, Fig 4b, it would be advantageous to have a geophysical method by which detailed anisotropy of fracture patterns could be mapped. Since the joint blocks have markedly weathered margins, Fig 29, substantial seismic anisotropy was predicted. The seismic refraction method is not an analogue of groundwater flow, as resistivity is, but data can be gathered in a wider range of ground conditions, and individual refractors may be mapped at depth.

Dowlen (1979) gathered a great deal of data in an M.Sc. thesis and his field arrays are summarised in Fig 19. He used a hammer source exclusively, and found difficulty in recording signals across faults. He found anisotropies of up to 160%, compared with a previously recorded maximum of about 15 to 29% for the Carboniferous limestone of the Northwest of England, Bamford and Nunn, 1977.

Functions 'DATAMAN2', 'ELLIPSEFIT', and 'BACKUSFIT' were written in APL, and a Fortran+*Ghost program was written to produce the plots of Figs 68 to 83. Greenkorn et al (1964), following Scheidegger (1954), provide a formula for curvefitting an inverse ellipse, Fig 3, expressed in terms of radius and azimuth. This curvefit was tried as well as the formula provided by Backus (1962, 1965) and used by Bamford and

Nunn (op cit). Backus's curve is not held to be theoretically valid above 10% anisotropy by Bamford and Nunn (op cit), and it seems from the results described by Dowlen (op cit) that an ellipse fits the data as well or better than the other two curves tried. An ellipse fits some of the data sets very well, especially if allowance is made for heterogeneity of joint frequency, by fitting subsets of the data with separate segments of ellipses, Dowlen (op cit).

Fig 68 shows the most anisotropic Array Three, fitted with an ellipse having an axial ratio of 2.6, after Dowlen (op cit). Figures 69 and 70 illustrate the improvement in fit that can be gained by dividing heterogeneous data into subsets. Array One is near the largest fault in Spaunton Moor Quarry and velocities on the side of the array nearest the fault are substantially reduced. This may be due to a higher joint frequency near to the fault; or to gape of the existing fissures, since the fault face is now a free surface. Figures 71 to 76 show a remarkable swing of the long axis of the fitted ellipse with a change in array size from 24m to 14m radius. There is a lot of scatter in this data from Dowlen's (op cit) Array Five, but the change in orientation is regular. This is interpreted as due to the increasing dominance of east-west oriented minor joints away from the mappable faults of the syncline, Figs 7 and 19.

In order to overcome the poor data transmission through faults reported by Dowlen, a dropweight was tried in the field. Transmission was observed through faults of up to one metre in throw, and the site of DBARRAY was chosen to study attenuation anisotropy, Figs 19 and 77. The gain levels of the Bison recorder were adjusted with successive drops until the

Fig 69:

Ellipse fit to P-wave seismic velocities from array three (Farrthree, of Fig 19), Spaunton Moor Quarry, after Dowlen (1979).

Fig 70:

Ellipse fit to P-wave seismic velocities from array one (Farrone, of Fig 19), Spaunton Moor Quarry, after Dowlen (1979).

Fig 71:

Data of Fig 70, ellipse fitted in two subsets.

ARRAY THREE, VELOCITIES AT 24M

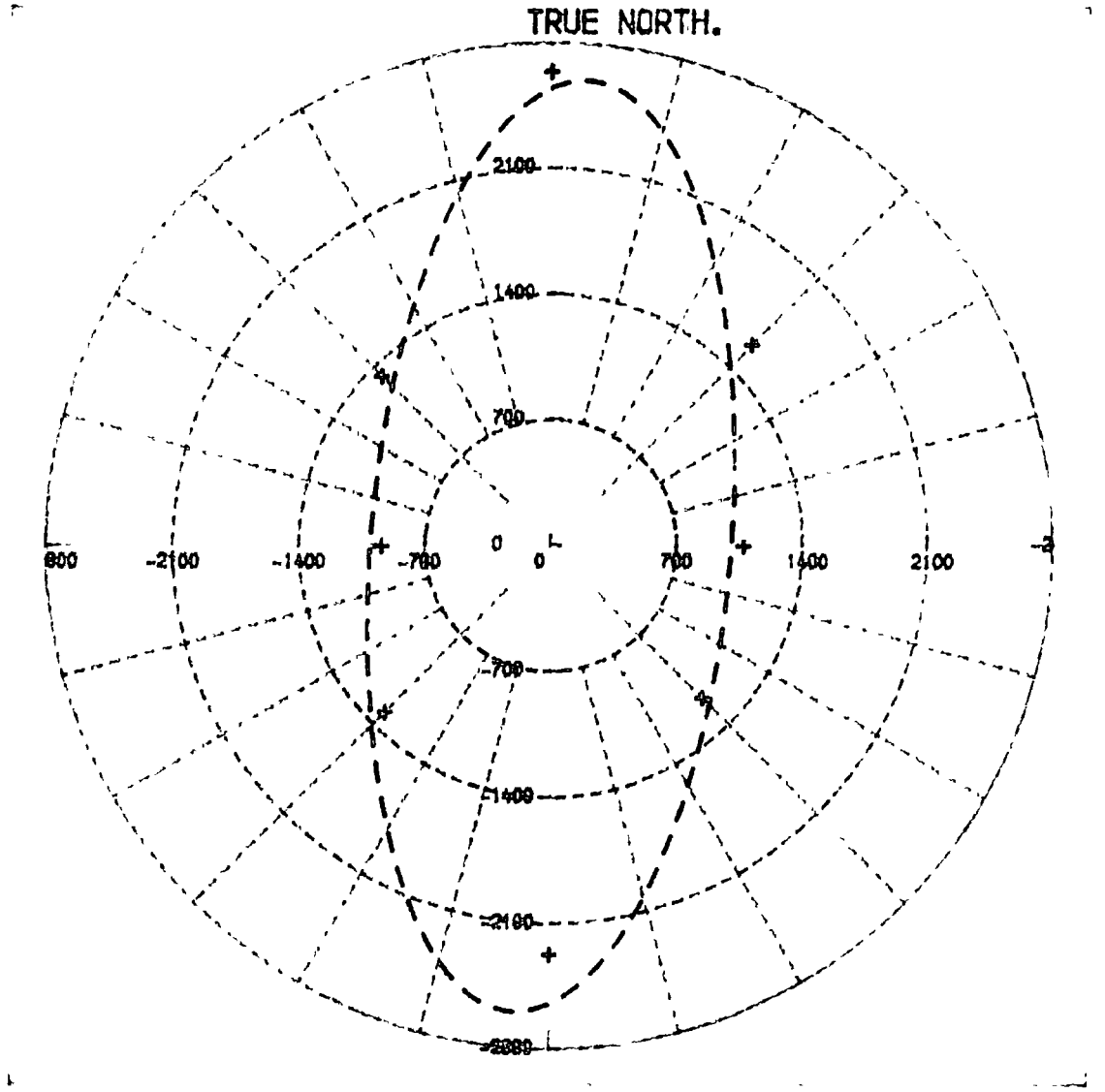

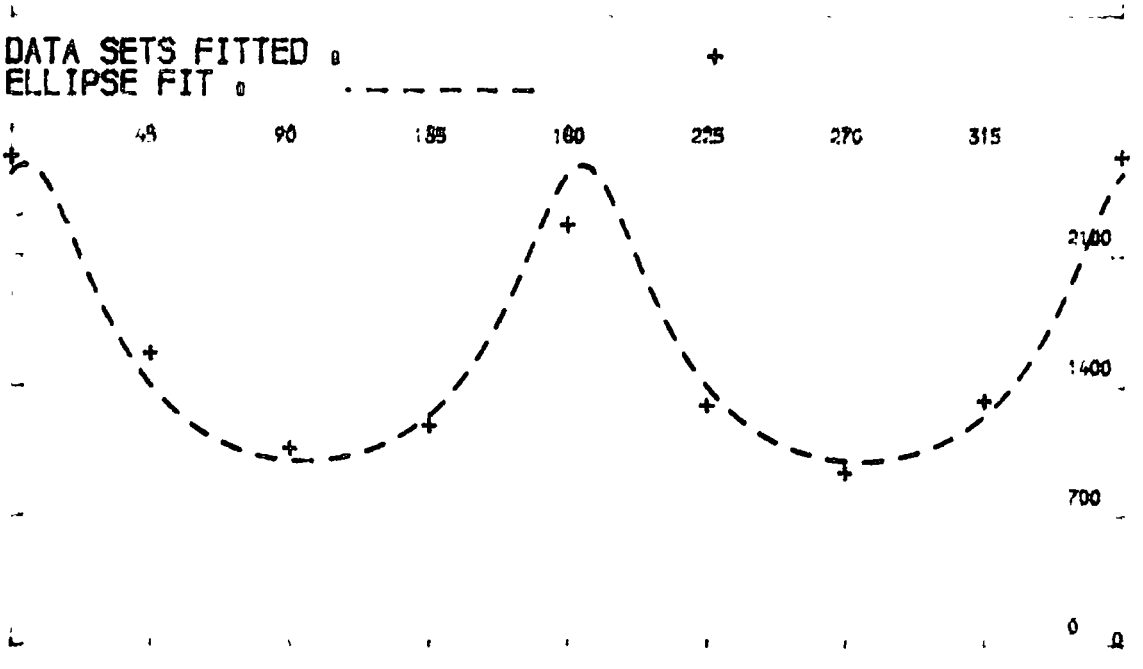

Fig 69

ARRAY ONE, VELOCITIES AT 12M

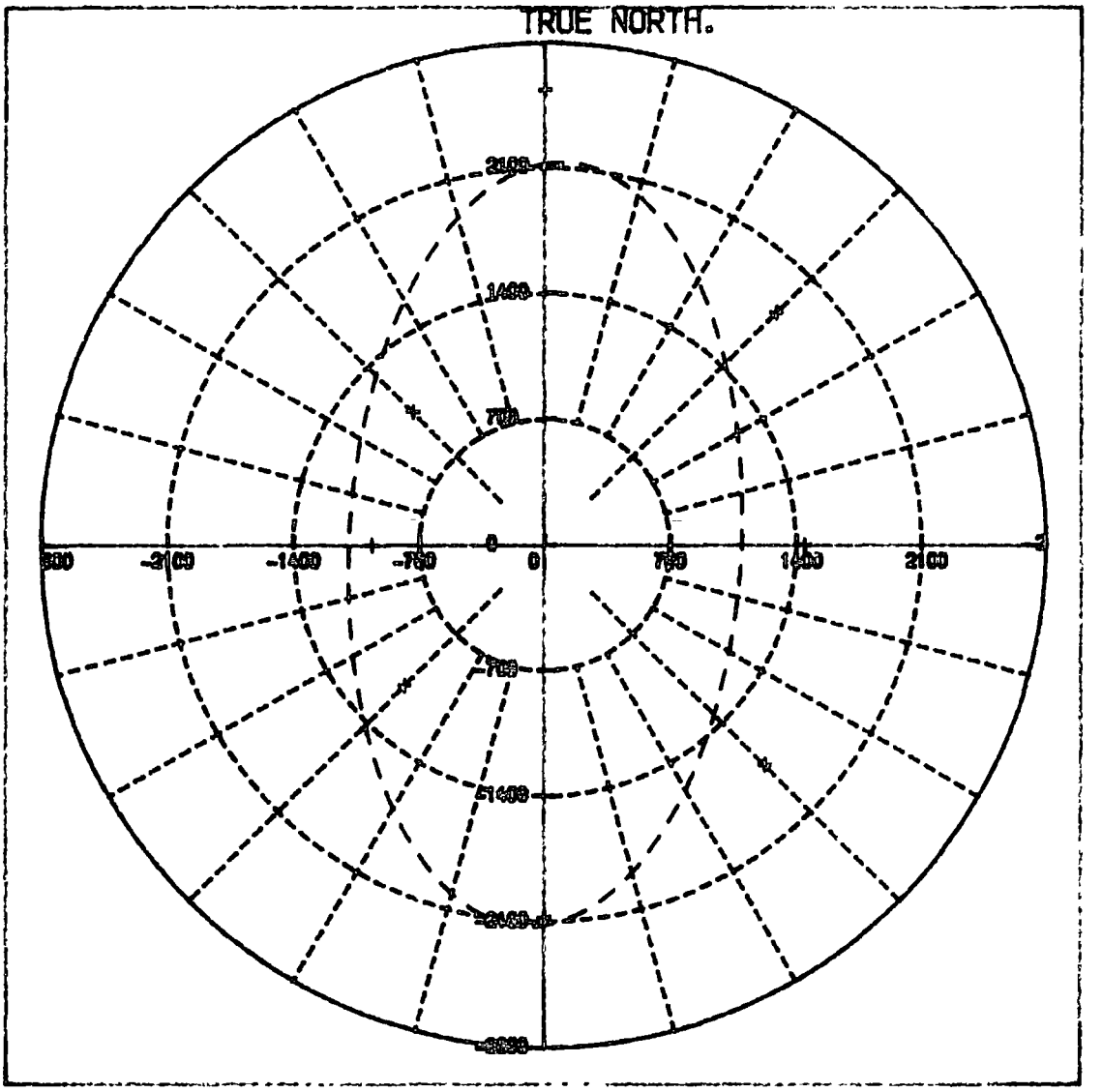

DATA SETS FITTED :
ELLIPSE FIT :

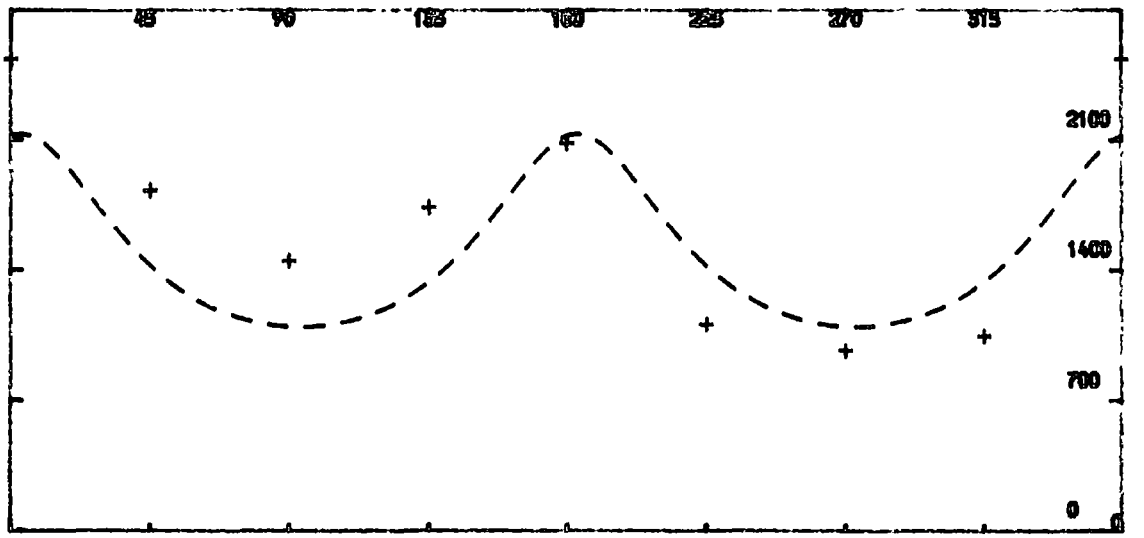

Fig 70

ARRAY ONE, VELOCITIES AT 12M

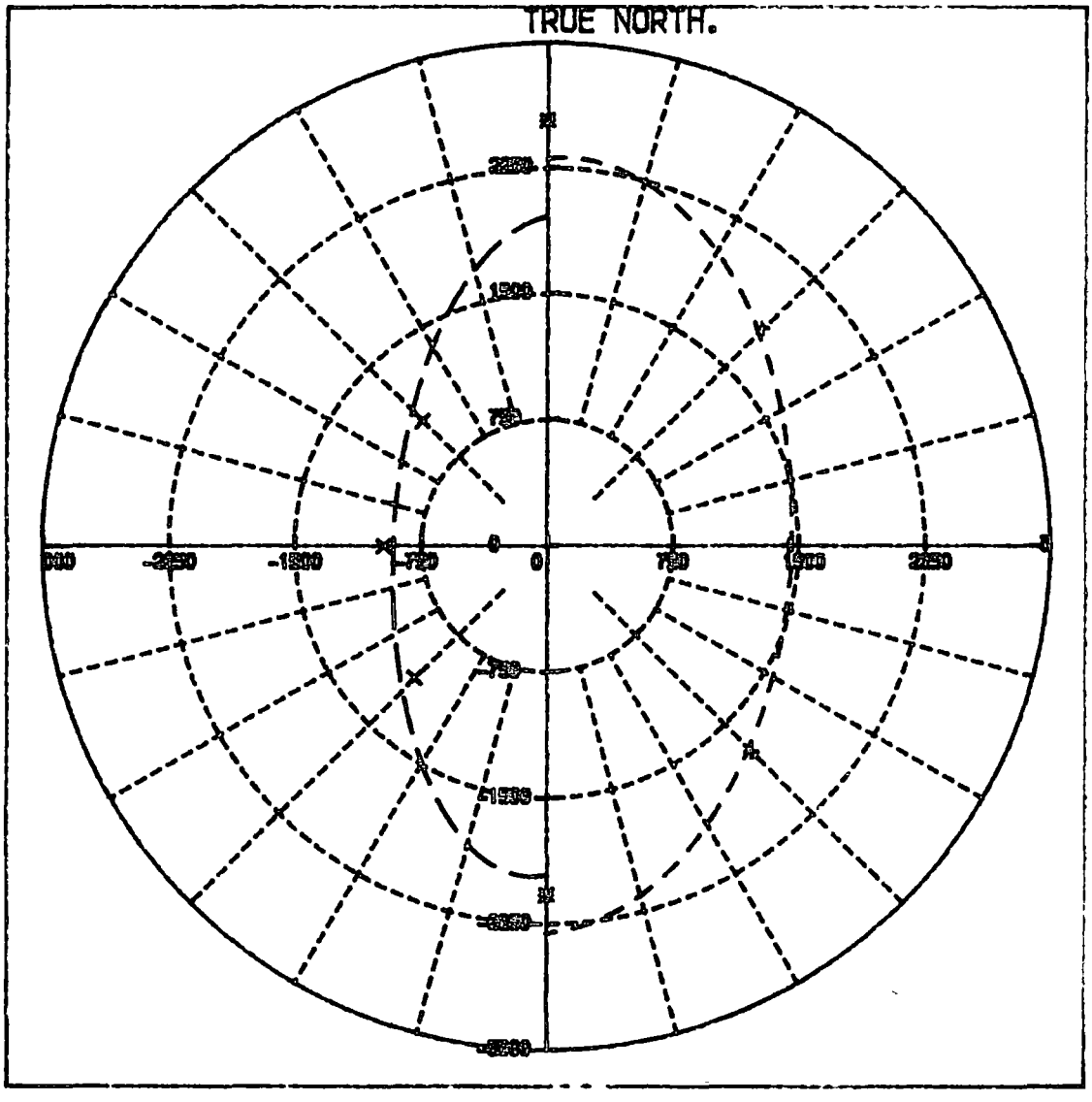

DATA SETS FITTED ▯ + ×
ELLIPSE FIT ▯ — — — —

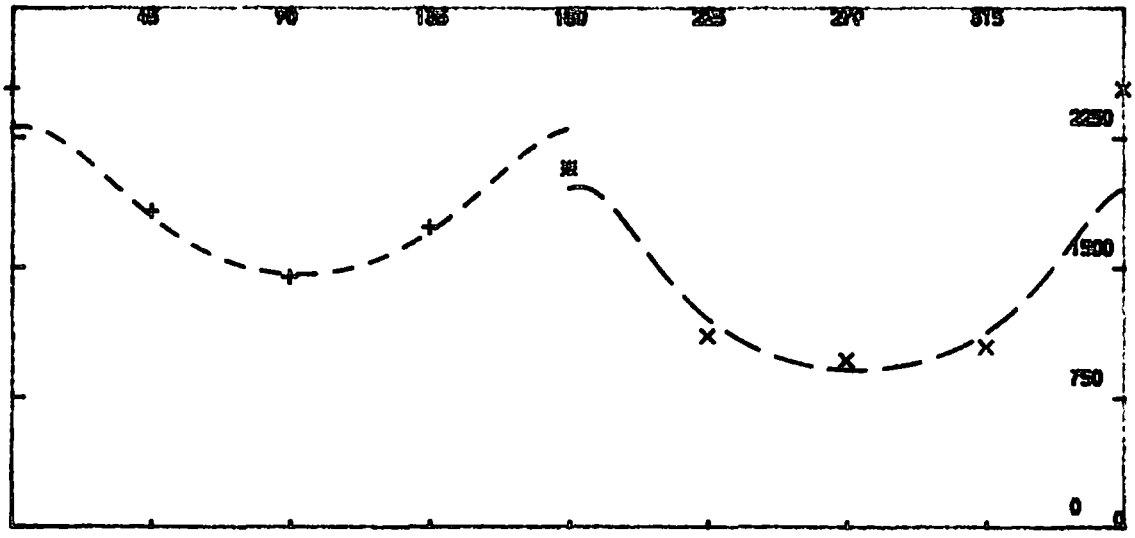

Fig 71

Fig 72:

Ellipse fit to P-wave seismic velocities from array five (Farrfive, of Fig 19), Spaunton Moor Quarry, after Dowlen (1979). Data from a radius of 24m.

Fig 73:

As Fig 72, but with data from a radius of 22m.

Fig 74:

As Fig 72, but with data from a radius of 20m.

Fig 75:

As Fig 72, but with data from a radius of 18m.

Fig 76:

As Fig 72, but with data from a radius of 16m.

Fig 77:

As Fig 72, but with data from a radius of 14m.

ARRAY FIVE, VELOCITIES AT 24M

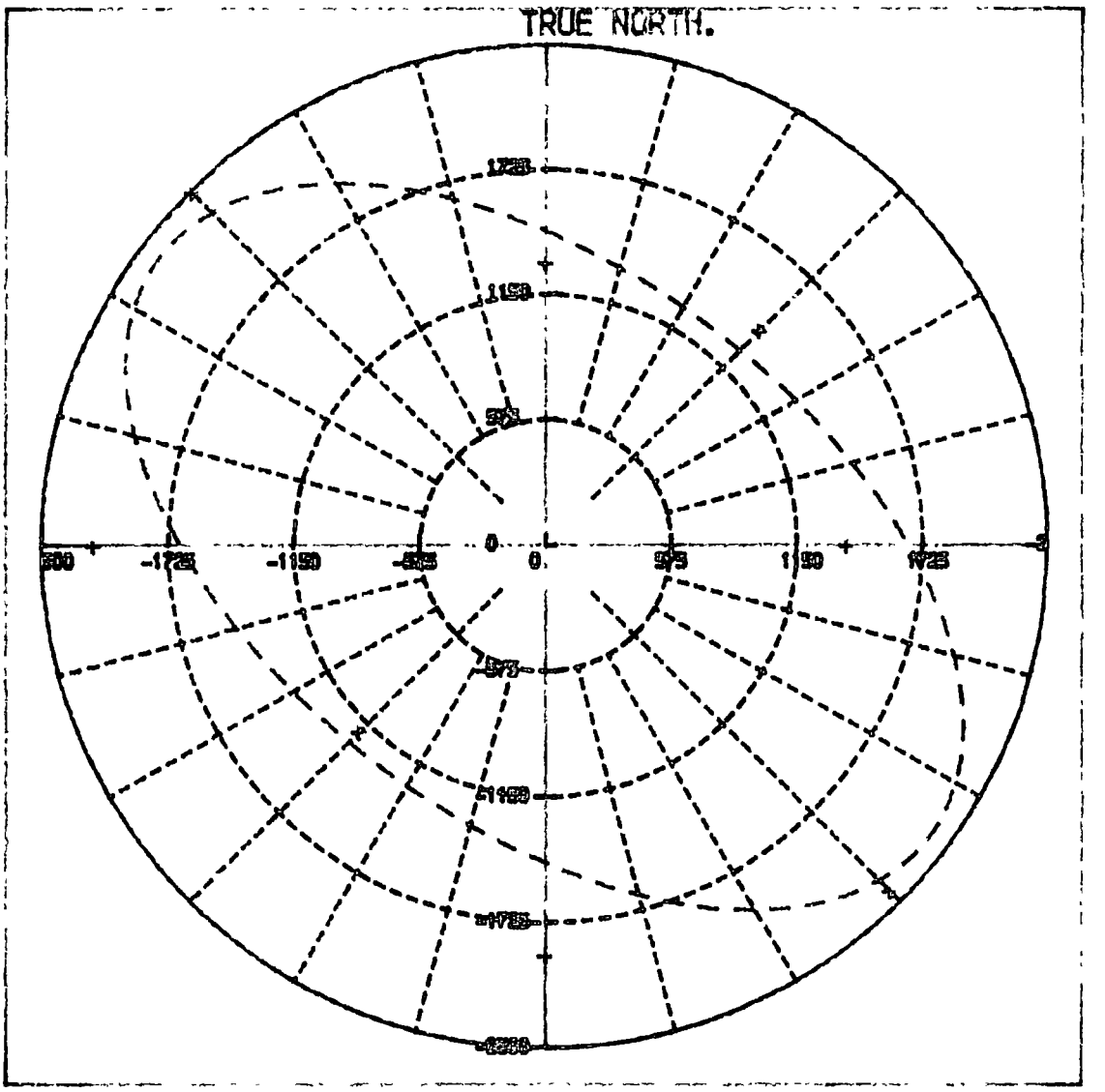

DATA SETS FITTED :
ELLIPSE FIT :

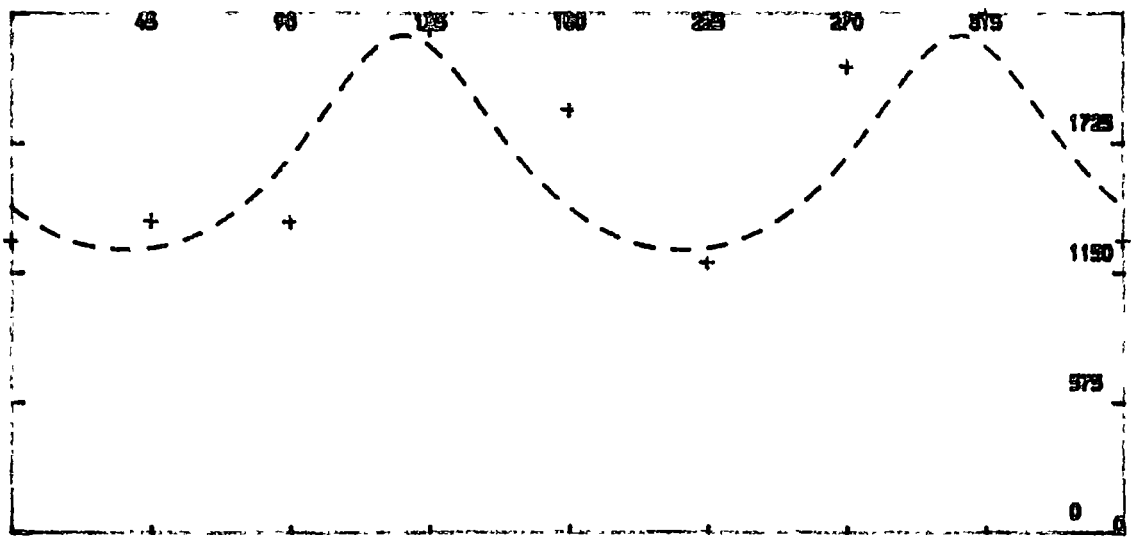

Fig 72

ARRAY FIVE, VELOCITIES AT 22M

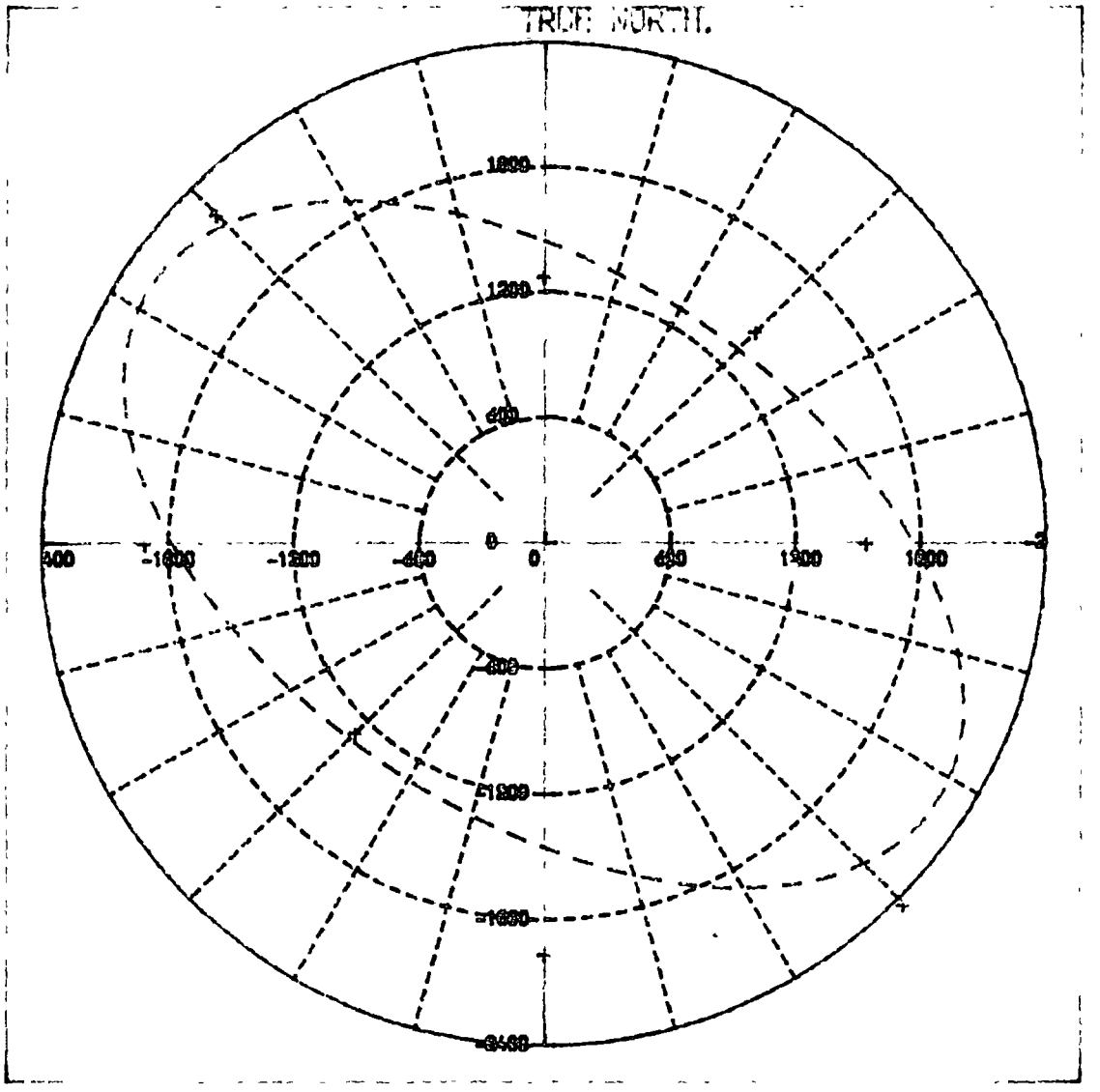

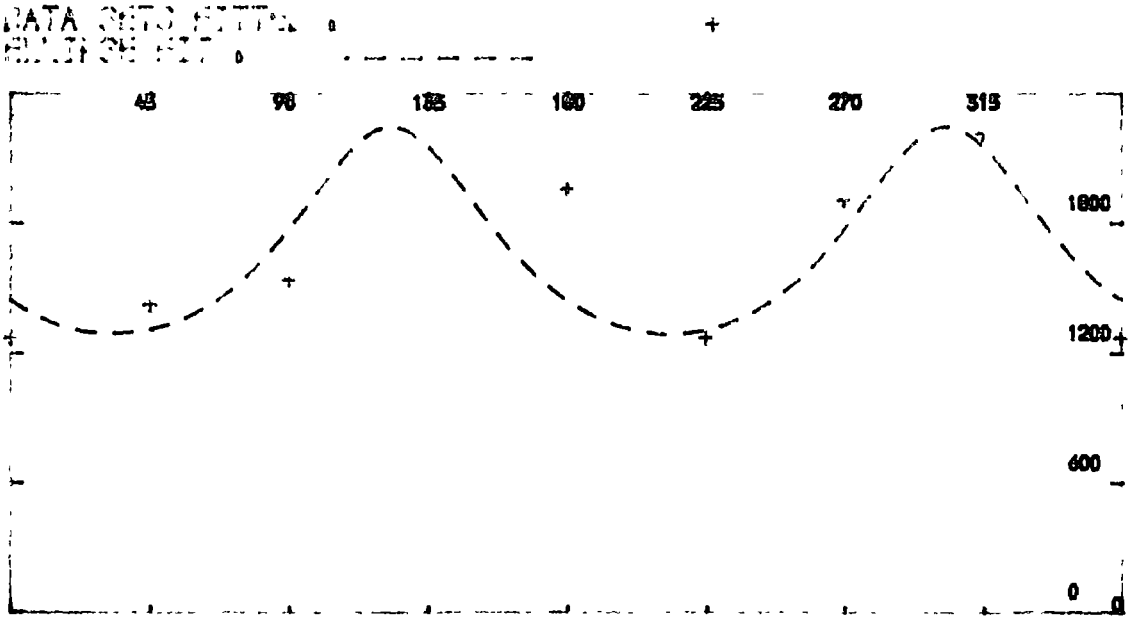

ARRAY M1/E, VELOCITIES AT 20M

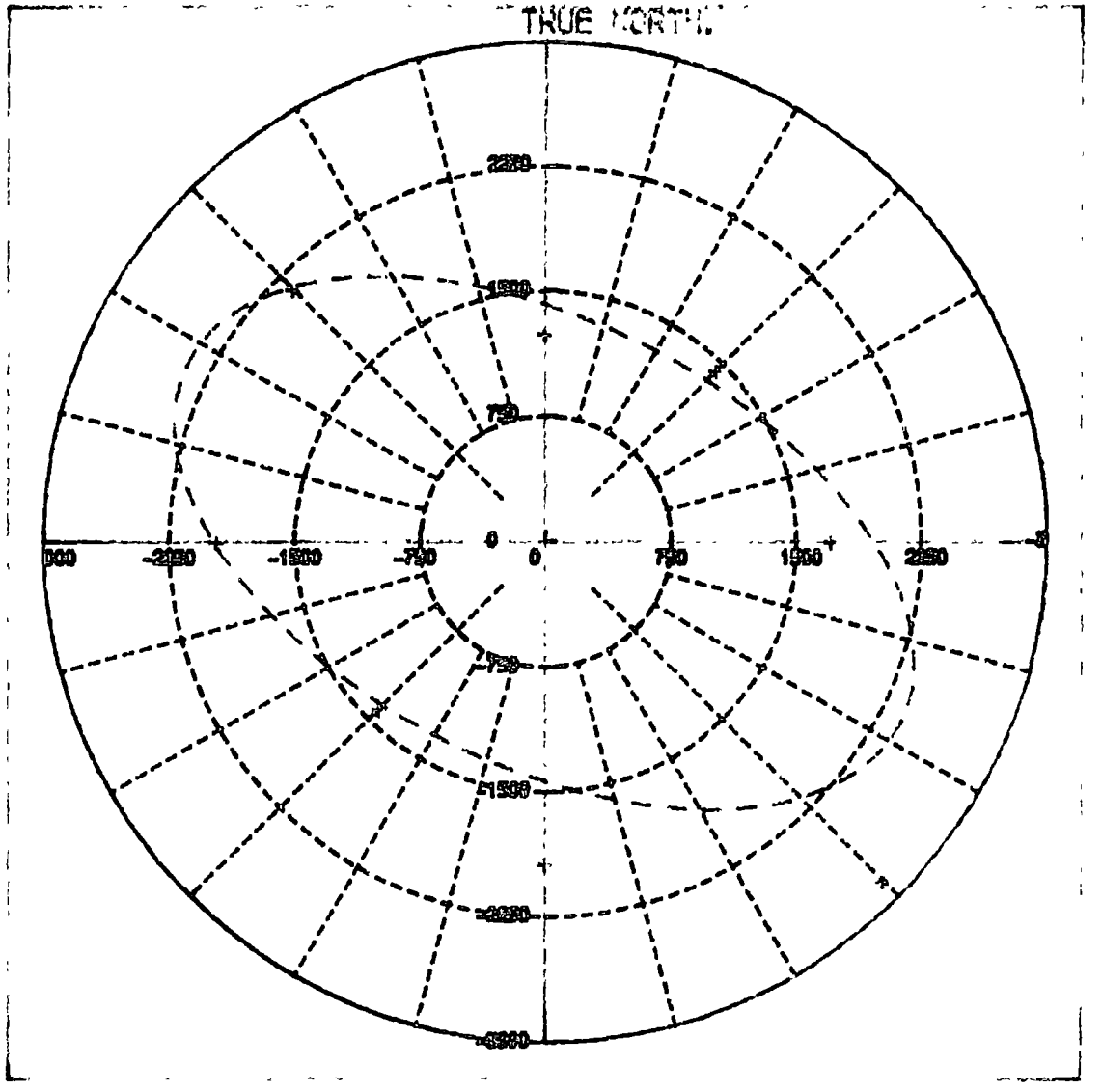

DATA SETS FITTED

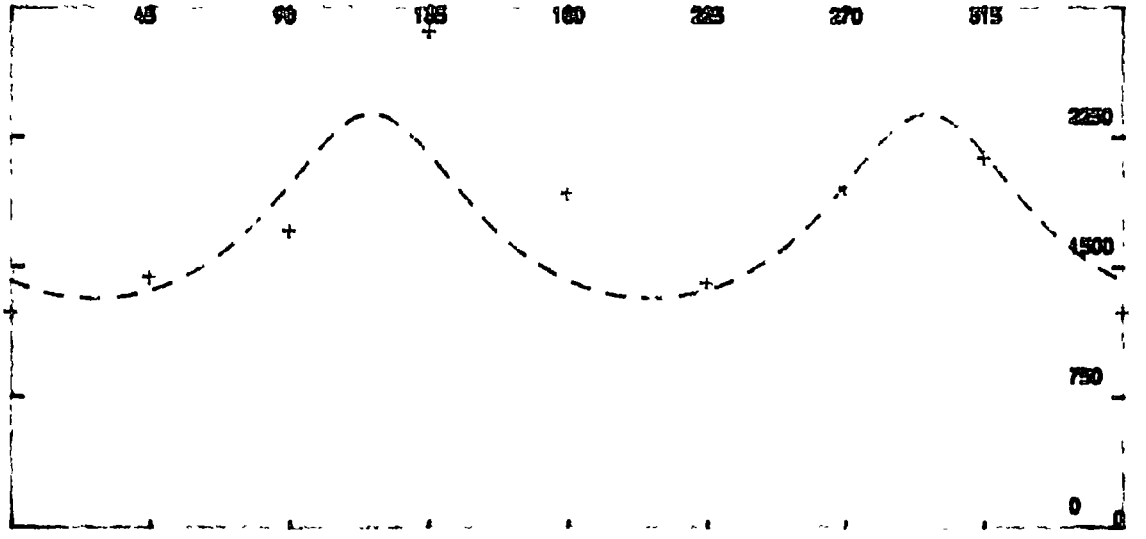

ARRAY FIVE, VELOCITIES AT 1811.

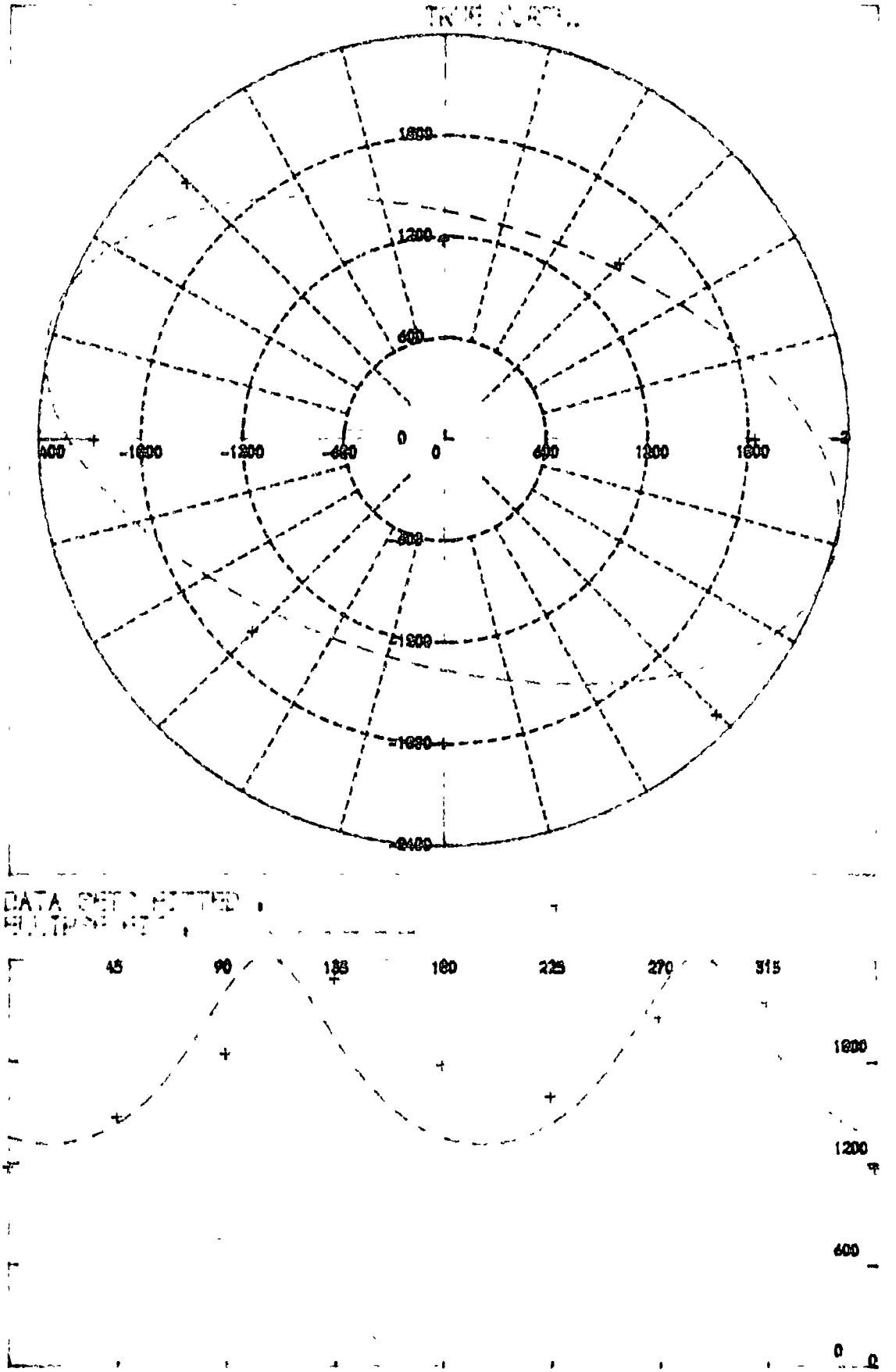

Fig 75

ARRAY FIVE, VELOCITIES AT 16M.

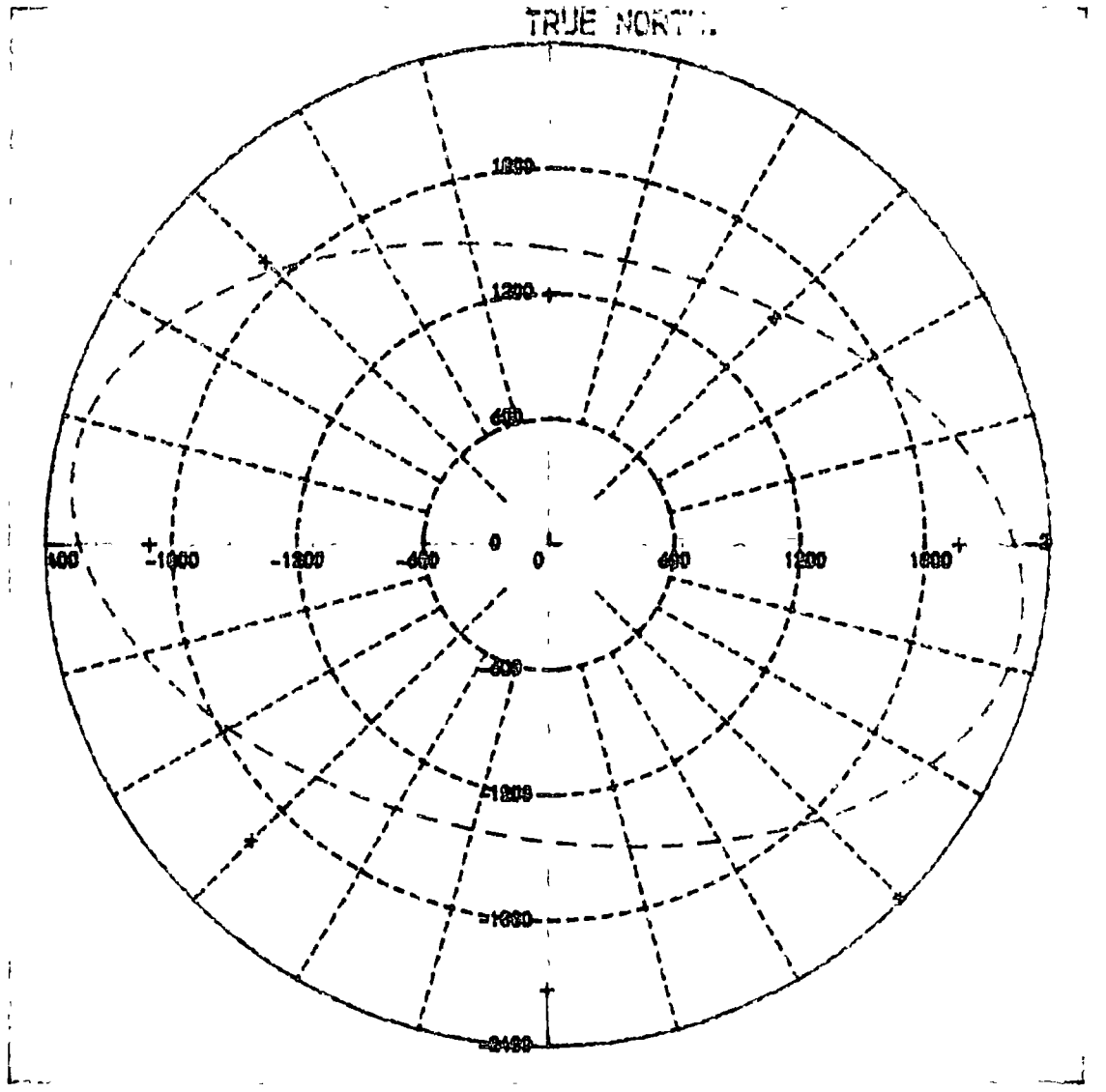

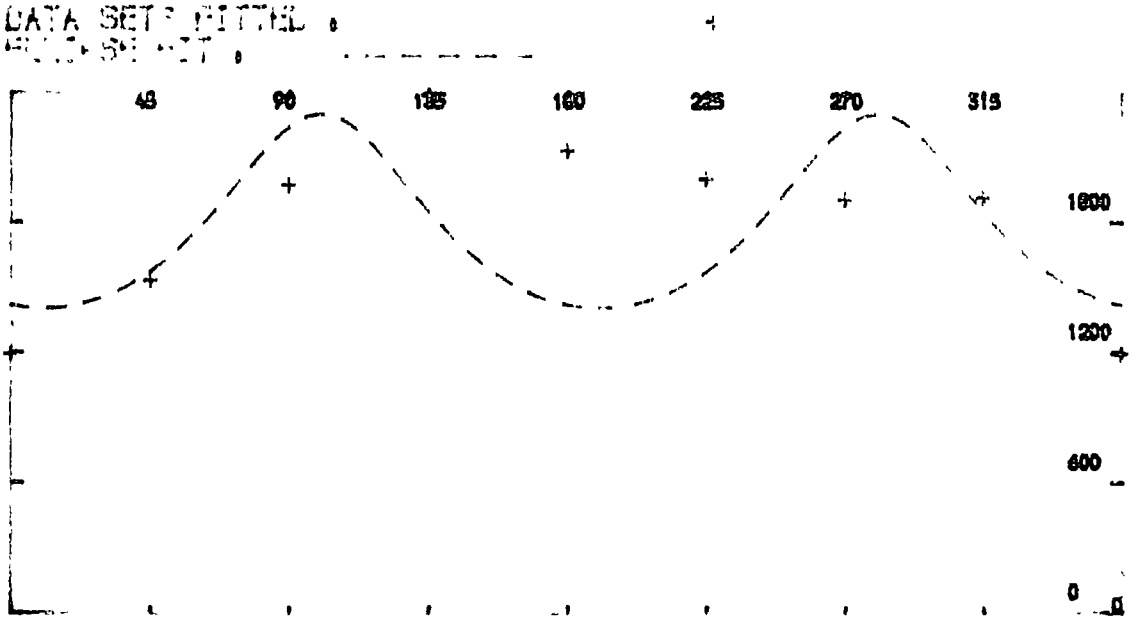

Fig 7

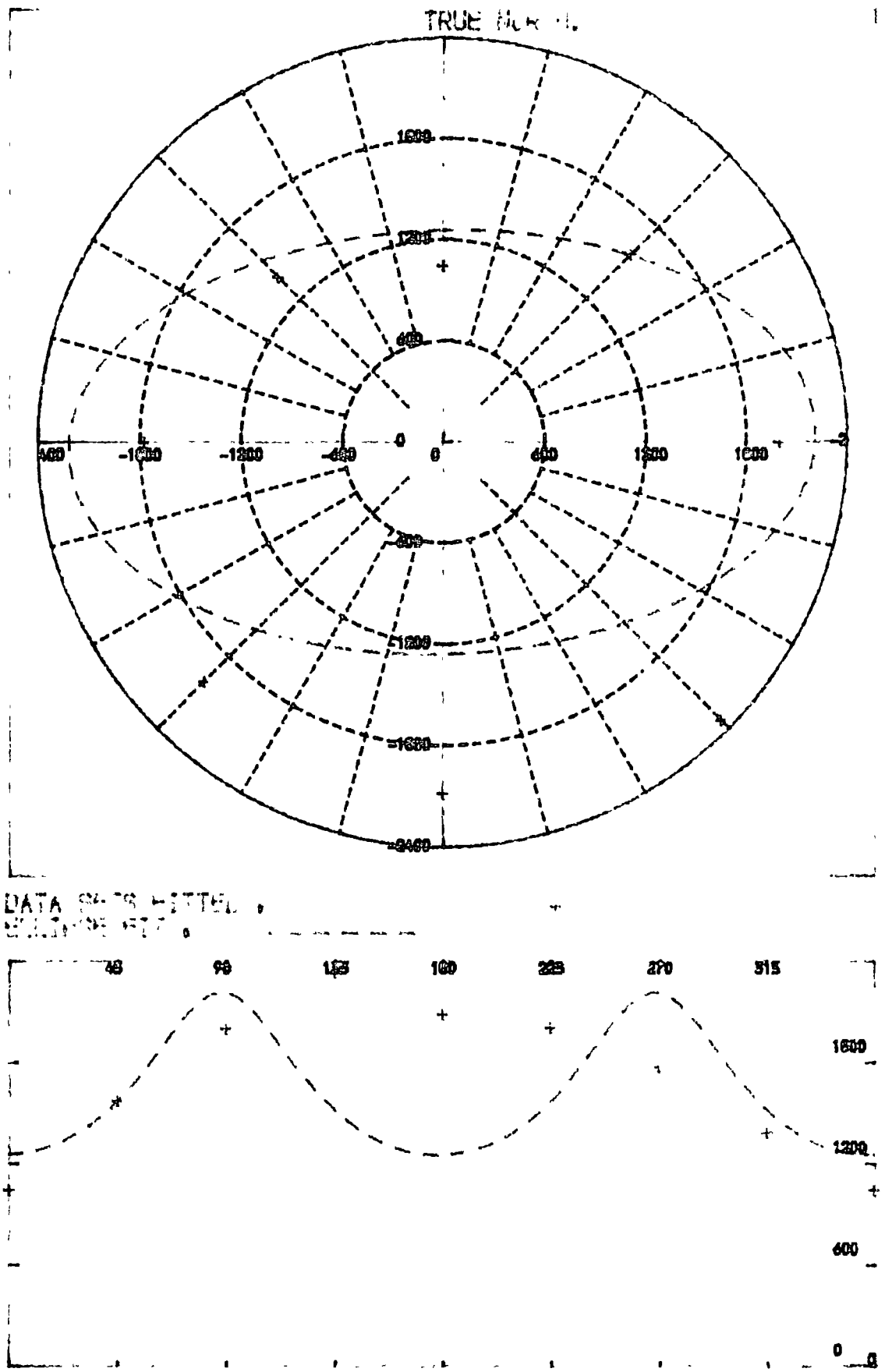
TRUE NORTH
1600
1200
800
400
0
-1600
-1200
-800
-400
0
400
800
1200
1600
-2400
45
90
135
180
225
270
315
1600
1200
800
400
0

Fig. 77

Fig 78:

Detail of the fault pattern and geophone positions in DBARRAY, of Fig 19.

Fig 79:

Ellipse fit and Backus's fit to velocities from DBARRAY.

Fig 80:

Inverse ellipse fit to velocities from DBARRAY.

Fig 81:

Ellipse fit and Backus's fit to attenuation at 35m in DBARRAY.

Fig 82:

Inverse ellipse fit to attenuation at 35m in DBARRAY.

Fig 83:

Ellipse fit and Backus's fit to the Loss Factor between 5 and 35m in DBARRAY.

Fig 84:

Inverse ellipse fit to the Loss Factor between 5 and 35m in DBARRAY.

Detail of fault pattern and geophone positions within DSARRAY, a radial seismic array on the top bed of The Malton Oolite, Spaunton Moor Quarry, North Yorkshire.

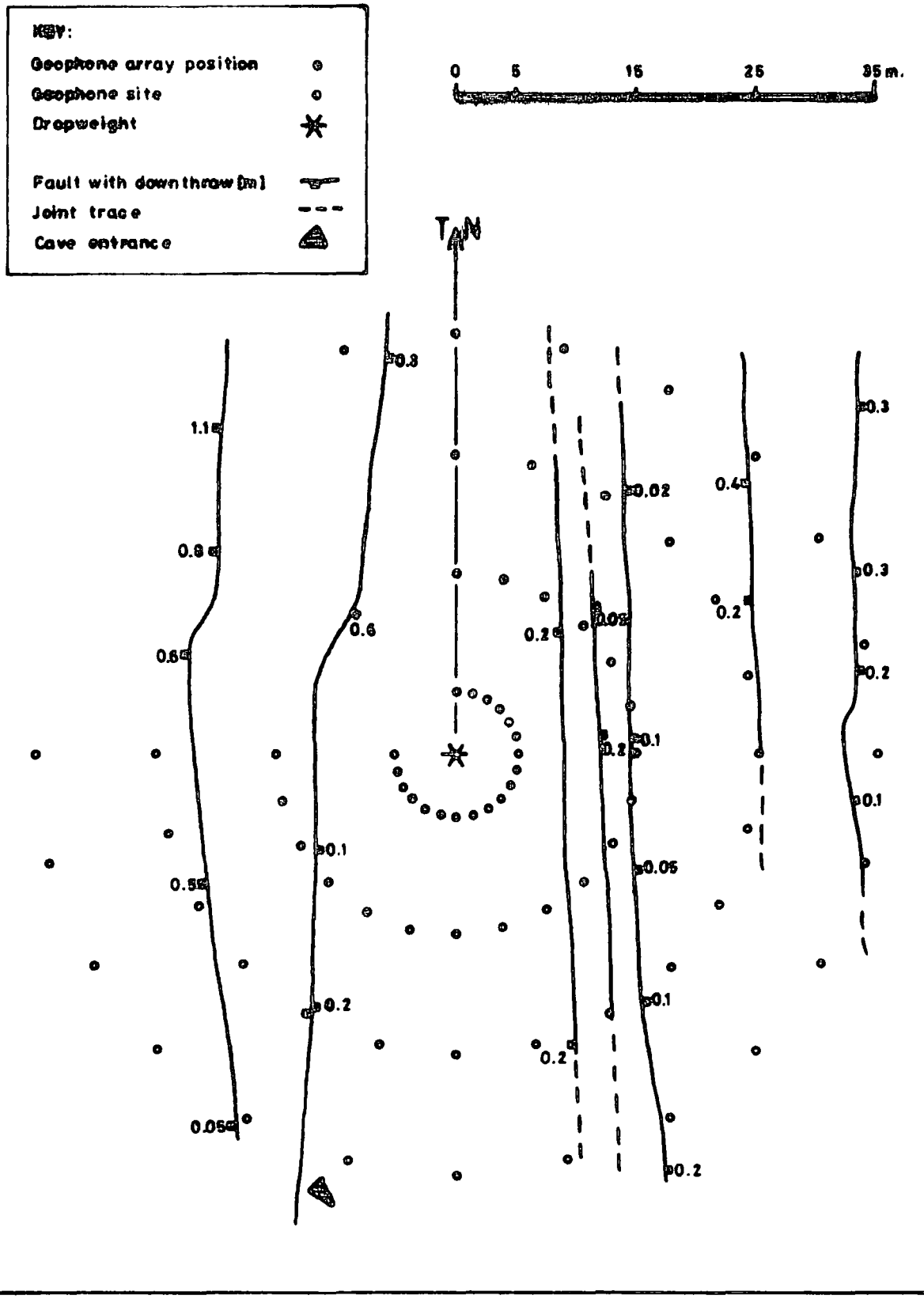

Fig 78

DROPWEIGHT ARRAY . VELOCITIES AT 35M. , METRES/SECOND .

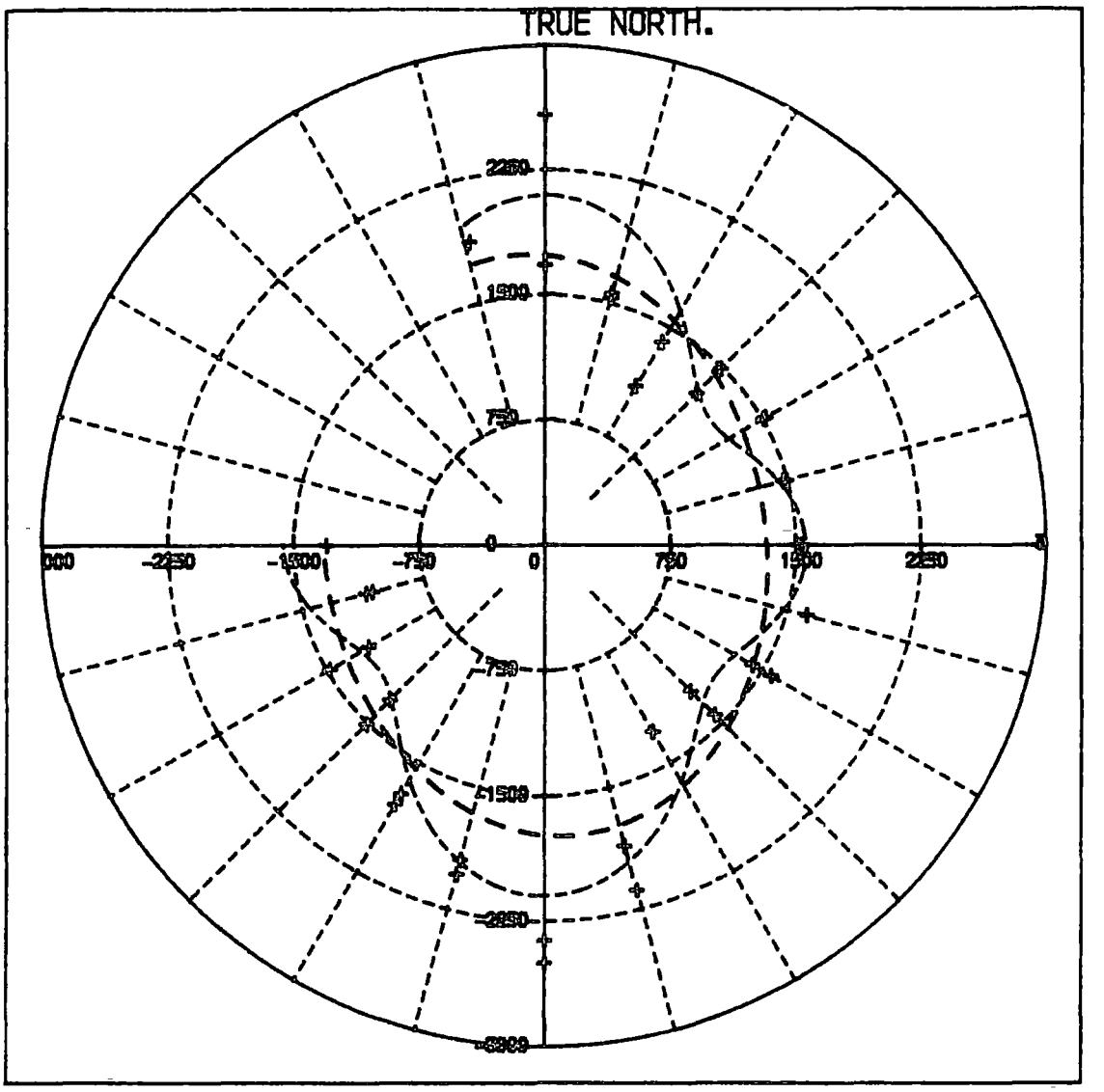

DATA SETS FITTED .
ELLIPSE FIT . BACKUS"S FIT .

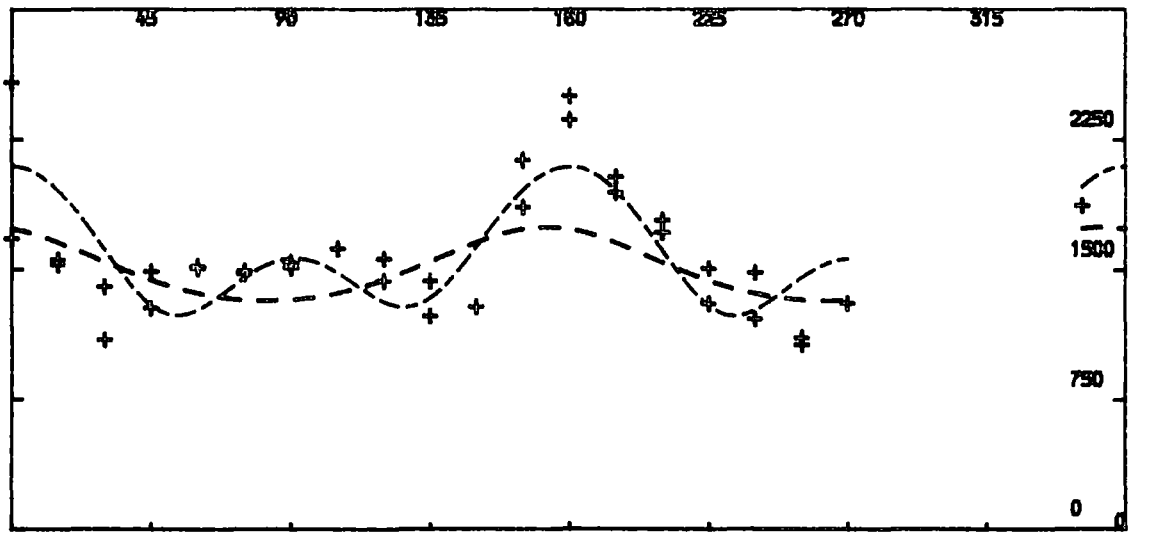

Fig 79

DROPWEIGHT ARRAY . VELOCITIES AT 35M. , METRES/SECOND .

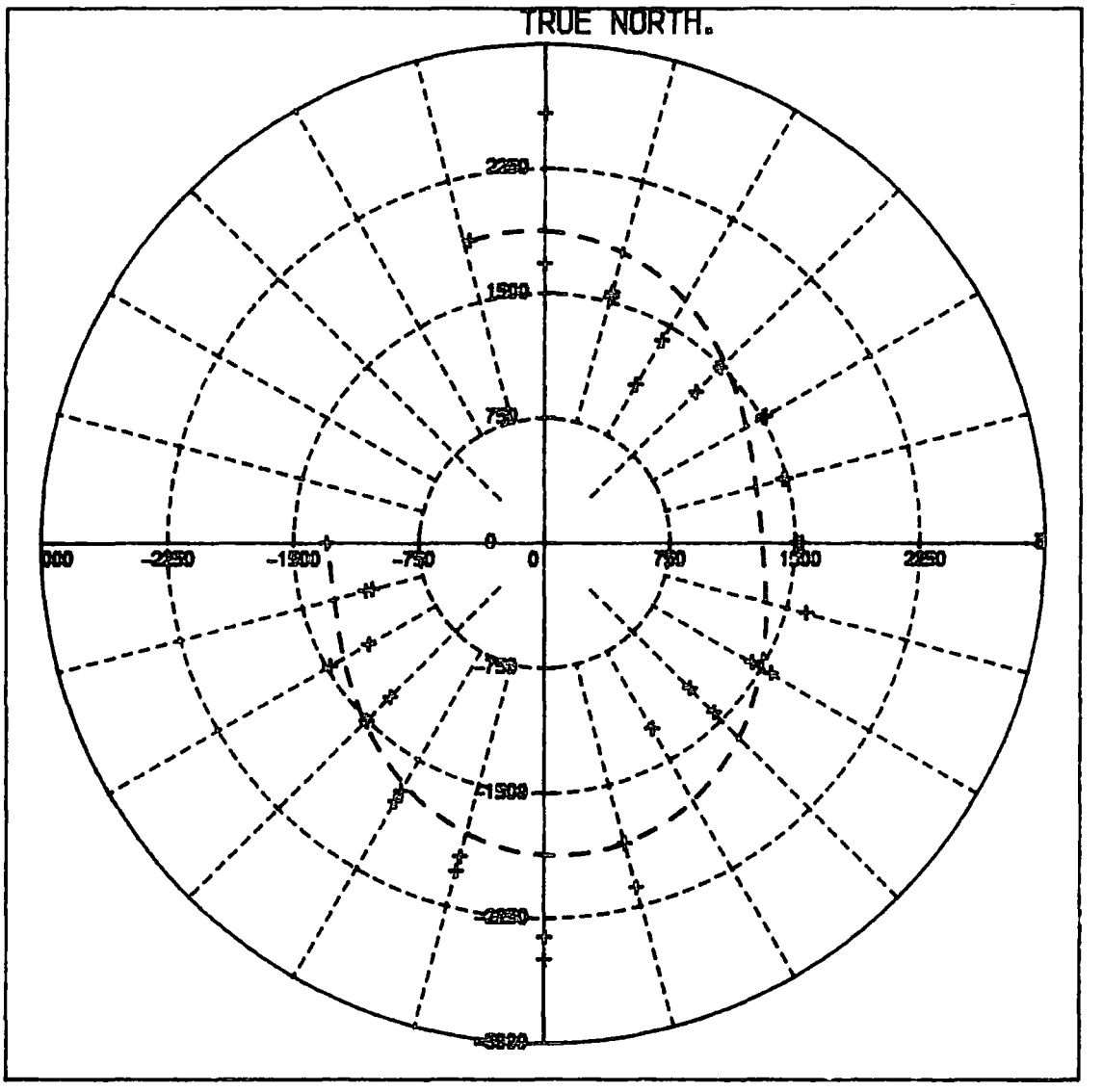

DATA SETS FITTED .
INV. ELLIPSE FIT .

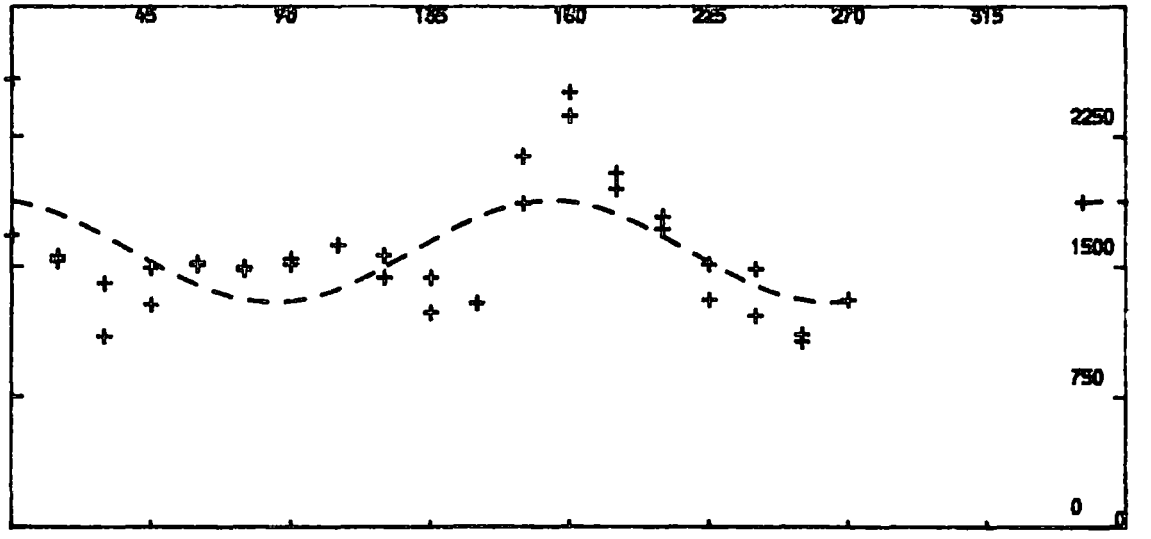

Fig 80

DROPWEIGHT ARRAY , ATTENUATION AT 35 METRES , DECIBELS.

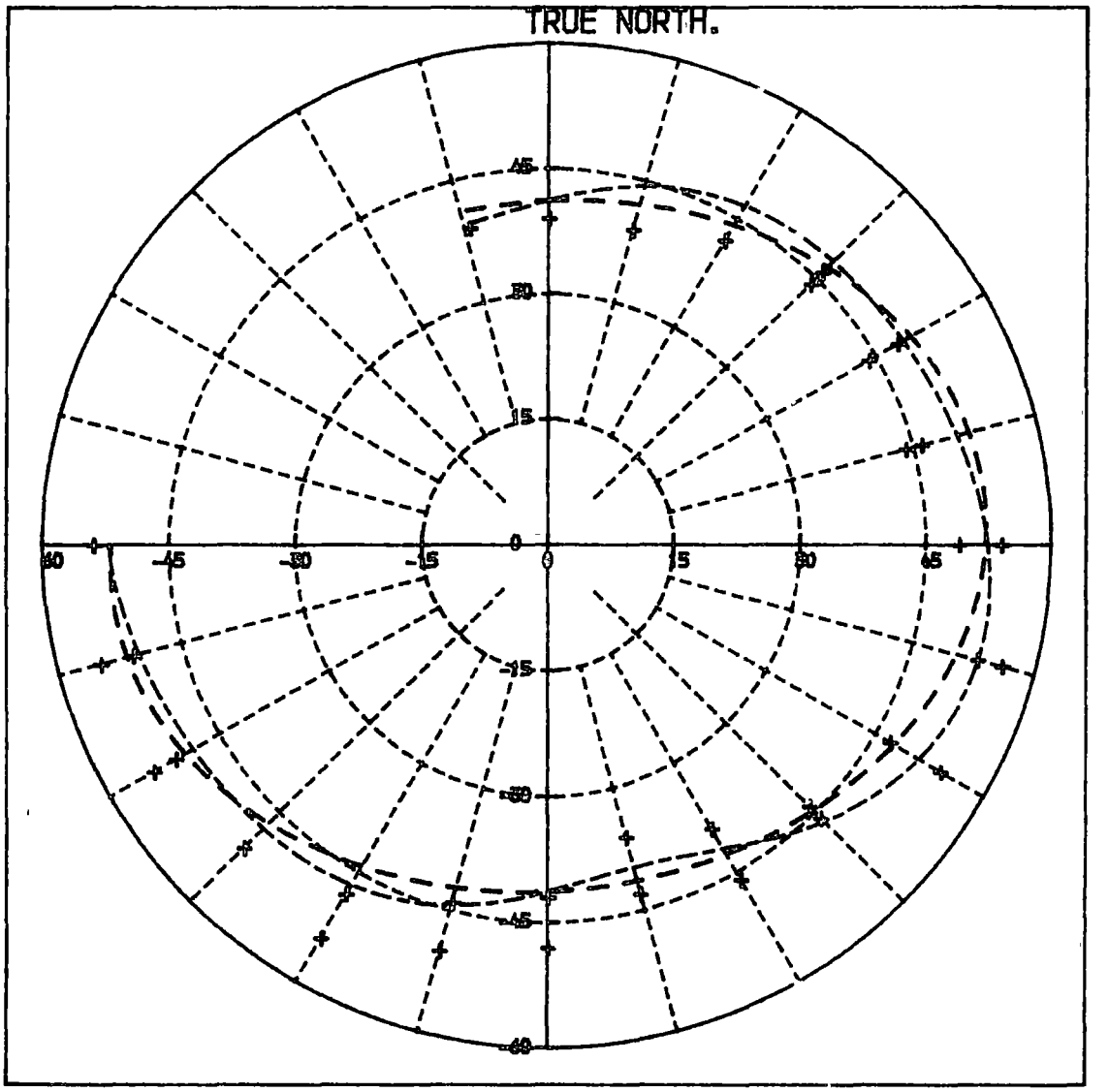

DATA SETS FITTED :
ELLIPSE FIT : - - - - - - BACKUS"S FIT : ---------

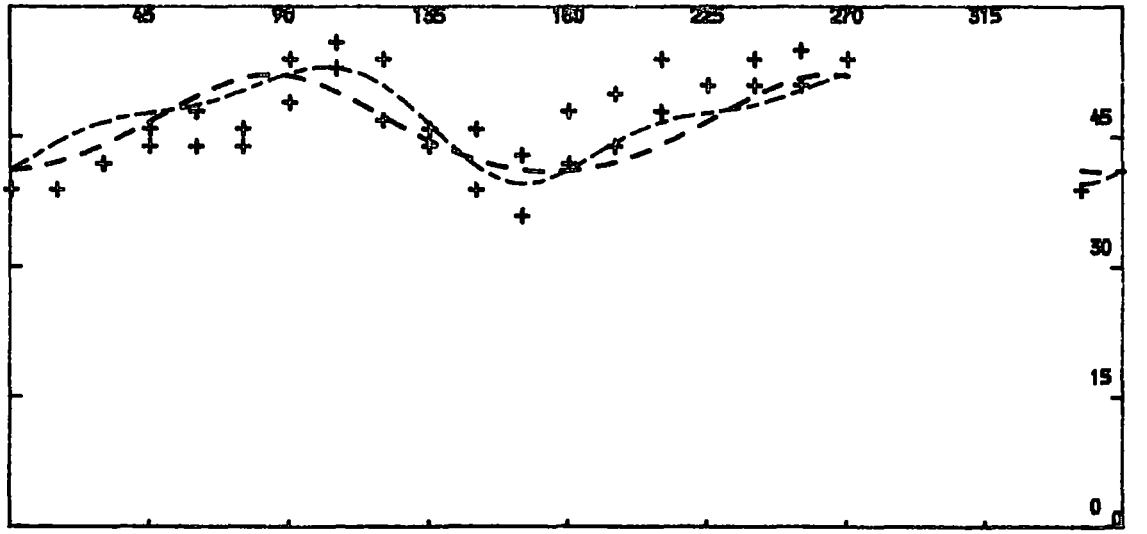

Fig 81

DROPWEIGHT ARRAY , ATTENUATION AT 35 METRES , DECIBELS .

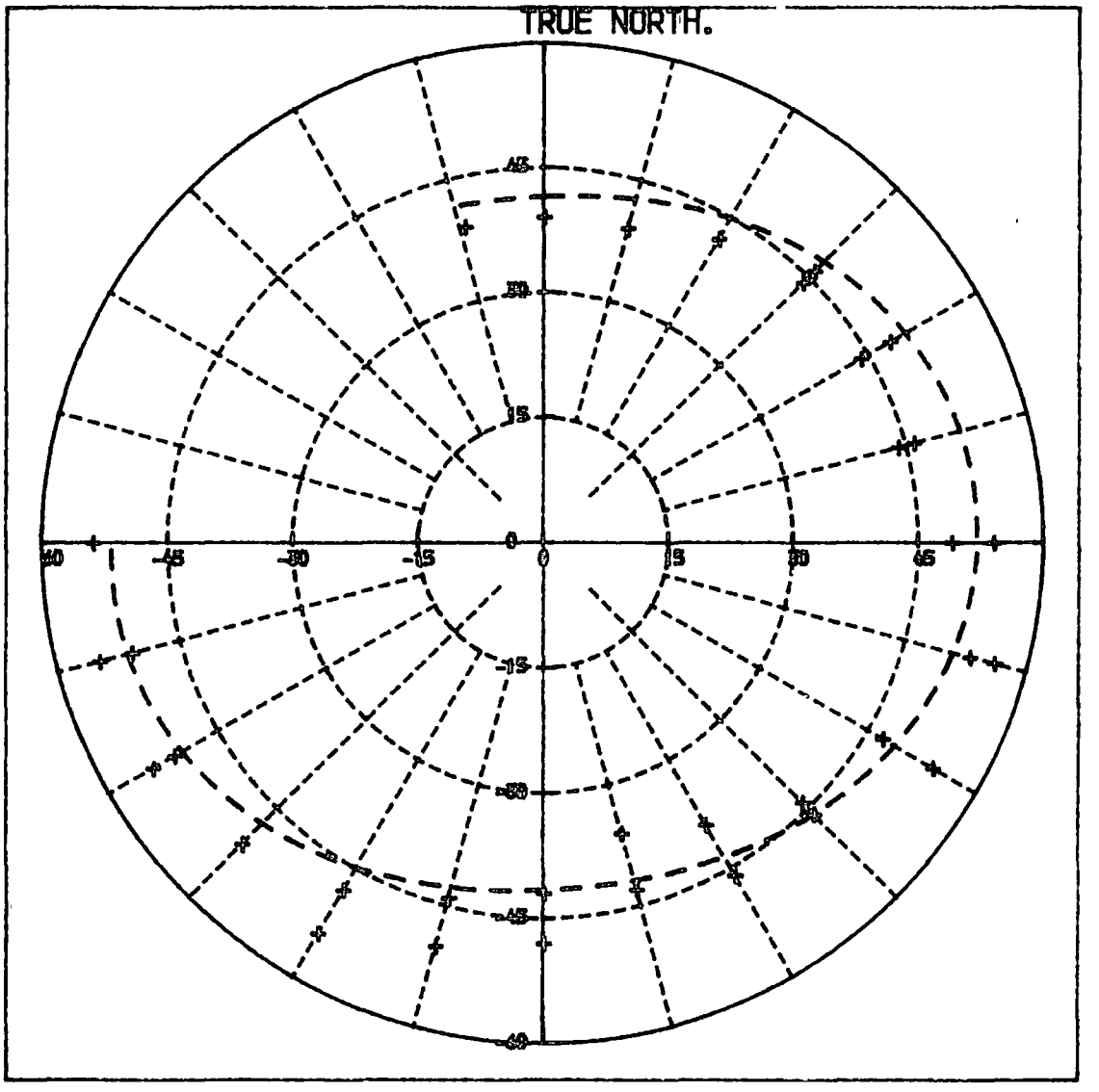

DATA SETS FITTED :
INV. ELLIPSE FIT :

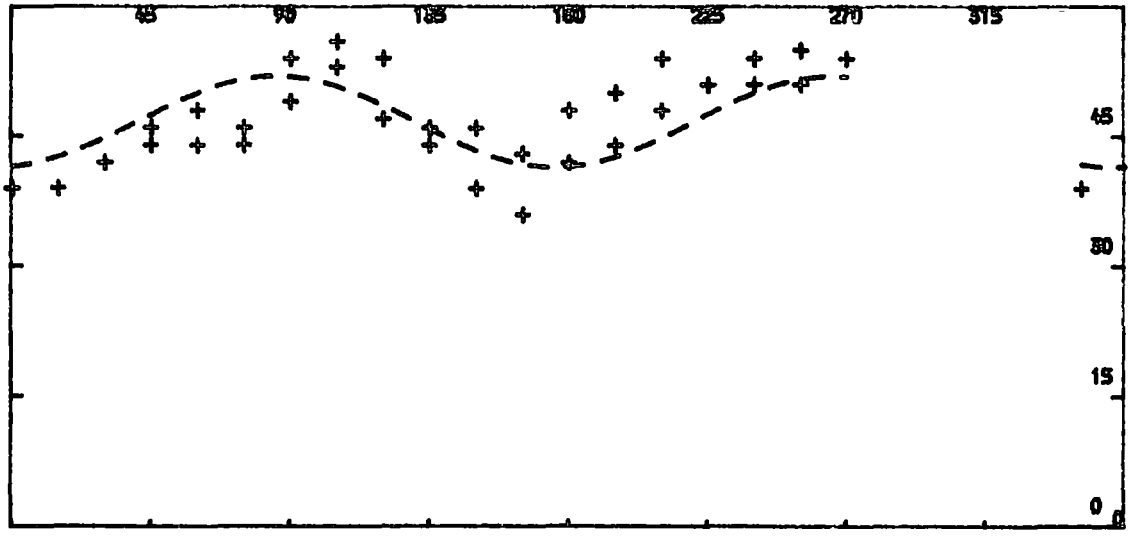

Fig 82

DROPWEIGHT ARRAY , LOSS FACTOR BETWEEN 5 AND 35 METRES.

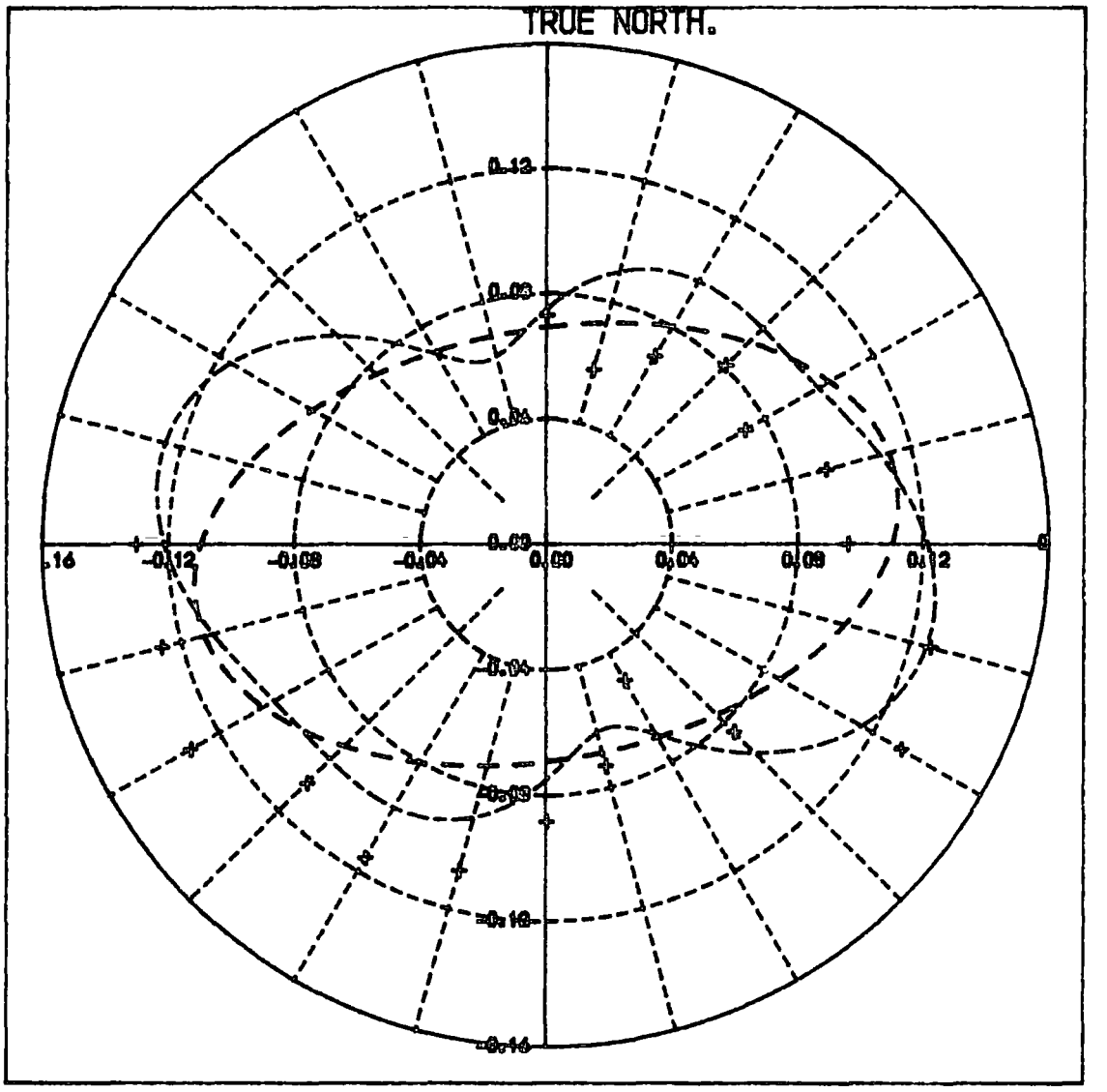

DATA SETS FITTED :
ELLIPSE FIT : - - - - - - BACKUS"S FIT : ---------

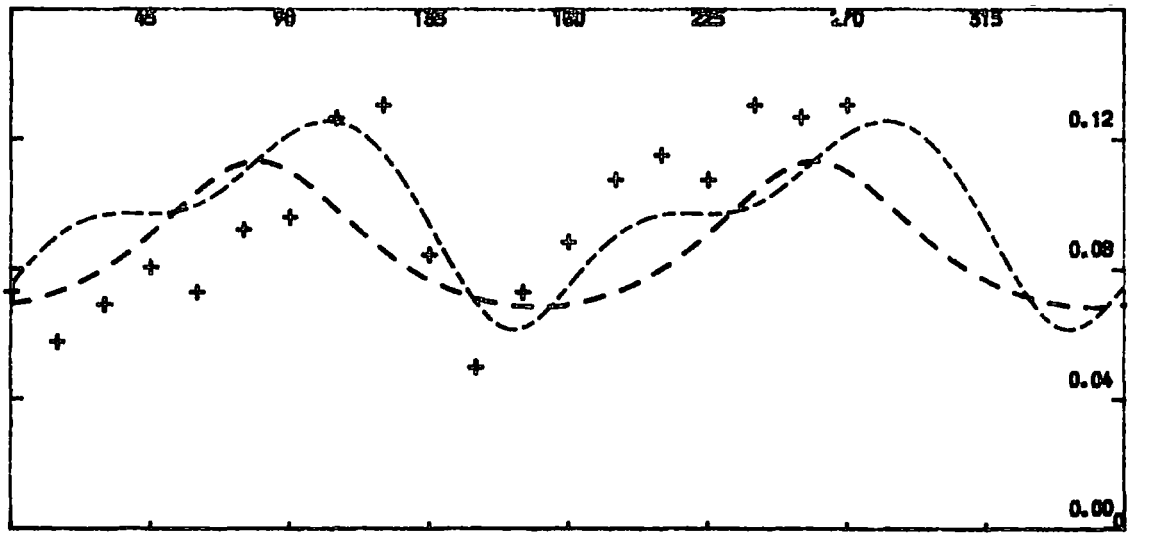

Fig 83

DROPWEIGHT ARRAY β LOSS FACTOR BETWEEN 5 AND 35 METRES.

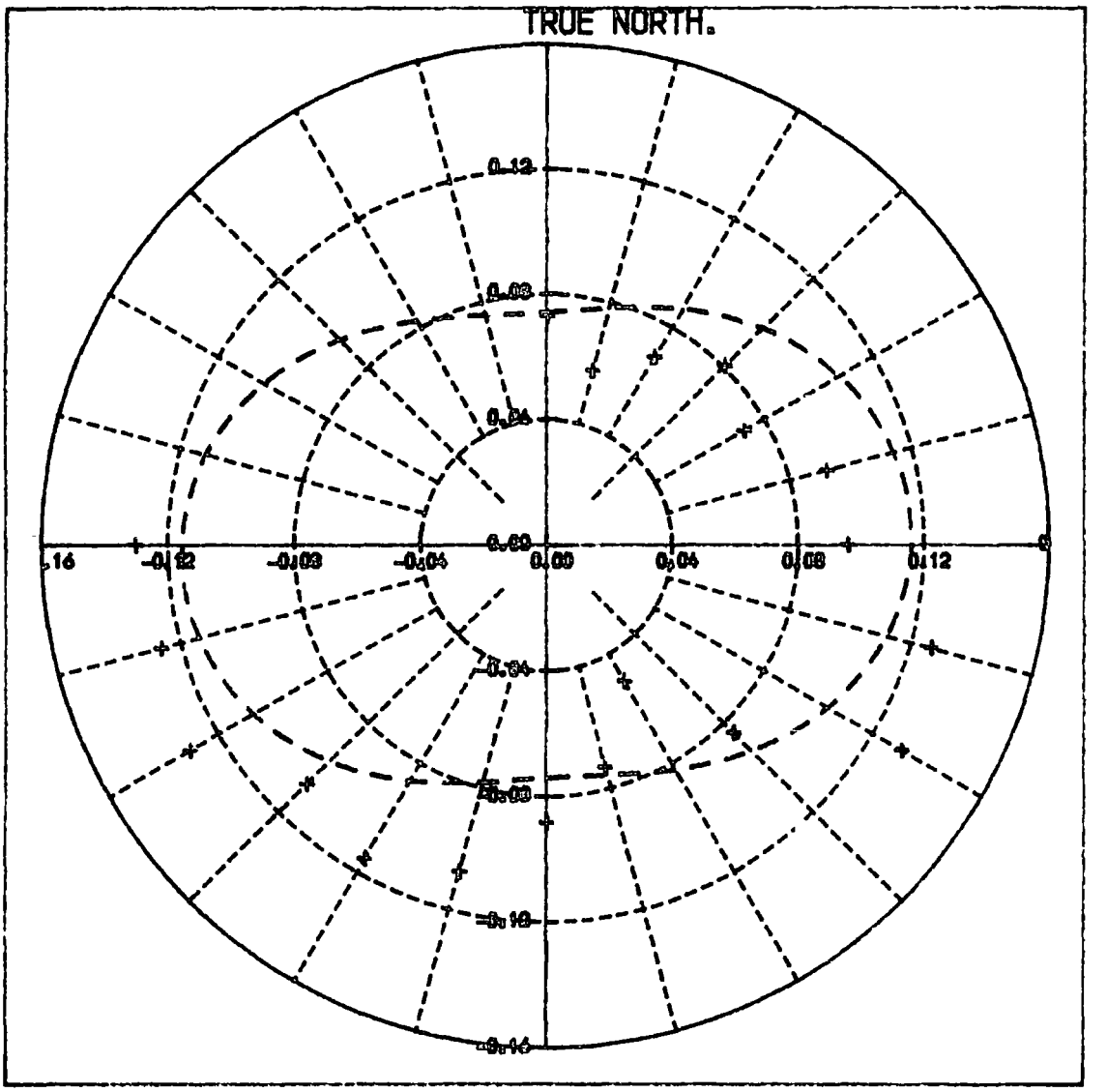

DATA SETS FITTED +
INV. ELLIPSE FIT

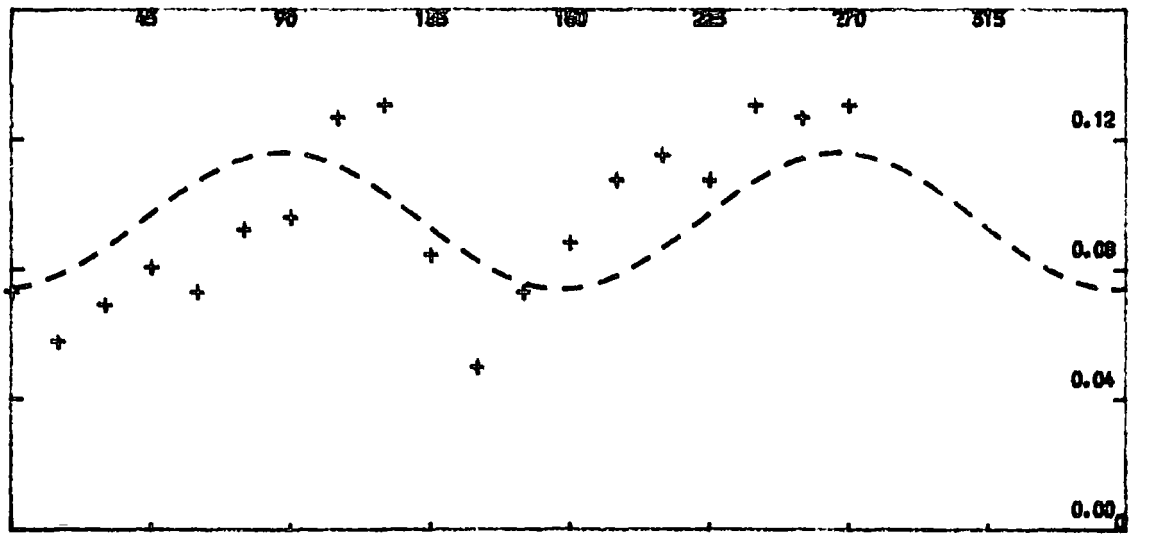

Fig 84

amplitudes shown for all radial geophones matched the amplitude on a reference trace, used as an overlay. A signal generator was used to calibrate the gain levels of the channels of the Bison recorder in decibels. Waveforms differed in an interesting manner, but recording facilities were not adequate enough to make a study of what could be a very revealing phenomenon. Some of the results from the DBARRAY or dropweight array are shown in Figs 78 to 83. Figs 78 and 79 show velocities at 35m, the radius at which two data sets were gathered on geophones four and five, Fig 77. Although there are now 38 data points, there is little to choose between the three curvefits.

Born (1941) gives an expression for a loss or attenuation factor for plane waves in terms of amplitude and distance. O'Brien (1967) discusses attenuation of seismic refraction signals in more detail, taking into account frequency and geometrical loss. Born's (op cit) loss factor is plotted in Figs 82 and 83. Because two data sets are involved the errors are combined and the scatter is greater. Backus's fit becomes unstable.

Tourenq et al (1971) give a relationship between a quality index and a combination of fissure and intrinsic porosity. Their quality index is the percentage ratio of the observed velocity: to the velocity in an equivalent fresh rock type of zero porosity. Because the profile of intrinsic porosity across a joint block margin is known at Spaunton Moor, (Riemer, 1979), one could in theory solve for the fracture spacing and mean fracture width. Unfortunately, the propagation of errors leads to unusable results, but it may be that the methods described could be refined, so that the axes of ellipses fitted to field

observations of seismic anisotropy will yeild a useful description of average, orthogonal maximum and minimum fissure porosities.

7.6 Finite element analysis of conjugate-shear bounded blocks.

7.6.1 Spaunton Moor shear joint sets.

The joint sets seen at Spaunton Moor Quarry are discussed in Section 2.1. In Chapter 4 the importance of an adequate description of patterns of jointing and faulting is discussed.

For a block bounded by conjugate shears to be rotationally stable, it is necessary that:

$$Tor(xy) = -Tor(yx) \quad \ldots\ldots\ldots\ldots\ldots\ldots\ldots\ldots (46)$$

where:

$Tor(xy)$, $Tor(yx)$ are the shear stresses along adjacent faces.

This is usually taken to be the case for engineering structures, where rotational stability is assumed. Rotation of a conjugate-shear bounded block may be initiated by an imbalance in the frictional resistance on two adjacent sides. Stick-slip is recognised as a mechanism by which individual faults move discretely and irregularly. Such rotation could induce a subsidiary fracture pattern within the block. The resulting overall fracture pattern would necessarily retain a two-fold axis of rotational symmetry, but would have lost all reflectional symmetry.

It may seem far-fetched at first sight to compare the shear joint sets of Spaunton Moor with the conjugate wrench fault controlled Scourie Dykes of the Loch Torridon area. However, it is maintained that they are mechanically similar. In the Lewisian, the fractures having the highest hydraulic conductivity are intruded by mappable basic dykes. Some light is therefore thrown onto the distribution of hydraulic conductivities within a naturally occurring fracture system.

The Finite-element model and the resulting discussion is intended to be relevant to both areas.

7.6.2 Scourie dyke emplacement near Loch Torridon.

The field evidence is discussed in detail in Westerman and Holland (submitted), and a brief review will be given here. Large scale structural variations were considered by Sutton (1949). Small scale structures have been described and classified by Cresswell (1969, 1972), and his notation is followed here. Those which affect the margins of Scourie dykes comprise: earlier (S4) and later (S6) subparallel foliations; drag folds affecting those foliations (F5, F7); and drag of earlier structures. Earlier structures include boudin trains parallel to S3, Fig 87b, and the S3 foliation itself. Two examples of the drag folds affecting dyke margins are shown in Figs 86 and 87a. Sites at which this evidence can be seen are marked in relation to the dykes in Fig 85a. Fig 85b shows an interpretation of the field evidence expressed as an overlay to Fig 85a. The 'PIPS' are areas in which post-D3 structures are rare, and the dyke swarms are areas in which D3 structures are strongly deformed in association with dyke injection. PIP 80 is proposed as a type area for the first phase of Scourie dyke injection.

PIP 80 is interpreted as a conjugate-shear bounded block which is preserved in the process of being invaded by secondary dextral shears. Ramsay (1980) has described brittle to ductile transition in shear zone deformational styles such as is seen in this area and he has commented (op cit) that, whilst conjugate shears are common, the two two shear sets do not seem able to operate synchronously. The concentration of drag folds

Fig 85:

a) Distribution map of the Scourie dykes, north of Loch Torridon, Ross-shire.

b) Overlay to Fig 85a, to show the distribution of small and large scale Inverian structures.

Fig 86:

a) View looking east, of the cross-section of a sinistral drag fold plunging 40/110 degrees TN, and affecting the margin of a Scourie dyke at NGR NG 811 587. Scale: Silva compass oriented north-south, of length 18cm.

b) View looking east at a folded early-amphibolite boudin train. The main S3 foliation trend is 230 degrees TN. Scale: Messrs. Mike and Chris Lucas, 19.Apr.1981.

Fig 87:

a) View looking east of the cross-section of a sinistral drag fold plunging 30/100 degrees TN, and affecting the foliation within a Scourie dyke, at NGR NG 822 591. Scale: Dr. Rob Taylor.

b) Overlay, structural sketch of Fig 87a.

Fig 88:

Capped yeild failure envelope to relate:

a) Badcallian, D3 and

b) Inverian, D4 to D7 stress fields.

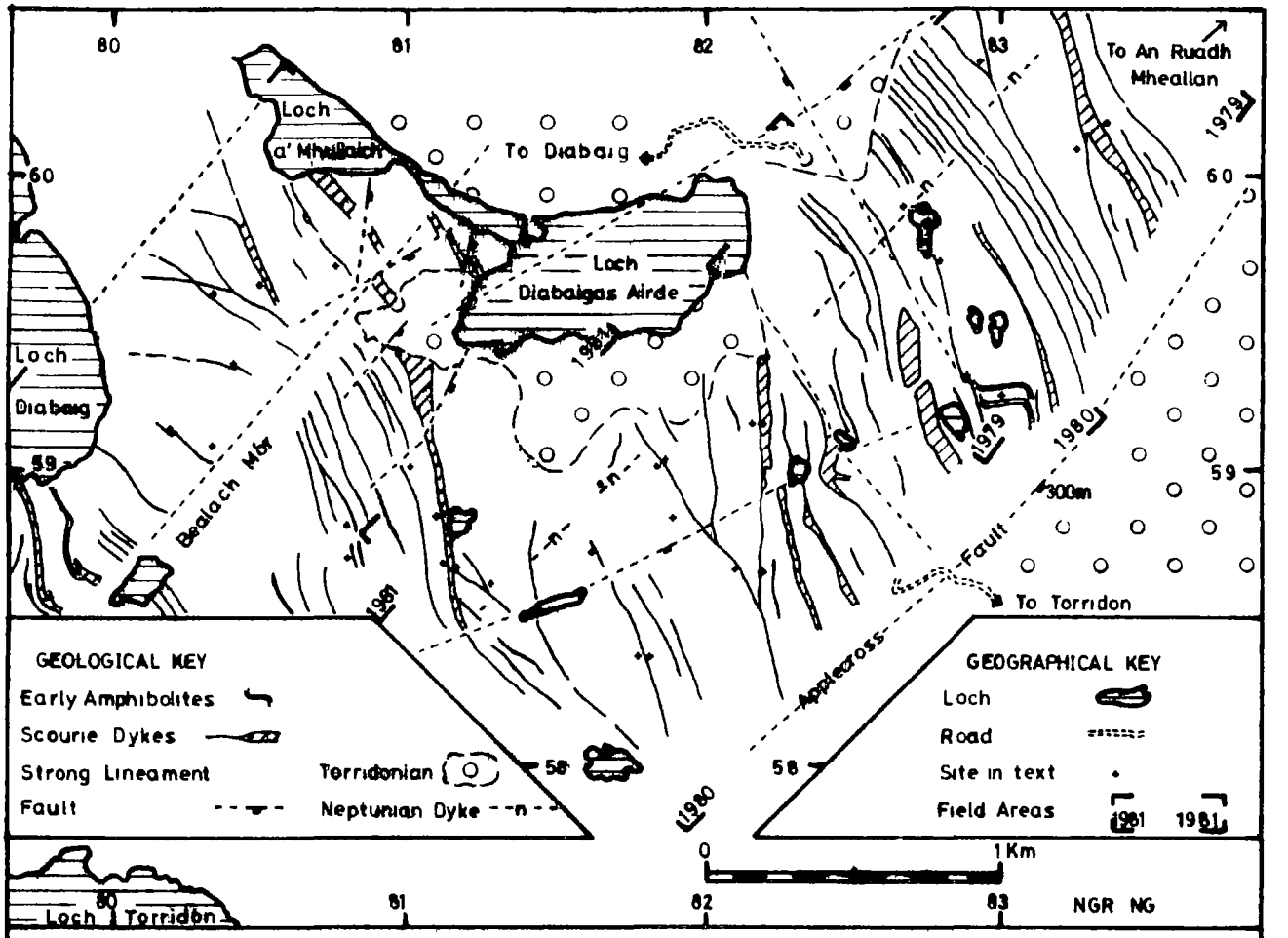

ABOVE Map to show Scourie Dyke distribution, BELOW Overlay defining Inverian structural units

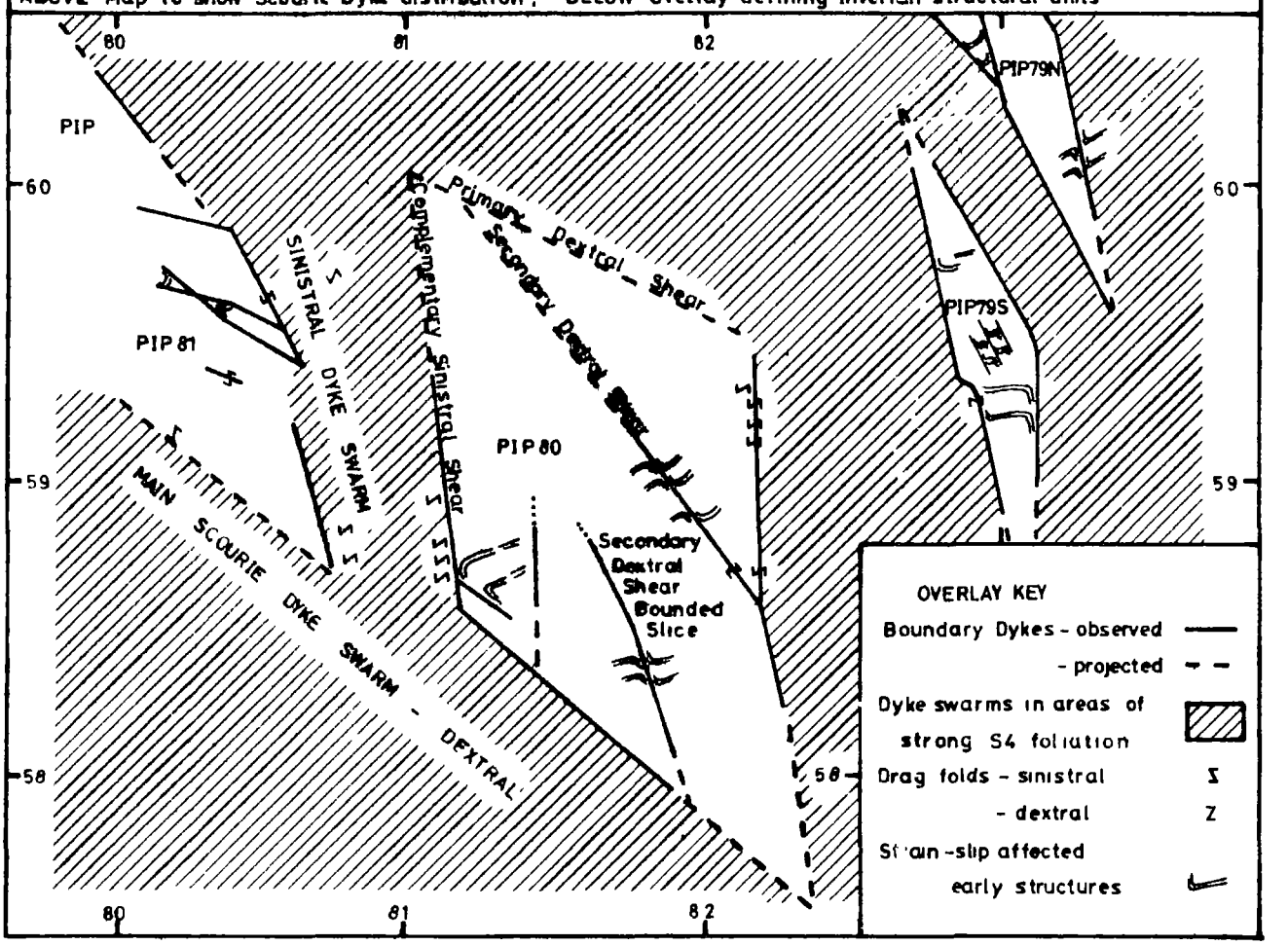

Fig 85

Fig 88

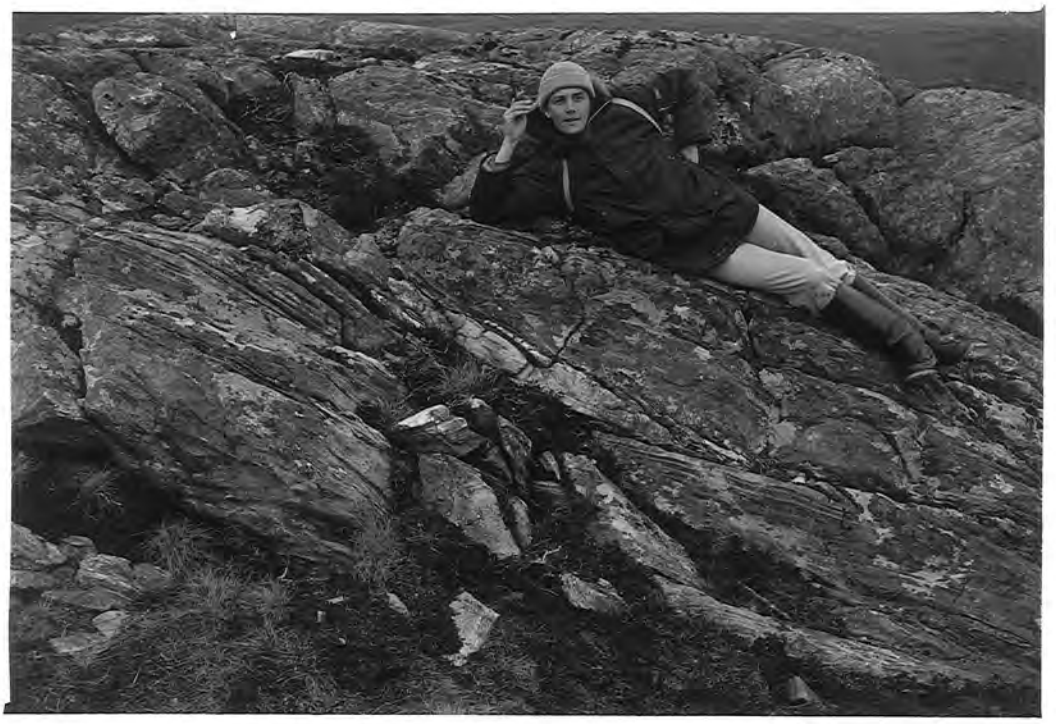

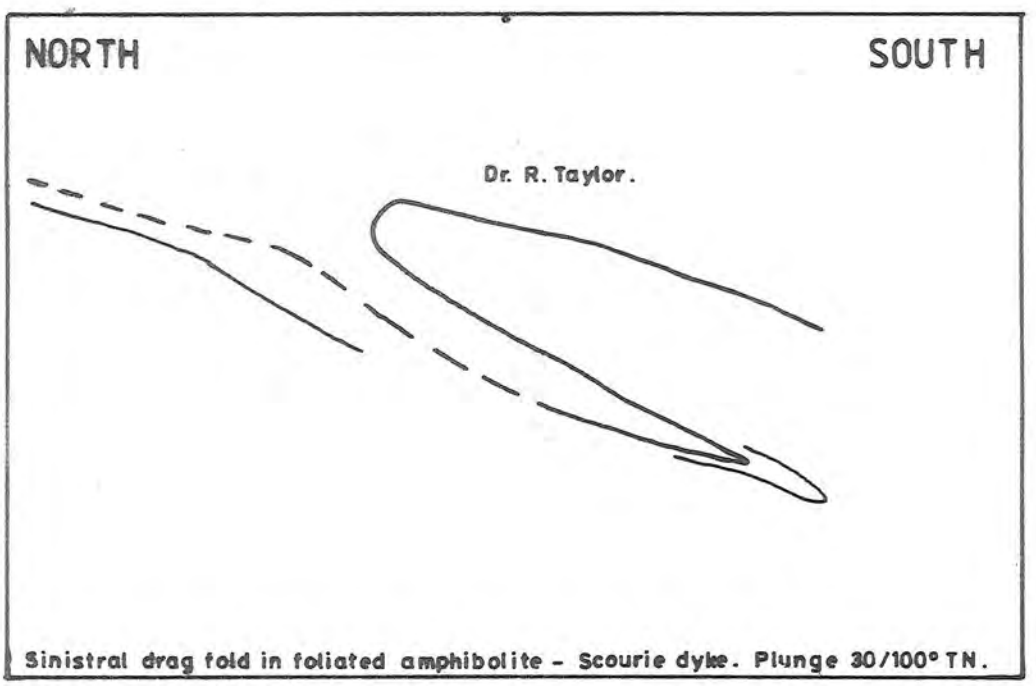

Sinistral drag fold in foliated amphibolite - Scourie dyke. Plunge 30/100° TN.

Fig 87

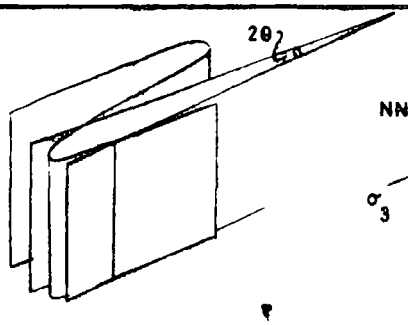

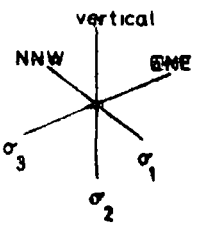

KEY

$\sigma_3, \sigma_2, \sigma_1$ minimum, intermediate, & maximum principal stresses

2θ angle subtended by failure surfaces and bisected by σ_3

ϕ angle of internal friction

EARLY SCOURIAN

(BADCALLIAN)

D3

SIMILAR FOLDS,

VERTICAL PLUNGE

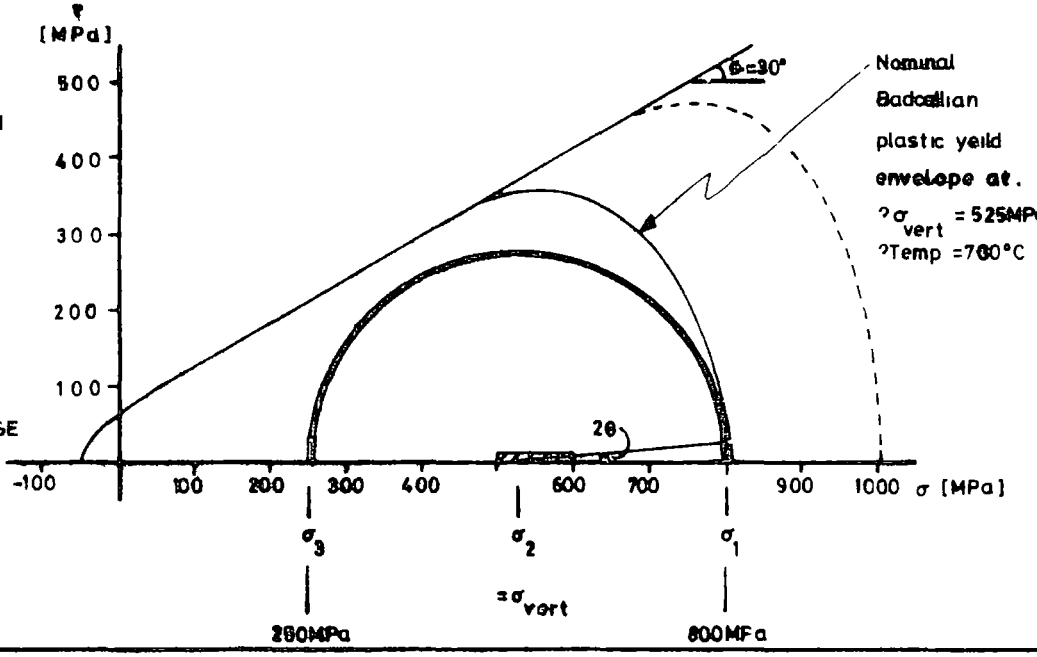

Capped yeild Mohr-Coulomb failure model to relate · Badcallian (ABOVE) and Inverian (BELOW) stress fields

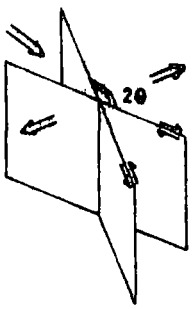

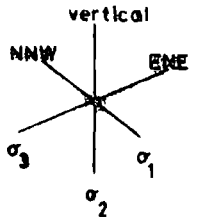

NOTE

$\sigma_2 = \sigma_{vertical} = \sigma_{hydrostatic} = \sigma_{dyke} > \sigma_n$

σ_n stress normal to failure surfaces

LATE SCOURIAN

(INVERIAN)

D4 - D7

CONJUGATE SHEAR,

DYKE INJECTION

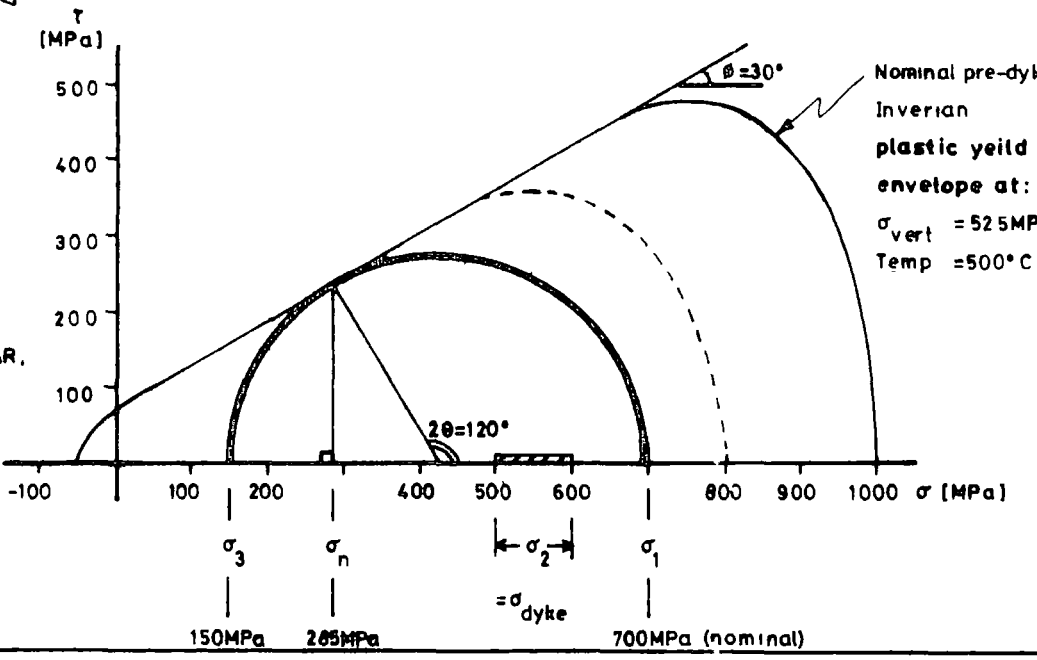

Fig 88

at two corners of PIP 80, and the two-fold rotational symmetry of the secondary dextral shears within it, suggest that it experienced a dextral couple as the northwesterly trending, dextral member of the conjugate shear set became dominant. Figure 8b shows a stress configuration which explains the observed phenomena; the dykes were injected during a shear regime, and the vertical, or hydrostatic stress exceeded the stress normal to the shear planes.

7.6.3 Model and results.

A Finite-element model was set up using PAFEC (Program for Automatic Finite Element Calculations). The pips and the shear zones were represented by the mesh shown in Figs 89 and 90. It was hoped to induce rotation of the central pip by seeding the shear zones adjacent to it with two elements having more rigid properties. It was hoped that the resulting stress distribution would show which parts of the pip were likely to fail first. Hence the mesh concentration in that area. In PAFEC level 3.1 (Henshell, 1975) plastic elements were not available. The shear zones were represented by lower elastic moduli. Rotation of the central pip did not occur, and stresses were distributed within it with reflectional symmetry, Fig 91. The stress distribution in the plattens does show a rotational symmetry, Fig 92.

For a Finite-element model to be useful, the ductile shear zones must be modelled by elements with plastic yeild criteria. Later versions of PAFEC may offer this facility, and node generation to simulate crack propagation. Then it will be possible to map the stress trajectories in a system of conjugate-shear bounded blocks as secondary shears begin to develop.

Fig 89:

Finite-element model to represent the large scale Inverian structural units, or conjugate-shear bounded blocks, of Fig 88b.

Fig 90:

Machine drawn Finite-element mesh of Fig 89, with displaced shape shown in dashed line.

Fig 91:

Stress distribution within the central one of nine conjugate-shear bounded blocks from Fig 89, representing PIP 80 of Fig 85b.

Fig 92:

Stress distribution within the plattens of Fig 89. Note the asymmetry due to the two elements of intermediate elastic modulus placed at the corners of the central block.

Diagram to show the representation of Laurian structures north of Loch Torridon, Ross-shire by a Finite-Element model.

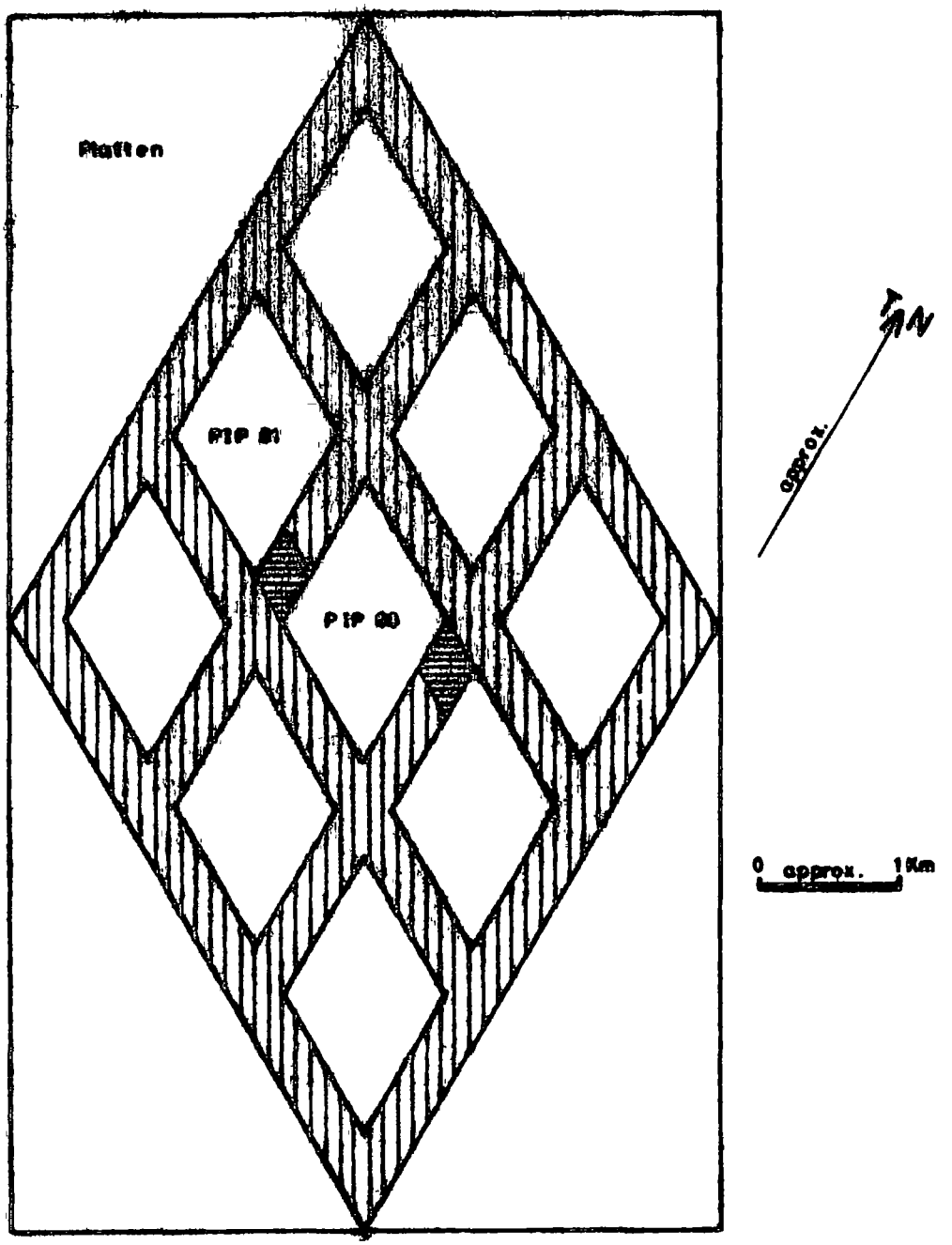

KEY:

Sets of elements representing conjugate-shear bounded blocks of cold gneiss (also plattens) with Young's Modulus = 1×10^4 MPa

Sets of elements representing dyke swarms, Y. M., E = 1×10^0 MPa

Two elements to give two-fold rotational symmetry, E = 1×10^2 MPa

Fig 89

Finite-element mesh, with displaced shape shown in dashed line. Constraints arrowed.

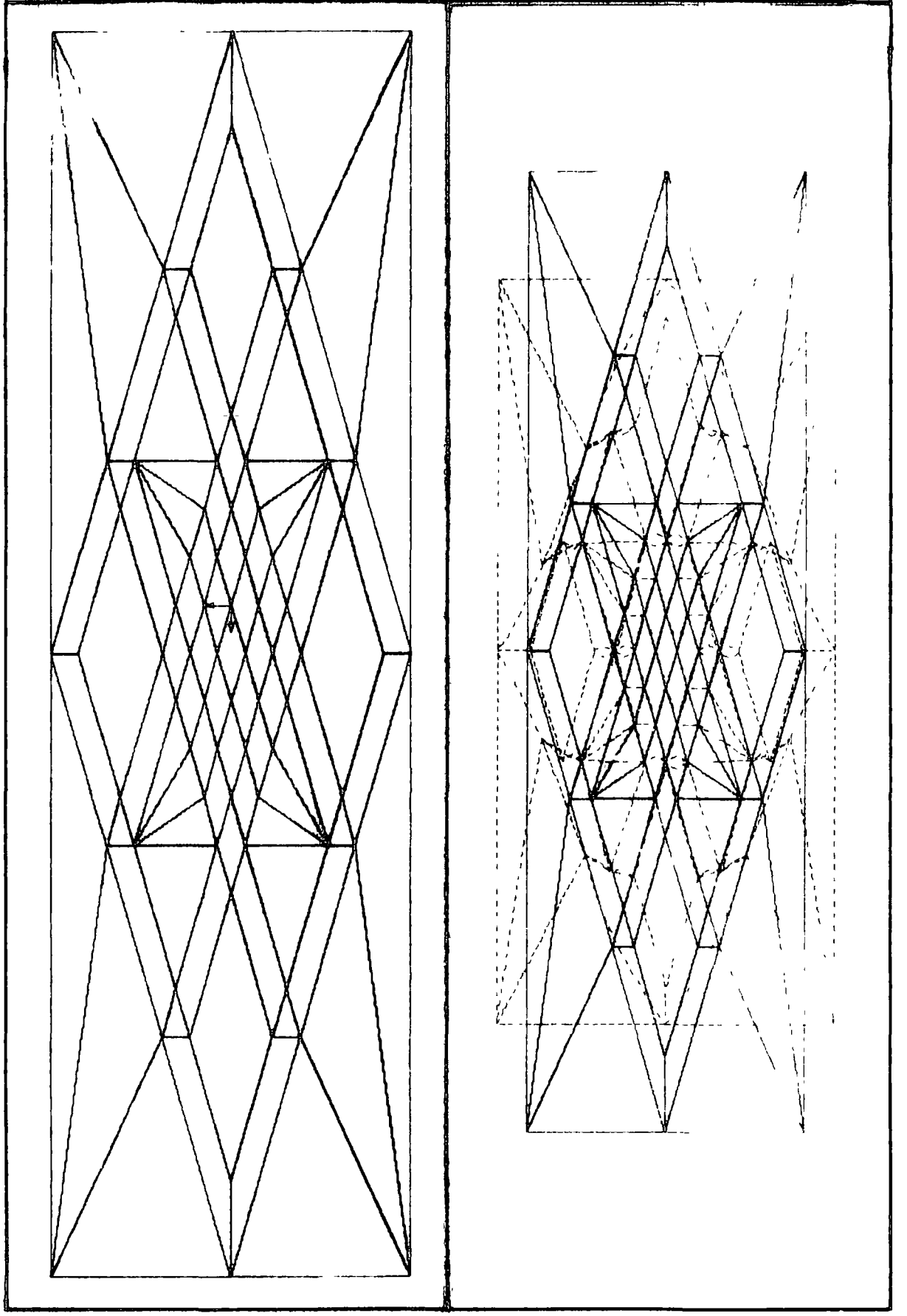

Fig 90

Stress distribution within the central block (PIP 80) of the Finite - Element model of conjugate shear.

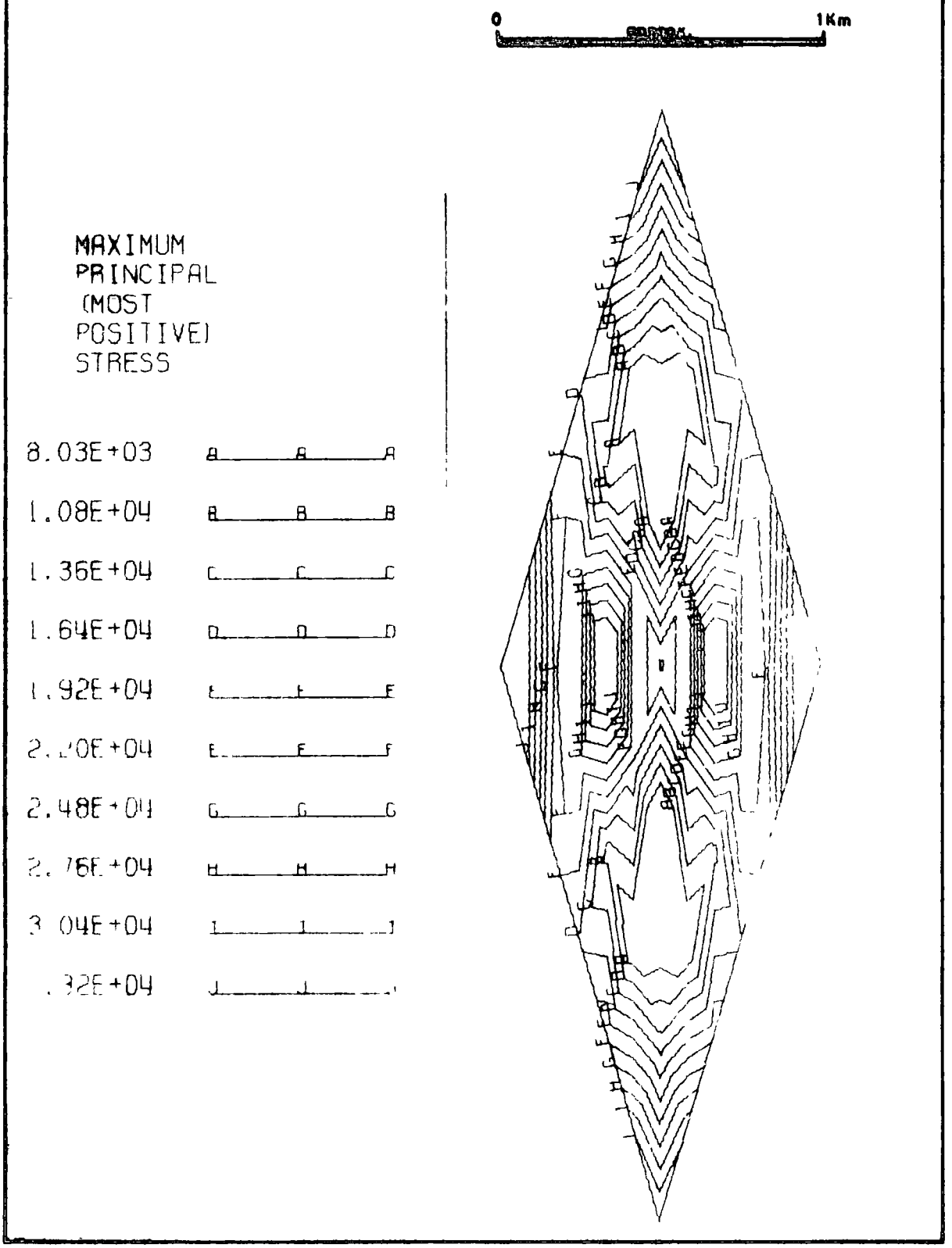

Fig 91

Stress distribution in the plattens of the Finite-Element model of conjugate shear.

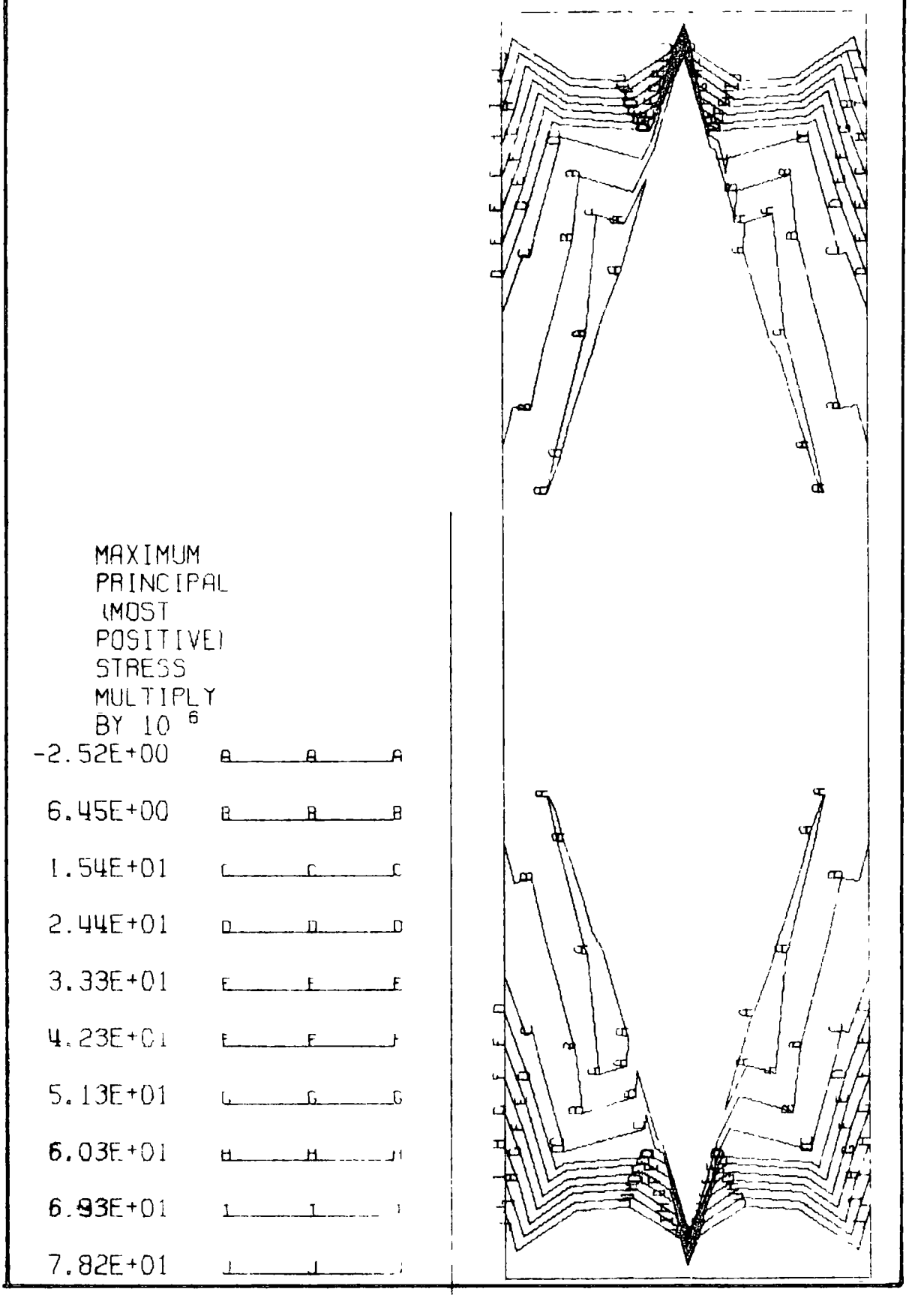

Fig 92

7.6.4 Capped-yeild failure criteria.

The deformational event, D3, which preceeded those associated with the intrusion of the Scourie dykes, (D4 to D7), is marked by similar folds having sub-vertical plunge, Fig 88a. The very last structures to affect the Scourian basement are late brittle normal faults, and neptunian dykes which have developed in Torridonian times at the back of fault scarps, Fig 85a. It would be useful to know if the entire sequence of deformational events described in the Lewisian are inter-related, Westerman and Holland (op cit). The discussion on fracture patterns and their heirarchical generation, Chapter 4, could lead to a coherent theory of crustal evolution, from early plastic to late brittle phases, given failure criteria which described both plastic and brittle failure modes. Plastic yeild caps have been diagrammatically added to Fig 88, and a possible form of equation is investigated in Fig 93. Lawn and Wilshaw (1975) describe the energy balance, or thermodynamic basis of Griffith's crack theory. Brace (1960) shows that this leads to a parabolic Mohr envelope in tension, Section 2.1, equation (24). Westerman and Holland (op cit) propose that in the plastic, or partial melt regime, melt porosity is not uniformly distributed but would be intersected in greatest abundance by a plane normal to the maximum principal stress. Paterson (1970) shows that this can be related to the variation in the local chemical potential of a non-hydrostatically stressed solid. The equation given and fitted to the notional yeild curve of Fig 93 can then be derived, Westerman and Holland (op cit).

Since the localised chemical potential, or Gibbs Free

Fig 93:

Trial curve fit of a possible form of equation to describe a capped-yeild failure envelope.

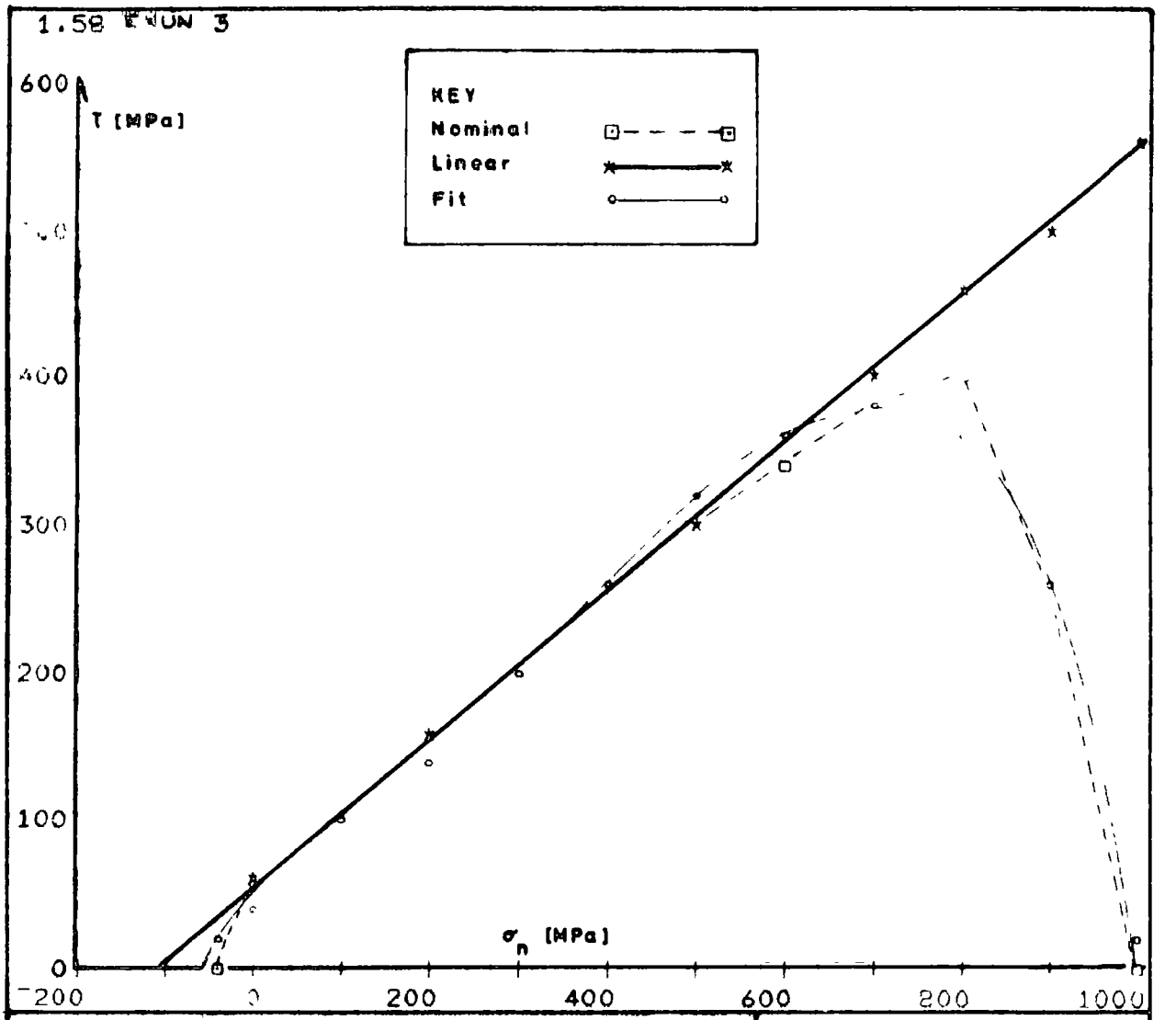

Table of shear stress values plotted T [MPa]

Nominal, T1	Linear, T2	Fit. T3	T1-T3
1.0	25.0	16.0	-15.0
50.0	50.0	38.3	11.7
100.0	100.0	91.4	8.6
150.0	150.0	148.9	1.1
200.0	200.0	206.5	-6.5
250.0	250.0	261.5	-11.5
300.0	300.0	311.1	-11.1
345.0	350.0	350.9	-5.9
390.0	400.0	373.0	17.0
400.0	450.0	360.1	39.9
250.0	500.0	265.7	-15.7
1.0	550.0	13.6	-12.6
RMS MN SD FOR T1-T3 :-			
	16.0	.0	16.7

APL Function.

```
    ∇EXUN[□]∇
∇ D EXUN N
[1]   L←-⍀T1-T2×D
[2]   SM←SN∘.*¯1+⍳N
[3]   X←L⌹SM
[4]   T3←T2×D×*-SM+.×X
[5]   ⍝KY SIZE
∇
```

Coefficients at T = 773°K

D = 1 58

X = ¯8827 6

Y = ¯32.901

Z = 4.019×10^{-2}

Summary of curve fit to the nominal Inverian capped yield criteria using the function :

$$T = (c + \sigma_n \tan\phi).[\, D.\exp(R.T/(X + Y\,\sigma_n + Z\,\sigma_n^2))]_{P,T,V}$$

Fig 93

Energy, is used as a measure of the proportion of melted or plasticised rock intersected by any given plane, this theory is contentious. It must be stressed that it is compared with a purely intuitive form of the failure envelope in Fig 93. However, a yeild cap of this form would explain the phenomena of conjugate ductile shears described by Ramsay (1980). Conjugate ductile shears have dihedral angles containing the minimum principal stress, which are less than 90 degrees, Fig 88. Conjugate brittle shears have dihedral angles which are greater than 90 degrees by the angle of internal friction (Phi).

7.7 Anaglyphs in geology.

Anaglyphs are convenient to project, and may be used to illustrate the development of three-dimensional structures through time. An interactive computer program is presented which outputs an anaglyph, a conventional stereopair, and orthoscopic views. Suppliers of suitable inks and filters are given.

The paper by Johnson and Richter (1979) is a stimulating reminder that stereoviews are not only an essential method of presenting remote sensing imagery to the analyst; but a very useful way of presenting three-dimensional geological data. In fact, geological problems are essentially four-dimensional, since structural relationships can be considered to change with time. If stereoviews are presented by means of anaglyphs, a rapid change of view is possible; and indeed commercial three-dimensional motion pictures have been successfully made.

Anaglyphs of line drawings have been made from two conoscopic projections, calculated on viewpoints about five degrees apart, and plotted in different colours. Spectacles are made from coloured plastic film. If the match between a colour filter and an ink is close enough then a drawing made in that ink will be invisible, or barely visible when viewed through the filter. The purity of cheaply and readily available filters, (such as Griffin and George's: primary green 030F; and primary red 010L), is sufficiently good for the purpose. The three filters which accompany Nature 284, 1980 are even better. Most red inks encountered were a very good match, but most green inks appear slightly red when viewed through the green filter: consequently that eye sees two images and it becomes

Fig 94:

Print of an anaglyph of a pipe network, equivalent to Figs 37 and 38, showing flowrates. The images for the right and left eye are superimposed, and drawn in green and red respectively in the original.

Fig 95:

Print of an anaglyph of a pipe network, equivalent to Figs 40 and 41, showing pipe sizes.

Fig 96:

Print of an anaglyph of a pipe network, equivalent to Figs 42 and 43, showing flowrates.

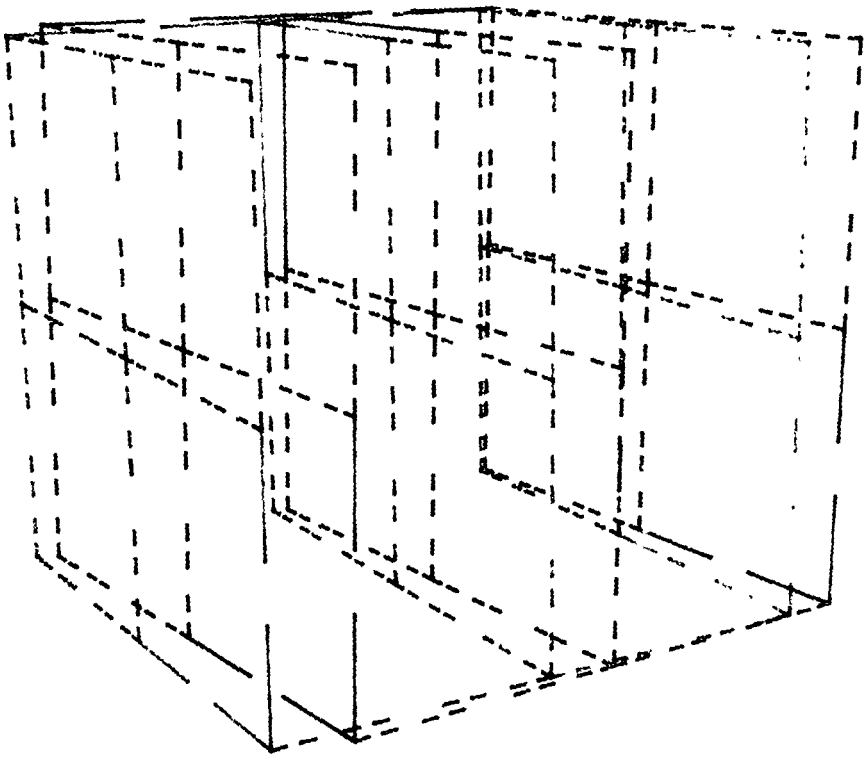

ANAGLYPH OF PIPE NETWORK :-

ITERATION NUMBER 2.

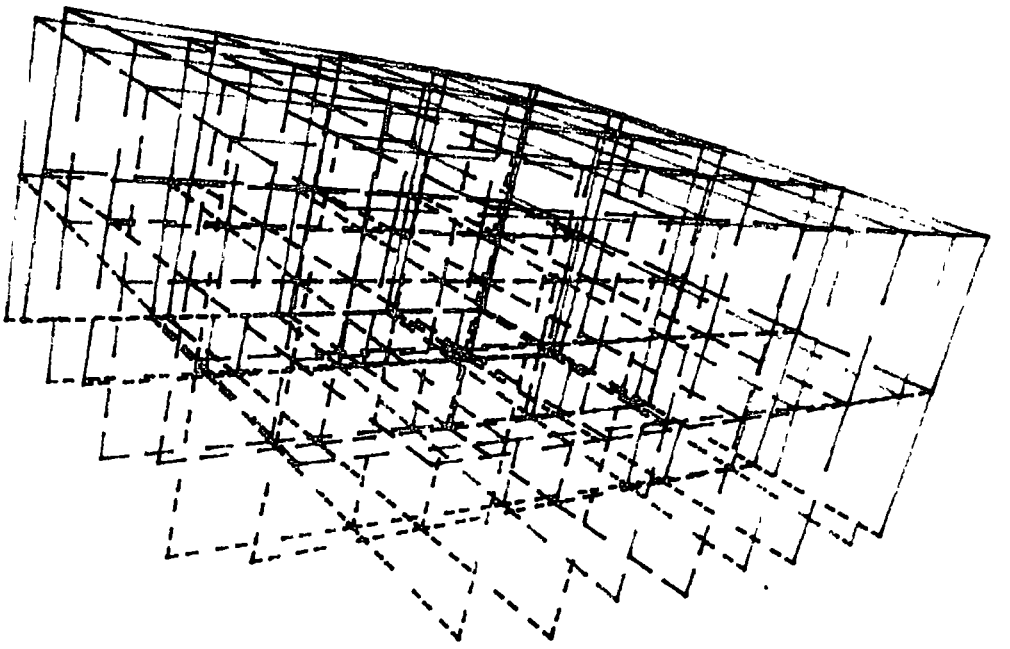

ANAGLYPH OF PIPE NETWORK :-

ITERATION NUMBER 0.

Fig 95

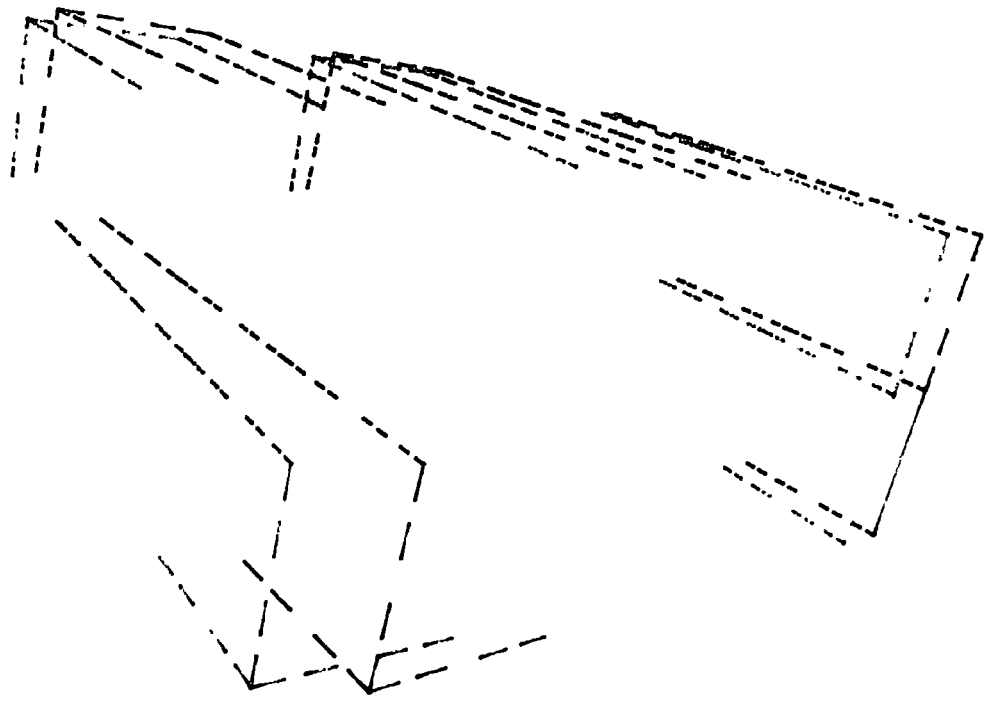

ANAGLYPH OF PIPE NETWORK :-

ITERATION NUMBER 2.

Fig 96

difficult to form a three dimensional mental image.

Output of computer-generated graphics would best be made directly onto microfilm, but access to the Rutherford Laboratory's 256 colour microfilm output device is reported to be difficult to obtain. Alternatively, 35mm photographs could be made directly from a colour TV screen, an output device which is not yet available in Durham.

The best green ink found was Green 5E56 for optical readers. This must be diluted with white spirit before using in felt tipped plotter pens. It is available from: BASF Farben + Fasern GB , Siemenstrasse 76, 7000 Stuttgart 30.

7.7.2 Program description.

Although the Figs 94 to 96 are not coloured in such a way as to be suitable for viewing as anaglyphs, they are included for comparison purposes. A succession of anaglyphs, showing the network as it develops would make a three dimensional motion picture of the dynamic processes involved. The program Ignet9 is given in Figs 97 to 107. It allows perspective and viewpoint to be chosen interactively, and a choice of anaglyph, stereopair, and three orthogonal orthoscopic views as output. Output is route to screen or plotter, depending on the way in which the program is invoked.

Figs 97 to 107:

Listing of Fortran+*Integrated Graphics program 'Ignet9'. An interactive stereographic net plotting program, with anaglyph, stereo pair, and three orthogonal orthoscopic views.

```
 1.000   C TO PLOT A 3D PIPE NETWORK ;
 2.000   C IN *IG
 3.000   C
 4.000         DIMENSION XS(3700), YS(3700), ZS(3700)
 5.000         DIMENSION XF(3700), YF(3700), ZF(3700)
 6.000         DIMENSION ITH(3700), ICOL(3700)
 7.000         DIMENSION CN(8,4)
 8.000         INTEGER*4 LHUE(3700), LINE
 9.000         INTEGER*4 BLACK, BLUE, RED
10.000         INTEGER NO /'N'/, YES /'Y'/
11.000         DATA CN /8*0.0, 0.2, 7*0.0, 0.1, 0.2, 0.1, 5*0.0, 0.05, 0.1, 0.05,
12.000        1     0.2, 0.05, 0.1, 0.05, 0.0/
13.000         DATA BLACK /'BLAC'/, BLUE /'BLUE'/, RED /'RED'/
14.000   C
15.000   C*****************************************************
16.000   C INPUT
17.000   C   4 , NETWORK GEOMETRY FROM STARTSQNET IN APL .
18.000   C   5 , CONDUCTIVITIES , COLOURS .
19.000   C   6 , INTERACTIVE TERMINAL I/P .
20.000   C   7 , INTERACTIVE TERMINAL O/P : = F7/8 IN SOFL(9,) .
21.000   C   8 , INPUT FROM F7/8 FOR HARD COPY RUN .
22.000   C*****************************************************
23.000   C
24.000   C R RADIUS OF SPHERE OF INTEREST .
25.000   C S , F START , FINISH COORDS OF PIPE .
26.000   C
27.000         DR = (ATAN(1.0)) / 45.0
28.000         READ (4,240) R
29.000         READ (5,270) ITS, ITF
30.000         READ (4,250) N
31.000         READ (4,260) (XS(I),YS(I),ZS(I),I=1,N)
32.000         READ (4,260) (XF(J),YF(J),ZF(J),J=1,N)
33.000   C
34.000   C SET INTERACTIVE I/P OFF OR ON .
35.000   C
36.000      10 PRINT 280
37.000         READ (6,300) INTERA
38.000         IF (INTERA .EQ. YES) GO TO 20
39.000         IF (INTERA .NE. NO) GO TO 10
40.000         PRINT 290
```

```
41.000          READ (6,300) IANAG
42.000          IF (IANAG .EQ. YES) GO TO 210
43.000    C
44.000    C ITH IS THE CODE FOR THE NO. OF DASHES IN A LINE.
45.000    C     1 FOR 80-100% FLOW ETC..
46.000    C
47.000    C IO IS :STEADY(1 , BLACK);GROWING(2 , BLUE);DECR.(3 , RED).
48.000    C
49.000    C SET COLOURS IN LHUE .
50.000    C
51.000       20 READ (5,270) (ITH(K),ICOL(K),K=1,N)
52.000          DO 50 L = 1, N
53.000            IF (ICOL(L) .EQ. 2) GO TO 30
54.000            IF (ICOL(L) .EQ. 3) GO TO 40
55.000            LHUE(L) = BLACK
56.000            GO TO 50
57.000       30   LHUE(L) = BLUE
58.000            GO TO 50
59.000       40   LHUE(L) = RED
60.000       50 CONTINUE
61.000    C
62.000    C*****************************************************
63.000    C FORM 3D NETWORK ; INTO OBJECT CALLED 'STOR' .
64.000    C*****************************************************
65.000    C
66.000          CALL IGINIT
67.000          CALL IGBGNO('STOR')
68.000          DO 70 K = 1, N
69.000            NK = ITH(K)
70.000            IF (NK .GE. 5) GO TO 70
71.000            LINE = IGBGNS(0)
72.000    C
73.000    C CANTOR SET :- A SEQUENCE OF BROKEN LINES SO THAT
74.000    C TOTAL DRAWN LENGTH = TOP END OF % FLOW RANGE
75.000    C AND ORTH. PERSP. SHOWS MAX. FLOW IN COLUMN OF PIPES .
76.000    C      XYZ R  RELATIVE MOVE = LENGTH OF PIPE AS X,Y,Z .
77.000    C       " CDR DRAWN LENGTH OF LINE IN CANTOR SET .
78.000    C       " CMR MOVED    "    "   "   "    "    "  (GAP) .
79.000    C
80.000            CALL IGMA(XS(K), YS(K), ZS(K))
```

```
 81.000            XR = XF(K) - XS(K)
 82.000            YR = YF(K) - YS(K)
 83.000            ZR = ZF(K) - ZS(K)
 84.000            ICN = 2 ** (NK - 1)
 85.000            XCDR = (XR - ((NK - 1)*XR*0.2)) / ICN
 86.000            YCDR = (YR - ((NK - 1)*YR*0.2)) / ICN
 87.000            ZCDR = (ZR - ((NK - 1)*ZR*0.2)) / ICN
 88.000            DO 60 LC = 1, ICN
 89.000              XCMR = XR * CN(LC,NK)
 90.000              YCMR = YR * CN(LC,NK)
 91.000              ZCMR = ZR * CN(LC,NK)
 92.000              CALL IGDR(XCDR, YCDR, ZCDR)
 93.000         60   CALL IGMR(XCMR, YCMR, ZCMR)
 94.000            CALL IGENDS(LINE)
 95.000            CALL IGHUE(LINE, LHUE(K))
 96.000         70 CONTINUE
 97.000            CALL IGENDO('STOR')
 98.000      C
 99.000      C*********************************************************
100.000      C*********************************************************
101.000      C STEREOSCOPIC PAIR .
102.000      C*********************************************************
103.000      C*********************************************************
104.000      C
105.000            IANSCH = NO
106.000         80 CALL IGBGNS('PICT')
107.000            CALL IGBGNS('FRAM')
108.000      C
109.000      C FRAME .
110.000      C
111.000            CALL IGMA(-0.179,  0.179)
112.000            CALL IGDA(-0.179, 1.0)
113.000            CALL IGDA(1.0, 1.0)
114.000            CALL IGDA(1.0, -0.179)
115.000            CALL IGDA(-0.179, -0.179)
116.000            CALL IGMA( 0.673, -1.0)
117.000            CALL IGDA(-0.673, -0.95)
118.000            CALL IGMA(-0.673, 0.95)
119.000            CALL IGDA( 0.673, 1.0)
120.000      C
```

```
121.000   C MOST OF TITLE .
122.000   C
123.000         CALL IGMA(0.0, -0.4)
124.000         CALL IGTXTH('STEREO PAIR OF PIPE NETWORK :- E ')
125.000   C
126.000         CALL IGBGNS('IMAG')
127.000         CALL IGMA(0.15, -0.6)
128.000         CALL IGTXTH(' LEFT IMAGE . E ')
129.000         CALL IGENDS('IMAG')
130.000   C
131.000         CALL IGMA(0.05, -0.8)
132.000         CALL IGTXTH('ITERATION NUMBER  E ')
133.000         CALL IGFMTH(ITS, 'I')
134.000         CALL IGTXTH('. E ')
135.000         CALL IGENDS('FRAM')
136.000         CALL IGHUE('FRAM', 'BLACK')
137.000   C
138.000   C*********************************************************
139.000   C INPUT NETWORK ('STOR') TO 'PICT' , AS SUBPIC 'STER' .
140.000   C*********************************************************
141.000   C
142.000         CALL IGPUTO('STOR', 'STER')
143.000   C
144.000   C SET SCALES FOR STEREO PAIR PROJECTION .
145.000   C
146.000         IF (IANSCH .EQ. YES) GO TO 100
147.000         IF (INTERA .EQ. YES) GO TO 90
148.000         READ (8,310) ROTX, ROTY, DIST, WSTER, WSTAR
149.000         GO TO 100
150.000      90 ROTX   15.0
151.000         ROTY = 30.0
152.000         DIST = R
153.000         WSTER - R
154.000         WSTAR - R
155.000   C
156.000   C*********************************************************
157.000   C TRANSFORM , I.E. :-
158.000   C ROTATE , PROJECT , AND SCALE .
159.000   C*********************************************************
160.000   C
```

```
161.000      100 CALL IGTRAN('STER', 'ROTX', ROTX*DR)
162.000          CALL IGTRAN('STER', 'CURR', 'ROTY', ROTY*DR)
163.000          CALL IGTRAN('STER', 'CURR', 'MOV3', 0.0, 0.0, DIST)
164.000          CALL IGTRAN('STER', 'CURR', 'PROJ', 0.0, 1.0/6.0*R)
165.000          CALL IGTRAN('STER', 'CURR', 'WIND', -WSTER, WSTER, -WSTER, WSTER)
166.000          CALL IGVWPT('STER', -0.179, 1.0, -0.179, 1.0)
167.000    C
168.000    C DRAW LEFT STEREO MAP
169.000    C
170.000          CALL IGENDS('PICT')
171.000          CALL IGDRON('TERMINAL')
172.000          IF (INTERA .EQ. NO) GO TO 110
173.000          PRINT 320
174.000          PRINT 340, ROTX, ROTY, DIST, WSTER
175.000          PRINT 330
176.000          READ (6,300) DUMMY
177.000    C
178.000    C REST OF TITLE :
179.000    C CHANGE FOR RIGHT STEREO IMAGE .
180.000    C
181.000      110 CALL IGBGNS('IMAG')
182.000          CALL IGMA(0.15, -0.6)
183.000          CALL IGTXTH(' RIGHT IMAGE F ')
184.000          CALL IGENDS('IMAG')
185.000    C
186.000    C REFORM STER AND
187.000    C ROTATE 5 DEGREES LESS FOR RIGHT EYE .
188.000    C
189.000          CALL IGTRAN('STER', 'ROTX', ROTX*DR)
190.000          CALL IGTRAN('STER', 'CURR', 'ROTY', (ROTY   5.0)*DR)
191.000          CALL IGTRAN('STER', 'CURR', 'MOV3', 0.0, 0.0, DIST)
192.000          CALL IGTRAN('STER', 'CURR', 'PROJ', 0.0, 1.0/6.0*R)
193.000          CALL IGTRAN('STER', 'CURR', 'WIND', -WSTER, WSTER, -WSTER, WSTER)
194.000          CALL IGVWPT('STER',  0.179, 1.0,  0.179, 1.0)
195.000    C
196.000    C DRAW RIGHT STEREO MAP
197.000    C
198.000          CALL IGDRON('TERMINAL')
199.000    C
200.000          IF (INTERA .EQ. NO) GO TO 130
```

```
201.000           PRINT 320
202.000           PRINT 340, ROTX, ROTY, DIST, WSTER
203.000           PRINT 350
204.000           READ (6,300) IANSCH
205.000           IF (IANSCH .EQ. NO) GO TO 120
206.000           PRINT 360
207.000           READ (6,340) ROTX, ROTY, DIST, WSTER
208.000           GO TO 80
209.000       120 WRITE (7,310) ROTX, ROTY, DIST, WSTER
210.000     C
211.000       130 CALL IGDELS('PICT')
212.000     C
213.000     C*****************************************************
214.000     C*****************************************************
215.000     C ORTHOSCOPIC VIEWS .
216.000     C*****************************************************
217.000     C*****************************************************
218.000     C
219.000     C IORTH=1,2,3 FOR X,Y,Z.
220.000     C
221.000           IORTH = 1
222.000       140 CALL IGBGNS('ORTH')
223.000           CALL IGMA(-0.179, -0.179)
224.000           CALL IGDA(-0.179, 1.0)
225.000           CALL IGDA(1.0, 1.0)
226.000           CALL IGDA(1.0, -0.179)
227.000           CALL IGDA(-0.179,  0.179)
228.000           CALL IGMA(-0.673, -1.0)
229.000           CALL IGDA(-0.673, -0.95)
230.000           CALL IGMA(-0.673, 0.95)
231.000           CALL IGDA( 0.673, 1.0)
232.000     C
233.000     C TITLE .
234.000     C
235.000           CALL IGMA(0.05, -0.4)
236.000           CALL IGTXTH('ORTHOSCOPIC PROJECTION , [ ')
237.000           CALL IGMA(0.0, -0.6)
238.000           CALL IGTXTH('VIEW DOWN  E ')
239.000     C
240.000     C*****************************************************
```

```
241.000   C INPUT NETWORK ('STOR') TO 'ORTH' ,AS SUBPIC 'STAR' .
242.000   C*****************************************************
243.000   C
244.000         CALL IGPUTO('STOR', 'STAR')
245.000   C
246.000   C 3 VIEWS .
247.000   C
248.000         IF (IORTH .EQ. 2) GO TO 160
249.000         IF (IORTH .EQ. 3) GO TO 170
250.000         CALL IGTXTH('X (SIDE) AXIS . E ')
251.000     150 CALL IGTRAN('STAR', 'ROTY', 90.0*DR)
252.000         CALL IGTRAN('STAR', 'CURR', 'MOV3', 0.0, 0.0, DIST)
253.000         CALL IGTRAN('STAR', 'CURR', 'PROJ', 0.0, 0.0)
254.000         CALL IGTRAN('STAR', 'CURR', 'WIND', -WSTAR, WSTAR, -WSTAR, WSTAR)
255.000         CALL IGVWPT('STAR', -0.179, 1.0, -0.179, 1.0)
256.000         GO TO 180
257.000     160 CALL IGTXTH('Y (VERTICAL) AXIS . E')
258.000         CALL IGTRAN('STAR', 'ROTX', 90.0*DR)
259.000         CALL IGTRAN('STAR', 'CURR', 'MOV3', 0.0, 0.0, DIST)
260.000         CALL IGTRAN('STAR', 'CURR', 'PROJ', 0.0, 0.0)
261.000         CALL IGTRAN('STAR', 'CURR', 'WIND', -WSTAR, WSTAR, -WSTAR, WSTAR)
262.000         CALL IGVWPT('STAR', -0.179, 1.0, -0.179, 1.0)
263.000         GO TO 180
264.000     170 CALL IGTXTH('Z (SIDE) AXIS . E.')
265.000         CALL IGTRAN('STAR', 'CURR', 'MOV3', 0.0, 0.0, DIST)
266.000         CALL IGTRAN('STAR', 'PROJ', 0.0, 0.0)
267.000         CALL IGTRAN('STAR', 'CURR', 'WIND', -WSTAR, WSTAR, -WSTAR, WSTAR)
268.000         CALL IGVWPT('STAR', -0.179, 1.0, -0.179, 1.0)
269.000     180 CALL IGENDS('ORTH')
270.000   C
271.000   C*****************************************************
272.000   C OUTPUT .
273.000   C*****************************************************
274.000   C
275.000         CALL IGDRON('TERMINAL')
276.000   C
277.000         IF (INTERA .EQ. NO) GO TO 190
278.000         PRINT 390, WSTAR
279.000         PRINT 350
280.000         READ (6,300) IANSCH
```

```
281.000          IF (IANSCH .EQ. NO) GO TO 190
282.000          PRINT 370
283.000          READ (6,310) WSTAR
284.000          IF (IANSCH .EQ. YES) IORTH = 1
285.000          IF (IANSCH .EQ. YES) GO TO 140
286.000      190 IORTH = IORTH + 1
287.000          IF (IORTH .LE. 3) GO TO 140
288.000          IF (INTERA .EQ. NO) GO TO 200
289.000          WRITE (7,310) WSTAR
290.000      200 ITS = ITS + 1
291.000          IF (ITS .LE. ITF) GO TO 20
292.000          IF (INTERA .EQ. NO) GO TO 400
293.000          PRINT 380
294.000          GO TO 400
295.000     C*************************************************
296.000     C*************************************************
297.000     C ANAGLYPHIC PLOT .
298.000     C*************************************************
299.000     C*************************************************
300.000     C
301.000     C*************************************************
302.000     C FORM 3D NETWORK ; INTO OBJECT CALLED 'STOR' .
303.000     C*************************************************
304.000     C
305.000       210 READ (5,270) (ITH(K),TCOL(K),K=1,N)
306.000          CALL IGINIT
307.000          CALL IGBGNO('STOR')
308.000          DO 230 K = 1, N
309.000            NK = ITH(K)
310.000            IF (NK .GE. 5) GO TO 230
311.000     C
312.000     C CANTOR SET :- A SEQUENCE OF BROKEN LINES SO THAT
313.000     C TOTAL DRAWN LENGTH = TOP END OF % FLOW RANGE
314.000     C AND ORTH. PERSP. SHOWS MAX. FLOW IN COLUMN OF PIPES .
315.000     C      XYZ R  RELATIVE MOVE = LENGTH OF PIPE AS X,Y,Z .
316.000     C       " CDR DRAWN LENGTH OF LINE IN CANTOR SET .
317.000     C       " CMR MOVED    "    "   "   "    "    " (GAP) .
318.000     C
319.000            CALL IGMA(XS(K), YS(K), ZS(K))
320.000            XR = XF(K) - XS(K)
```

```
321.000            YR = YF(K) - YS(K)
322.000            ZR = ZF(K) - ZS(K)
323.000            ICN = 2 ** (NK - 1)
324.000            XCDR = (XR - ((NK - 1)*XR*0.2)) / ICN
325.000            YCDR = (YR - ((NK - 1)*YR*0.2)) / ICN
326.000            ZCDR = (ZR - ((NK - 1)*ZR*0.2)) / ICN
327.000            DO 220 LC = 1, ICN
328.000              XCMR = XR * CN(LC,NK)
329.000              YCMR = YR * CN(LC,NK)
330.000              ZCMR = ZR * CN(LC,NK)
331.000              CALL IGDR(XCDR, YCDR, ZCDR)
332.000      220   CALL IGMR(XCMR, YCMR, ZCMR)
333.000      230 CONTINUE
334.000          CALL IGENDO('STOR')
335.000    C
336.000    C*********************************************************
337.000    C*********************************************************
338.000    C STEREOSCOPIC PAIR .
339.000    C*********************************************************
340.000    C*********************************************************
341.000    C
342.000          CALL IGBGNS('PICT')
343.000          CALL IGBGNS('FRAM')
344.000    C
345.000    C FRAME .
346.000    C
347.000          CALL IGMA(-0.179, -0.179)
348.000          CALL IGDA(-0.179, 1.0)
349.000          CALL IGDA(1.0, 1.0)
350.000          CALL IGDA(1.0,  0.179)
351.000          CALL IGDA( 0.179,  0.179)
352.000          CALL IGMA(-0.673, -1.0)
353.000          CALL IGDA(-0.673, -0.95)
354.000          CALL IGMA(-0.673, 0.95)
355.000          CALL IGDA(-0.673, 1.0)
356.000    C
357.000    C MOST OF TITLE .
358.000    C
359.000          CALL IGMA(0.0, -0.4)
360.000          CALL IGTXTH('ANAGLYPH OF PIPE NETWORK :- E ')
```

```
      C
            CALL IGMA(0.05, -0.8)
            CALL IGTXTH('ITERATION NUMBER  E')
            CALL IGFMTH(ITS, 'I')
            CALL IGTXTH('. E ')
            CALL IGENDS('FRAM')
            CALL IGHUE('FRAM', 'BLACK')
      C
      C*********************************************************
      C INPUT NETWORK ('STOR') TO SUBPICS 'STLR' AND 'STLB' .
      C*********************************************************
      C
            CALL IGPUTO('STOR', 'STLR')
            CALL IGHUE('STLR', 'RED ')
            READ (8,310) ROTX, ROTY, DIST, WSTER, WSTAR
      C
      C*********************************************************
      C TRANSFORM , I.E. :-
      C ROTATE , PROJECT , AND SCALE .
      C*********************************************************
      C
            CALL IGTRAN('STLR', 'ROTX', ROTX*DR)
            CALL IGTRAN('STLR', 'CURR', 'ROTY', ROTY*DR)
            CALL IGTRAN('STLR', 'CURR', 'MOV3', 0.0, 0.0, DIST)
            CALL IGTRAN('STLR', 'CURR', 'PROJ', 0.0, 1.0/6.0*R)
            CALL IGTRAN('STLR', 'CURR', 'WIND', -WSTER, WSTER, -WSTER, WSTER)
            CALL IGVWPT('STLR', -0.179, 1.0, -0.179, 1.0)
      C
      C ROTATE 5 DEGREES LESS FOR RIGHT EYE .
      C
            CALL IGPUTO('STOR', 'STRB')
            CALL IGTRAN('STRB', 'ROTX', ROTX*DR)
            CALL IGTRAN('STRB', 'CURR', 'ROTY', ROTY*DR)
            CALL IGTRAN('STRB', 'CURR', 'MOV3', 0.0, 0.0, -R)
            CALL IGTRAN('STRB', 'CURR', 'ROTY', -5.0*DR)
            CALL IGTRAN('STRB', 'CURR', 'MOV3', 0.0, 0.0, R)
            CALL IGTRAN('STRB', 'CURR', 'MOV3', 0.0, 0.0, DIST)
            CALL IGTRAN('STRB', 'CURR', 'PROJ', 0.0, 1.0/6.0*R)
            CALL IGTRAN('STRB', 'CURR', 'WIND', -WSTER, WSTER,  WSTER, WSTER)
            CALL IGVWPT('STRB', -0.179, 1.0, -0.179, 1.0)
```

```
401.000          CALL IGHUE('STRB', 'BLUE')
402.000    C
403.000          CALL IGENDS('PICT')
404.000          CALL IGDRON('TERMINAL')
405.000          ITS = ITS + 1
406.000          IF (ITS .LE. ITF) GO TO 210
407.000    C
408.000      240 FORMAT (21X, F10.4)
409.000      250 FORMAT (21X, I10)
410.000      260 FORMAT (3E10.2)
411.000      270 FORMAT (1X, 2I10)
412.000      280 FORMAT ('DO YOU WANT TO CHANGE PROJECTION VARIABLES', /, '
413.000         1               INTERACTIVELY ? ')
414.000      290 FORMAT (/, 'DO YOU WANT JUST THE ANAGLYPHIC PLOT ?', /, 'THE ALTER
415.000         1NATIVE IS A STANDARD STEREO-', 'PAIR AND ORTHOSCOPIC PLOTS :=')
416.000      300 FORMAT (A1)
417.000      310 FORMAT (F10.4)
418.000      320 FORMAT ('PRESENT VALUES ARE :-   ', /, '      ROTX;     ROTY;MOV3(
419.000         1DIST); WIND(W):')
420.000      330 FORMAT ('RETN=CONTINUE')
421.000      340 FORMAT (4F10.4)
422.000      350 FORMAT ('DO YOU WANT TO CHANGE ?')
423.000      360 FORMAT ('INPUT : ROTX , ROTY , DIST , W ; 4F10.4 .', /, 'START.000
424.000         10     .0000     .0000     .0000')
425.000      370 FORMAT ('INPUT NEW VALUE , F10.4 .', /, 'START.0000')
426.000      380 FORMAT ('FOR HARD COPY WITH CHOSEN PARAMETERS :- $SO SGFIL(J2,)')
427.000      390 FORMAT ('PRESENT VALUE OF HALF-WINDOW EDGE (WSTAR) IS : ', F10.4)
428.000      400 STOP
429.000          END
```

Anderson, E.M. (1942)

'The dynamics of faulting and dyke formation, with applications to Britain.' Edinburgh.

Anon (1978)

'APL Language.' International Business Machines Corporation publication number GC 26-3847-3, file no. 5370-22 Systems.

Anon (undated)

'Musterbuch F246.' BASF Farben+Fasern AG, Siemenstrasse 76, 7000 Stuttgart 30.

Anon (undated)

'Operating manual, Ruska Gas Permeameter'. Ruska Instrument Corporation, P.O.Box 36010, Houston, Texas, 77036.

Anon (undated)

'Operating manual, Ruska porometer'. Ruska Instrument Corporation, P.O.Box 36010, Houston, Texas, 77036.

Ashton, K. (1965)

'Preliminary report on a new hydrological technique'. Cave Res. Gp. G.B, Newsletter, v98, pp2-5.

Ashton, K. (1966)

'The analysis of flow data from karst drainage systems'. Trans. Cave Res. Gp. G.B., v7, no2, pp161-204, March 1966.

Backus, G.E. (1962)

'Long wave elastic anisotropy produced by horizontal layering'. J. Geophys. Res., v67, no11, pp4427-4440. Oct 1962.

Backus, G.E. (1965)

'Possible forms of seismic anisotropy of the uppermost mantle under oceans'. J. Geophys. Res., v70, no14, pp3429-3439, July 15 1965.

Bamford, D. and Nunn, K.R. (1979)

'In situ seismic measurement of crack anisotropy in the Carboniferous limestone of Northwest England'. Geophys. Prospecting, v27, no2, pp322-338, June 1979.

Bear, M. (1972)

'Dynamics of fluid in porous media'. American Elsevier, N. York.

Bedinger, M.S. (1966)

'Electric-analogue study of cave formation'. Nat. Speleo. Soc. Bull., v28, no3, pp127-132, July 1966.

Bogli, A. (1971)

'Corrosion by mixing of Karst waters'. Trans. Cave Res. Gp. G.B., v13, no2, pp109-114, June 1971.

Bollobas B. (1979)

'Graph theory- an introductory course'. Springer-Verlag, N. York, 180pp.

Born, W.T. (1941)

'The attenuation constant of earth materials'. Geophysics, v6, pp132-148.

Brace, W.F. (1960)

'An extension of Griffith's theory of fracture to rocks'. J. Geophys. Res., v65, no10, pp3477-3480.

Broadbent, S.R. and Hammersley, J.M. (1957)

'Percolation processes, 1. Crystals and mazes, 2. The connective constant'. Proc. Camb. Phil. Soc., 53, 629-45.

Brook, A., Brook, D., Davies, G.M. and Long, M.H. (1976)
'Northern caves, volume two, Penyghent and Malham.' Dalesman Books, Clapham. 120pp.

Brook, D., Davies, G.M., Long, M.H., and Ryder, P.F. (1974)
'Northern caves, volume five, The Northern Dales'. Dalesman Books, Clapham. 160pp.

Brown, A. (1968)
'Statistical physics.' Edinburgh University Press. 307pp.

Budworth, D.W. (1970)
'Introduction to ceramic science'. Pergammon, Oxford.

Calhoun, J.C. and Yuster, S.T. (1947a)
'A study of the flow of homogeneous fluids through ideal porous media, continued.' Producers Monthly, v11, August 1947, pp32-38.

Calhoun, J.C. and Yuster, S.T. (1948b)
'A study of the flow of homogeneous fluids through ideal porous media, conclusion.' Producers Monthly, Sept 1947, pp22-27

Celestino, T.B. and Goodman, R.E. (1979)
'Path dependency of rough joints in bi-directional shearing'. In Proc. 4th Int. Symp. Rock Mech., v1, pp9-98, Montreux, Switzerland, Sept 1979.

Chadha, D.(1979) pers comm.

Chatzis, I. and Dullien, F.A.L. (1977)
'Modelling pore structure by 2-dimensional and 3-dimensional networks with application to sandstones'. J. Canad. Petrol. Tech., Jan-Mar 1977, pp97-108.

Chinnery, M.A. (1966)
'Secondary faulting, 1. Theoretical aspects'. Canad. J. Earth Sci., v3, pp163-174.

Chinnery, M.A. (1966)

'Secondary faulting, 2. Geological aspects'. Canad. J. Earth Sci., v3, pp175-190.

Coats, K.H. and Smith, B.D. (1964)

'Dead end pore volume and dispersion in porous media'. Soc. Petrol. Eng. J. AIME., v231, pp73-84, Mar 1964.

Cresswell, D. (1969)

'The geology of the Lewisian rocks north of Loch Torridon, Ross-shire, Scotland.' Unpublished Ph.D. Thesis, University of Keele.

Cresswell, D. (1972)

'The structural development of the Lewisian rocks on the North shore of Loch Torridon, Ross-shire.' Scott. J. Geol., v8, pt.4, pp293-308.

Darcy, H. (1865)

'Les fontaines publiques de la ville de Dijon'. Paris

David, M. (1977)

'Geostatistical ore reserve estimation'. Elsevier, N.Y., 364pp.

Deo, N. (1974)

'Graph theory with applications to engineering and computer science.' Prentice-Hall, Eaglewood Cliffs, N.J.

de Wijs, H.J. (1953)

'Statistics of ore distribution, Part II, Theory of binomial distribution applied to sampling and engineering problems'. Geol. en Mijnbouw, v15, pp12-24.

Doughty, P.S. (1968)

'Joint densities and their relation to lithology in the Great Scar limestone'. Proc. Yorks. Geol. Soc., v36, pt4, no27, pp479-512.

Dowlen, G.R. (1979)

'Velocity anisotropy and attenuation as studied under laboratory and field conditions.' Unpublished M.Sc. Thesis, University of Durham.

Duguid, J.O. and Abel, J.F. (1974)

'Finite-element galerkin method for analysis of flow in fractured porous media'. (In Oden, J.T., Zienkiewicz, O.C., Gallagher, R.H. and Taylor, C. (eds.) 'Finite-element methods in flow problems') Univ. Alabama, pp599-615.

Evers, J.F., Preston, F.W., Sadiq, S., and Swift, G.W. (1967)

'Preparation and testing of low permeability porous media to meet scaling requirements for gas reservoir modelling.' Society of Petroleum Eng. J. of AIME, v240, pp189-194.

Ewers, R.O. (1966)

'Bedding plane anastomoses and their relation to cavern passages'. Nat. Speleo. Soc. Bull., v28, no3, p133-140, July 1966.

Flanagan, F.J. (1969)

'U.S. Geological Survey Standards-II. First compilation of data for the new U.S.G.S. Rocks'. Geochim. et Cosmochim. Acta, v33, pp81-120.

Ford, T.D. (1971)

'Structures in limestones affecting the initiation of caves'. Trans. Cave Res. Gp. G.B., v13, no2, pp65-72, June 1971.

Ford, T.D. and Cullingford, C.H.D. (eds.), (1976)

'The Science of Speleology'. Academic Press Inc, London.

Ford, L.R.Jr. and Fulkerson D.R. (1957)

'A simple algorithm for finding maximal network flows and an application to the Hitchcock problem'. Canad. J. Math., v9, pp210-218.

Fox-Stangeways, C. (1881)

'The geology of the Oolitic and Liassic rocks north and west of Malton'. Mem. Surv. Eng. and Wales, 96, Malton, HMSO, London.

Francis, H.A. (1977)

'Applications of spherical indentation mechanics to reversible and irreversible contact between rough surfaces'. Wear, v45, pp221-269.

Gash, P.J.S. (1971)

'A study of surface features relating to brittle and semi-brittle fracture'. Tectonophysics, v12, pp349-391.

Grassie, D. (in preparation)

'Optimum Isorhythm interpolation in digital modelling'. University of Durham, Ph.D. Thesis.

Greenkorn, R.A., Johnson, C.R. and Shallenberger L.K. (1964)

'Directional permeability of heterogeneous anisotropic porous media'. Soc. Petrol. Eng. Jour. AIME., v231, pp124-132, and discussion pp363-4.

Griffith, A.A. (1920)

'The phenomena of rupture and flow in solids'. Phil. Trans. Roy. Soc. Lond., Ser(A), v221, pp163-198.

Groves, A.W. (1951)

'Silicate analysis.' Alan and Unwin, London. 336 pp.

Harris, A.B., Lubensky, T.C., Holcomb, W.K. and Dasgupta, C. (1975)

'Renormalisation-Group approach to percolation problems'. Phys. Rev. Lett., v35, no6, pp327-330, Aug 1975.

Harrison, I.B. (1973)

'The hydrogeology of the Vale of Pickering'. Unpubl. Ph.D. Thesis, Univ. Leeds, Sept 1973.

Henshell, R.D. (1975)

'PAFEC 75- Theory, Results'. Pafec Ltd., Pafec House, 40, Broadgate, Beeston, Nottingham.

Herbert, R. and Rushton, K.R. (1966)

'Groundwater flow studies by resistance networks'. Geotechnique, v16, no1, pp53-75.

Hoek, E. and Bray, J. (1974)

'Rock Slope Engineering'. J. Mining Metal., London.

Howard, G.C. and Fast, C.R. (1970)

'Hydrodynamic Fracturing'. SPE Monograph, vII.

Hoyle, F. (1953)

'On the formation of gas clouds into galaxies and stars'. Astrophys. J., v118, pp513-528.

Hunter, R.H. (1980), pers comm

Huskey, W.L. and Crawford, P.B. (1967)

'Performance of petroleum reservoirs containing vertical fractures in a matrix'. Soc. Petrol. Eng. J. AIME., v240, pp221-228, June 1967.

Jennings, A. (1977)

'Matrix computation for engineers and scientists.' John Wiley and Sons, Chichester, New York. 330pp.

Jeppson, R.W. (1977)

'Analysis of flow in pipe networks'. Ann Arbor Science, Michigan.

Johnson, C.E. and Richter, F.M. (1979)

'Stereo views of seismicity associated with subduction zones.' J. Geology, v87, pp467-474.

Johnson, M.R.W. and Frost, R.T.C. (1977)

'Fault and lineament patterns in the Southern Highlands of Scotland'. Geol. en Mijnbouw, v56, no4, pp287-294.

Jonasson, H. (1980)

'A preliminary study of the small scale roughness of rock surfaces'. Unpubl. M.Sc. Thesis, Univ. Durham.

Jones, R.H. and Hurt, K.G. (1978)

'An osmotic method for determining rock and aggregate suction characteristics with application to frost heave studies.' Q. J. Eng. Geol., v11, pp245-252.

Kendrick, R.I. (1979)

'Some aspects of flow network tracing in the Corallian aquifer, North Yorkshire'. Unpubl. M.Sc. Thesis, Univ. Durham.

Kent, P.E. (1967)

'Outline geology of the Southern North Sea Basin'. Proc. Yorks. Geol. Soc., v36, ptl, ppl-22.

Kent, P.E. (1974)

'Structural History'. (In Rayner, D.H. and Hemingway, J.E. (eds.), (1974), 'The geology and mineral resources of Yorkshire'). Yorks. Geol. Soc., pp20-21.

Klinkenberg, L.J. (1941)

'The permeability of porous media to liquids and gases'. API Drilling and Production Practice, pp200-213.

Krutter, H. and Day, R.J. (1941)

'Modification of permeability measurements'. Oil Weekly, v104, pp24-32.

Ladeira, F.L. and Price, N.J. (1981)

'Relationship between fracture spacing and bed thickness'. J. Struct. Geol., v3, no2, pp179-183.

Lange, A. (1959)

'Introductory notes on the changing geometry of cave structures'. Cave Studies, no11, pp69-90, May 1959.

Lange, A. (1968)

'The changing geometry of cave structures part 1: The constant solution gradient'. Caves and Karst, v10, no1, pp1-10, Jan/Feb 1968.

Lawn, B.R. and Wilshaw, T.R. (1975)

'Fracture of brittle solids'. Camb. Univ. Press.

Legeza, L. (1975)

'Tao magic, the secret language of diagrams and calligraphy'. Thames and Hudson, London.

Louis, C. and Maini, Y.N. (1967)

'Determination of in situ hydraulic parameters in jointed rock'. Proc. 2nd. congr. Internat. Soc. Rock Mech. (Belgrave).

Longuet-Higgins, M.S. (1957)

'Statistical properties of an isotropic surface'. Phil. Trans. Roy. Soc., A250, 157.

Lucas, J.M. and Holland, J.G. (1980)

'X-ray data reduction using MIDAS.' Read at 13th. Philips X-ray Spectometer conference, Durham.

Mandelbrot, B. B. (1977)

'Fractals, form chance and dimension.' W. H. Freeman and Co., San Francisco. 365pp.

Mercado,A. (1972)

'The kinetics of mineral dissolution in aquifers and their use for hydrologic investigation'. Unpubl. Ph.D. Thesis, North Mexico Inst. Mining and Technol., Sorocco.

Mierzejewski, J.K. (1978)

'Groundwater tracing in the Vale of Pickering using the Fluorescein/activated charcoal method'. Unpubl. M.Sc. Thesis, Univ. of Durham, Sept 1978.

Moseley, F. and Ahmed, S.M. (1967)

Carboniferous joints in the North of England and their relation to earlier and later structures'. Proc. Yorks. Geol. Soc., v36, pt1, no4, pp61-90.

Moseley, F. (1973)

'Orientation and origins of joints, faults and folds in the Carboniferous limestone of the Northwest of England'. Trans. Cave Res. Gp. G.B., v15, no2, pp99-106, June 1973.

Morrow, N.R. (19759

'The effects of surface roughness on contact angle with special reference to petroleum recovery'. J. Canad. Petrol. Tech., pp42-53, Dec 1975.

Mowat, G.D. (1962)

'Progressive changes of shape by solution in the laboratory'. Cave Notes, v4, pp45-49.

Muehlberger, W.R. (1960)

'Conjugate joint sets of small dihedral angle'. Geological notes, pp211-219.

Nayak, (1971)

'Random process model of rough surfaces'. Trans. ASME. J. Lub. Tech., F93, pp398-407.

New, B.M. and West, G. (1980)

'The transmission of compressional waves in jointed rock'. Engng. Geol., v15, pp151-161.

Nooshin, H. (1979)

'Formex formulation of double layer grids'. Space Structures Research Centre, Dept. Civil Engineering, Univ. Surrey.

Norton, D. and Knapp, R. (1977)

'Transport phenomena in hydrothermal systems: the nature of porosity'. Am. J. Sci., v277, pp913-936, Oct 1977.

Novikov, E.A. and Stewart, R.W. (1964)

'The intermittency of turbulence and the spectrum of energy dissipation fluctuations'. Izvestia Academii Nank. SSR Seria Geofizicheskaia, v3, pp408-413.

Nikuradse, J. (1933)

(In german). Ver. deutsch Ing. Forschungshaft, no361.

NUMAC Computing Services, (1977)

'The use of *IG in MTS.' The Universities of Newcastle-upon-Tyne and Durham.

Nye, J.F. (1957)

'Physical properties of crystals: their representation by tensors and matrices'. Oxford Clarendon Press, 322p.

O'Brien, P.N.S. (1967)

'The use of amplitudes in seismic refraction survey'. (In Musgrave, A.W. (ed.) 'Seimic Refraction Prospecting'), The Soc. Explor. Geophys., Tulsa, Oklahoma.)

Ollos, G. (1961)

'Possibilities of model investigations into water movements occuring in fissured rocks'. Proc. 9th. conv. on hydraul. res., Int. Assoc. Hyraul. Res., Dubrovnik, Jugoslavia., pp485-494.

Paterson, M.S, (1970)

'Non-hydrostatic thermodynamics and it's geologic applications'. Rev. Geophys. Space Phys., v11, pp355-389.

Patir, N. (1978)

'A numerical proceedure for random generation of rough surfaces'. Wear, v47, pp263-277.

Patir, N. and Cheng, H.S. (1978)

'An average flow model for determining effects of 3-dimensional roughness on partial hydrodynamic lubrication'. Trans. ASME. J. Fluids Engng., v100, pp12-17, Jan 1978.

Patsoules, M. (1980), pers comm.

Ph.D. Thesis, Univ. Sheffield, in preparation.

Patsoules, M. and Cripps, J.C. (in preparation)

'A qualitative analysis of chalk pore geometry using resin casts'.

Pickell, J.J., Swanson, B.F. and Hickman, W.B. (1966)

'Application of air-mercury and oil-air capillary pressure data in the study of pore structure and fluid distribution'. Soc. Petrol. Eng. J. AIME., v237, pp55-61, Mar 1966.

Picknett, R.G. and Stenner, R.D. (1978)

'Enhanced calcite solubility in dilute magnesium carbonate solutions'. Trans. Brit. Cave Res. Assoc., v5, no1, pp47-54, Mar. 1978.

Pittman, E.D. and Duschatho, R.W. (1970)

'Use of pore casts and scanning electron microscope to study pore geometry.' J. Sed. Pet., v40, pp1153-1157.

Pitty, A.F. (1968)

'The scale and significance of the solutional loss from the limestone tract of the Southern Pennines'. Proc. Geol. Assoc., v79, pp153-177.

Price, N.J. (1966)

'Fault and joint development in brittle and semi-brittle rock.' Pergamon Press, Oxford. 176pp.

Purcell, W.R. (1949)

'Capillary pressures- their measurement using mercury and the calculation of permeability therefrom.' Petroleum Transactions, AIME, v186, pp39-48

Ramberg, I.B., Gabrielsen, R.H., Larsen, B.T. and Solli, A. (1977)

'Analysis of fracture patterns in Southern Norway'. Geol. en Mijnbouw, v56, no4, pp295-310.

Ramsay, J.G. (1980)

'Shear zone geometry: a review'. J. Struct. Geol., v2, pp83-99.

Rats, M.V. and Chernyashov, S.N. (1965)

'Statiscical aspect of the problem on the permeability of the jointy rocks'. S. Hydrol. Fract., pp227-236.

Raudkivi, A.J. and Callander,R.A. (1976)

'Analysis of groundwater flow.' Edward Arnold Ltd., London. 214pp.

Redshaw, S.C. (1948)

'An electrical potential analyser'. Proc. Instn. Mech. Engnrs., v159, pp55-62.

Reeves, M.J. (1973a)

'Groundwater chemistry of the Vale of Pickering'. Unpubl. Rept. to the Yorks. River Authority.

Reeves, M.J. (1973b)

'Aquifer properties and the nature of groundwater flow in the Vale of Pickering'. Unpubl. Rept. to the Yorks. River Authority.

Reeves, M.J. (1977)

'Groundwater flow in early mesozoic and palaeozoic aquifers'. Proc. Conf. on Rock Engng., Core-UK., 4-7 Apr 1977.

Reeves, M.J., Parry, E.L. and Richardson,G. (1978)

'Preliminary evaluation of the groundwater resources of the western part of the Vale of Pickering'. Q. J. Engng. Geol., v11, pp253-262.

Reeves, M.J. (1979)

'Recharge of the English Chalk: some possible mechanisms'. Eng. Geol., v14, pp231-240.

Richardson, L.F. (1961)

'The problem of contiguity: an appendix of statistics of deadly quarrels'. General Systems Yearbook, v6, pp139-187.

Riemer, K.L. (1979)

'The effects of weathering and test procedures on the strength of joint margins in the Corallian Limestones from Spaunton Moor Quarry.' Unpublished M.Sc. Thesis, Univ. Durham. Sept 1979.

Romm, J.S. (1966)

'Flow phenomena in fissured rock'. (Russian), Nedra, Moskau, 284pp.

Rose, W.D. (1948)

'Permeability and gas slippage phenomena'. API Meetings, Chicago, Illinois, pp127-135, Nov 1948.

Rowlands, N.J. and Sampey, D. (1977)

'Zipf's law- an aid to resource inventory prediction in partially explored areas'. Math. Geol., v9, no4.

Russell, S. quoted in Schaffer R.J. (1972)

Ryder, P.F. and Stevens, G. (1973)

'Kirkdale Cave Survey'. Moldywarps Speleological Journal, v3. P.F.Ryder, 147, Heavygate Rd., Sheffield.

Sayles, R.S and Thomas,T.R. (1978)

'Surface topography as a nonstationary random process'. Nature, v271, 2.2.1978.

Schaffer, R.J. (1972)

The weathering of natural building stones.' Dept. Sci. Ind. Res., Build. Res. Spec. Report no. 18, 139pp.

Scheidegger, A.E. (1954)

'Directional permeability of porous media to homogeneous fluids'. Geofis. Pura Appl., v28, pp75-90.

Scheidegger, A.E. (1956)

'On directional permeability'. Geofis. Pura Appl., v33, pp111-113.

Scheidegger, A.E. (1957)

'The physics of flow through porous media'. Univ. Toronto Press.

Scheidegger, A.E. (1958)

'Principles of geodynamics.' Springer-Verlag, Berlin.

Sharir, M.R. and Howard, C.D.D. (1968)

'Water distribution systems analysis'. J. Hydraul. Div. ASCE., v94, pp219-234.

Sheppard, T. (ca. 1902, but undated)

'Geological rambles in East Yorkshire.' A. Brown and Sons Ltd., Hull. 235pp.

Smith, C.M.Jr. (29 Feb 1972)

'Matrix inverses and the APL Inverse operator.' Share SSD#220, Share secretary, Computation Centre, Pennsylvania State University.

Snow, D.T. (1968)

'Hydraulic character of fractured metamorphic rocks of the front range and implications to the Rocky Mountain Arsenal Well'. Q. Colorado School of Mines. v63, pp167,199.

South Wales Caving Club (undated)

'Ogof Ffynon Ddu'. Map. South Wales Caving Club, Penwyllt, Brecknockshire.

Sutton, J. (1949)

'The geology of the Lewisian rocks of the Loch Torridon area.' Unpubl. Ph.D. Thesis, London University.

Swanson, B.F. (1979)

'Visualising pores and nonwetting phase in porous rock.' J. Petroleum Technology, January 1979, pp10-18

Thomas, T.R. and King, M. (1977)

'Surface topography in engineering: a state-of-the- art review and bibliography'. Brit. Hydromech. Res. Assoc., Cranfield.

Thomas, T.R. and Sayles, R.S. (1978)

'Some problems in the tribology of rough surfaces'. Tribology International, pp163-168, June 1978.

Toureng, C., Fourmaintraux, D. and Denis, A. (1971)

'Propagation des ondes et discontinuites des roches'. Proc. Symp. Int. Mecanique des Roches. Nancy, 1971, 'Rock Fracture'.

Turner, P.A. (1977)

'Hydrological laboratory methods and apparatus used for routine analysis.' ILR669, June 1977, Water Research Centre, Medmenham Laboratory, Medmenham, Bucks..

Walsh, J.B. and Brace, W.F. (1966)

'Elasticity of Rock: A review of some recent theoretical studies'. Rock Mech. and Engng. Geol., IV/4, pp283-297.

Waltham, A.C. (1971)

'Controlling factors in the development of caves'. Trans. Cave Res. Gp. G.B., v13, no2, pp73-80, June 1981.

Waltham, A.C. (1974)

'Caves'. Macmillan, London.

Waltham, A.C. and Brooks, D.B. (1980)

'Three Counties Cave Systems'. Map, Brit. Cave Res. Assoc..

Weissbach, G. (19789

'A new method for the determination of the roughness of rock joints in the laboratory'. Int. J. Rock Mech. and Min. Sci., v15, pp131-133.

Westbrook, G.K., Holland, J.G. and Hardy, R.G. (1974)

'Non-linear optimisation of inter-element influence factors in X-ray fluorescence analysis.' Proc. 9th. X-ray analytical conference, Exeter. Philips.

Westerman, A.R. and Holland, J.G. (submitted)

'Structural control of Scourie dykes, north of Loch Torridon, Ross-shire, Scotland.' submitted to J. Struct. Geol.

Whitehouse, and Archard (1970)

'The properties of a random surface of significance in their contact'. Proc. Roy. Soc. Lond., ser A, 32, 316.

Whiteman, A., Naylor, D., Pegrum, R. and Rees, G. (1975)

'North sea troughs and plate tectonics'. Tectonophysics, v26, pp39-54.

Williamson, J.B.P., Pullen, J. and Hunt, R.T. (1969)

'The shape of solid surfaces'. Am. Soc. Mech. Enginrs., N.York.

Wilson, K.G. (1975)

'Renormalisation Group Methods'. Advances in Math., v16, no4, pp170-186.

Wilson, K.G.

'Problems in physics with many scales of length'. Sci. Am., pp140-157. Aug 1979.

Wilson, V. (1948)

'British Regional Geology: East Yorkshire and Lincolnshire'. Inst. Geol. Sci., HMSO, 94pp.

Wittke, W. (1970)

'Three-dimensional percolation of fissured rock'. (In Rensburg, P.W.J. (ed.) 'Open Pit Mining Symposium, pp181-191).

Wittke, W., Rissler, P. and Semprich, S. (1972)

'Three-dimensional laminar and turbulent flow through fissured rock according to discontinuous and continuous models'. Symp. on Percolation through fissured rock. Stuttgart, 1972, paper T1-H.

Wood, D.A. (1978)

'Major and trace element variations in the Tertiary lavas of E. Greenland and their significance with respect to the Iceland geochemical anomaly.' J. Petrology, v19, pt3, pp393-436.

Wright, T.L. and Doherty, P.C. (1970)

'A linear programming and least squares computer method for solving petrological mixing problems.' Bull. Geol. Soc. Am., v81, pp1995-2008.

Ziman, J.M. (1979)

'Models of disorder'. Camb. Univ. Press, 492pp.

TACHYMETRIC SURVEY OF SPAUNTON MOOR QUARRY,
NR. KIRKBYMOORSIDE, YORKS. : TOP BENCH.

TRUE NORTH IS PARALLEL THE SIDES.
ALL DISTANCES & HEIGHTS IN METRES.

HORIZONTAL RMS ERROR : 1.2M/100M
VERTICAL RMS ERROR : 0.4M/100M HORIZONTAL.

SCALE 1:500

R.J.KENDRICK & A.R.WESTERMAN
30.6-1.7.1979

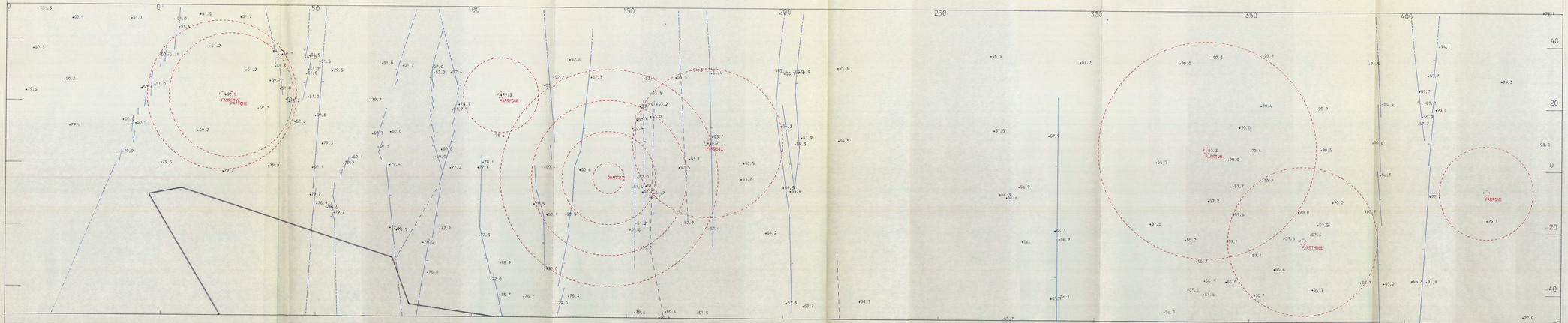

PROJECTED FAULT LINE :
SMALL THROW
OVER 0.2M. THROW.

DOWNTHROWN SIDE.

QUARRY FACE.

CIRCLES INDICATE POSITION OF SEISMIC ARRAYS.

Fig 8